AD NUMBER

AD905291

NEW LIMITATION CHANGE

TO

Approved for public release, distribution unlimited

FROM

Distribution authorized to U.S. Gov't. agencies only; Test and Evaluation; 11 AUG 1972. Other requests shall be referred to Air Force Avionics Laboratory, Attn: NVA-698DF, Wright-Patterson AFB, OH 45433.

AUTHORITY

AFAL ltr, 21 Sep 1978

PERFORMANCE SYNTHESIS

(ELECTRO OPTICAL SENSORS)

—

Frederick A. Rosell
Robert H. Willson
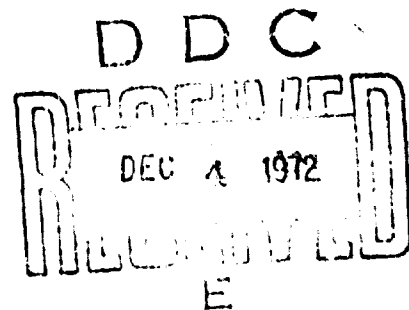
FOREWORD

This program involved the improvement of mathematic models and performance of psychophysical experiments as part of the continuation effort of the 698DF development project for a high-resolution low-light-level television system for tactical airborne application. The models are couched in similar terminology as in the literature. It is felt that these studies have led to a better understanding of electro-optical sensors and their operation and could lead to improved sensors, improved methods of sensory system specification and a reduced need for costly laboratories and flight testing of systems due to the more realistic predictions of detection, recognition and identification ranges that are now possible.

The Air Force Project Director on this program was Frank A. McCann, AFAL/NVA(698DF). The Westinghouse effort was conducted principally by Frederick A. Rosell and Robert H. Willson. The program was performed by the Westinghouse Systems Development Division, Baltimore, Maryland, under Air Force Contract F33615-70C-1461.

This report was submitted by Frederick A. Rosell and Robert H. Willson.

This technical report has been reviewed and is approved for publication.
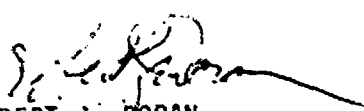
ROBERT J. DORAN
Deputy Director
Navigation & Weapon Delivery Division
Air Force Avionics Laboratory

ABSTRACT

This effort is a continuation of the Performance Synthesis
Study (Electro-Optical Sensors) reported in Technical Report AFAL-TR-71-
137, dated May 1971. Analytical models are developed for evaluating
and predicitng the performance of observers augmented by electro-optical
sensors for laboratory test images such as rectangles and periodic bar
patterns and for a limited number of real world objects. The models
developed are improved, and modified to bring them into closer agreement
with those models proposed by other investigators for the purpose of ob-
taining greater acceptance and making available a wider body of technical
literature. In the models developed, a signal-to-noise ratio is associated
with an image based on the image's irradiance and spatial dimensions.
Through psychophysical experimentation, the observer's thresholds for discri-
mination of these images are determined.

Methods of predicting the range capability of sensor-augmented
observers are developed and applied to both range-gated active and passive
low-light-level television systems. These models take into account proper-
ties of the scene, atmosphere and level of target discrimination. Also,
pure image motion effects, observer effects due to motion, and sensor effects
due to motion are analyzed. The general area of system specification is
discussed.

TABLE OF CONTENTS

LIST OF ILLUSTRATIONS

1.0 Introduction and Summary

The objectives of the Performance Synthesis Study for electro-optical sensors, performed under Contract Number F33615-70C-1461 are to determine the fundamental limitations of long range air-to-ground detection, recognition and identification of tactical military targets; to determine methods of realizing maximum range performance through optimum spatial, temporal and electrical filtering of the received image signals; and to devise methods of predicting maximum range performance taking into account the parameters of real targets, backgrounds, illumination sources, atmospherics and sensory systems. The results are to be applicable to all imaging sensors whether passive or active and are to include low light level television, forward looking infrared scanners and direct view light amplifiers.

The current effort is a continuation of the program previously reported in the technical report AFAL-TR-71-137 dated May 1971. The approach taken is to devise analytical models to describe sensory system operation including the observer as an integral part of the system. Psychophysical experiments were performed to obtain the necessary constants required to quantitatively evaluate the analytical models devised. It is felt that these studies have led to a better understanding of electro-optical sensors and their operation and will lead to improved sensors, improved methods of sensory system specifications and a reduction of costly laboratory and flight testing of systems.

In the previous program, the emphasis in the experimentation and analysis was placed on images of simple geometry such as squares and rectangles in order to focus on fundamentals, and to form firm analytical bases. However, preliminary efforts were made to analyze and obtain psychophysical constants for periodic test patterns, and to correlate the discernibility of the periodic test patterns with the recognizability of "real world" objects such as vehicles of different types. In the continuation effort reported here, the main emphasis has been on periodic test patterns and on the recognition and identification of the "real world" objects. However, studies were also initiated or extended into the areas of eye limitations to range performance and to sensor time constant effects. In the eye limitations area, we have investigated retinal fluctuation-generated noise problems, images of large angular extent, display viewing distance-to-height ratio and the effect of images in motion. In the sensor time constant area, image build-up and decay times and dynamic resolution effects were studied.

The detailed results of this Performance Synthesis Study are presented in Sections 2 through 6. In Section 2, we present a range analysis for both a passive and an active television system. A passive system views a scene which is illuminated, or irradiated, by natural sources of light such as the sun, moon, stars, sky glow, etc. An active system includes its own scene irradiator. In the active system case, we focused most attention on sources which are pulsed and used in conjunction with sensors which incorporate range gating. The purpose of the range gating is to reduce image contrast degrading atmospheric backscatter effects.

In the analytical models which we develop in Section 3, we
associate a signal-to-noise ratio or SNR with an image detail. This SNR
is a function of the image's size, irradiance level, contrast, location
relative to background clutter and the sensor parameters such as the
objective lens diameter, photosurface sensitivity, modulation transfer
characteristic and various signal and system generated noises. In partic-
ular, we wish to note the SNR's functional relationship to the size of an
image detail. In our analysis, we select the image detail size on the
basis of the level of object discrimination desired. For this report, we
use three levels of discrimination definitions; detection, recognition and
identification. It is quite clear that a higher res lving power is needed
to identify an object than to merely detect it. Many years ago, methods
for determining the resolution required for a given level of discrimination
were experimentally determined. Also, a parallel requirement for
"sufficient" SNR was imposed although the method of determining the SNR
required was not explicitly given. The parallel requirements of SNR and
resolution are avoided in our treatment because we define SNR as a function
of the image detail size. Image detail size is selected on the basis of
the level of discrimination. For detection, the selected image detail
size is large while for identification, it is small. The SNR required
for detection is, however, the same as for identification and thus it
follows that detection range will be longer than identification range.

The analytical model of Section 3 together with the psychophysical
experiment results of Section 4 are used in Section 2 to predict sensor
range capability. For the passive sensor, we discuss properties of the
scene irradiance and the effect of the atmosphere intervening between the

3

source and the observer. It is seen that the principal effect of the
atmosphere was to degrade the apparent image contrast. In this connection,
we note that the amount of contrast degradation depends not only upon
meteorological visibility but upon the object's background reflectivity,
the sky condition, source to object viewing angle and many other parameters
which are neglected by many systems' designers, more often than not.

Since the image contrast is range dependent, the sensor/observer
SNR equation, written as a function of range, is solved for image contrast.
When the SNR obtainable from the sensor/observer combination is set equal
to its threshold value, the image contrast becomes the minimum detectable
contrast. We then plot the sensor-augmented-observer's minimum detectable
contrast vs range and on the same coordinates, we plot the apparent
image contrast vs range. The intersection of the apparent image contrast
and minimum detectable image contrast gives threshold range.

The atmosphere can also reduce the apparent image contrast for
range gated active systems although contrast degradation is not the principal
effect for a well designed system as is discussed at length in Section 2.
Rather, the principal effect is the absorption of source radiation, both
on its way to the scene and on its way back to the sensor. For this reason
it is more convenient to plot scene irradiance as a function of range for
the source. The SNR equation for the sensor and observer is solved for
differential scene irradiance level as a function of range. Again, the
SNR is set equal to its threshold value and the differential scene
irradiance level becomes the minimum detectable scene irradiance. Finally,
the minimum detectable scene irradiance and scene irradiance curves are
plotted vs range using the same coordinates and once again, the intersections

4

of these two curves gives threshold range.

In the earlier Performance Synthesis Study Report, an analytical model for sensor prediction was developed and it was shown that good agreement between measured and predicted results was obtained. However, the model differs in certain respects from that developed by Schade. These differences are mainly conceptual and have only minor impact on sensor predictions. However, in order to obtain a closer agreement between investigators and to make available a wider body of literature and data couched in similar if not identical terminology, it was decided to adopt many of the features of Schade's analysis. Neither the previous model developed in the Performance Synthesis Study nor that of Schade can be considered to be completely verified but both are considered adequate for first order analysis.

The elementary model described in Section 3 is believed to be generally accepted by the majority of investigators in the field and has been experimentally verified. The elementary model, however, only applies to images which are undistorted by optical and sensor apertures, i.e., optical transfer functions or OTF. The effect of an OTF on image discernability can only be estimated in many cases. For isolated aperiodic images, the Schade theory holds that image detection is made more difficult by OTF's preceding a point of noise insertion but are made easier by OTF's following a point of noise insertion. With periodic patterns, an OTF severely reduces signal amplitude whether it precedes a point of noise insertion or not but an OTF has some noise filtering effect if it follows a point of noise insertion. The effects of OTF on an isolated object's detectability or its effects on noise filtering are subtle. Preliminary attempts to verify current theories have not yet borne fruit. The first

order effect of an OTF on periodic signals seems quite clear however.

In the current model, it is assumed that any noise at spatial frequencies below that of a periodic image's spatial frequency will adversely affect the periodic image's discernability while noise at higher spatial frequencies will not. However, there is considerable evidence suggesting that noise at or near the signal frequency is more serious than noise at other frequencies. This notion needs further verification.

In any event, the updated model is applied to the SEBIR and I-SEBIR camera tubes and its resolution vs input signal current and input irradiance characteristic is calculated. We have found these predictions to be quite accurate.

In Section 4, we report the results of an extensive series of psychophysical experimentation. Test images used included aperiodic, periodic and "real world" imagery. The aperiodic test images used were mainly images of large angular extent relative to the observer's eye. In the earlier study, we noted the eye's ability to integrate over very large angles; over 6° in one direction. However, the images used were long thin rectangles. In the literature, it has been observed that the eye is not effective in integrating over angular subtenses much larger than about $\frac{1}{3}^{\circ}$. This conclusion was determined mainly on the basis of square or round images. It was hypothesized that the eye is actually a differentiator and that it uses only the image's edges in the detection process. The very high detectability of the long thin rectangles is explained on the basis that they are nearly all edge. This is apparently the case as we show. Interpreted in this light, our results are computable with the results reported by other investigators.

Much of the psychophysical experimentation was devoted to the discernability of bar patterns. In the earlier study, we hypothesized that the eye uses only one bar in the pattern and that the discernability of the bar pattern is proportional to the area of the single bar. This appears to be the case. It was found that the threshold signal-to-noise ratio required to detect a bar pattern did decrease with increase in bar pattern spatial frequency when viewing distance was near optimum. This could be due to the eye's inability to effectively integrate along the length of a low frequency bar or to the notion that noise at the signal frequency is more important than noise far removed in spatial frequency as we noted above.

The influence of display viewing distance to display height was experimentally studied. As we expected, the observer should increase his viewing distance to see low frequency patterns and decrease his viewing distance to see high frequency patterns. The effects of image motion from a psychophysical viewpoint were deemed negligible for the magnitude of image motion normally expected. Image detectability limitations due to retinal fluctuation noise are a reality and can be the limiting noise under certain conditions. More effort in this area is needed to include this noise effect in the analytical model.

A considerable experimental effort was mounted in the object recognition and identification area. In the first series of experiments, four different vehicle types were randomly displayed at randomly selected signal-to-noise ratios. Data was taken in the form of the probability of correct recognition vs the signal-to-noise ratio. It was found that the SNR required to correctly recognize a vehicle on a 50% probability level

7

and computed on the basis of a strip equal to 1/8 the area of the vehicle was nearly identical to that required to discern an "equivalent bar pattern." The equivalent bar pattern was one with bars of length equal to the length of the object and width equal to the object's minimum dimension divided by 8. This equivalent bar pattern approach has a historical basis which was the reason for its selection.

The identification experiments were performed in a similar manner except that five vehicles, all of the same type (tanks in this case), were used. As expected, higher resolution is required to identify an object than to recognize it. Again, the "equivalent bar pattern" approach appears to have merit. For the identification case, the equivalent bar pattern is one which has bars of length equal to the length of the object and of width equal to the minimum object width divided by 13. Again, the signal-to-noise ratio needed to identify the object was about the same as that required to discern the equivalent bar pattern for a given level of probability.

The results obtained in comparing the discernability of the equivalent bar pattern and the recognition or identification of an object were almost too good to be true and indeed they probably are. The essential difference between a bar pattern and an object is that the bar pattern is periodic while the "real world" object is an assemblage of aperiodic objects. Thus, the effects of OTF will be different for the object and the bar pattern. This subject needs further work and will be studied in the continuation effort. In the interim, the equivalent bar pattern is considered to be a useful and viable concept and can be used. It is felt that range predictions using the equivalent bar pattern will tend to be

somewhat pessimistic but not greatly so.

In Section 5, we have made some initial efforts to determine the effect of image motion on overall system performance. We first studied the geometrical aspects of motion and showed that some scene motion will nearly always exist and that the magnitude of the motion is enough to cause sensor time constants to come into play. Next, considerable numbers of exploratory sensor experiments were performed by the Westinghouse Electronic Tube Division under the direction of Dr. A. Laponsky. These measurements included both readin and readout time constants and dynamic resolution measurements. Attempts were also made to measure the modulation transfer function or MTF using bar patterns in motion with the hope that these measurements would explain the very large sensitivity losses noted in making dynamic resolution measurements. However, the sensitivity losses noted were far larger than the MTF losses. Further studies are indicated and will be emphasized in the continuation effort. We consider motion effects to be a first order effect having major impact on sensory system performance. Though these effects are very significant, they are not now included in range prediction analysis.

In Section 6, we discuss the general area of system specification. By specification, we do not mean the physical details of the equivalent such as the finish of part, vulnerability to fungus or the like. Though these features are important to the final product utilization, the concern is with providing the procuring agency with some assurance that the equipment being proposed for a given mission will have some reasonable expectation of actually meeting the mission requirement. Toward this end, we discuss scene and sensor parameters. We highlight the areas where

9

parameters are misused or incorrectly defined or specified. Where a number of definitions are involved, we make recommendations for a selection.

While the various individual scene and sensor parameters are important, it is the overall performance of the ensemble that matters. Thus, we recommend that a system proposer be required to make range predictions to show that mission requirements will probably be met.

While manufacturers can be requested or even forced to supply data and calculations, the quantities supplied will be of little use unless some degree of standardization is imposed. It is also reasonably clear that standards and specifications are of little use unless they are generally accepted and there is little likelihood that this will happen unless most of the major military and industrial organizations take part in their generation. Thus, we recommend the establishment of such a committee.

2.0 The Range of An Electro-Optical Sensor

"On a clear day, one can see forever." While this popular
statement is undoubtedly optimistic, it is certainly true that one can see
the sun by clear day, and the stars by clear night, at considerable distance.
From a more practical viewpoint, the objects of our attention are more likely
to be more mundane terrestrial objects at modest range. These objects may
be seen with greater or lesser clarity depending on the acuity and sensi-
tivity of the observer and the range, size and incremental luminance of the
object. Sometimes it will not matter whether the object is seen at a given
level of discrimination or not, while at other times it may be vital. In
general, our concern in this report will tend to favor those conditions
under which the observer is highly motivated to observe scene objects
with some intended purpose in mind such as navigating in a boat or aircraft,
detecting a criminal act or differentiating between friend or foe. If we
suppose the observer has some purpose in searching for scene objects, it
follows that he must observe the object at sufficient range if the intended
purpose is to be served.

Thus, the range at which an object can be observed with sufficient
clarity to perform some useful task is of considerable interest. The words
"sufficient clarity" should be stressed. In one case, it may be sufficient
to merely detect a blob such as a channel buoy while in other cases, a much
higher level of object detail is needed. For example, it is of no use to
televise and record a burgulary if the recording's acuity is insufficient to
identify the burgular in a court of law. In the usual case, by range, we
imply the maximum range at which we can just barely resolve the object if it

11

is the mere presence of the object we are interested in. If the object such as the burgular, is to be identified, then we would be interested in the maximum range at which the subject's features can be barely discerned. In short, range implies a threshold but the threshold depends upon the level of object discrimination required. The various levels of discrimination are usually defined as detection, orientation, recognition and identification and are discussed in Section 3.3.

We proceed next to the discussion of the various factors which go into determining range. The primary interest herein is in the performance of a man augmented by an electro-optical sensor. The general procedure is to associate a signal-to-noise ratio with an image as it appears on the output of the sensor's display and then the signal-to-noise ratio required by the observer is determined through experimentation. By relating the signal-to-noise ratio required by the observer to that provided by the sensor, threshold range can be computed. In this analysis, the image signal-to-noise ratio is computed on the basis of an equivalent test object of simple geometry but with characteristics like the real object. The premise is that the detectability of a simple test object can be correlated with the detectability, recognizability or identifiability of the real object by suitably selecting the parameters of the test object.

2.1 Properties of the Scene

The scene to be viewed consists of a source or a number of sources of radiant energy, an atmosphere intervening between the source and an object, the object itself and its background, and the atmosphere intervening between the object and the observer or electro-optical sensor. The sources may be either natural such as the sun, moon and stars, or auxiliary such as a

12

searchlight. At times, the sources can be a combination of natural and auxiliary sources. However, for the sake of simplicity, we will consider sources to be either predominately one or the other and analyze the cases separately because a slightly different approach is indicated in each case.

2.2 Natural Sources of Scene Radiance - Passive* Sensors

A wide variety of "natural" sources can exist, including the sun, the stars, the moon and the skyglow. "Unnatural" sources such as city lights reflected off low clouds and even scene floodlighting when the floodlights are not at or near the sensor's location will nevertheless be considered as natural sources on the basis that the scene radiance passes only once through the atmosphere from the object to the sensor rather than twice as is the case for the auxiliary source. The two primary classes of natural sources are those which provide mainly diffuse scene irradiance and those which provide predominantly directional scene radiance. Clear night starlight and heavy overcast sunlight or moonlight represent diffuse sources while clear day sunlight and clear night moonlight would be examples of directional sources. There are obviously cases where both classes of source exist together and are of near equal importance such as in light overcast sun or moonlight or when the moon is new or when either the sun or moon are low on the horizon sky.

In diffuse light, the detectability of objects would be expected to be relatively independent of viewing angle since the lighting is nearly

---

* By passive it is meant those sensors which use natural scene irradiance rather than auxiliary sources of radiation.

13

uniform in all directions, and the objects are shadowless or nearly so. The average scene contrasts also would be expected to be lower than in the case where lighting is directional. With the directional lighting, one expects sharp contrast shadows but object features may become unrecognizable except at certain viewing and source angles. For example, a black and white bar pattern on a panel may be clearly discerned when the moon is behind the observer, but with the moon behind the panel, the panel appears black.

Naturally irradiated scenes can assume an infinite variety depending on the relative aspect angles between the scene object, observer and the source, or type of source and it becomes most difficult to divide the number of objects into a reasonable number of cases for analytical purposes. Hence, it is usual to assume that the source is primarily directional or primarily diffuse. If directional, it is assumed that an equivalent diffuse source can be defined.

The irradiance levels we expect to find, whether day or night, are ordinarily tabulated for typical scenes. Usually, the irradiance levels are measured with photometers which are compensated to have a spectral response similar to that of the unaided human eye. The resulting curves such as that shown in Fig. 1 may or may not be relevant to electro-optical sensors which can have an entirely different spectral bandpass.[1] This subject is discussed in some detail in Ref. (2) and (3). However, it is assumed that by some means, a natural source and scene object can be approximated by an apparent source and object of known geometry and radiance level. Usually, the apparent object and its background are assumed to be diffusely reflecting.
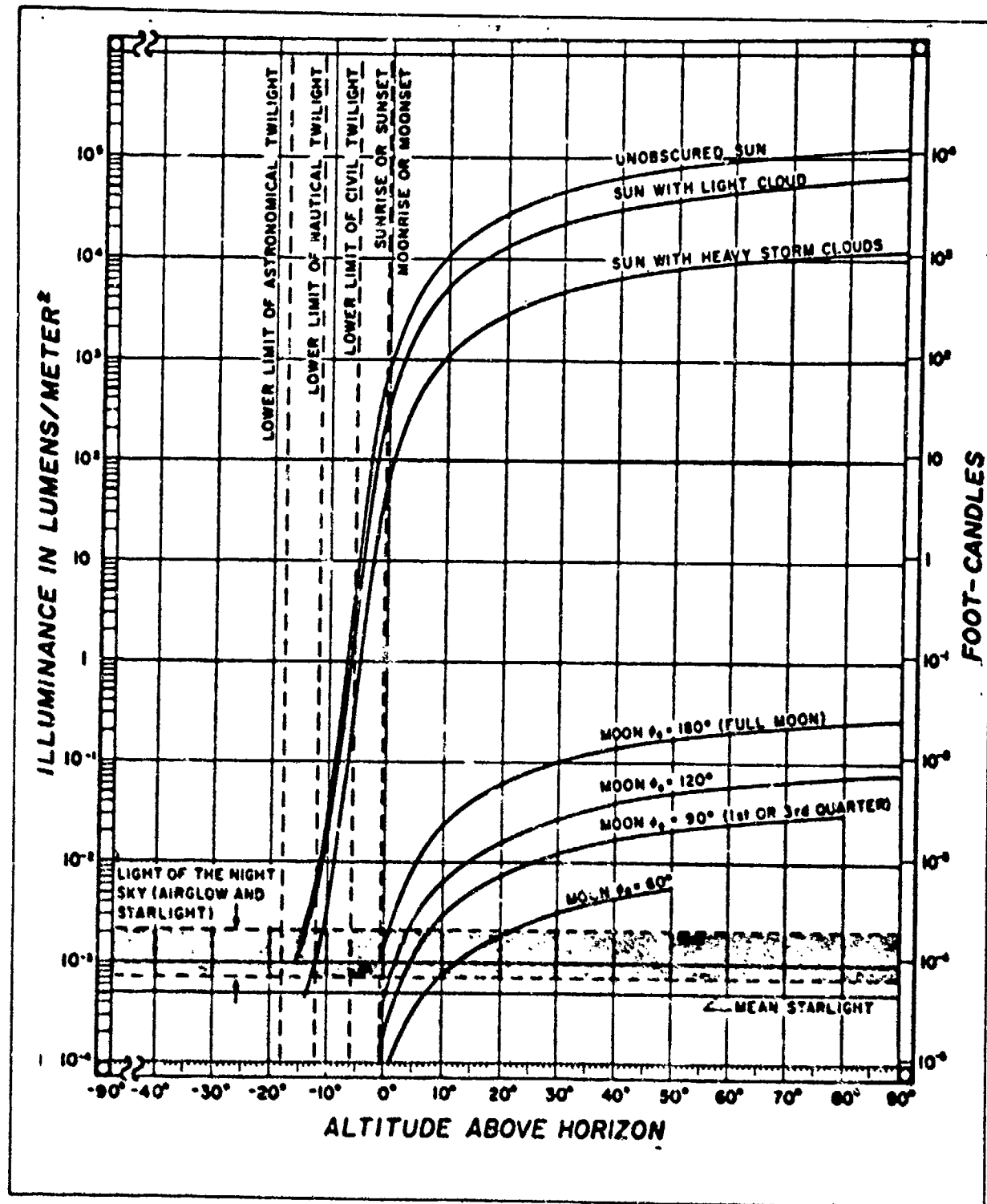
Fig. 1. Illuminance Levels on the Surface of the Earth due to the Sun, the Moon, and the Light of the Night Sky.

15

2.3 The Atmosphere, Source-to-Object and Object-to-Observer for Passive
Sensors

The atmosphere between the source and object, or surrounding the
object has three principal effects on passive imaging sensors. First, the
atmosphere may be, in effect, the natural source as is the case of the sun
just below the horizon. In this case, the light scattered by the atmosphere
is the principal source. Secondly, the scene irradiance is diminished due
to absorption and to scattering of the natural source radiation out of the
path between the source and object and finally, a portion of the sources
radiant energy may be scattered into the sensors line-of-sight. The levels
of natural scene irradiance are not ordinarily calculated except in special
instances but rather, are taken from tables and curves as we noted above.

The main effect of atmosphere scattering of radiation into the
line of sight is to decrease image contrast.

Many definitions of image contrast are in current use. Two
definitions that are commonly used in sensor analysis are, the isolated
image contrast, C_I, and the modulation contrast C_M. The isolated image
contrast, C_I, is defined as

$$C_I = \frac{N_{max} - N_{min}}{N_{max}} \qquad (1)$$

and the modulation contrast, C_M, is defined as

$$C_M = \frac{N_{max} - N_{min}}{N_{max} + N_{min}} \qquad (2)$$

where N_{max} and N_{min} are the radiances of the object and background with
N_{max} representing either the object or background depending upon which is
the brighter. With these definitions, contrast is always positive and can

16

range in value between 0 and 1 only. The isolated image contrast definition is preferred for small objects against an extensive uniform background while the modulation contrast is preferred for detailed objects against variegated backgrounds. In the special case where the objects are diffusely reflecting, the radiance N may be written as H/π where H is the scene irradiance and contrast becomes the incremental irradiance divided by the background irradiance or sum of object and background radiance as appropriate. The two definitions of contrast are actually equivalent* descriptions and are related by the equations

$$C_I = \frac{2\,C_M}{1 + C_M} \,, \tag{3}$$

and

$$C_M = \frac{C_I}{2 - C_I} \,. \tag{4}$$

These relations are plotted in Fig. 2.

In dealing with atmospheric effects on contrast, it is usual to define two contrasts; the "inherent" contrast and the "apparent" contrast. The "inherent" contrast is the contrast of the object at zero range along the line of sight from the observer's actual position at range, R, to the object. The apparent contrast is the actual contrast of the image at the observer's location. The most general law for atmospheric contrast

---

* For positive contrasts only.
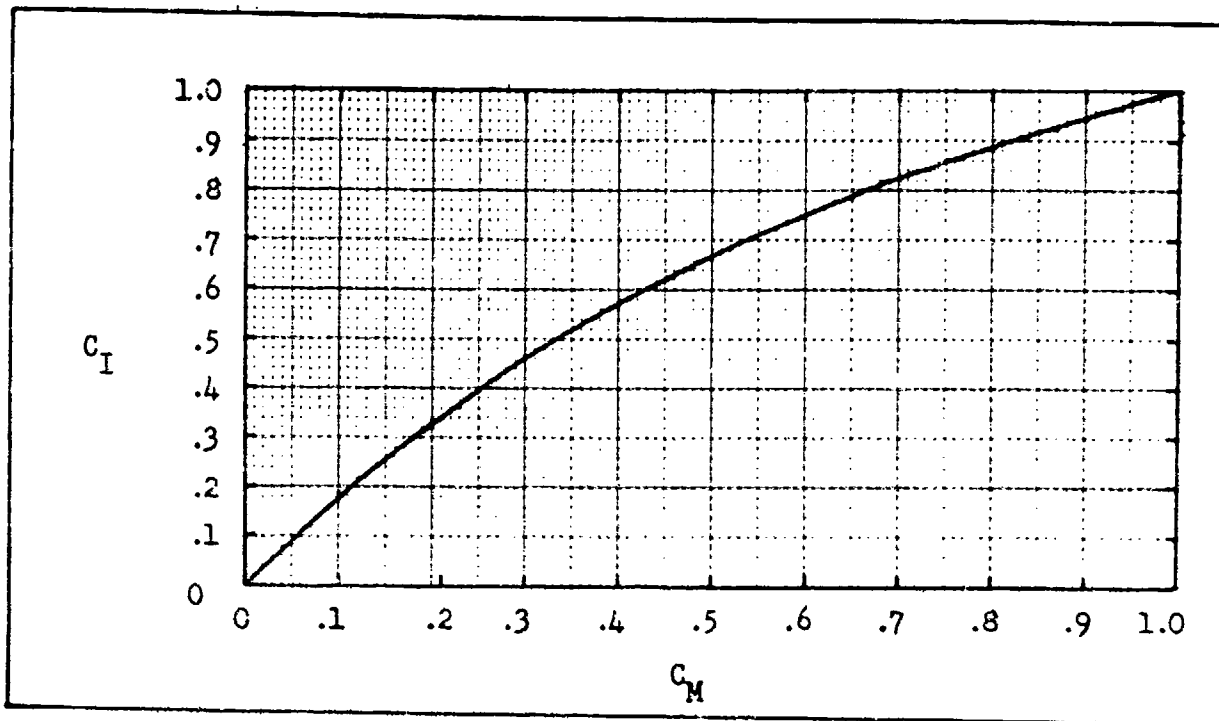
Fig. 2. Isolated Object Contrast, C_I, versus Object Modulation Contrast, C_M.

reduction is given by Middleton[4] as

$$C_{\bar{R}} = C_0 \left(\frac{N_{oo} - N_{bo}}{N_{oR} - N_{bR}} \right) e^{-\alpha_o \bar{R}} , \tag{5}$$

where N_{oo} and N_{bo} are the object and background radiance at zero range respectively and N_{oR} and N_{bR} are the corresponding quantities at range, R. Also, α_o is the value of the atmospheric attenuation, or extinction, coefficient at zero range and $\bar{R}$ is the "optical slant range" and represents the equivalent distance in a homogeneous atmosphere for which the attenuation is the same as that actually encountered along the true path of length R.

The optical slant range is obtained from an equation of the form

$$\bar{R} = \int f(r) dr . \tag{6}$$

Visibility n. miles	Extinction Coefficient n. miles^{-1}	ft^{-1}	Subjective Visibility
– 100	– 0.39	– 6.52×10^{-6}	Exceptionally Clear
– 38	– 0.12	– 1.58×10^{-6}	Very Clear
– 10	– 0.39	– 6.52×10^{-5}	Clear
– 5	– 0.78	– 1.3×10^{-4}	Light Haze
– 2	– 1.95	– 3.26×10^{-4}	Haze
– 1	– 3.9	– 6.52×10^{-4}	

Fig. 3. Atmospheric Extinction Coefficient as a Function of Meteorological and Subjective Visibility.

For an optical standard atmosphere, Middleton (after Duntley) gives

$$\bar{R} = \int_{R_1}^{R_2} e^{-r \sin \theta / 30,000} \, dr \ , \tag{7}$$

where $r \sin \theta$ is the altitude of either object or observer above sea level and θ is the angle between the observer and the horizontal. For the above formulation, a single vertical structure is assumed for the atmosphere which is usually not the case. An alternative approach is to use the actual slant path and correct the sea level extinction coefficient, α_a of Fig. 3 by means of the curves of Fig. 4 (Ref. 5).

The general law of contrast reduction has been specialized for

19
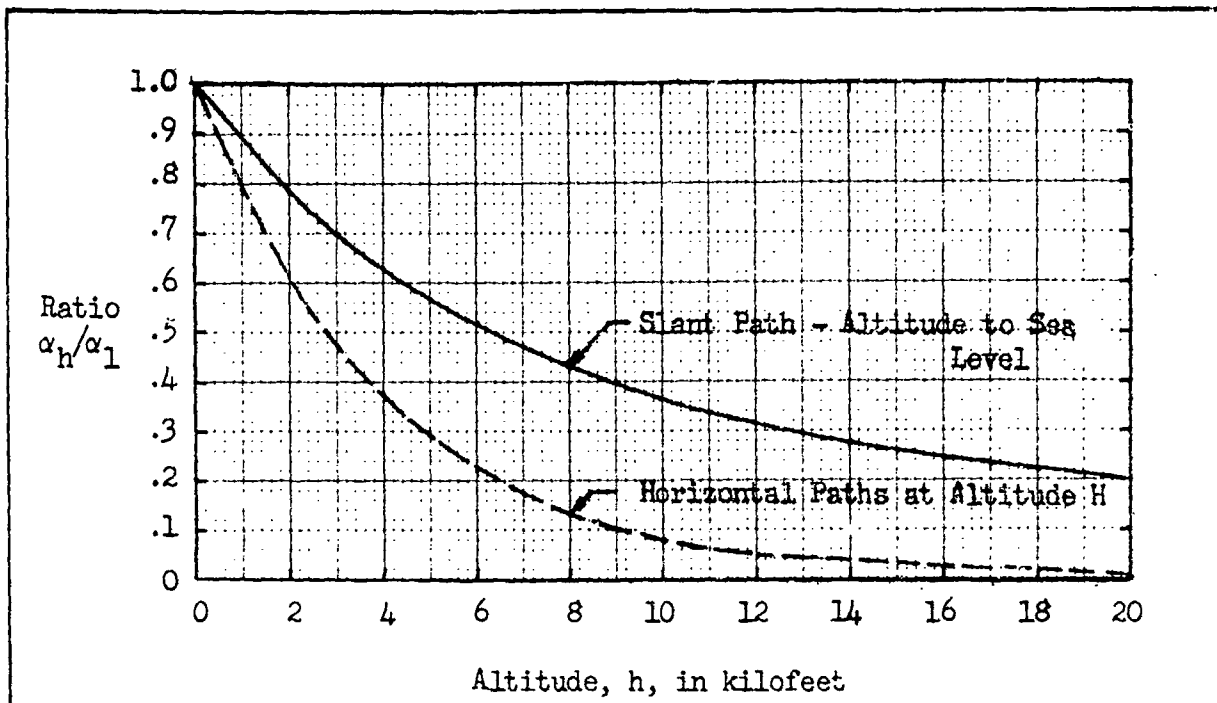
Fig. 4. Approximate ratio of the Atmospheric Extinction Coefficient, α_h, at Altitude h to its value, α_1, at Sea Level for Slant and Horizontal Paths neglecting Water Vapor and Carbon Dioxide Absorption.

three cases by Middleton as follows.

1. Horizontal Vision - When the observer is looking at an object imaged against a horizon sky background, the general case simplifies to

$$ C_R = C_0 e^{-\alpha_0 R} \quad , \tag{8} $$

which holds for objects of both positive and negative contrast. This equation is often erroneously used even when the object is not imaged against the horizon sky.

2. The Observer Looking Upward - For this case, Middleton gives

$$ C_R = C_0 e^{-\alpha_0 \bar{R}} \left[\frac{1 - \exp\left(-\alpha_0 \bar{R}_{R \to \infty}\right)}{1 - \exp\left(-\alpha_0 \bar{R}_{0 \to \infty}\right)} \right] , \tag{9} $$

20

Sky Condition	Ground Condition	S_k/G_d
Clear	Fresh snow	0.2
Clear	Desert	1.4
Clear	Forest	5
Overcast	Fresh Snow	1
Overcast	Desert	7
Overcast	Forest	25

Fig. 5.   Typical Values of the Sky to Ground Ratio in the Visible Spectrum.

where

$$\bar{R}_{R \to \infty} = \int_{R}^{\infty} f(r)dr \text{ and, } \bar{R}_{0 \to \infty} = \int_{0}^{\infty} f(r)dr. \tag{10}$$

3. Vision Downward - This is the most important case in aerial surveillance. For this case,

$$C_R = C_0 [1 - \frac{S_k}{G_d} (1 - e^{+\alpha_0 \bar{R}})]^{-1}, \tag{11}$$

where S_k/G_d is a quantity dubbed the "sky-to-ground ratio" and represents the sky-to-ground brightness ratio. Its value is estimated to be inversely proportional to the background reflectivity, ρ, i.e.,

21
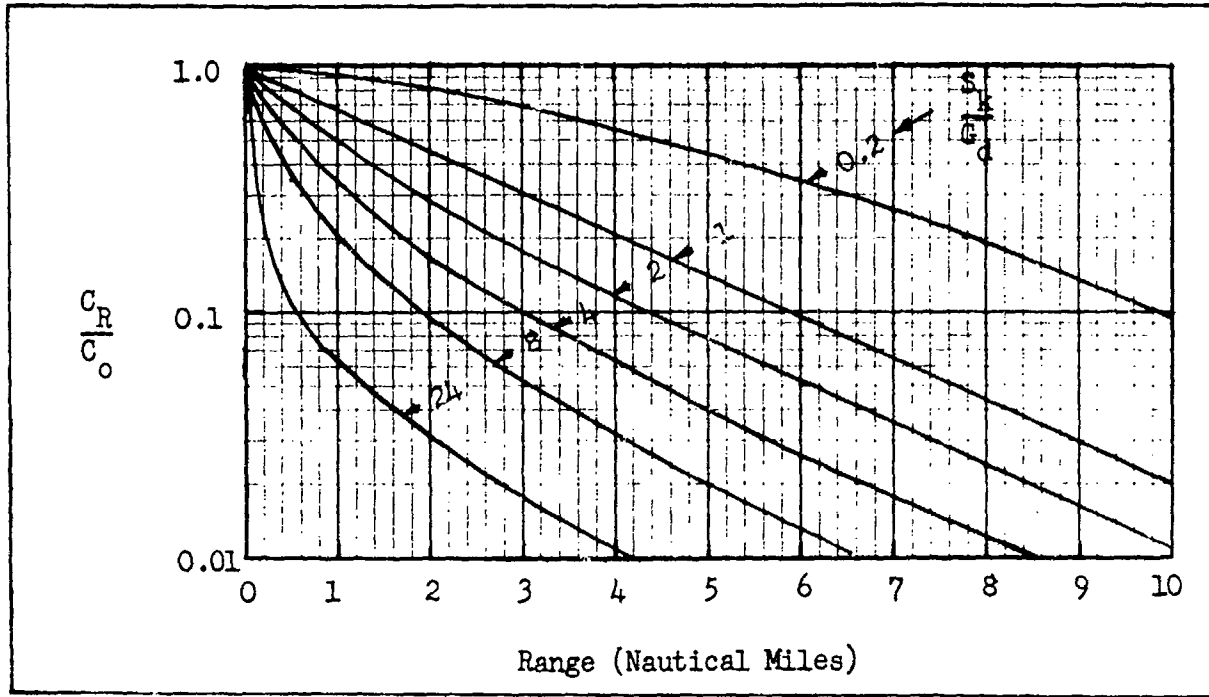
Fig. 6.   Ratio of Apparent to Inherent Contrast vs Range for Various Values
of Sky-to-Ground Ratio for a Meteorlogical Visibility of 10 Nautical Miles.

$$\frac{S_k}{G_d} = \frac{1}{\rho} \qquad \text{(overcast sky)} \ , \qquad\qquad (12)$$

$$= \frac{0.2}{\rho} \qquad \text{(clear sky)} \ . \qquad\qquad (13)$$

Typical values of S_k/G_d are given in Fig. 5 for the visible spectrum.
The Eq. (11) is plotted in Fig. 6 for a meteorological visibility of 10 n.
miles. Note that these curves apply to the visible spectrum. In the near
infrared, the reflectivity of forests is much higher than in the visible
and hence, the sky-to-ground ratio is correspondingly lower.

The main point of the above discussion is to note that the
reduction in contrast due to atmosphere is not always a simple exponential

22

as is commonly taken to be the case but instead varies with the sky condition, the background and the viewing direction.

2.4 Auxiliary or System Sources - Active Sensors

The auxiliary or system source may be a simple searchlight, or a complex light emitting diode array or laser. These sources may be used in conjunction with a simple passive sensor or with a range gated sensor. In either case, the system is considered to be an "active" system if an auxiliary source of scene irradiance is used and if the system source is near the observer.

The primary system source parameters are the average transmitted source power, P_s, and the solid angle Ω_s into which it radiates. Thus, the average source radiant intensity, J_s, is

$$J_s = \frac{P_s}{\Omega_s} . \tag{14}$$

The system source may be continuous wave, CW, as in the case of an ordinary searchlight, or pulsed wave (PW) as in the case of a pulsed laser. If pulsed, the pulse duration, T, will be a primary source parameter. Also, the pulsed source is monochromatic in which case J_s becomes $J_{s\lambda}$.

In the absence of atmosphere, the scene radiance normal to the line-of-sight is given for a diffuse reflector by

$$N_s = \frac{\rho \, P_s}{\pi \Omega R^2} . \tag{15}$$

23

where ρ is the scene reflectance, P_s is the source radiant power in Watts, and Ω is the solid angle into which the source radiates in steradians. In normalized form, this equation becomes

$$\frac{N_s}{\rho P_s} = \frac{1}{\pi \Omega R^2} \frac{\text{Watts/m}^2 \text{-sr}}{\text{Watt}} , \tag{16}$$

which is plotted in Fig. 7.

2.5 The Atmosphere, Source-to-Object and Object-to-Observer

The atmosphere intervening between the source and object has two principal effects on active imaging systems. First, the scene radiance is diminished due to scattering of source radiation out of the line-of-sight and secondly, a portion of the source radiation may be backscattered into the sensor's line-of-sight. The reduction of source radiant intensity by the atmosphere at range, R, compared to that in a vacuum is given by

$$\frac{J_s}{J_{sv}} = e^{-\alpha_o \overline{R}} , \tag{17}$$

where J_{sv} is the radiant intensity under vacuum condition. Then, the actual scene radiance becomes

$$N_s = \frac{\rho P_s \exp(-\alpha_o \overline{R})}{\pi \Omega R^2} . \tag{18}$$

However, the reflected scene radiance must travel through the atmosphere once more on its trip to the observer and thus, the apparent scene radiance becomes
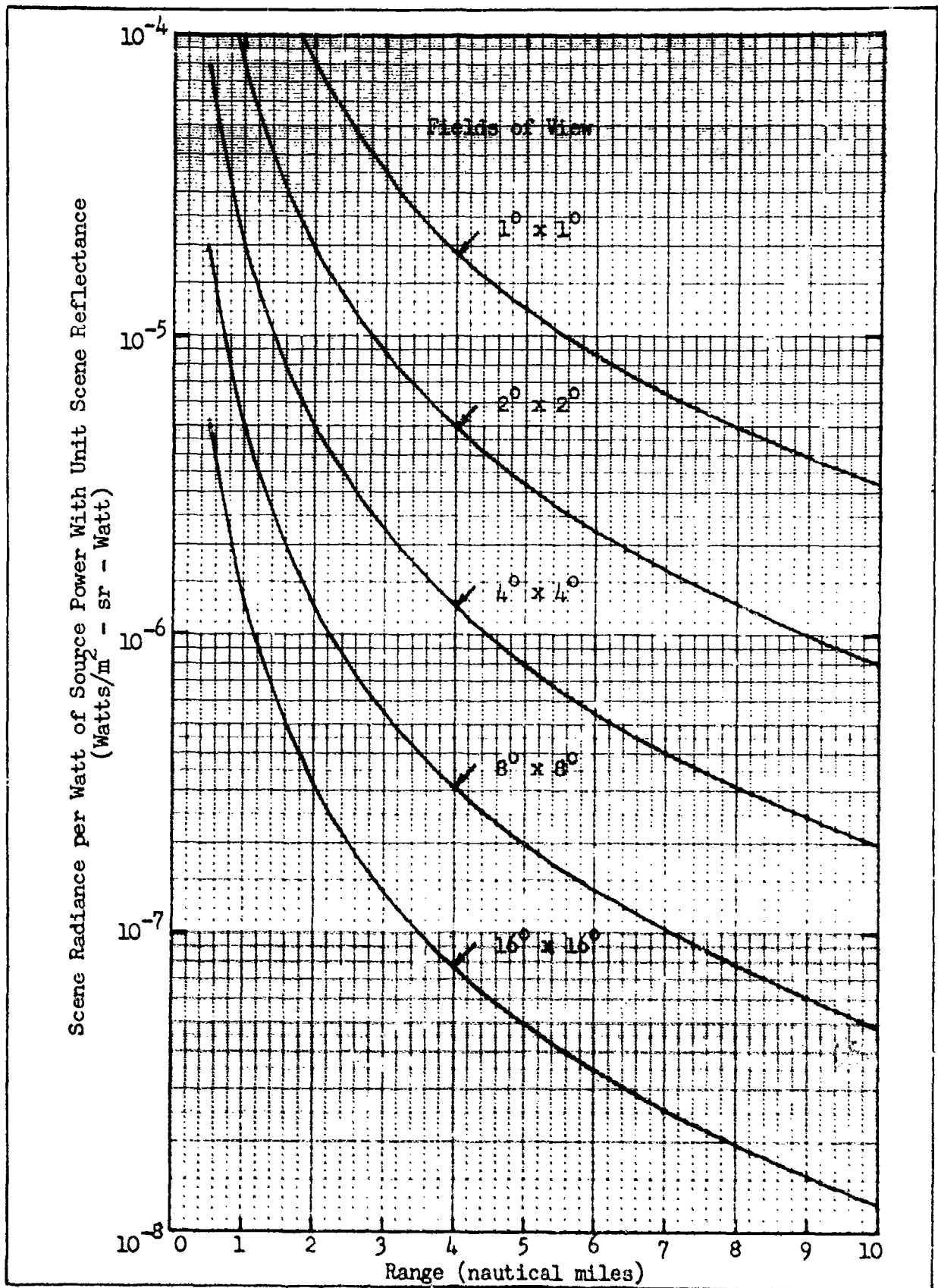
Fig. 7. Scene Radiance per Watt of Source Power vs Range for Scenes of Unit Reflectivity, Infinite Visibility and Various Optical Fields of View.

25
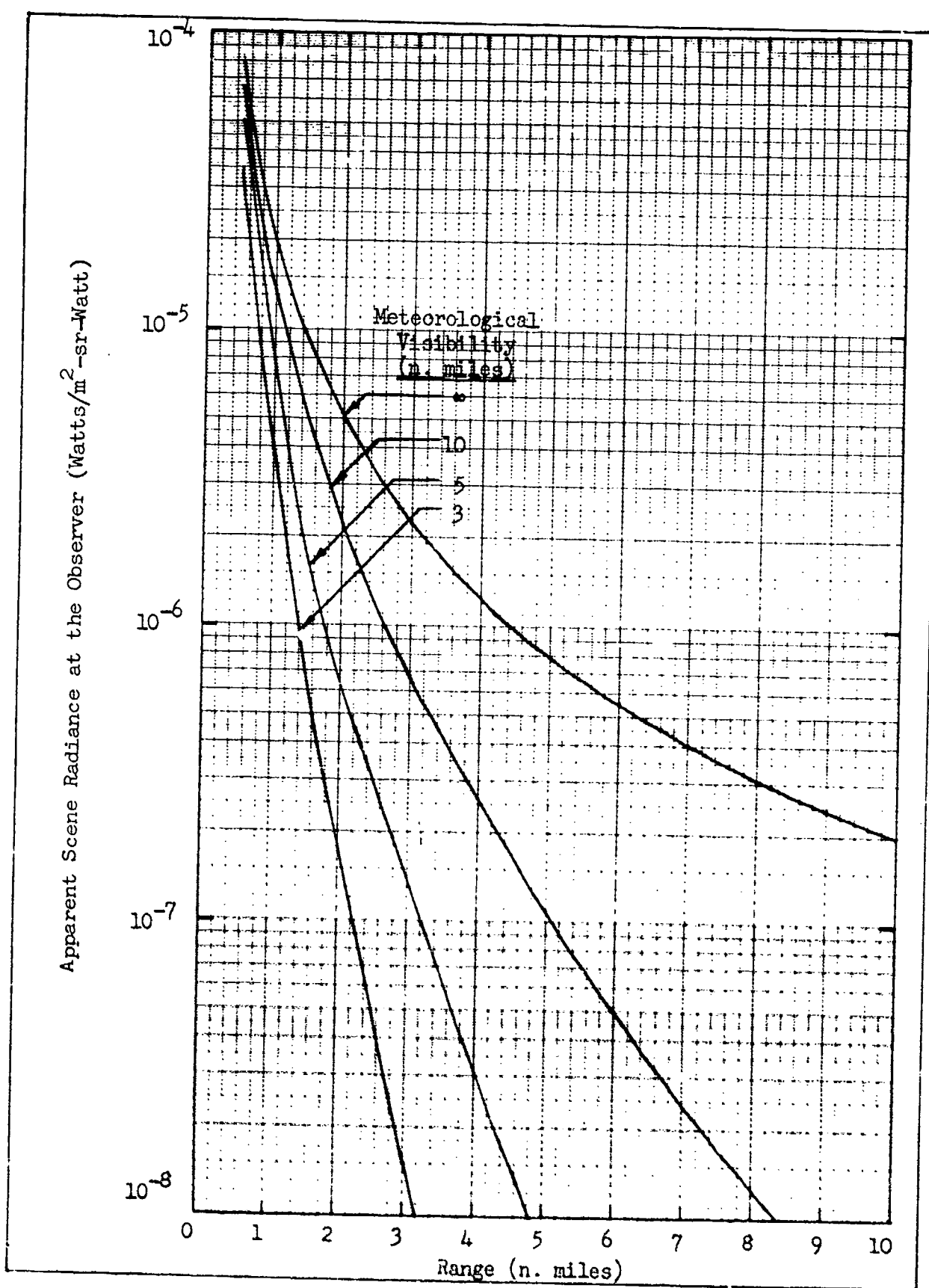
Fig. 8. Apparent Scene Radiance at Observer's Location per Watt of Source Power for Scenes of Unit Reflectivity. Field of View is 4° x 4° and the Radiation Wavelength is 0.86 micrometers.

26

Visibility n. miles	Extinction Coefficient		
	$\alpha \ (ft)^{-1}$	$\alpha \ (n. \ Miles)^{-1}$	$\alpha \ (meters)^{-1}$
1	4.72×10^{-4}	2.27	9.15×10^{-4}
2	2.18	1.33	6.65
3	1.37	0.832	4.18
4	9.82×10^{-5}	0.597	2.99
5	7.58	0.461	2.31
6	6.1	0.371	1.86
7	5.1	0.310	1.55
8	4.32	0.263	1.32
9	3.8	0.231	1.16
10	3.3	0.201	1.0
15	1.99	0.12	6.08×10^{-5}
20	1.39	0.0845	4.24

Fig. 9. Values of the Extinction Coefficient at 0.86 Micrometers vs Meteorological Visibility.

$$N_s \ = \ \frac{\rho \ P_s \ \exp \ (-2\alpha_0 \overline{R})}{\pi \Omega R^2} \quad , \tag{19}$$

which is plotted in normalized form, $(N_s/\rho \ P_s)$ in Fig. 8 for a $4^\circ \times 4^\circ$ field of view with λ = 0.86 micrometers and various sea level visibilities. The value of α_0 for the curves is obtained from the relation given by Steingold and Strauch[6] as

$$\alpha_0(\lambda) \ = \ \frac{3.91 \cdot 10^{-3}}{V} \ [\frac{0.55}{\lambda}]^{\ 0.585V^{\frac{1}{3}}} \quad , \tag{20}$$

where $\alpha_0(\lambda)$ is the attenuation per meter when V is the meteorological visibility in kilometers and λ is in micrometers. The Eq. (20) is tabulated in Fig. 9 for λ = 0.86 micrometers. As can be seen from Fig. 8, the atmosphere strongly influences the apparent scene radiance.

27
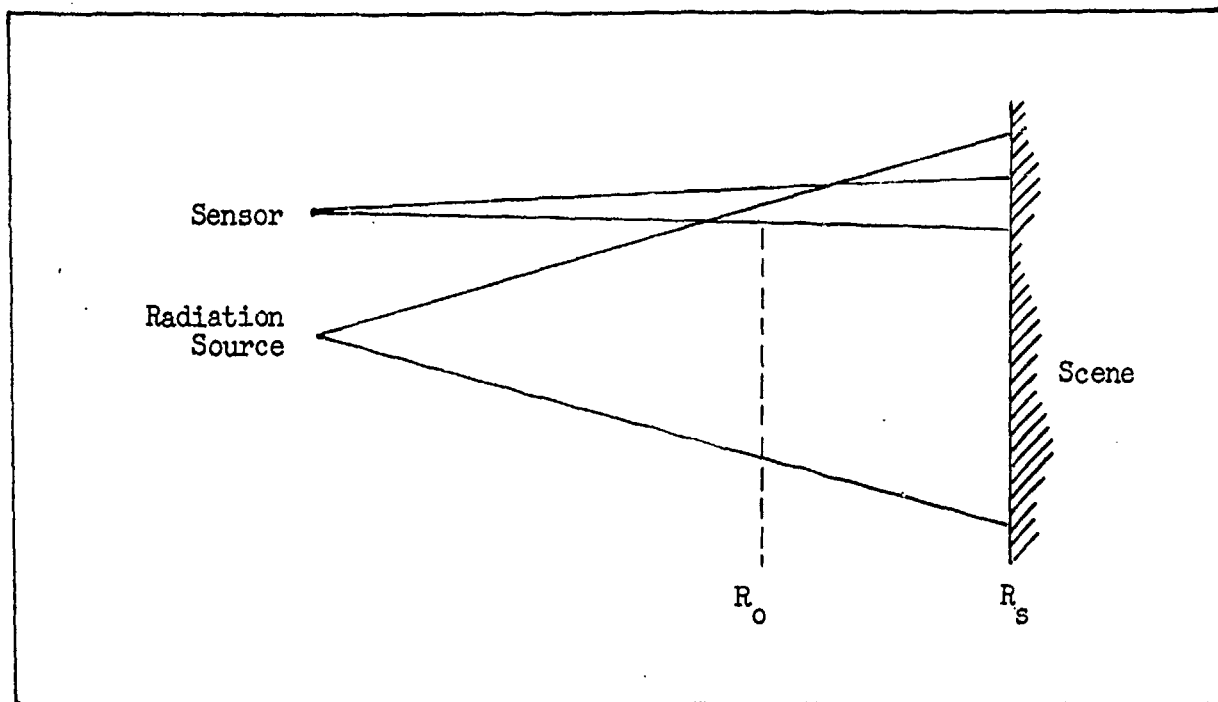
Fig. 10. Geometry for Backscatter Calculation - Sensor Not Range Gated.

The second major effect of atmosphere on an active system is to decrease image contrast as is discussed in some detail by Rampolla in Ref. (3). The contrast reduction in general terms is given by

$$\frac{C_R}{C_0} = [1 + \frac{F_b}{F_s}]^{-1} \quad , \tag{21}$$

where F_b is the total flux returned to the sensor by backscattering and F_s is the total signal flux.

For continuous wave, or CW, systems the ratio F_b/F_s is given by *

$$\frac{F_b}{F_s} = \frac{\alpha_a R_s^2 (\exp 2\alpha_a R)}{8 \rho} \int_{R_o}^{R_s} \frac{\exp (-2\alpha_a R) \, dR}{R^2} \quad , \tag{22}$$

---

* In this formulation, we use the extinction coefficient, α_a, which is corrected for slant path.
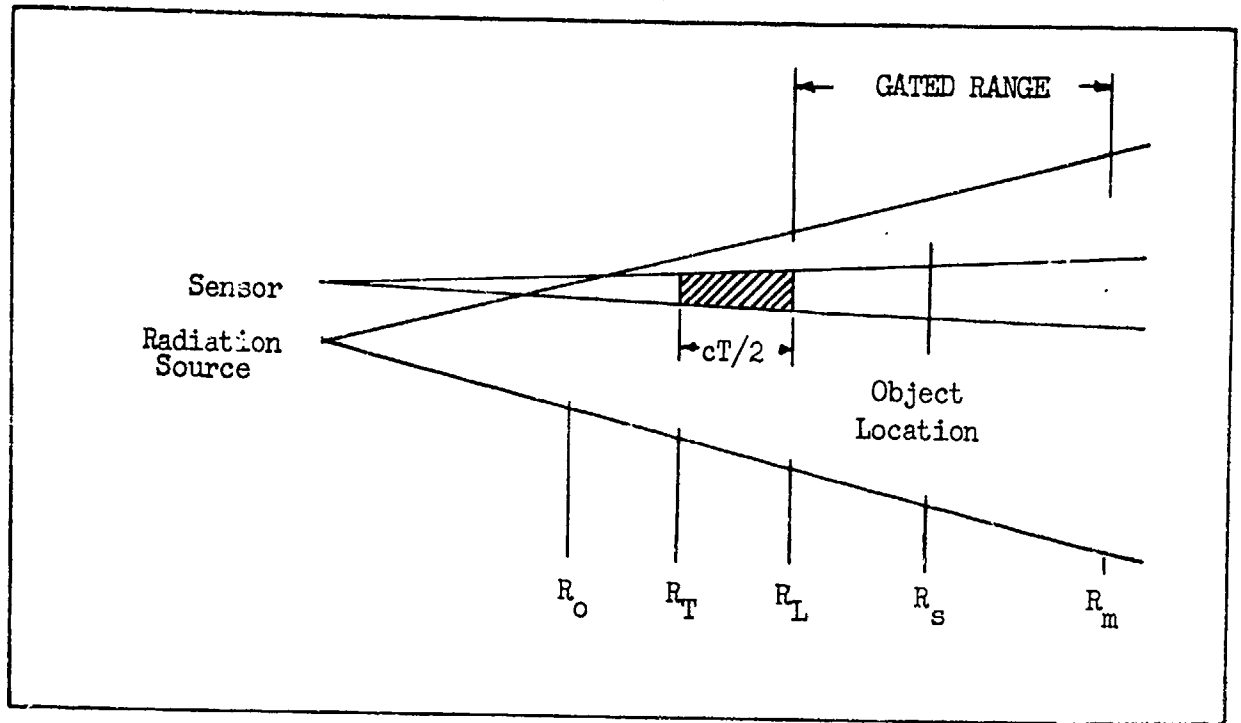
Fig. 11.   Geometry for Backscatter Calculation - Range Gated Sensor.

where the distance limits, R_o and R_s, are obtained from the geometry of Fig. 10. The above equation cannot be solved in closed form but can be evaluated using the series expansion (Dwight 568.2 and 568.1),

$$\frac{\exp(-2\alpha_a R)\ dR}{R^2} = \frac{-e^{-2\alpha_a R}}{R} - 2\alpha_a\ [\ln R - 2\alpha_a R + \frac{(2\alpha_a R)^2}{2\cdot2!}$$

$$+ \frac{(2\alpha_a R)^3}{3\cdot3!} ------ + \frac{(2\alpha_a R)^n}{n\cdot n!}\ ] \ . \qquad (23)$$

For the range gated active system, the contrast reduction by the atmosphere can be expected to be smaller, but the contrast reduction calculations will be found to be much more complex. Hence, a number of

29

simplifications are in order. The simplified geometry to be used is shown in Fig. 11. The duration of the radiation pulse is taken to be T seconds, and, the range increment corresponding to the pulse packet is $cT/2$ where c is the velocity of light (9.835×10^8 ft/sec). If the radiation pulse is initiated at time zero, and if the sensor is gated on at time t_1, the leading edge of the pulse can be located at range R_L and the trailing edge at range R_T. These ranges are

$$R_L = ct_1/2$$

$$R_T = c(t_1 - T)/2 . \tag{24}$$

The sensor is gated off at some time t_2 and there will be a range R_m corresponding to this time. A scene object to be detected must be located approximately between the range limits R_L and R_m. (At slightly longer or shorter ranges, the object may be detected because of the radiator's finite pulse duration but the effective object radiance is reduced because only a part of the returned pulse is sensed.)

The ratio of F_b/F_s is determined from the relation

$$\frac{F_b}{F_s} = \frac{\alpha_a\left[\int_{R_1}^{R_2} \frac{\exp(-2\alpha_a R)}{R^2} \left(\frac{R-R_T}{cT/2}\right)dR + \int_{R_2}^{R_s} \frac{\exp(-2\alpha_a R)}{R^2} dR\right]}{\alpha_o \exp(-2\alpha_a R_s)/R_s^2} , \tag{25}$$

where the limits are

$$R_1 = R_o \quad \text{if } R_o \geq R_T \text{ @ } t_1 ,$$

$$R_1 = R_T \quad \text{if } R_o < R_T \text{ @ } t_1 ,$$

$$R_2 = R_L \quad \text{if } R_s > R_L \text{ @ } t_1 ,$$

$$(26)$$

$$R_2 = R_s \quad \text{if } R_s \leq R_s \text{ @ } t_1 .$$

The first term in Eq. (26) which is designated $(F_b/F_s)_1$, is repeated below as

$$[\frac{F_b}{F_s}]_1 = \frac{\alpha_a \left[\int_{R_1}^{R_2} \frac{\exp(-2\alpha_a R)}{R^2} (\frac{R-R_T}{cT/2}) \, dR \right]}{\varepsilon_o \exp(-2\alpha_a R_s)/R_s^2} \qquad (27)$$

is the component of backscatter due to the range interval from R_T to R_L in Fig. 11. Suppose that the object is at distance R_L. Then, the second term in Eq. (25) is zero and only Eq. (27) applies. A typical result for this special case is calculated using Eq.'s (27 and 21) and is plotted in Fig. 12. For this calculation, the radiation wavelength was taken to be 0.86 microns and a visibility of 10 n. miles was assumed for the purpose of obtaining the atmospheric extinction coefficient. The scene reflectivity used was 0.2.

For comparison purposes, the contrast degradation due to atmosphere is shown for a passive system on the same figure. Observe

31
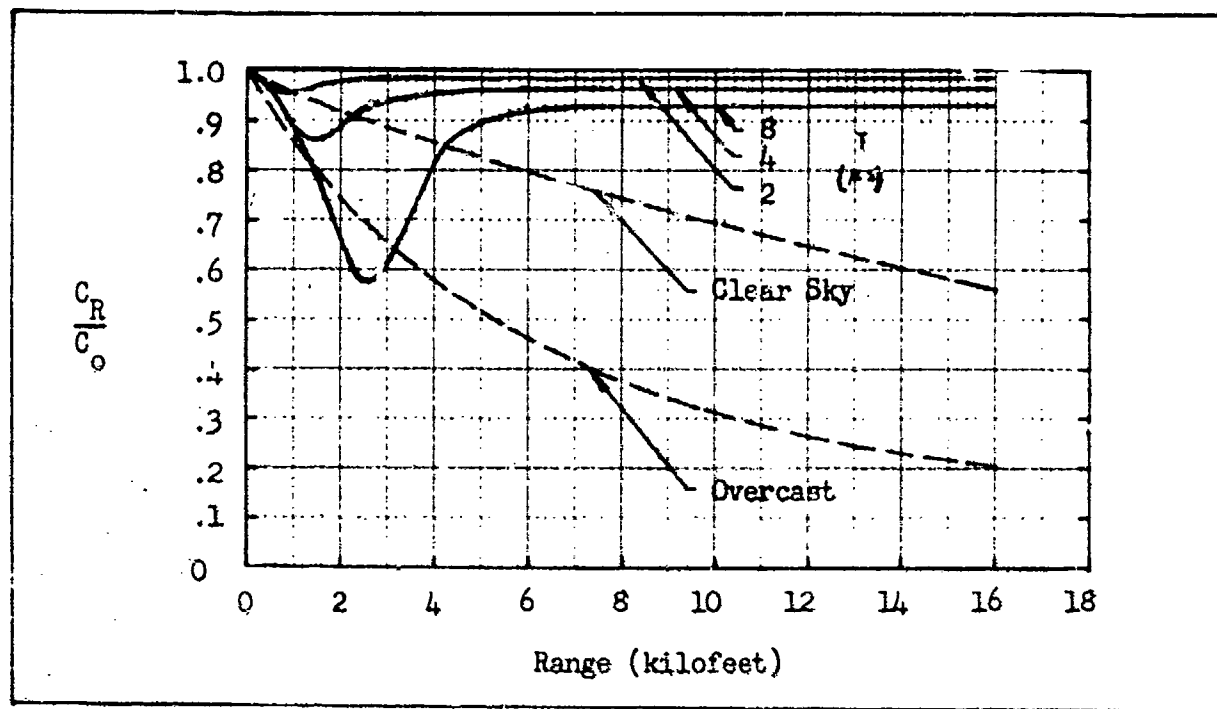
Fig. 12.   Ratio of Apparent-to-Inherent Contrast for (———) Range Gated Active and (- - -) Passive Sensors for Background Reflectivity of 20% and 10 Nautical Mile Visibility.

that at short ranges, that the active system is inferior to the passive system while the converse is true at long range. The inferior result at short range is due to the fact that very little of the atmosphere is range grted for close in targets and the backscatter from the radiation source is larger than from an atmosphere irradiated by a natural source such as the moon.

In the general case, the object will be at some range R_s greater than R_L. In this case, we will prefer to determine the ratio F_b/F_s in the form

$$\frac{F_b}{F_s} = \frac{K}{r}\left[[F_b{}' (T, R_L)]_1 + [F_b{}' (R_s)]_2 - [F_b{}' (R_L)]_2 \right], \quad (28)$$

where

$$K = \frac{.R_s^2}{8 \exp(-2\alpha_a R_s)} \quad , \tag{29}$$

and

$$[F_b'(T, R_L)]_1 = \alpha_a \int_{R_L-cT/2}^{R_L} \frac{\exp(-2\alpha_a R)}{R^2} \frac{[R-(R_L-cT/2)]\, dR}{cT/2} \quad , \tag{30}$$

and

$$[F_b'(R_s)]_2 = \alpha_a \int_{R_k}^{R_s} \frac{\exp(-2\alpha_a R)\, dR}{R^2} \quad , \tag{31}$$

and

$$[F_b'(R_L)]_2 = \alpha_a \int_{R_k}^{R_L} \frac{\exp(-2\alpha_a R)\, dR}{R^2} \quad . \tag{32}$$

The function $[F_b'(T, R_L)]_2$ is computer calculated and tabulated for various visibilities and two pulse durations in Fig. 13. The functions $[F_b'(R_s)]_2$ and $[F_b'(R_L)]_2$ are actually the same function evaluated between the same lower limit but different upper limits. Thus,

$$[F_b'(R_s)]_2 - [F_b'(R_L)]_2 = \alpha_a \int_{R_L}^{R_s} \frac{\exp(-2\alpha_a R)\, dR}{R^2} \quad , \tag{33}$$

which is the desired result. The function $[F_b'(R)]_2$ and K are tabulated in Fig. 14.

33

Fig. 13(a) Tabulation of $[F_b' (T, R_L)]_1$ for T = 2 microseconds and Various Meteorological Visibilities.

Visibility = 3 n. m. T = 2 μs

$R_L=$	$F_b=$
2000.	1.72621E-8
2500	8.59359E-9
3000	4.86324E-9
3500	2.97855E-9
4000	1.92564E-9
4500	1.29510E-9
5000	8.97720E-10
5500	6.37277E-10
6000	4.61216E-10
6500	3.39172E-10
7000	2.52798E-10
7500	1.90593E-10
8000	1.45123E-10
8500	1.11460E-10
9000	8.62577E-11
9500	6.72052E-11
10000	5.26768E-11
10500	4.15129E-11
11000	3.28750E-11
11500	2.61501E-11
12000	2.08850E-11
12500	1.67419E-11
13000	1.34663E-11
13500	1.08656E-11
14000	8.79268E-12
14500	7.13439E-12
15000	5.80336E-12
15500	4.73169E-12
16000	3.86635E-12
16500	3.16574E-12
17000	2.59706E-12
17500	2.13440E-12
18000	1.75714E-12

Visibility = 5 n. m. T = 2 μs

$R_L=$	$F_b=$
2000.	1.15849E-8
2500	6.14720E-9
3000	3.70390E-9
3500	2.41404E-9
4000	1.66034E-9
4500	1.18776E-9
5000	8.75624E-10
5500	6.61033E-10
6000	5.08735E-10
6500	3.97814E-10
7000	3.15276E-10
7500	2.52738E-10
8000	2.04616E-10
8500	1.67090E-10
9000	1.37485E-10
9500	1.13888E-10
10000	9.49099E-11
10500	7.95218E-11
11000	6.69542E-11
11500	5.66227E-11
12000	4.80790E-11
12500	4.09756E-11
13000	3.50404E-11
13500	3.00589E-11
14000	2.58605E-11
14500	2.23063E-11
15000	1.92923E-11
15500	1.67230E-11
16000	1.45275E-11
16500	1.26461E-11
17000	1.10294E-11
17500	9.63687E-12
18000	8.43446E-12
18500	7.39394E-12
19000	6.49164E-12
19500	5.70766E-12
20000	5.02520E-12
20500	4.43009E-12
21000	3.91026E-12
21500	3.45548E-12
22000	3.05701E-12
22500	2.70738E-12
23000	2.40018E-12
23500	2.12991E-12
24000	1.89184E-12
24500	1.68189E-12
25000	1.49651E-12
25500	1.33267E-12
26000	1.18770E-12
26500	1.05931E-12
27000	9.45485E-13
27500	8.44486E-13
28000	7.54789E-13
28500	6.75060E-13
29000	6.04134E-13
29500	5.40989E-13
30000	4.84730E-13

Visibility = 10 n. m. T = 2 μs

$R_L=$	$F_b=$
2000.	5.77697E-9
2500	3.20466E-9
3000	2.01746E-9
3500	1.37332E-9
4000	9.86329E-10
4500	7.37712E-10
5000	5.67015E-10
5500	4.46873E-10
6000	3.59020E-10
6500	2.93062E-10
7000	2.42446E-10
7500	2.02675E-10
8000	1.71446E-10
8500	1.46137E-10
9000	1.25512E-10
9500	1.08524E-10
10000	9.43993E-11
10500	8.25570E-11
11000	7.25526E-11
11500	6.40431E-11
12000	5.67599E-11
12500	5.04911E-11
13000	4.50672E-11
13500	4.03521E-11
14000	3.62350E-11
14500	3.26256E-11
15000	2.94492E-11
15500	2.66441E-11
16000	2.41588E-11
16500	2.19501E-11
17000	1.99816E-11
17500	1.82225E-11
18000	1.66465E-11
18500	1.52313E-11
19000	1.39576E-11
19500	1.28088E-11
20000	1.17705E-11
20500	1.08305E-11
21000	9.97780E-12
21500	9.20302E-12
22000	8.49790E-12
22500	7.85517E-12
23000	7.26846E-12
23500	6.73213E-12
24000	6.24119E-12

Vis. = 10 n. m. (cont.) T = 2 μs				
24500	5.79123E-12	47500	3.33100E-13	
25000	5.37832E-12	48000	3.15560E-13	
25500	4.99895E-12	48500	2.99011E-13	
26000	4.65002E-12	49000	2.83390E-13	
26500	4.32873E-12	49500	2.68642E-13	
27000	4.03259E-12	50000	2.54714E-13	
27500	3.75935E-12	50500	2.41557E-13	
28000	3.50701E-12	51000	2.29125E-13	
28500	3.27374E-12	51500	2.17376E-13	
29000	3.05791E-12	52000	2.06268E-13	
29500	2.85806E-12	52500	1.95765E-13	
30000	2.67284E-12	53000	1.85830E-13	
30500	2.50104E-12	53500	1.76432E-13	
31000	2.34157E-12	54000	1.67538E-13	
31500	2.19344E-12	54500	1.59121E-13	
32000	2.05574E-12	55000	1.51152E-13	
32500	1.92764E-12	55500	1.43606E-13	
33000	1.80840E-12	56000	1.36460E-13	
33500	1.69733E-12	56500	1.29690E-13	
34000	1.59381E-12	57000	1.23275E-13	
34500	1.49726E-12	57500	1.17196E-13	
35000	1.40716E-12	58000	1.11434E-13	
35500	1.32304E-12	58500	1.05971E-13	
36000	1.24445E-12	59000	1.00790E-13	
36500	1.17098E-12	59500	9.58773E-14	
37000	1.10228E-12	60000	9.12167E-14	

Vis. = 10 n. m. (cont.)		Visibility = 20 n. m. T = 2 μs		
		RL=	FB=	
37500	1.03799E-12	2000	2.58514E-9	11500	4.13113E-11
38000	9.77808E-13	2500	1.46311E-9	12000	3.73200E-11
38500	9.21439E-13	3000	9.39272E-10	12500	3.38389E-11
39000	8.68617E-13	3500	6.51907E-10	13000	3.07867E-11
39500	8.19097E-13	4000	4.77334E-10	13500	2.80976E-11
40000	7.72652E-13	4500	3.63464E-10	14000	2.57177E-11
40500	7.29073E-13	5000	2.85172E-10	14500	2.36027E-11
41000	6.88165E-13	5500	2.29104E-10	15000	2.17158E-11
41500	6.49749E-13	6000	1.87628E-10	15500	2.00264E-11
42000	6.13658E-13	6500	1.56122E-10	16000	1.85087E-11
42500	5.79739E-13	7000	1.31655E-10	16500	1.71410E-11
43000	5.47849E-13	7500	1.12297E-10	17000	1.59048E-11
43500	5.17855E-13	8000	9.67338E-11	17500	1.47845E-11
44000	4.89635E-13	8500	8.40473E-11	18000	1.37664E-11
44500	4.63074E-13	9000	7.35793E-11	18500	1.28390E-11
45000	4.38067E-13	9500	6.48490E-11	19000	1.19923E-11
45500	4.14514E-13	10000	5.74981E-11	19500	1.12175E-11
46000	3.92323E-13	10500	5.12559E-11	20000	1.05071E-11
46500	3.71409E-13	11000	4.59142E-11	20500	9.85446E-12
47000	3.51693E-13			21000	9.25373E-12
				21500	8.69981E-12
				22000	8.18819E-12
				22500	7.71488E-12
				23000	7.27633E-12
				23500	6.86941E-12
				24000	6.49129E-12
				24500	6.13948E-12
				25000	5.81170E-12
				25500	5.50595E-12
				26000	5.22042E-12
				26500	4.95345E-12
				27000	4.70356E-12
				27500	4.46943E-12
				28000	4.24984E-12
				28500	4.04367E-12
				29000	3.84993E-12
				29500	3.66771E-12
				30000	3.49617E-12
				30500	3.33455E-12
				31000	3.18215E-12
				31500	3.03832E-12
				32000	2.90250E-12
				32500	2.77413E-12
				33000	2.65271E-12
				33500	2.53781E-12
				34000	2.42898E-12
				34500	2.32585E-12
				35000	2.22805E-12

35

Vis. = 20 n. m. (cont.) T = 2 μs					
35500	2.13525E-12	58500	4.11769E-13	82500	1.05888E-13
36000	2.04714E-12	59000	3.99192E-13	83000	1.03167E-13
36500	1.96344E-12	59500	3.87056E-13	83500	1.00523E-13
37000	1.88389E-12	60000	3.75343E-13	84000	9.79541E-14
37500	1.80823E-12	60500	3.64035E-13	84500	9.54576E-14
38000	1.73623E-12	61000	3.53116E-13	85000	9.30313E-14
38500	1.66769E-12	61500	3.42572E-13	85500	9.06730E-14
39000	1.60241E-12	62000	3.32386E-13	86000	8.83806E-14
39500	1.54020E-12	62500	3.22546E-13	86500	8.61520E-14
40000	1.48088E-12	63000	3.13038E-13	87000	8.39853E-14
40500	1.42431E-12	63500	3.03849E-13	87500	8.18785E-14
41000	1.37032E-12	64000	2.94967E-13	88000	7.98298E-14
41500	1.31877E-12	64500	2.86379E-13	88500	7.78374E-14
42000	1.26954E-12	65000	2.78075E-13	89000	7.58996E-14
42500	1.22250E-12	65500	2.70045E-13	89500	7.40148E-14
43000	1.17753E-12	66000	2.62277E-13	90000	7.21813E-14
43500	1.13453E-12	66500	2.54762E-13	90500	7.03977E-14
44000	1.09339E-12	67000	2.47491E-13	91000	6.86623E-14
44500	1.05402E-12	67500	2.40454E-13	91500	6.69738E-14
45000	1.01633E-12	68000	2.33643E-13	92000	6.53307E-14
45500	9.80227E-13	68500	2.27050E-13	92500	6.37317E-14
46000	9.45643E-13	69000	2.20667E-13	93000	6.21756E-14
46500	9.12497E-13	69500	2.14486E-13	93500	6.06609E-14
47000	8.80720E-13	70000	2.08500E-13	94000	5.91866E-14
47500	8.50245E-13	70500	2.02702E-13	94500	5.77514E-14
48000	8.21009E-13	71000	1.97085E-13	95000	5.63541E-14
48500	7.92953E-13	71500	1.91643E-13	95500	5.49938E-14
49000	7.66020E-13	72000	1.86369E-13	96000	5.36692E-14
49500	7.40159E-13	72500	1.81259E-13	96500	5.23794E-14
50000	7.15316E-13	73000	1.76305E-13	97000	5.11234E-14
50500	6.91452E-13	73500	1.71503E-13	97500	4.99002E-14
51000	6.68514E-13	74000	1.66848E-13	98000	4.87088E-14
51500	6.46464E-13	74500	1.62333E-13	98500	4.75463E-14
52000	6.25260E-13	75000	1.57956E-13	99000	4.64179E-14
52500	6.04865E-13	75500	1.53710E-13	99500	4.53167E-14
53000	5.85243E-13	76000	1.49591E-13	100000	4.42439E-14
53500	5.66359E-13	76500	1.45596E-13	100500	4.31986E-14
54000	5.48182E-13	77000	1.41719E-13	101000	4.21802E-14
54500	5.30680E-13	77500	1.37957E-13	101500	4.11878E-14
55000	5.13825E-13	78000	1.34307E-13	102000	4.02207E-14
55500	4.97588E-13	78500	1.30764E-13	102500	3.92782E-14
56000	4.81943E-13	79000	1.27325E-13	103000	3.83596E-14
56500	4.66864E-13	79500	1.23986E-13	103500	3.74643E-14
57000	4.52332E-13	80000	1.20745E-13	104000	3.65916E-14
57500	4.38319E-13	80500	1.17597E-13	104500	3.57409E-14
58000	4.24805E-13	81000	1.14541E-13	105000	3.49116E-14
		81500	1.11572E-13	105500	3.41031E-14
		82000	1.08689E-13	106000	3.33148E-14

36

Fig. 13(b) Tabulation of $[F_b'(T, R_L)]_1$ for $T = 4$ microseconds and Various Meteorological Visibilities.

Visibility = 3 n. m.
$T = 4\ \mu s$

RL=	FB=
4000.	5.60843E-9
4500	3.60586E-9
5000	2.41945E-9
5500	1.67573E-9
6000	1.18956E-9
6500	8.61274E-10
7000	6.33763E-10
7500	4.72711E-10
8000	3.56666E-10
8500	2.71787E-10
9000	2.08901E-10
9500	1.61785E-10
10000	1.26139E-10
10500	9.89367E-11
11000	7.80183E-11
11500	6.18217E-11
12000	4.92034E-11
12500	3.93179E-11
13000	3.15340E-11
13500	2.53766E-11
14000	2.04851E-11
14500	1.65841E-11
15000	1.34618E-11
15500	1.09545E-11
16000	8.93491E-12
16500	7.30343E-12
17000	5.98198E-12
17500	4.90896E-12
18000	4.03565E-12

Visibility = 5 n. m.
$T = 4\ \mu s$

RL=	FB=
4000.	4.54841E-9
4500	3.11834E-9
5000	2.22933E-9
5500	1.64430E-9
6000	1.24259E-9
6500	9.57493E-10
7000	7.49710E-10
7500	5.94939E-10
8000	4.77529E-10
8500	3.87072E-10
9000	3.16442E-10
9500	2.60651E-10

RL	FB
10000	2.16130E-10
10500	1.80281E-10
11000	1.51183E-10
11500	1.27393E-10
12000	1.07818E-10
12500	9.16146E-11
13000	7.81311E-11
13500	6.68561E-11
14000	5.73855E-11
14500	4.93976E-11
15000	4.26348E-11
15500	3.68889E-11
16000	3.19911E-11
16500	2.78035E-11
17000	2.42129E-11
17500	2.11260E-11
18000	1.84657E-11
18500	1.61675E-11
19000	1.41779E-11
19500	1.24518E-11
20000	1.09514E-11
20500	9.64489E-12
21000	8.50511E-12
21500	7.50917E-12
22000	6.63757E-12
22500	5.87363E-12
23000	5.20312E-12
23500	4.61380E-12
24000	4.09519E-12
24500	3.63823E-12
25000	3.23513E-12
25500	2.87913E-12
26000	2.56440E-12
26500	2.28587E-12
27000	2.03912E-12
27500	1.82033E-12
28000	1.62615E-12
28500	1.45366E-12
29000	1.30032E-12
29500	1.16387E-12
30000	1.04237E-12

Visibility = 10 n. m.
$T = 4\ \mu s$

RL=	FB=
4000.	2.59338E-9
4500	1.85961E-9
5000	1.38971E-9
5500	1.07109E-9

RL	FB
6000	8.45597E-10
6500	6.80588E-10
7000	5.56544E-10
7500	4.61204E-10
8000	3.86547E-10
8500	3.27152E-10
9000	2.79245E-10
9500	2.40142E-10
10000	2.07886E-10
10500	1.81030E-10
11000	1.58483E-10
11500	1.39411E-10
12000	1.23169E-10
12500	1.09253E-10
13000	9.72621E-11
13500	8.68772E-11
14000	7.78409E-11
14500	6.99438E-11
15000	6.30145E-11
15500	5.69118E-11
16000	5.15185E-11
16500	4.67367E-11
17000	4.24843E-11
17500	3.86919E-11
18000	3.53009E-11
18500	3.22612E-11
19000	2.95300E-11
19500	2.70706E-11
20000	2.48514E-11
20500	2.28448E-11
21000	2.10271E-11
21500	1.93776E-11
22000	1.78782E-11
22500	1.65131E-11
23000	1.52684E-11
23500	1.41316E-11
24000	1.30922E-11
24500	1.21404E-11
25000	1.12677E-11
25500	1.04667E-11
26000	9.73051E-12
26500	9.05320E-12
27000	8.42937E-12
27500	7.85421E-12
28000	7.32340E-12
28500	6.83305E-12
29000	6.37967E-12
29500	5.96009E-12

Fig. 13(b) continued. Tabulation of $[F_b{}'(T, R_L)]_1$ for T = 4 microseconds and Various Meteorological Visibilities.

Vis. = 10 n. m. (cont.)
T = 4 μs

R_L	F_B
30000	5.57147E-12
30500	5.21123E-12
31000	4.87703E-12
31500	4.56675E-12
32000	4.27846E-12
32500	4.01042E-12
33000	3.76104E-12
33500	3.52885E-12
34000	3.31254E-12
34500	3.11090E-12
35000	2.92280E-12
35500	2.74725E-12
36000	2.58331E-12
36500	2.43013E-12
37000	2.28692E-12
37500	2.15297E-12
38000	2.02761E-12
38500	1.91024E-12
39000	1.80029E-12
39500	1.69725E-12
40000	1.60064E-12
40500	1.51002E-12
41000	1.42498E-12
41500	1.34514E-12
42000	1.27016E-12
42500	1.19971E-12
43000	1.13349E-12
43500	1.07122E-12
44000	1.01265E-12
44500	9.57542E-13
45000	9.05667E-13
45500	8.56820E-13
46000	8.10809E-13
46500	7.67457E-13
47000	7.26595E-13
47500	6.88070E-13
48000	6.51736E-13
48500	6.17459E-13
49000	5.85112E-13
49500	5.54579E-13
50000	5.25749E-13
50500	4.98521E-13
51000	4.72798E-13
51500	4.48492E-13
52000	4.25517E-13
52500	4.03796E-13
53000	3.83255E-13
53500	3.63825E-13
54000	3.45442E-13
54500	3.28046E-13
55000	3.11580E-13
55500	2.95990E-13
56000	2.81228E-13
56500	2.67245E-13
57000	2.53998E-13
57500	2.41446E-13
58000	2.29550E-13
58500	2.18273E-13
59000	2.07582E-13
59500	1.97443E-13
60000	1.87826E-13

Visibility = 20 n. m.
T = 4 μs

R_L =	F_B =
4000.	1.23288E-9
4500	9.01930E-10
5000	6.87484E-10
5500	5.40358E-10
6000	4.35002E-10
6500	3.56985E-10
7000	2.97632E-10
7500	2.51460E-10
8000	2.14861E-10
8500	1.85384E-10
9000	1.61313E-10
9500	1.41417E-10
10000	1.24797E-10
10500	1.10782E-10
11000	9.88638E-11
11500	8.86510E-11
12000	7.98394E-11
12500	7.21894E-11
13000	6.55098E-11
13500	5.96470E-11
14000	5.44765E-11
14500	4.98961E-11
15000	4.58220E-11
15500	4.21842E-11
16000	3.89245E-11
16500	3.59939E-11
17000	3.33510E-11
17500	3.09607E-11
18000	2.87928E-11
18500	2.68218E-11
19000	2.50252E-11
19500	2.33840E-11
20000	2.18814E-11
20500	2.05030E-11
21000	1.92360E-11
21500	1.80693E-11
22000	1.69929E-11
22500	1.59984E-11
23000	1.50780E-11
23500	1.42248E-11
24000	1.34328E-11
24500	1.26967E-11
25000	1.20114E-11
25500	1.13729E-11
26000	1.07770E-11
26500	1.02203E-11
27000	9.69970E-12
27500	9.21226E-12
28000	8.75542E-12
28500	8.32682E-12
29000	7.92433E-12
29500	7.54600E-12
30000	7.19002E-12
30500	6.85493E-12
31000	6.53909E-12
31500	6.24120E-12
32000	5.96002E-12
32500	5.69442E-12
33000	5.44334E-12
33500	5.20583E-12
34000	4.98100E-12
34500	4.76803E-12
35000	4.56616E-12
35500	4.37470E-12
36000	4.19300E-12
36500	4.02045E-12
37000	3.85651E-12
37500	3.70066E-12
38000	3.55242E-12
38500	3.41135E-12
39000	3.27702E-12
39500	3.14905E-12
40000	3.02709E-12
40500	2.91079E-12
41000	2.79985E-12
41500	2.69396E-12
42000	2.59285E-12

Fig. 13(b) continued. Tabulation of $[F_b{}'(T, R_L)]_1$ for $T = 4$ microseconds and Various Meteorological Visibilities.

Vis. = 20 n. m. (cont.) $T = 4 \mu s$					
42500	2.49627E-12	65500	5.48192E-13	89500	1.49821E-13
43000	2.40398E-12	66000	5.32380E-13	90000	1.46103E-13
43500	2.31575E-12	66500	5.17084E-13	90500	1.42487E-13
44000	2.23136E-12	67000	5.02286E-13	91000	1.38969E-13
44500	2.15062E-12	67500	4.87968E-13	91500	1.35546E-13
45000	2.07334E-12	68000	4.74110E-13	92000	1.32215E-13
45500	1.99935E-12	68500	4.60697E-13	92500	1.28973E-13
46000	1.92848E-12	69000	4.47711E-13	93000	1.25819E-13
46500	1.86058E-12	69500	4.35139E-13	93500	1.22749E-13
47000	1.79549E-12	70000	4.22964E-13	94000	1.19761E-13
47500	1.73308E-12	70500	4.11173E-13	94500	1.16853E-13
48000	1.67323E-12	71000	3.99751E-13	95000	1.14021E-13
48500	1.61580E-12	71500	3.88686E-13	95500	1.11264E-13
49000	1.56069E-12	72000	3.77965E-13	96000	1.08580E-13
49500	1.50778E-12	72500	3.67576E-13	96500	1.05967E-13
50000	1.45697E-12	73000	3.57507E-13	97000	1.03422E-13
50500	1.40816E-12	73500	3.47747E-13	97500	1.00944E-13
51000	1.36126E-12	74000	3.38285E-13	98000	9.85301E-14
51500	1.31618E-12	74500	3.29111E-13	98500	9.61792E-14
52000	1.27284E-12	75000	3.20216E-13	99000	9.38894E-14
52500	1.23116E-12	75500	3.11589E-13	99500	9.16587E-14
53000	1.19107E-12	76000	3.03222E-13	100000	8.94857E-14
53500	1.15249E-12	76500	2.95105E-13	100500	8.73686E-14
54000	1.11537E-12	77000	2.87231E-13	101000	8.53059E-14
54500	1.07963E-12	77500	2.79591E-13	101500	8.32960E-14
55000	1.04521E-12	78000	2.72177E-13	102000	8.13374E-14
55500	1.01207E-12	78500	2.64982E-13	102500	7.94288E-14
56000	9.80134E-13	79000	2.57998E-13	103000	7.75687E-14
56500	9.49365E-13	79500	2.51219E-13	103500	7.57558E-14
57000	9.19710E-13	80000	2.44638E-13	104000	7.39888E-14
57500	8.91121E-13	80500	2.38248E-13	104500	7.22664E-14
58000	8.63555E-13	81000	2.32043E-13	105000	7.05873E-14
58500	8.36969E-13	81500	2.26017E-13	105500	6.89504E-14
59000	8.11323E-13	82000	2.20165E-13	106000	6.73545E-14
59500	7.86578E-13	82500	2.14480E-13	106500	6.57986E-14
60000	7.62698E-13	83000	2.08958E-13	107000	6.42814E-14
60500	7.39648E-13	83500	2.03593E-13	107500	6.28021E-14
61000	7.17395E-13	84000	1.98380E-13	108000	6.13594E-14
61500	6.95908E-13	84500	1.93314E-13	108500	5.99525E-14
62000	6.75155E-13	85000	1.88392E-13	109000	5.85804E-14
62500	6.55108E-13	85500	1.83607E-13	109500	5.72421E-14
63000	6.35740E-13	86000	1.78957E-13	110000	5.59367E-14
63500	6.17023E-13	86500	1.74436E-13	110500	5.46634E-14
64000	5.98934E-13	87000	1.70041E-13	111000	5.34213E-14
64500	5.81447E-13	87500	1.65768E-13	111500	5.22096E-14
65000	5.64541E-13	88000	1.61613E-13	112000	5.10274E-14
		88500	1.57573E-13	112500	4.96740E-14
		89000	1.53643E-13	113000	4.87487E-14

Fig. 14 Tabulation of $[F_b' \, (R_S \text{ or } R_L)]_2$ and K for Various Visibilities.

Visibility = 3 n. m.

FB =	RS=	K=
2.71668E-9	3500	3.99516E+6
4.47099E-9	4000	5.98435E+6
5.66052E-9	4500	8.68601E+6
6.49018E-9	5000	1.22980E+7
7.08201E-9	5500	1.70654E+7
7.51201E-9	6000	2.32912E+7
7.82925E-9	6500	3.13484E+7
8.06634E-9	7000	4.16949E+7
8.24549E-9	7500	5.48918E+7
8.38218E-9	8000	7.16248E+7
8.48733E-9	8500	9.27299E+7
8.56883E-9	9000	1.19224E+8
8.63242E-9	9500	1.52344E+8
8.68232E-9	10000	1.93587E+8
8.72168E-9	10500	2.44768E+8
8.75288E-9	11000	3.08077E+8
8.77772E-9	11500	3.86160E+8
8.79758E-9	12000	4.82206E+8
8.81351E-9	12500	6.00052E+8
8.82633E-9	13000	7.44310E+8
8.83668E-9	13500	9.20519E+8
8.84506E-9	14000	1.13532E+9
8.85186E-9	14500	1.39668E+9
8.85740E-9	15000	1.71413E+9
8.86191E-9	15500	2.09905E+9
8.86561E-9	16000	2.56506E+9
8.86863E-9	16500	3.12841E+9
8.87111E-9	17000	3.80848E+9
8.87315E-9	17500	4.62837E+9
8.87483E-9	18000	5.61559E+9

Visibility = 5 n. m.

FB =	RS=	K=
2.23261E-9	3500	2.60305E+6
3.76619E-9	4000	3.66764E+6
4.87185E-9	4500	5.00738E+6
5.69178E-9	5000	6.66876E+6
6.31365E-9	5500	8.70463E+6
6.79404E-9	6000	1.11750E+7
7.17094E-9	6500	1.41479E+7
7.47023E-9	7000	1.77002E+7
7.71073E-9	7500	2.19192E+7
7.90585E-9	8000	2.69031E+7
8.06542E-9	8500	3.27627E+7

8.19691E-9	9000	3.96229E+7
8.30597E-9	9500	4.76242E+7
8.39696E-9	10000	5.69247E+7
8.47327E-9	10500	6.77015E+7
8.53758E-9	11000	8.01539E+7
8.59201E-9	11500	9.45050E+7
8.63827E-9	12000	1.11005E+8
8.67771E-9	12500	1.29933E+8
8.71147E-9	13000	1.51602E+8
8.74044E-9	13500	1.76362E+8
8.76538E-9	14000	2.04603E+8
8.78690E-9	14500	2.36762E+8
8.80552E-9	15000	2.73324E+8
8.82167E-9	15500	3.14831E+8
8.83571E-9	16000	3.61668E+8
8.84793E-9	16500	4.15166E+8
8.85859E-9	17000	4.75414E+8
8.86791E-9	17500	5.43462E+8
8.87607E-9	18000	6.20237E+8
8.88323E-9	18500	7.06766E+8
8.88951E-9	19000	8.04191E+8
8.89504E-9	19500	9.13778E+8
8.89990E-9	20000	1.03693E+9
8.90419E-9	20500	1.17532E+9
8.90798E-9	21000	1.33036E+9
8.91133E-9	21500	1.50427E+9
8.91429E-9	22000	1.69908E+9
8.91692E-9	22500	1.91714E+9
8.91925E-9	23000	2.16104E+9
8.92131E-9	23500	2.43368E+9
8.92315E-9	24000	2.73823E+9
8.92478E-9	24500	3.07821E+9
8.92623E-9	25000	3.45753E+9
8.92752E-9	25500	3.88048E+9
8.92868E-9	26000	4.35183E+9
8.92970E-9	26500	4.87682E+9
8.93062E-9	27000	5.46125E+9
8.93144E-9	27500	6.11152E+9
8.93216E-9	28000	6.83470E+9
8.93283E-9	28500	7.63858E+9
8.93342E-9	29000	8.53175E+9
8.93394E-9	29500	9.52370E+9
8.93441E-9	30000	1.06249E+10

Fig. 14 continued. Tabulation of $[F_b' (R_S \text{ or } R_L)]_2$ and K for Various Visibilities.		

Visibility = 10 n. m.					
FB =	RS =	K =	6.28146E-9	26000	4.70009E+8
1.28206E-9	3500	1.92916E+6	6.28569E-9	26500	5.04641E+8
2.20156E-9	4000	2.60426E+6	6.28963E-9	27000	5.41440E+8
2.89356E-9	4500	3.40659E+6	6.29331E-9	27500	5.80524E+8
3.42922E-9	5000	4.34678E+6	6.29674E-9	28000	6.22017E+8
3.85329E-9	5500	5.43606E+6	6.29995E-9	28500	6.66051E+8
4.19521E-9	6000	6.68641E+6	6.30294E-9	29000	7.12764E+8
4.47515E-9	6500	8.11053E+6	6.30574E-9	29500	7.62299E+8
4.70732E-9	7000	9.72188E+6	6.30835E-9	30000	8.14809E+8
4.90200E-9	7500	1.15348E+7	6.31080E-9	30500	8.70451E+8
5.06682E-9	8000	1.35643E+7	6.31310E-9	31000	9.29394E+8
5.20753E-9	8500	1.58266E+7	6.31524E-9	31500	9.91812E+8
5.32855E-9	9000	1.83386E+7	6.31726E-9	32000	1.05789E+9
5.43332E-9	9500	2.11183E+7	6.31914E-9	32500	1.12782E+9
5.52455E-9	10000	2.41849E+7	6.32092E-9	33000	1.20180E+9
5.60441E-9	10500	2.75584E+7	6.32258E-9	33500	1.28004E+9
5.67466E-9	11000	3.12603E+7	6.32414E-9	34000	1.36278E+9
5.73672E-9	11500	3.53130E+7	6.32561E-9	34500	1.45023E+9
5.79175E-9	12000	3.97405E+7	6.32699E-9	35000	1.54265E+9
5.84075E-9	12500	4.45680E+7	6.32828E-9	35500	1.64028E+9
5.88450E-9	13000	4.98220E+7	6.32950E-9	36000	1.74341E+9
5.92370E-9	13500	5.55308E+7	6.33065E-9	36500	1.85230E+9
5.95892E-9	14000	6.17240E+7	6.33173E-9	37000	1.96725E+9
5.99065E-9	14500	6.84330E+7	6.33275E-9	37500	2.08858E+9
6.01930E-9	15000	7.56910E+7	6.33370E-9	38000	2.21660E+9
6.04523E-9	15500	8.35327E+7	6.33461E-9	38500	2.35166E+9
6.06875E-9	16000	9.19952E+7	6.33546E-9	39000	2.49410E+9
6.09013E-9	16500	1.01117E+8	6.33626E-9	39500	2.64430E+9
6.10960E-9	17000	1.10940E+8	6.33702E-9	40000	2.80264E+9
6.12736E-9	17500	1.21506E+8	6.33773E-9	40500	2.96954E+9
6.14359E-9	18000	1.32861E+8	6.33841E-9	41000	3.14542E+9
6.15844E-9	18500	1.45053E+8	6.33905E-9	41500	3.33073E+9
6.17206E-9	19000	1.58133E+8	6.33965E-9	42000	3.52592E+9
6.18455E-9	19500	1.72154E+8	6.34022E-9	42500	3.73150E+9
6.19604E-9	20000	1.87171E+8	6.34075E-9	43000	3.94798E+9
6.20661E-9	20500	2.03244E+8	6.34126E-9	43500	4.17588E+9
6.21636E-9	21000	2.20435E+8	6.34174E-9	44000	4.41577E+9
6.22534E-9	21500	2.38809E+8	6.34220E-9	44500	4.66824E+9
6.23364E-9	22000	2.58435E+8	6.34263E-9	45000	4.93389E+9
6.24132E-9	22500	2.79385E+8	6.34303E-9	45500	5.21338E+9
6.24842E-9	23000	3.01734E+8	6.34342E-9	46000	5.50736E+9
6.25500E-9	23500	3.25564E+8	6.34378E-9	46500	5.81655E+9
6.26110E-9	24000	3.50956E+8	6.34413E-9	47000	6.14168E+9
6.26676E-9	24500	3.78004E+8	6.34445E-9	47500	6.46351E+9
6.27202E-9	25000	4.06795E+8	6.34476E-9	48000	6.84286E+9
6.27691E-9	25500	4.37429E+8	6.34506E-9	48500	7.22055E+9
			6.34533E-9	49000	7.61747E+9
			6.34560E-9	49500	8.03453E+9

Visibility = 10 n. m. (Continued)

6.34585E-9	50000	8.47270E+9
6.34609E-9	50500	8.93298E+9
6.34631E-9	51000	9.41642E+9
6.34652E-9	51500	9.92411E+9
6.34673E-9	52000	1.04578E+10

Visibility = 20 n. m.

FB =	R.S=	K=
6.11071E-10	3500	1.68773E+6
1.05787E-9	4000	2.23524E+6
1.40062E-9	4500	2.68657E+6
1.71106E-9	5000	3.59101E+6
1.88929E-9	5500	4.40594E+6
2.06865E-9	6000	5.31683E+6
2.21834E-9	6500	6.32723E+6
2.34487E-9	7000	7.44080E+6
2.45302E-9	7500	8.66130E+6
2.54635E-9	8000	9.99257E+6
2.62757E-9	8500	1.14386E+7
2.69676E-9	9000	1.30034E+7
2.76159E-9	9500	1.46911E+7
2.81735E-9	10000	1.65061E+7
2.86711E-9	10500	1.84527E+7
2.91172E-9	11000	2.05354E+7
2.95189E-9	11500	2.27568E+7
2.98820E-9	12000	2.51277E+7
3.02115E-9	12500	2.76470E+7
3.05115E-9	13000	3.03215E+7
3.07854E-9	13500	3.31565E+7
3.10362E-9	14000	3.61571E+7
3.12665E-9	14500	3.93287E+7
3.14785E-9	15000	4.26769E+7
3.16740E-9	15500	4.62073E+7
3.18549E-9	16000	4.99257E+7
3.20224E-9	16500	5.38380E+7
3.21779E-9	17000	5.79503E+7
3.23224E-9	17500	6.22688E+7
3.24571E-9	18000	6.67999E+7
3.25427E-9	18500	7.15502E+7
3.27001E-9	19000	7.65264E+7
3.28099E-9	19500	8.17354E+7
3.29128E-9	20000	8.71842E+7
3.30093E-9	20500	9.28800E+7
3.31000E-9	21000	9.88302E+7
3.31852E-9	21500	1.05042E+8
3.32655E-9	22000	1.11524E+8
3.33411E-9	22500	1.18284E+8
3.34124E-9	23000	1.25330E+8
3.34798E-9	23500	1.32669E+8
3.35434E-9	24000	1.40312E+8
3.36037E-9	24500	1.48266E+8
3.36607E-9	25000	1.56540E+8
3.37147E-9	25500	1.65144E+8
3.37659E-9	26000	1.74086E+8
3.38145E-9	26500	1.83378E+8
3.38607E-9	27000	1.93027E+8
3.39046E-9	27500	2.03044E+8
3.39463E-9	28000	2.13443E+8
3.39860E-9	28500	2.24229E+8
3.40238E-9	29000	2.35415E+8
3.40598E-9	29500	2.47013E+8
3.40942E-9	30000	2.59032E+8
3.41269E-9	30500	2.71486E+8
3.41582E-9	31000	2.84386E+8
3.41880E-9	31500	2.97744E+8
3.42165E-9	32000	3.11572E+8
3.42438E-9	32500	3.25883E+8
3.42699E-9	33000	3.40690E+8
3.42948E-9	33500	3.56007E+8
3.43187E-9	34000	3.71846E+8
3.43415E-9	34500	3.88222E+8
3.43634E-9	35000	4.05149E+8
3.43844E-9	35500	4.22641E+8
3.44046E-9	36000	4.40714E+8
3.44239E-9	36500	4.59382E+8
3.44424E-9	37000	4.78662E+8
3.44602E-9	37500	4.98568E+8
3.44772E-9	38000	5.19118E+8
3.44936E-9	38500	5.40327E+8
3.45094E-9	39000	5.62214E+8
3.45245E-9	39500	5.84794E+8
3.45391E-9	40000	6.08087E+8
3.45531E-9	40500	6.32109E+8
3.45666E-9	41000	6.56881E+8
3.45796E-9	41500	6.82420E+8
3.45921E-9	42000	7.08746E+8
3.46041E-9	42500	7.35880E+8
3.46157E-9	43000	7.63840E+8
3.46268E-9	43500	7.92649E+8
3.46376E-9	44000	8.22327E+8
3.46480E-9	44500	8.52895E+8
3.46580E-9	45000	8.84377E+8
3.46676E-9	45500	9.16794E+8

Fig. 14. (continued) Tabulation of $[F_b' (R_S \text{ or } R_L)]_2$ and K for Various Visibilities.					

Visibility = 20 n. m. (Continued)					
FB	RS	K	3.48886E-9	68000	3.82753E+9
			3.48908F-9	68500	3.93838F+9
			3.48930E-9	69000	4.05202F+9
3.46769E-9	46000	9.50170F+8	3.48951F-9	69500	4.16850E+9
3.46859F-9	46500	9.84529E+8	3.48972F-9	70000	4.28789F+9
3.46946E-9	47000	1.01989E+9	3.48992F-9	70500	4.41024F+9
3.47029F-9	47500	1.05629F+9	3.49011F.-9	71000	4.53563E+9
3.47110F-9	48000	1.09374F+9	3.49030F-9	71500	4.66411E+9
3.47188E-9	48500	1.13228F+9	3.49048E-9	72000	4.79578E+9
3.47264E-9	49000	1.17192E+9			
3.47337E-9	49500	1.21270F+9			
3.47407F-9	50000	1.25464F+9			
3.47475E-9	50500	1.29777F+9			
3.47541E-9	51000	1.34213E+9			
3.47605E-9	51500	1.38773F+9			
3.47666E-9	52000	1.43461F+9			
3.47726E-9	52500	1.48280F+9			
3.47783F-9	53000	1.53233F+9			
3.47839F.-9	53500	1.58323F+9			
3.47893E-9	54000	1.63554E+9			
3.47945E-9	54500	1.68928E+9			
3.47996E-9	55000	1.74450E+9			
3.48045E-9	55500	1.80123F+9			
3.48092F.-9	56000	1.85950E+9			
3.48138F-9	56500	1.91935F+9			
3.48183F-9	57000	1.98081F+9			
3.48226F-9	57500	2.04393F+9			
3.48268F-9	58000	2.10874F+9			
3.48308F-9	58500	2.17528F+9			
3.48348F-9	59000	2.24359F+9			
3.48386F-9	59500	2.31372F+9			
3.48423F-9	60000	2.38570F+9			
3.48459F.-9	60500	2.45958F+9			
3.48494F.-9	61000	2.53540F+9			
3.48527F.-9	61500	2.61321E+9			
3.48560F.-9	62000	2.69304F+9			
3.48592F-9	62500	2.77496F+9			
3.48623E-9	63000	2.85900F+9			
3.48653F-9	63500	2.94522F+9			
3.48682F-9	64000	3.03366F+9			
3.48710F-9	64500	3.12437F+9			
3.48737F.-9	65000	3.21741F+9			
3.48764F-9	65500	3.31263F+9			
3.48790E-9	66000	3.41066F+9			
3.48815F.-9	66500	3.51102F+9			
3.48839F-9	67000	3.61390F+9			
3.48863F.-9	67500	3.71939F+9			

Object Range (n. m.)

$\frac{C_R}{C_o}$

R_{L1} R_{L2} R_{L3} R_{L4} R_{L5} R_{L6}

Object Range (kilofeet)
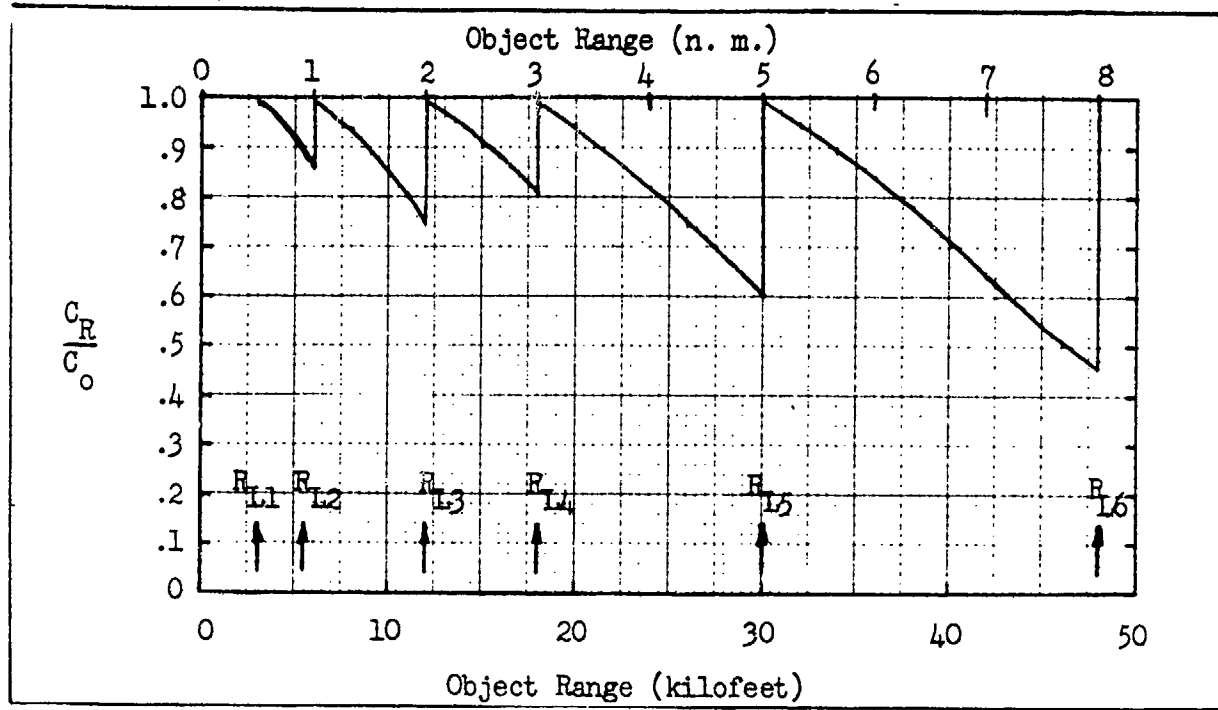
Fig. 15.   Ratio of Apparent to Inherent Object Contrast vs Range for a Near
Point Range Gate Fixed at R_{Ln} for Objects in the Range Interval R_{Ln}
to R_{Ln+1}. Visibility at 0.86 micrometers is 10 n.m. with Average
Scene Reflectance = 0.2.   T=2 μs.

To illustrate the use of the tables and to give insight into the

operation of an active sensor, two cases are considered. In the first case,

the leading edge, or the near point range gate, of the pulse is fixed at a

range R_{L1} and the ratio of apparent-to-inherent contrast is calculated as

the object is moved from range R_{L1} to R_{L2}. Then, the leading edge is moved

to R_{L2} and the object is moved from R_{L2} to R_{L3}, etc., as shown in Fig. 15.

In this figure, and the next, the radiation wavelength was 0.86 micrometers,

the scene reflectivity was 0.2, the pulse duration was 2 μs, and the

meteorological visibility was 10 n. m. With the visibility of 10 n. m., and

radiation pulse duration of 2 μs, the contrast degradation due to the finite

pulse duration [the first term in Eq. (28)] can be neglected. Note in the

Fig. 15, that the observer can increase the apparent contrast of the object

to nearly its inherent value at anytime by adjusting the near point range
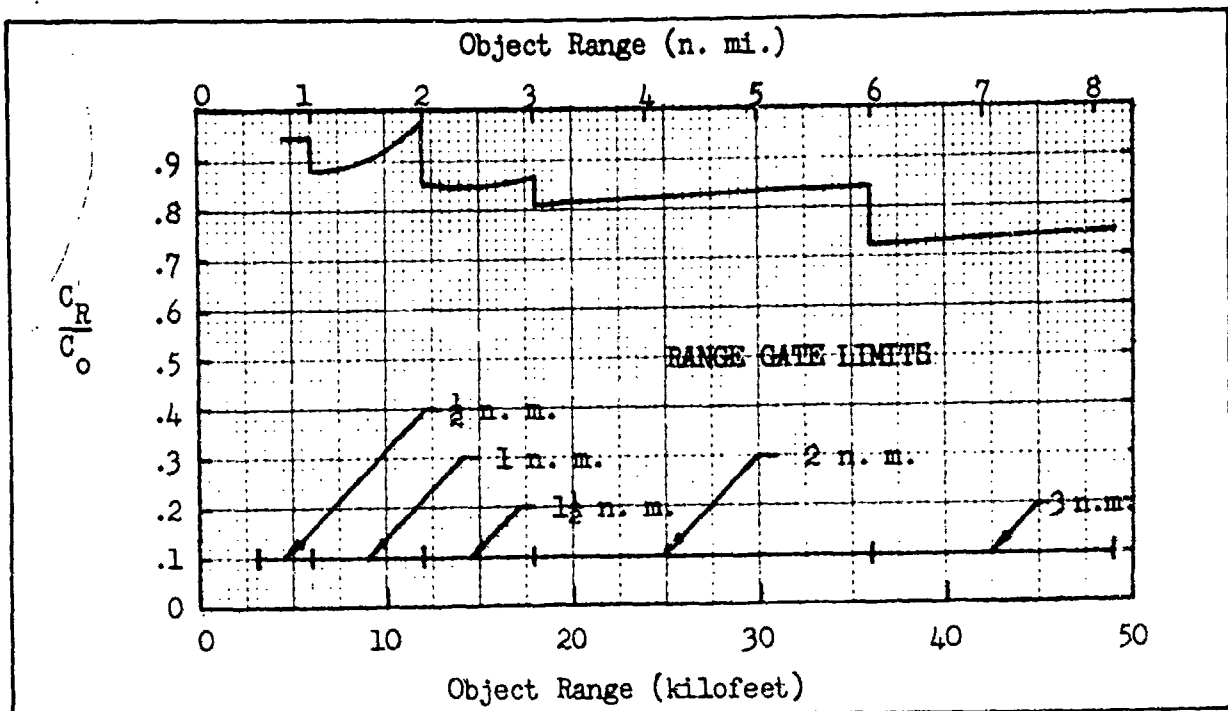
Fig. 16. Ratio of Apparent to Inherent Contrast vs Range for Objects in the Middle of the Range Gate Limits. Visibility at 0.86 micrometers is 10 n. m. with Average Scene Reflectance = 0.2. $T = 2 \mu s$.

gate so that it falls just in front of the object being viewed.

In a more practical situation, we assumed that the range gate was moveable and that the object was located in the center of the range gate, i.e., midway between the near point as set by sensor turn on time, t_1, and the far point as set by the sensor turn off time, t_2. The results are shown in Fig. 16. In this calculation, the range gate was made progressively larger as distance was increased to illustrate the effect of various range gate widths. This figure is probably representative of the typical search condition. Once an object has been detected, the observer will probably adjust the range gate near point to increase the object contrast.

2.6 Lens Parameters

Scene radiant flux is collected and imaged onto the image plane by a lens. For the purposes of illustration and first order analysis,

45
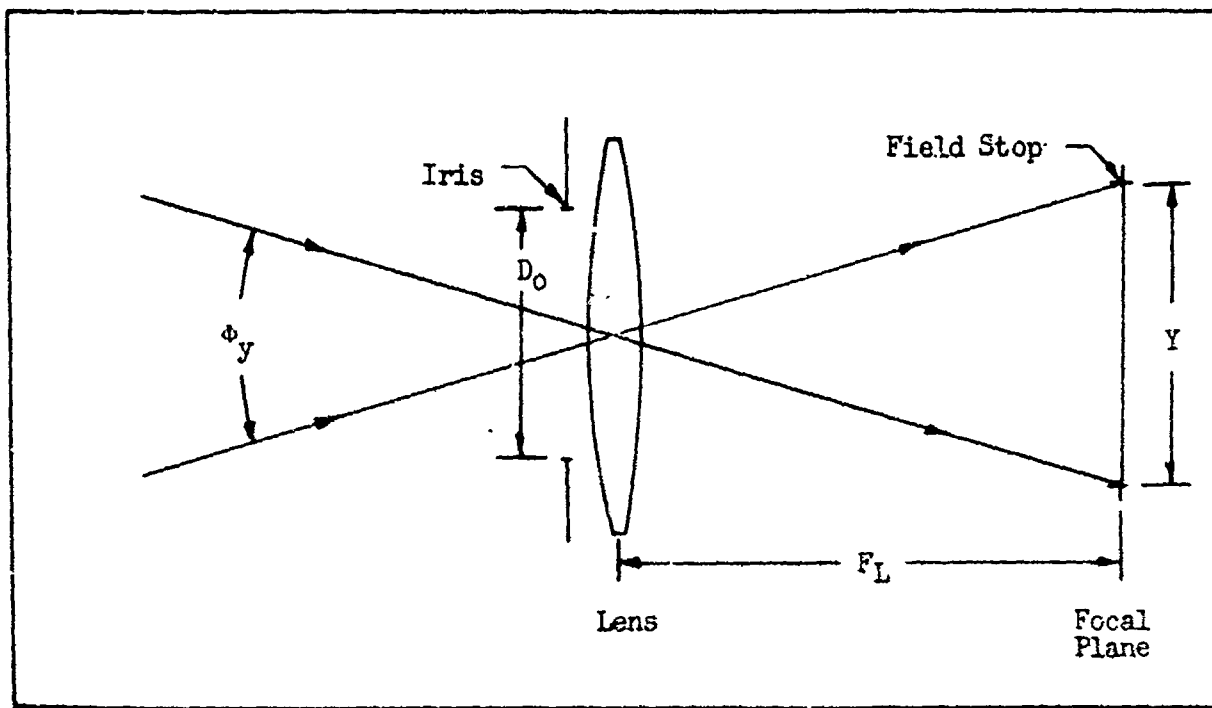
Fig. 17.   Schematic of the Lens.

the lens is assumed to be thin and the scene is assumed to be at long range
such that the lens magnification is zero. The first order lens parameters
of primary interest are, the

(a) Lens Aperture, D_O. - The lens aperture is the effective lens diameter
and is sometimes called the clear aperture or entrance pupil. The entrance
pupil is the image of the aperture stop from object space (the scene side
of the lens). In Fig. 17, the iris is the aperture stop and entrance pupil.
The maximum diameter of the entrance pupil in the thin lens case is the
diameter of the lens itself.

(b) Lens Focal Length, F_L. - Parallel light rays from distant objects are
focused on the focal plane at distance, F_L, from the lens plane.

(c) Lens Focal Ratio, f. - The ratio of lens focal length to clear aperture,
or F_L/D, is called the lens focal ratio.

46

(d) _Lens Transmittance_, T_o. - The transmittance of the optical elements on the optical axis.

(e) _Lens T stop_, T. - The lens T stop is numerically equal to $f/\sqrt{T_o}$ and is used to relate focal plane irradiance to the scene radiance levels as discussed below.

(f) _Field Stop_, X, Y. - For the thin lens case, the dimensions of the field stop X and Y are given by the dimensions of the effective photosensitive area of the sensor. In photography, the field stop is the size of the film being exposed; while in TV, it is the area scanned out by the electron beam referenced to the input photosurface.

(g) _Sensor Field of View_, φ_x, φ_y. - The sensor field of view is numerically equal to $\varphi_x = 2 \tan^{-1} X/2 \, F_L$ and $\varphi_y = 2 \tan^{-1} Y/2 \, F_L$. For small fields of view, $\varphi_x \cong X/F_L$ and $\varphi_y \cong Y/F_L$.

(h) _Lens Point Spread Function_, r_o (x,y). - The waveform of an image of a point source. This is sometimes known as the lens's _impulse response_.

(i) _Lens Line Spread Function_, $r_o(x)$ or $r_o(y)$. - The waveform of an image of a line source.

(j) _Lens Aperture Frequency Response_*, $R_o(k_x, k_y)$. - The lenses' complex steady-state frequency response to a point source as discussed in Section 3 $R_o(k_x, k_y)$ is the Fourier transform of $r_o(x,y)$. The quantities k_x, k_y are called _spatial frequencies_ and are generally expressed in line pairs, or cycles, per millimeter.

---

* In this report, spatial frequency is generally given as N lines per picture height rather than k_x line pairs/mm. Note that $N = 2 k_x Y$ where Y is the picture height in mm.

47

(k) <u>Lens Optical Transfer Function</u>, $R_o(k_x)$ or $R_o(k_y)$. - The lens's complex steady state frequency response to a line source.

(1) <u>Modulation Transfer Function</u>, $R_o(k_x)$, $R_o(k_y)$ or MTF. - The magnitude of the optical transfer function.

2.7 Photosurface Irradiance Level

We next wish to relate the photosurface irradiance level to that at the scene. Suppose the radiance of a small area a_o on the scene is N_s Watts/m^2-sr. If the scene is diffuse, then

$$N_s = \frac{W_s}{\pi} \quad , \tag{34}$$

where W_s is the radiant emittance of the scene in Watts/m^2. The flux, P_o, incident on the sensor's lens will be

$$P_o = \frac{W_s a_o A_o T_o}{\pi R^2} \quad , \tag{35}$$

where A_o is the effective area of the objective lens and T_o is its transmittance. Since $A_o = \pi D_o^2/4$,

$$P_o = \frac{W_s a_o D_o^2 T_o}{4 R^2} \quad . \tag{36}$$

For an infinity focused lens,

$$\frac{a_o}{R^2} = \frac{a_i}{F_L^2} \quad , \tag{37}$$

48

where a_i is the image area. Now,

$$P_o = \frac{W_i a_i T_o}{4F_L^2/D_o^2} \quad , \tag{38}$$

and the image irradiance,

$$H_i = \frac{P_o}{a_i} = \frac{W_s}{4T^2} \quad , \tag{39}$$

where T is the lens T stop as previously defined. The above equation may also be written as

$$H_i = \frac{\pi N_s}{4T^2} \quad . \tag{40}$$

In the analysis of sensory system performance, the image irradiance must be related to the photocurrent of the input photosurface to progress with the sensor analysis. This relationship is obtained from the general relationship

$$i = A \left[\sigma_p \int_{-\infty}^{\infty} R_\lambda H_\lambda d\lambda \right]^\gamma \tag{41}$$

where σ_p is the peak responsivity of the photosurface in Amps/Watts*, R_λ is the photosurface's relative spectral sensitivity, H_λ is its spectral irradiance, and γ is the slope of the signal current vs irradiance

---

* When the gamma is different than 1, σ_p and R_λ are functions of the operating point on the signal transfer characteristic.

49

characteristic. Spectral sensitivity curves are shown for a number of common photoemitters in Fig. 18 and for a silicon diode matrix photoconductor in Fig. 19. For these surfaces, the gamma is equal to or near unity. In many cases, particularly in the laboratory, the response to a standard light source, such as a tungsten source operated at 2854° K, is specified. In this case

$$i = A \left[\sigma_T H_T \right]^\gamma \tag{42}$$

where the subscript is used to denote a response to a specific source.

2.8 Resolution vs Discrimination Range

An electro-optical sensor is of little use if it does not provide sufficient resolution of scene detail to serve some intended purpose. As we noted in Section 2.0, the level of required resolution can vary depending on the task at hand. In Section 3, the levels of discrimination of scene objects have been arbitrarily divided into three major classes; namely, detection, recognition and identification with simple detection being the lowest level of discrimination and identification being the highest. The conceptual differences between these various levels are discussed in detail in Section 3 and also in Section 4.

Suppose the object in the scene is of rectangular shape of dimensions l_g in the horizontal and w_g in the vertical. Let the corresponding quantities in the focal plane of the sensor's objective lens be l and w. These quantities are related to one another by the formula

50

Fig. 19. Spectral Response of the Silicon Vidicon

Fig. 18. Spectral Responsivity Versus Wavelength for Photoemissive Photocathodes

51

$$\frac{l_g}{R} \cdot \frac{w_g}{R} = \frac{1}{F_L} \cdot \frac{w}{F_L} \qquad . \tag{43}$$

As we discuss in Section 3, a signal-to-noise ratio can be associated with an image and thi₃ signal-to-noise ratio is proportional to the image's area, a, i.e.,

$$SNR_I \; \alpha \; (a/A)^{\frac{1}{2}} \qquad . \tag{44}$$

Note that we show the signal-to-noise ratio as being proportional to the ratio of image area to the useful, or effective, focal plane area rather than the image area alone. This is an analytical convenience rather than a necessity. While the scene object may have specific dimensions such as its length and width, the image area of a rectangle to be used in the signal-to-noise ratio calculation is a variable depending on the level of object discrimination required. If the object is isolated and amid a uniform background, the area, a, is identical to that of the object's image. If the object is amid clutter, then, the area is taken to be equal to 1/2 the minimum object dimension times the object length. For the object to be recognized, we specify the area to be 1/8 the minimum object dimension times the object length and for identification, 1/13 the minimum object dimension times its length. The rationale behind these area choices is discussed in detail in Section 3 and verified, or at least, made reasonable through the psychophysical experiments of Section 4.

52
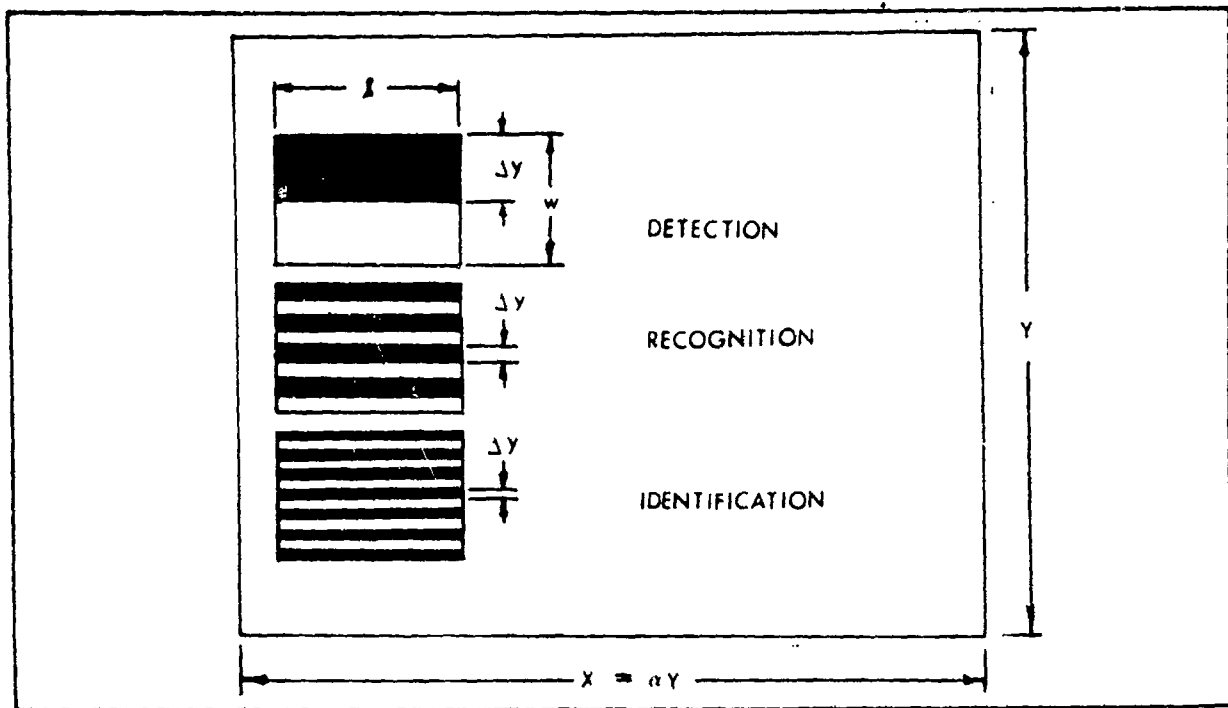
Fig. 20.   Image Dimensions to be used in the Calculation of Signal-to-Noise in the Focal Plane, XY, for Various Levels of Object Discrimination.

For ease in calculating and plotting results in a common format, we define a distance Δy on the object as shown in Fig. 20 and further define

$$N = \frac{Y}{\Delta y} \quad , \tag{45}$$

where Y is the effective focal plane, or "picture" height, such that the units of N are "lines per picture height". Then, for the isolated object in a uniform background, the ratio, a/A, becomes

$$\frac{a}{A} = \frac{lw}{XY} = \frac{2(l\Delta y)}{\alpha Y^2} = \frac{2n_v \Delta y^2}{\alpha Y^2} = \frac{2 n_v}{\alpha N^2} \quad , \tag{46}$$

where α is the picture aspect ratio (h/v)*, and n_v is the length-to-width

———————————

* h is the horizontal dimension, v is the vertical dimension.

53

ratio, $1/\Delta y$. For the detection of an object in clutter or, for recognition or identification,

$$\frac{a}{A} = \frac{1 \Delta y}{\alpha Y^2} = \frac{n_v}{\alpha N^2} \tag{47}$$

Next, we observe that by analogy to Eq. (43), that

$$\frac{w_r}{R} = \frac{\Delta Y}{F_L} = \frac{Y}{N \cdot F_L} \cong \frac{\varphi_y}{N} \quad, \tag{48}$$

and,

$$R = \frac{N \cdot F_L \cdot w_r}{Y}$$

$$\cong \frac{N \cdot w_r}{\varphi_y} \quad, \tag{49}$$

where φ is approximately the vertical field of view for small angles φ. The quantity w_r is designated the "ground resolution".

In the Fig. 20, the image is shown as a bar pattern rather than as a real object. This stems from the concept promulgated by Johnson[7] wherein the detectability of a bar pattern is correlated with levels of target discrimination. That such correlation exists, is shown experimentally in Section 4. In the above discussion, the isolated object case is separated

from the cluttered scene detection and the recognition and identification cases. The only apparent difference at this point is a factor of 2 in the a/A ratio but considerably larger differences will be noted with respect to the effect of apertures on the object detectability in the discussion below.

2.9 Sensor Signal-to-Noise Ratio

For illustrational purposes, a specific low light level television camera example will be used in the following description. This camera will be the 40/40 mm I-SEBIR* which has been discussed and analyzed in Section 3. It is assumed that the I-SEBIR is operated with sufficient gain before electron beam image readout so as to insure that the sensor is photoelectron-noise-limited. As discussed in Section 3, the signal-to-noise ratio for detection of the isolated object in a uniform background case is written

$$SNR_D = [\frac{2n_v t}{\alpha}]^{\frac{1}{2}} \frac{1}{N} \frac{2C_M(i_{av}/e)^{\frac{1}{2}}}{(\xi_{lw})^{\frac{1}{2}}} \quad , \tag{50}$$

(isolated object)

where t is the integration time of the eye, i_{av} is the average input photo-surface photocurrent, e is the charge of an electron and ξ_{lw} is a noise correction factor. For the objects in clutter, or for recognition and identi-

---

* I-SEBIR means the Intensified, Silicon-Electron-Bombardment Induced Response.

fication,

$$\mathrm{SNR}_D = [\frac{n_v t}{\alpha}]^{\frac{1}{2}} \cdot \frac{2C_M\, R_{SF}(N)}{N} \; (\frac{i_{av/e}}{\beta\, \xi_1})^{\frac{1}{2}} \; , \tag{51}$$

(objects in clutter)

where β is a noise equivalent bandpass and R_{SF} is the square wave flux response.

For the isolated object case, the function, ξ_{1w}, is given by the relations

$$\xi_{1w} = \xi_1 \cdot \xi_w \; , \tag{52}$$

and

$$\xi_1 = \frac{[1 + (\frac{N}{n_v\, N_{eL}})^2\,]}{[1 + (\frac{N}{n_v\, N_{eL}})^2 + (\frac{N}{n_v\, N_{eT}})^2\,]^{\frac{1}{2}}} \; , \tag{53}$$

and

$$\xi_w = \frac{[1 + (\frac{N}{2\, N_{eL}})^2]}{[1 + (\frac{N}{2\, N_{eL}})^2 + (\frac{N}{2\, N_{eT}})^2\,]^{\frac{1}{2}}} \; , \tag{54}$$

where N_{eL} and N_{eT} are the noise equivalent passbands of the lens and camera

56
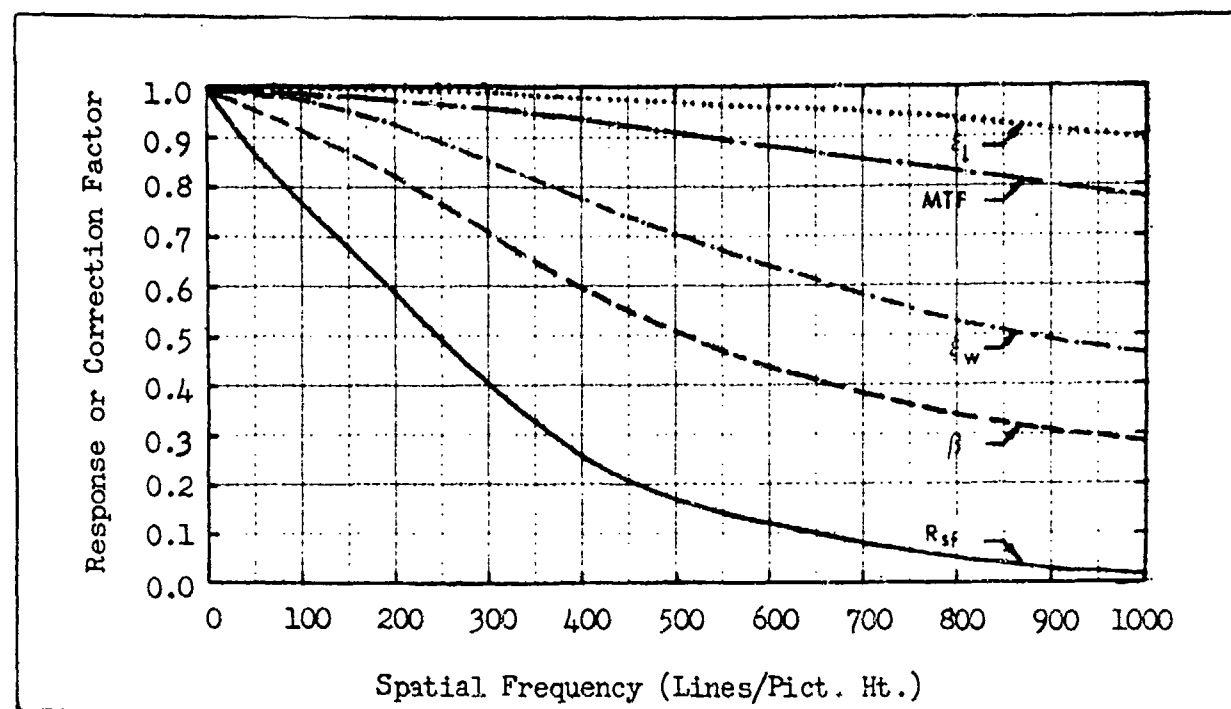
Fig. 21. Lens Modulation Transfer Function, MTF, Sensor Noise Correction Factors ε_1, ε_w, and β, and Square Wave Flux Responses, R_{sf} for the Overall System. Lens is of 10" Focal Length and Sensor is the 40/40 mm I-SEBIR.

tubes respectively. These functions are plotted in Fig. 21 for $n_v = 4$, $N_{eL} = 1,875$ and $N_{eT} = 241$. It is implicitly assumed that the various sensor and lens MTF's are equal in x and y and that x and y are independent and separable variables.

For the objects in clutter, we use the function ε_1 and calculate β from

$$\beta = \frac{\int_{o}^{N} \left| R_{oT}(N) \right|^2 \, dN}{N} \quad , \tag{55}$$

where R_{oT} is the sensor MTF. In the above, it is assumed that there are only two principal MTF's, the lens and the camera tube. The quantity β is obtained from Fig. 54 of Section 3. The square wave flux response

is computed from

$$R_{SF} = \frac{8}{\pi^2} \sum_k \frac{[R_{oL}(kN) \cdot R_{oT}(kN)]}{k^2} \, , \qquad (56)$$

$$k = 1, 3, 5 \ldots$$

and plotted in Fig. 21. In the above, $R_{oL}(N)$ is the lens MTF.

For calculation purposes, we will assume that $t = 0.1$ seconds, $n_v = 4$ and $\alpha = 4/3$. Then, Eq. (50) may be written as

$$SNR_D = 3.86 \times 10^9 \frac{C_M}{N} \left(\frac{i_{av}}{\xi_{1w}}\right)^{\frac{1}{2}}. \qquad (57)$$

(isolated object)

For the objects in clutter, Eq. (51) becomes

$$SNR_D = 2.736 \times 10^9 \frac{C_M R_{SF}(N)}{N} \left(\frac{i_{av}}{\beta\xi_1}\right)^{\frac{1}{2}} . \qquad (58)$$

(objects in clutter)

2.10 Threshold Signal-to-Noise Ratio

The equations of Section 2.9 provide a means of determining the signal-to-noise ratio of the displayed image as provided by the sensor. To determine range performance, it is necessary to determine the observer's signal-to-noise ratio requirements as a function of the sensor's signal current and the bar pattern spatial frequency. In this connection, recall that we postulated that bar pattern detectability can be correlated with

58
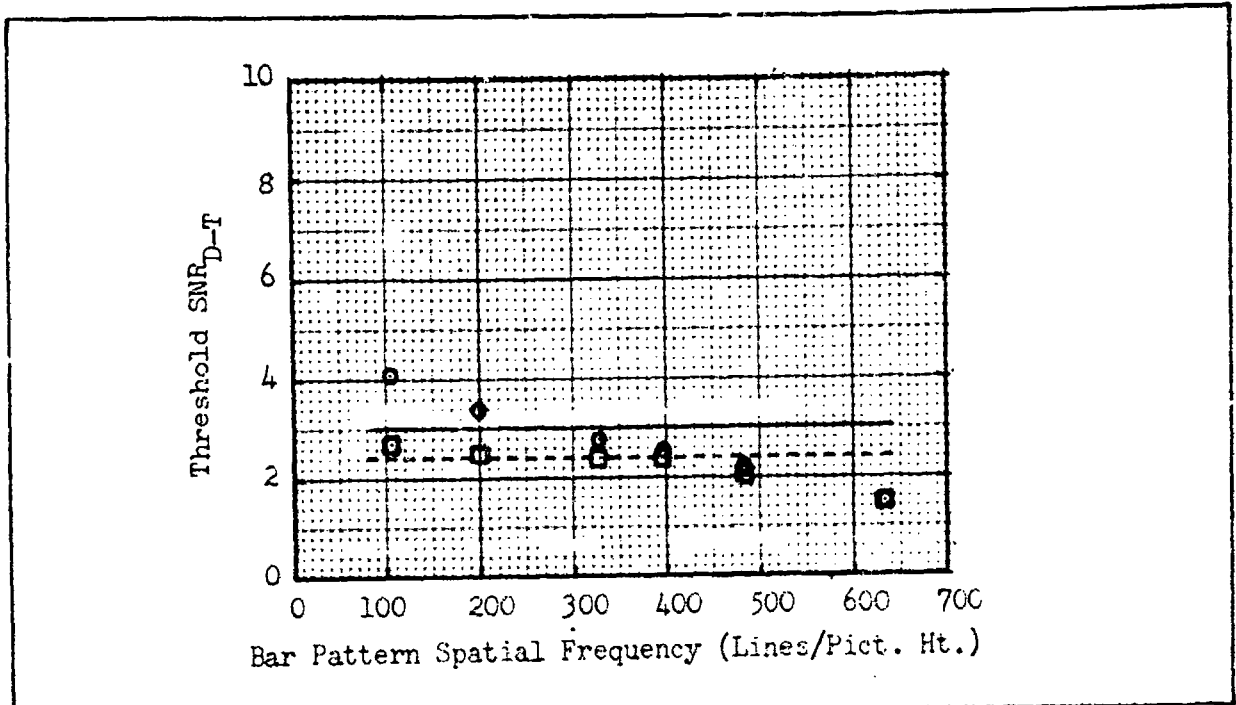
Fig. 22. Threshold Display Signal-to-Noise Ratio vs. Bar Pattern Spatial Frequency for □ Optimal Viewing Distance and ○ 28" Viewing Distance for One Observer.

the detectability of real world targets. The signal-to-noise ratio thresholds for bar patterns have been investigated at length through psychophysical experimentat: with the results summarized below.

In Fig. 22, the experimental data points are shown for the value of the threshold display signal-to-noise ratio as a function of bar pattern spatial frequency for two different observer conditions. In the first case, represented by the circle data points, the observer's sat 28" from the display. As can be seen, there is a progressive drop in threshold signal-to-noise ratio with increase in spatial frequency. The average value is 3.0 and this is the value that the solid curve was drawn through. In the second case, the observer was allowed to vary his distance at each signal-to-noise value in such a manner so as to resolve the highest spatial frequency possible for that signal-to-noise ratio. The data is represented

59

by the squares in Fig. 22. This is the so-called "optimal viewing" case and as can be seen, the threshold value of signal-to-noise ratio is virtually independent of spatial frequency. The average value is 2.4 and this is the value that the dashed curve was drawn through. For calculations, either 3.0 or 2.4 will be used, depending on operator conditions. A threshold value of 3.0 also applies to isolated images.

By "threshold" signal-to-noise ratio, a 50% probability of discerning the pattern is implied, i.e., 50% of the patterns were detected at a given signal-to-noise ratio and 50% were not. In order to increase the probability to near unity, the signal-to-noise ratio required is approximately twice that needed at threshold.

2.11 Minimum Detectable Contrast - Passive Sensors

In the passive system case discussed in Section 2.4, we noted that the primary effect of atmosphere on object detectability, was to degrade the object's contrast with typical results as shown in Fig. 6. Thus, it is most useful to solve the signal-to-noise ratio expression of Eqs. (50 and 51) for contrast. In the special case [numerically evaluated forms of Eqs. (57 and 58)], the equation for the isolated object becomes

$$ C_N = 2.59 \times 10^{-10} \; N \; (\frac{i_{1N}}{i_{av}})^{\frac{1}{2}} \cdot SNR_D \quad , \tag{59} $$

(isolated object)

and for the object in clutter

$$ C_N = 3.65 \times 10^{-10} \; \frac{N}{R_{SF}(N)} \; (\frac{B_{i_1}}{i_{av}})^{\frac{1}{2}} \cdot SNR_D \quad . \tag{60} $$

(object in clutter)

If now, the SNR_D is set equal to its threshold value SNR_{D-T}, then C_M becomes the minimum detectable object contrast, C_{M-MIN}.

To be used in a range calculation, the resolution term, N, must be converted to range using Eq. (49) which is repeated below as

$$R \cong \frac{N w_r}{\varphi y} \quad .$$

(61)

The level of discrimination wanted is obtained by setting w_g, the minimum object dimensions equal to

$$w_r = \frac{w_g}{K_D} \quad ,$$

(62)

where $K_D = 2$ for detection, 8 for recognition and 13 for identification. However, when the Eqs. (59 or 60) are evaluated using range instead of line number N, it becomes specific for a certain object dimension and no other. Hence, it becomes more convenient to plot the equations as a function of N and convert to range as a second step.

The Eqs. (59 and 60) are evaluated for 4 values of signal current and plotted in Fig. 23. It can be seen that the minimum detectable contrast is much lower for the isolated object than for the object in clutter. This is particularly true at the higher line numbers. To relate the Fig. 23 to the detection of a scene object we must first assume scene irradiance
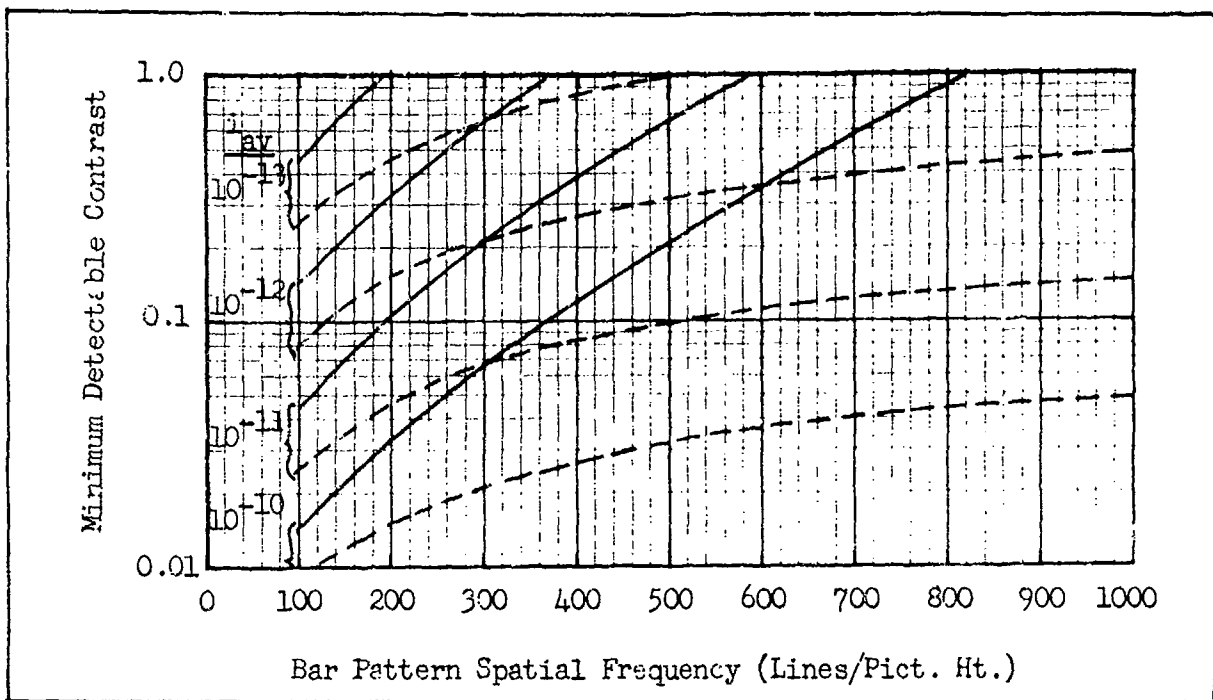
Fig. 23. Minimum Detectable Contrast for (– – –) Isolated Objects
and (———) Objects in Clutter for the Assumed Photoelectron-Noise-
Limited Sensor.

characteristics. In the case where the sun or moon are natural sources,

the scene radiance will be a function of the number of air masses through

which the source radiance must pass as shown in Fig. 24. Knowing the number

of air masses, the scene irradiance can be approximated from Figs. 25 and

26 which are taken from Ref. (2). From these figures, we can also

obtain the radiometric responsivity for a typical S-25 photocathode which

is seen to be 2.34×10^{-2} Amperes/Watt on the average over the 0.4 to 0.85

micron spectral band. With this value of responsivity, σ, the signal current

vs scene irradiance characteristic can be obtained from the relation

$$ i_{av} = \frac{\sigma A \rho_{av} H_s}{4T^2} \tag{63} $$

Sun or
Moon

δ

Optical Air Mass	δ (deg)
m = 1	0
m = 2	60.0
m = 3	70.5
m = 4	75.5
m = 5	78.5

P = 760 mm pressure

W = 2.0/cm water vapor*

D = 300 dust particles/cm^3

Ozone = 0.28 atmo - cm

* per unit of optical air mass

71-0530-V-90
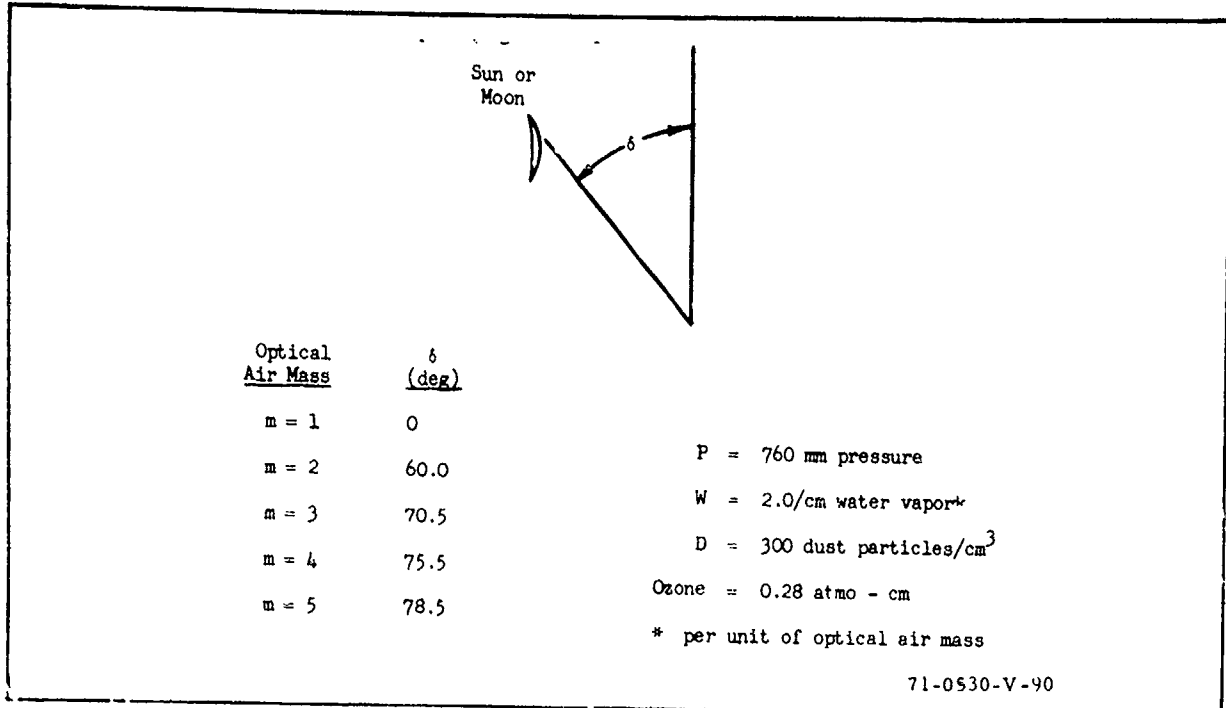
Fig. 24.   Optical Air Mass vs Source Declination.

	FULL MOON PLUS AIRGLOW			0.3 FULL MOON PLUS AIRGLOW		
	1 air mass	2 air masses	3 air masses	1 air mass	2 air masses	3 air masses
Natural Illuminance fc	1.532×10^2	1.228×10^2	1.004×10^2	4.602×10^3	3.696×10^3	3.013×10^3
Natural Irradiance W/m^2	1.066×10^3	8.718×10^{-4}	7.309×10^{-4}	3.237×10^{-4}	2.624×10^4	2.199×10^4
Radiant Sensitivity A/m^2	2.537×10^5	2.042×10^5	1.676×10^5	7.063×10^6	6.146×10^6	5.04×10^6
Radiometric Responsivity A/W	2.379×10^2	2.343×10^2	2.294×10^2	2.367×10^2	2.342×10^2	2.291×10^2
Luminous Sensitivity A/lm	1.983×10^{-4}	1.983×10^{-4}	1.983×10^{-4}	1.983×10^4	1.983×10^4	1.983×10^4
Correction Factor t_{pc} illuminance basis / t_{pc} irradiance basis	1.287	1.281	1.277	1.279	1.281	1.274

Fig. 25.   Relationship between Radiometric and Psychometric Quantities
with an S-25 Photocathode for 1.0 and 0.3 Full Moon.

63

	0.1 FULL MOON PLUS AIRGLOW			0.03 FULL MOON PLUS AIRGLOW		
	1 air mass	2 air masses	3 air masses	1 air mass	2 air masses	3 air masses
Natural Illuminance fc	1.539×10^{-3}	1.22×10^{-3}	1.011×10^{-3}	4.672×10^{-4}	3.766×10^{-4}	3.089×10^{-4}
Natural Irradiance W/m^2	1.087×10^{-4}	8.82×10^{-5}	7.408×10^{-5}	3.336×10^{-5}	2.724×10^{-5}	2.3×10^{-5}
Radiant Sensitivity A/m^2	2.567×10^{-6}	2.061×10^{-6}	1.693×10^{-6}	7.832×10^{-7}	6.317×10^{-7}	5.211×10^{-7}
Radiometric Responsivity A/W	2.363×10^{-2}	2.336×10^{-2}	2.285×10^{-2}	2.347×10^{-2}	2.319×10^{-2}	2.266×10^{-2}
Luminous Sensitivity A/lm	1.983×10^{-4}	1.983×10^{-4}	1.983×10^{-4}	1.983×10^{-4}	1.983×10^{-4}	1.983×10^{-4}
Correction Factor $\dfrac{i_{pc}\ \text{illuminance basis}}{i_{pc}\ \text{irradiance basis}}$	1.278	1.261	1.273	1.2716	1.2713	1.2635

Fig. 26.   Relationship between Radiometric and Psychometric Quantities with an S-25 Photocathode for 0.1 and 0.03 Full Moon.

where A, the effective photosurface area is taken to be $7.68 \times 10^{-4}\ m^2$, ρ_{av}, the average scene reflectivity is either 1.0 or 0.3, H_s is the scene radiance in Watts/m^2, and the T-stop is taken to be 1.58. The result is plotted in Fig. 27. Typical scene irradiances are also shown in this figure for various moon conditions assuming three air masses.

Next, we plot the object contrast as a function of range for a sea level meteorological visibility of 10 n. miles and a sky-to-ground ratio of 4 in Fig. 28. Two values of inherent image contrast of 100% and 30% are shown. Then, the minimum detectable contrast curves of Fig. 23 are converted to range using Eq. (61 and 62) and by assuming an object width of 8', a discrimination factor K_D of 2 and a field of view, φ_y, of 0.1 radians (5.73°) in the vertical. The converted results are plotted for two values of signal current of 10^{-10} and 10^{-12} Amperes on the Fig. 28. The threshold
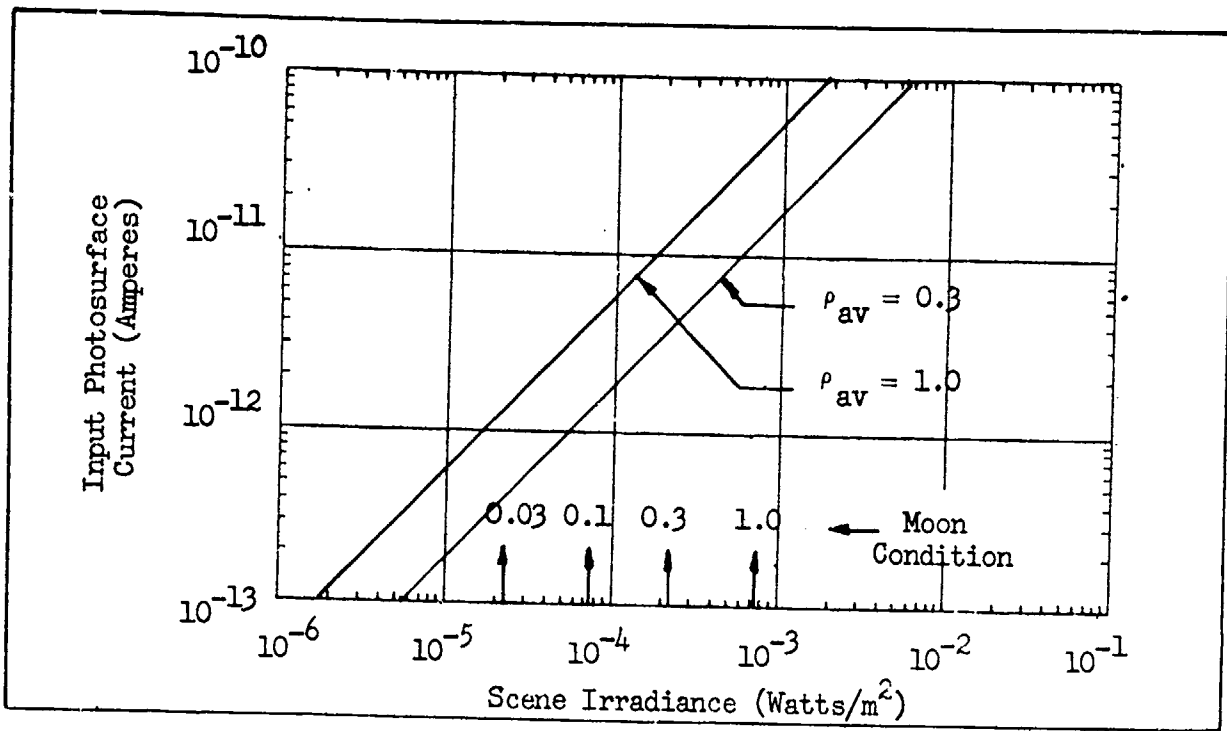
Fig. 27.   Input Photosurface Current vs Scene Irradiance for a Typical
S-25 Photosurface with T/1.58 Lens and Two Scene Reflectivities
of $\rho = 0.3$ and 1.0.
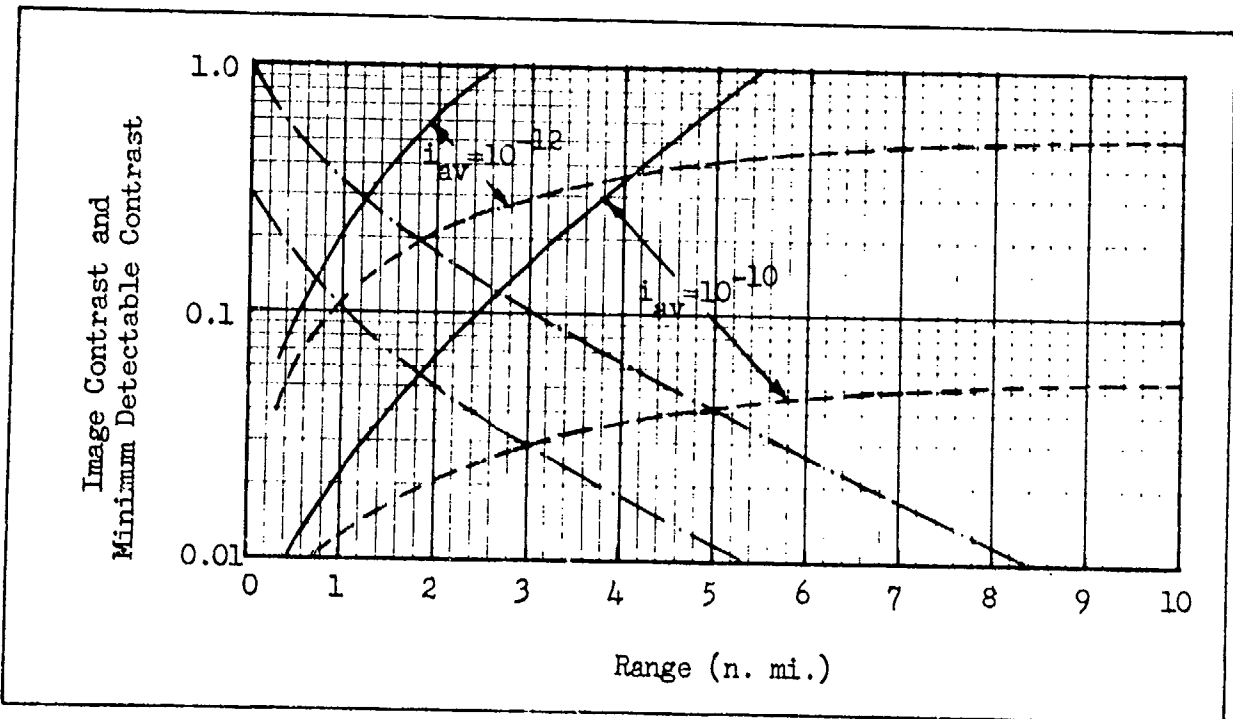
Fig. 28.   Minimum Detectable Contrast for (——) Objects in Clutter and
(- - -) Isolated Objects and (-·-) Image Contrast as a Function
of Range for the Assumed Sensor. Meteorological Range is 10
n. miles and Sky-to-Ground Ratio is 4. Object is 16x8 feet.

65

Input Photocurrent (Amps)	Object Contrast	Threshold Detection Range (n.mi.)	
		Object in Clutter	Isolated Object
10^{-12}	100%	1.25	1.82
10^{-10}		2.65	4.95
10^{-12}	30%	0.7	0.95
10^{-10}		1.85	3.05

Fig. 29.   Threshold Detection Range as Functions of Input Photocurrent and Modulation Contrast for the Assumed Passive Sensor, Atmospheric Visibility and Scene Object.

detection range is then determined by the intersections of the minimum

detectable contrast curves and the image contrast curves. The results are

summarized in Fig. 29. Again, note that isolated objects can be detected

at considerably longer range particularly at the higher signal currents.

Recall that the signal current can be related to scene irradiance by curves

of the form of Fig. 27.

2.12 Minimum Detectable Scene Radiance - Active Sensor

For the active sensor case, the primary effect of atmosphere is to

attenuate the image irradiance although, as we have seen, the received image

contrast may be somewhat reduced depending upon the object's location in

the gated range and the meteorological visibility. In any event, since

image irradiance is the primary factor being limited by atmosphere, it is

most appropriate to solve the signal-to-noise ratio equation for image

irradiance or some related quantity.

To proceed, we note that the input photocathode current may be written as

$$i_{av} = \pi \sigma A N_{av}/4T^2 \tag{64}$$

by analogy to Eq. (63) if N_{av}, the apparent scene radiance of Eq. (19) is equal to $\rho_{av} N_s$. This is approximately the case if the object and its background are diffuse such that

$$N_{av} = (\frac{\rho_o + \rho_b}{2}) N_s$$

$$= \rho_{av} N_s \tag{65}$$

In the graphical solution to follow, N_{av} will be plotted as a function of range for a number of average object and background reflectivities.

Next, we solve Eqs. (57 and 58) for N_{av} using the Eq. (65) as

$$N_{av-min} = \frac{4T^2 \varepsilon_{1w}}{\pi \sigma A C_M^2} [\frac{N \cdot SNR_{D-T}}{3.86 \times 10^9}]^2 \tag{66}$$

(isolated object)

and

$$N_{av-min} = \frac{4T^2 \beta \varepsilon_1}{\pi \sigma A C_M^2} [\frac{N}{R_{SF}(N)} \cdot \frac{SNR_{D-T}}{2.74 \times 10^9}]^2 \tag{67}$$

(objects in clutter)
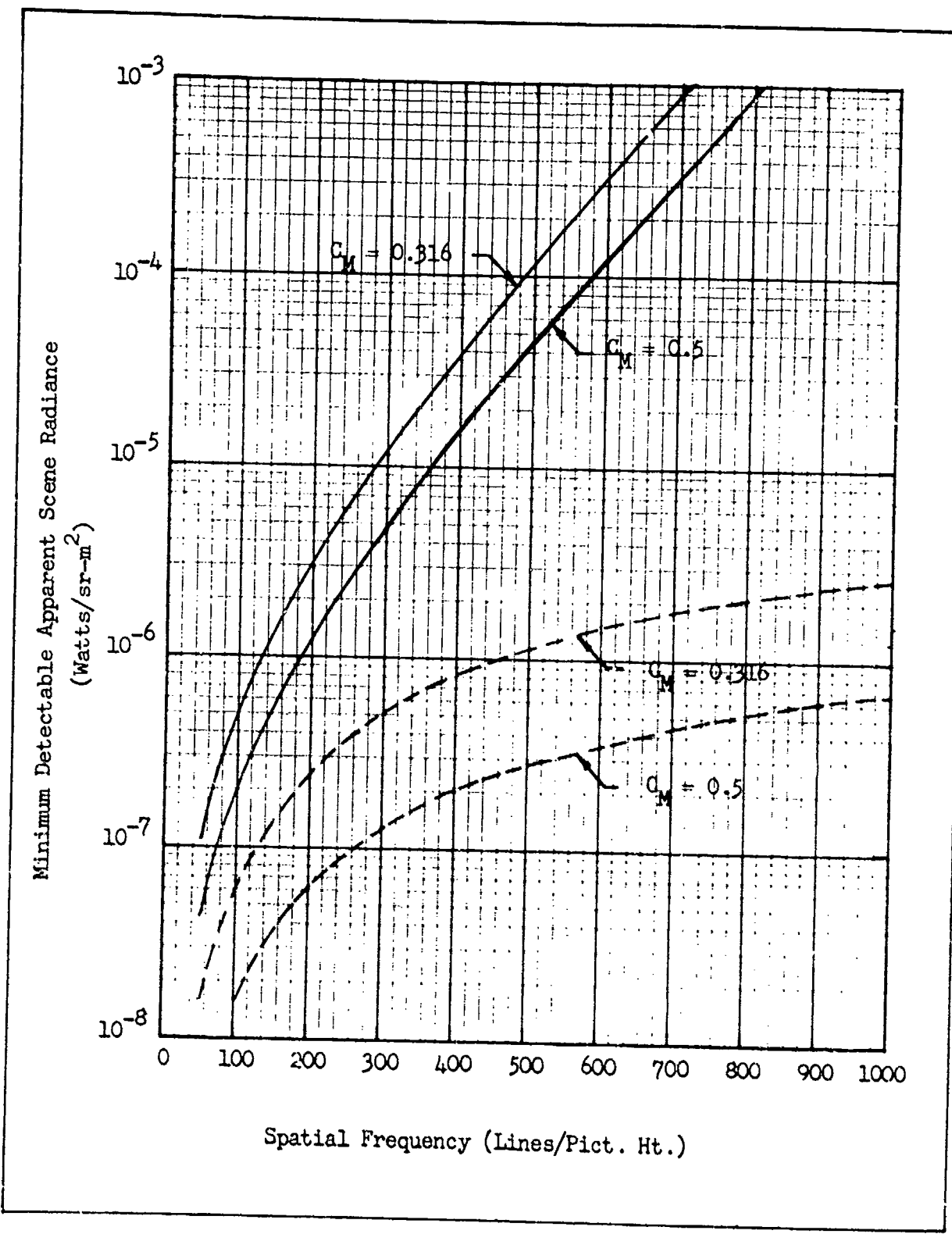
Fig. 30. Minimum Detectable Apparent Scene Radiance vs Bar Pattern
Spatial Frequency for the Assumed Sensor with (- - -) Isolated
Scene Objects and (——) Scene Objects in Clutter.

68
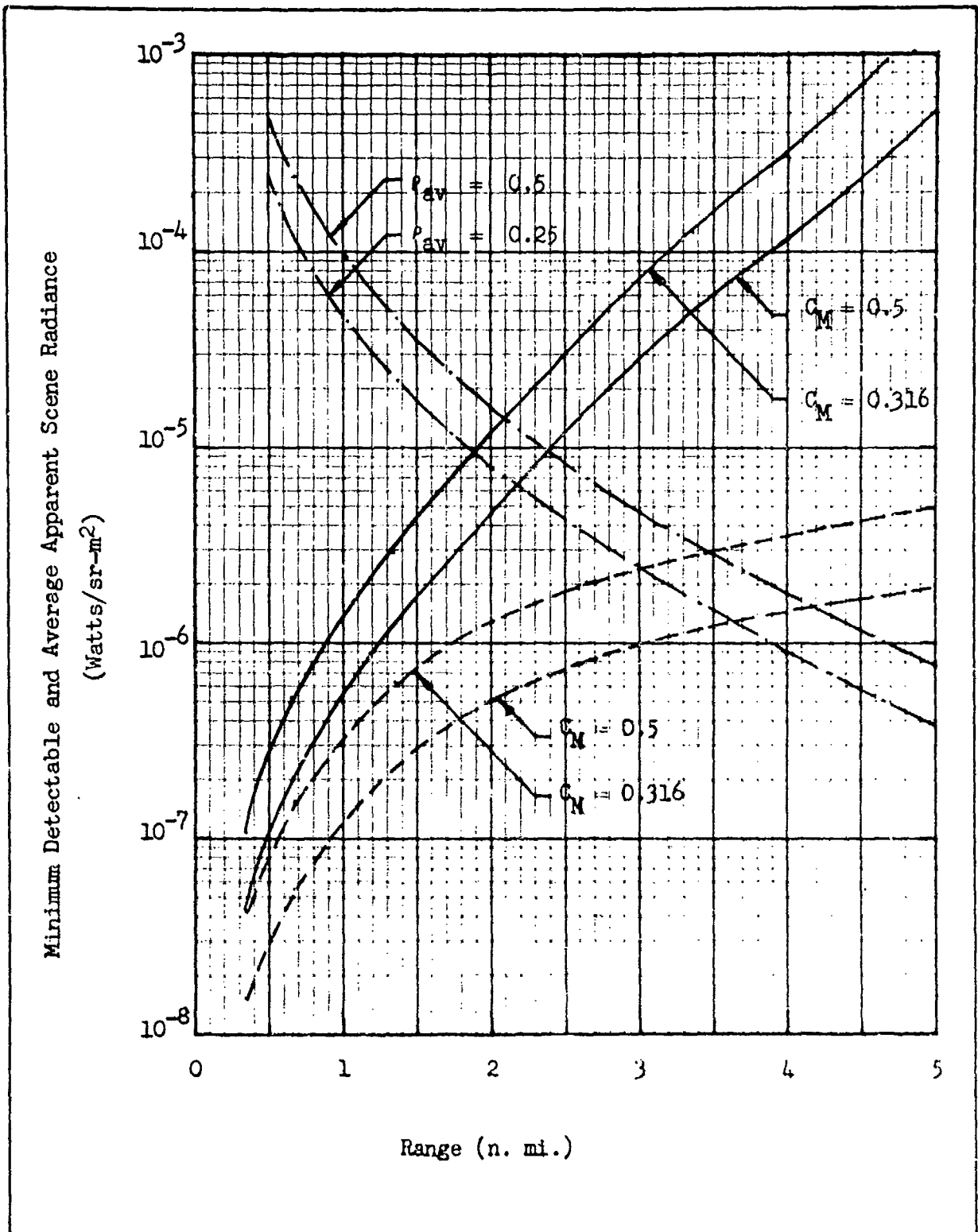
Fig. 31.   Minimum Detectable and Average Apparent Scene Radiance vs
            Range for the Assumed Active Sensor with 40 Watt Source,
            10 n. mi. Visibility and ⌐   8' Scene Object. (-.-)
            Scene Radiance, (--) Iso⌐   . Object, (—) Object in Clutter.

Average Scene Reflectivity	Object Contrast	Threshold Detection Range (n.mi.)	
		Object in. Clutter	Isolated Object
0.5	31.6%	2.1	3.45
	50 %	2.75	3.65
0.25	31.6%	1.75	3.0
	50%	2.18	3.25

Fig. 32.   Threshold Detection Range as Function of the Average Scene Reflectivity and Modulation contrast for the Assumed Active Sensor, Radiation Source Meteorological Visibility and Scene Object.

These equations are plotted in Fig. 30 for a sensor of responsivity 15 mA/Watt. Again, note the much greater detectability of the isolated object. Next, the apparent scene radiance is plotted in Fig. 31, for scene reflectances of 0.5 and 0.25 and a meteorological visibility of 10 n. miles using Eq. (15). The field of view was 5.7^o by 7.6^o or .0133 sr. Also plotted are the minimum detectable apparent scene radiances for the isolated objects and the objects in clutter. As before, threshold range is obtained from the intersections between the minimum detectable and the apparent scene radiances. The results, for the case considered are summarized in Fig. 32.

The minimum detectable apparent scene radiance for recognition of the 8' x 16' object is plotted for the conditions above and $\rho_{av} = 0.5$ and C_M 0.5 in Fig. 33. Also shown is the same quantity for detection. The recognition range at threshold is seen to be 0.97 n. miles as opposed to 2.38 n. miles for detection of a cluttered object.
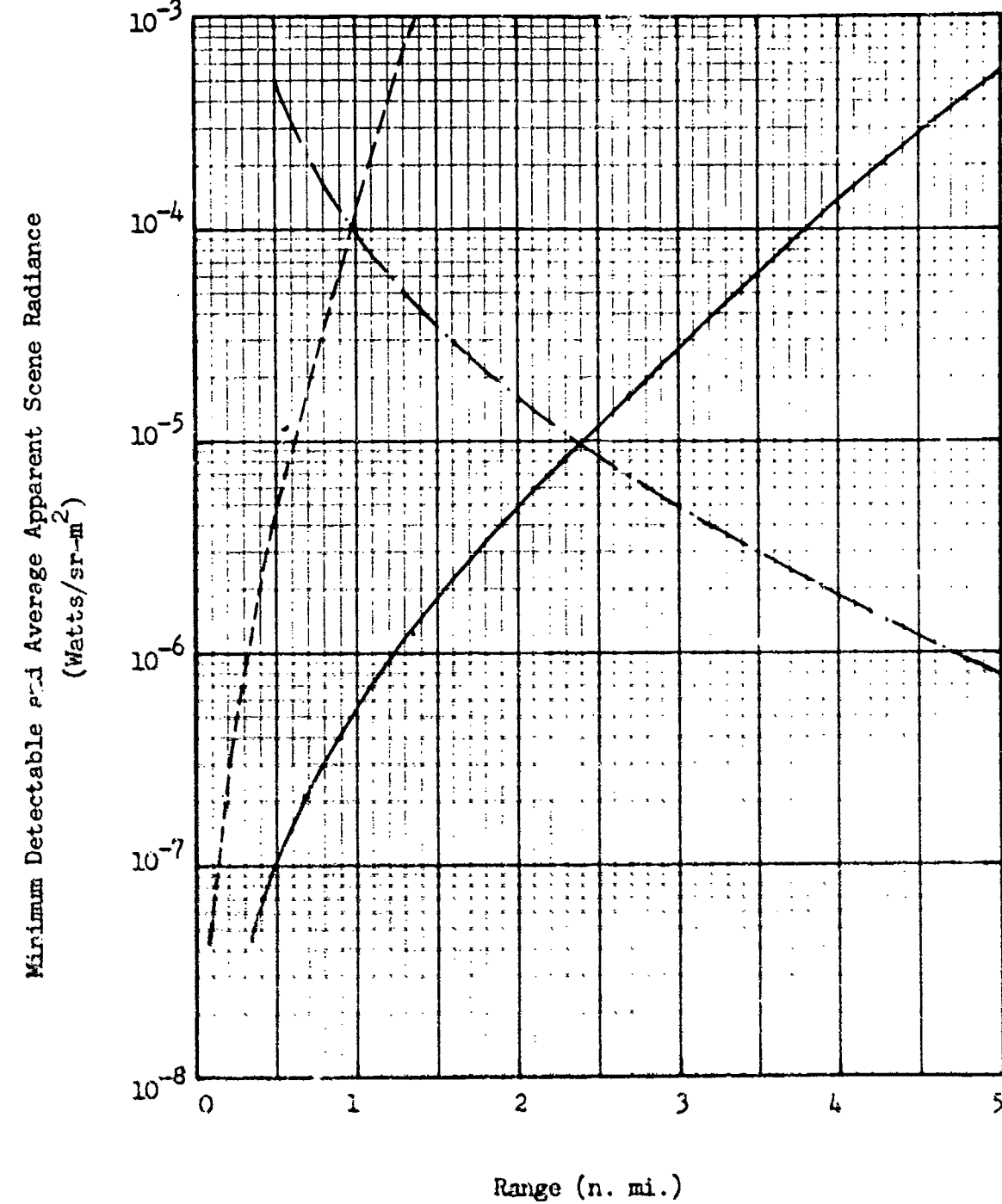
Fig. 33. Minimum Detectable Scene Radiance for (——) Detection and (— — —) Recognition and (— · —) Apparent Scene Radiance vs Range for $C_M=0.5$ and $\rho_{av} = 0.5$. Visibility is 10 n. mi. and Object is 16' x 8'.

3.0 Analytical Model Up-Date

In the previous Performance Synthesis Study Report, (Ref. 2), an analytical model for sensor prediction was developed and it was shown that good agreement between measured and predicted results were obtained. However, the model did differ in some respects with that developed by Schade[8]. These differences are mainly conceptual and have minor impact on sensor predictions, i.e., the numerical results calculated with either model are nearly identical. However, in order to obtain a closer agreement between investigators and to make available a wider body of literature and data couched in similar if not identical terminology, it has been decided to adopt many of the features of Schade's analysis. Neither the previous model nor that of Schade can be considered to be completely verified but both are adequate for first order analysis.

3.1 Elementary Prediction Model

We will first consider the very simple imaging geometry of Fig. 34 The image of the scene in this case consists of a small rectangle of area, a, amid a uniform background. This rectangle may be viewed either directly by the eye or through the auxiliary electro-optical sensor as shown. Suppose first that the eye is viewing the image directly using light that is emitted or reflected from it and its background. Photons received from the scene may be considered noiseless. The lens degrades the signal from the scene due to its finite aperture but does not add noise. However, the retinal photon-to-sensory impulse conversion process is

73
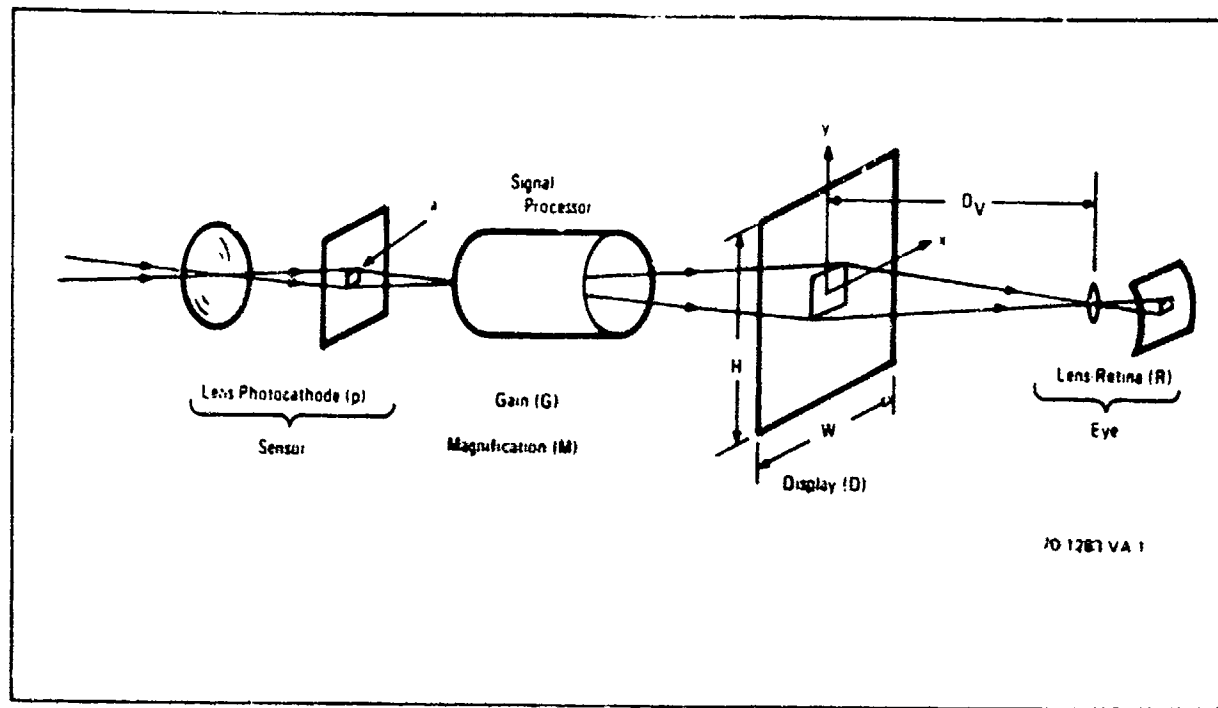
Fig. 34. Electro-Optical Imaging Process

considered noisy and thus, a signal-to-noise ratio is established at the
output of the retina which inherently limits the detectability of scene
objects.

In viewing the object indirectly through the auxiliary sensor, the
scene and lens are again considered noiseless and once again, th. photon-to-
electron conversion process is considered noisy. An image signal-to-noise
ratio is therefore established at the output of the sensor's photo-surface.
This image is then passed to the signal processor whose main purpose is to
amplify and magnify the signals and noises alike. If the signals are not
further degraded by the finite apertures of the processor or the display
and if the processor is noise-free, then the signal-to-noise ratio of the
image on the display will be identical to that of the input photosurface.
Furthermore, if the gain and magnification of the signal processor and

74

display combination is sufficient so that the observer's eye is neither light level nor image size limited, then the image's signal-to-noise ratio at the output of the eye's retina will be identical to that on the display and in turn to that at the output of the sensor's photo-surface. This condition can be achieved in practice for a range of image sizes, signal amplifications, apertures, display luminances, image magnifications and observer viewing distances. In many other cases, the noise added within the auxiliary sensor's signal processor will exceed that generated in the primary photoprocess but the other conditions are such that the signal-to-noise ratio of the displayed image is essentially identical to that at the retina's output.

In general, the signal-to-noise ratio which limits the images detectability may be that generated primarily by the sensor alone, or that generated primarily by the retinal photoprocess alone or that generated by a combination of the auxiliary sensor and the retinal photoprocess. In any experiment, it is important to distinguish between these various possibilities.

In 1932, Barnes and Czerny[9] suggested that the photon imaging and conversion process could be subject to statistical fluctuation. This notion was mathematically formulated by de Vries[10] in 1943 and further modified by Schade as follows. If the average number of photoelectrons generated in the photoprocess by an image of uniform amplitude and area, a, is $\bar{n}_o$ and if the average number generated by an equivalent area containing only background is $\bar{n}_b$, then the signal $\Delta\bar{n}$ is equal to

$$\Delta\bar{n} = \bar{n}_o - \bar{n}_b = (\dot{\bar{n}}_o - \dot{\bar{n}}_b) \, at, \qquad (68)$$

where $\dot{\bar{n}}$ is the average rate of photoelectron generation per unit area and time. The noise associated with the inherent fluctuations in the photoprocess was assumed to follow the Poisson probability distribution law which infers that the fluctuations have a standard deviation equal to the square root of the average number photoconverted in the sampling area and period. For the case of an object imaged against a uniform background, the mean square noises from each are assumed to be the average of their sum in quadrature so that the image signal-to-noise ratio becomes

$$SNR_I = (\bar{n}_0 - \bar{n}_b)/[(\bar{n}_0 + \bar{n}_b)/2]^{\frac{1}{2}}$$

$$= (\dot{\bar{n}}_0 - \dot{\bar{n}}_b)(2at)^{\frac{1}{2}}/[(\dot{\bar{n}}_0 + \dot{\bar{n}}_b)]^{\frac{1}{2}} \quad , \tag{69}$$

which is the model which we shall use hereafter. De Vries further postulated that to be liminally detectable (with 50% probability) that the SNR_I must equal or exceed some threshold constant SNR_T. This postulate was verified, or, at least, made reasonable by Rose[11] using noisy photographic imagery. Rose also showed that this simple model could be fit to the Blackwell[12] disk detection data for the unaided eye over a range of light levels. We must note, however, that in the noisy photographic case, the image signal-to-noise ratio is that inherent in the photograph which is separate and distinct from a signal-to-noise ratio established by the observer's retinal photoprocess. In viewing the photographs, the observer's eye-brain combination is usually operating well above any inherent thresholds as may be set by the eye's photoconversion or brain interpretation process, temporal or spatial integration capability or by their apertures. On the

other hand, if these other effects are taken into account, the threshold levels as set by the retinal photoprocess will be found to be very much like those set by any other photoprocess. Thus, tests made with noisy imagery at light levels and of spatial detail above eye thresholds should apply to the eye's own threshold over a reasonable range.

Our initial concern will be with image signal and noise levels which are substantially above any eye thresholds due to inherent accuity or light limits. Instead of noisy photographic imagery, noisy televised test imagery will be employed. In viewing such imagery, the condition that the test imagery signal and noise levels exceed the eye-brain thresholds can be readily achieved by permitting the observer to adjust his viewing distance and the display's brightness and contrast at will. However, in most of the experiments reported below, viewing distances and other parameters will be fixed in any given case and then varied to show the effect of the observer's eye limitations as appropriate.

For Eq. (69), it is assumed that the eye-brain can spatially integrate over the entire image area, a, for a constant integration period t. It is further assumed that the eye compares the area, a, containing signal, with some comparison area of the same size containing background but no signal. Before proceeding, we will define image modulation contrast C_M specifically as

$$C_M = \Delta \bar{\dot{n}} / [(\bar{\dot{n}}_0 + \bar{\dot{n}}_b)]$$

$$= \Delta \bar{\dot{n}} / 2\bar{\dot{n}}_{ave} , \tag{70}$$

so that Eq. (69) becomes

$$SNR_T = (at)^{\frac{1}{2}} \, 2 \, C_M \, (\dot{\bar{n}}_{ave})^{\frac{1}{2}} \quad . \tag{71}$$

As our next step, we note that the auxiliary sensor may be limited not only by photoconversion noise but by noises generated internally within the system. If these added noises, referred to the output of the photosurface, result in a photoelectron count in the signal (or sampling area) of $\dot{n}_s$ and its equally sized comparison area, then Eq. (71) becomes

$$SNR_I = (at)^{\frac{1}{2}} \, \frac{2 \, C_M \, (\dot{\bar{n}}_{ave})}{[\dot{\bar{n}}_{ave} + \dot{\bar{n}}_s]^{\frac{1}{2}}} \quad . \tag{72}$$

Suppose further that $\dot{\bar{n}}_s \gg \dot{n}_{ave}$ which implies that the auxiliary sensor is limited by internally generated system noise rather than by photoconversion noise, then Eq. (72) simplifies to

$$SNR_D = (at)^{\frac{1}{2}} \, \frac{2 \, C_M \, (\dot{\bar{n}}_{ave})}{(\dot{\bar{n}}_s)^{\frac{1}{2}}} \quad . \tag{73}$$

The above equation is designated SNR_D with the subscript I of Eq. (72) changed to D to imply that the image signal-to-noise ratio is referenced to the auxiliary sensor's display rather than the output of the input photocathode. This is a convenience when observer eye effects are to be taken into account.

Continuing, we write the photoelectron rates as

$$\dot{n} = \frac{i}{eA} \quad , \tag{74}$$

where i is the photocurrent in Amperes, e is the charge of an electron in Coulombs and A is the total effective photosurface area in m^2. Combining Eqs. (73 and 74)

$$SNR_D = [t(\frac{a}{A})]^{\frac{1}{2}} \frac{2 C_M i_{ave}}{[e i_s]^{\frac{1}{2}}} \quad . \tag{75}$$

Next, the numerator and denominator of Eq. (75) are multiplied by $2 \Delta f_V$, the video bandwidth in Hz, so that

$$SNR_D = [2 t \Delta f_V (a/A)]^{\frac{1}{2}} [\frac{2 C_M i_{ave}}{(2 e i_s \Delta f_V)^{\frac{1}{2}}}] \quad . \tag{76}$$

Those familiar with the analysis of television equipments will recognize the second bracketed term as the video signal-to-noise ratio SNR_V, i.e.,

$$SNR_D = [2 t \Delta f_V (a/A)]^{\frac{1}{2}} \cdot SNR_V \quad . \tag{77}$$

This relationship between the image signal-to-noise ratio on the display and the signal-to-noise ratio as measured in the video channel was originally suggested by Coltman and Anderson[13] and provides a very convenient method for generating noisy test imagery for use in psychophysical experiments for the purpose of determining detection thresholds as shown in Section 5. It should be noted that the above equation only holds for images which are unlimited by finite sensor apertures and applies only to isolated rectangular images whereas in practice, it is more common to employ periodic

79

test patterns.

These test patterns take various forms from sine wave patterns, to bar pattern wedges, to bursts of bar patterns. Whatever their form, the notion is to project patterns of various spatial frequencies onto the sensor. Then, an observer is asked to determine the pattern of highest spatial frequency which can be just barely detected as the pattern's signal-to-noise ratio is varied by increasing or decreasing its irradiance. The resolution so measured is called the sensor's "limiting resolution", and it is plotted versus the pattern's highlight irradiance.

The limiting resolution versus photocathode irradiance characteristic is now used by nearly all the major sensor manufacturers to specify and compare the performance of their products with others. Test procedures though not standardized have come to be an accepted if not a thoroughly reliable method of comparison. The measurements which are subjective and statistically variable, are usually made by a single observer in a very limited number of trials and using test patterns of widely different parameters. Observers must, of course, be experienced. The evaluation of sensors in this manner can be extremely costly — particularly where new developmental sensors or combinations of sensors, such as television pickup tubes with cascaded intensifiers, are involved. Rosell[14] found that, given certain data of the type ordinarily supplied by sensor manufacturers, the limiting resolution versus absolute irradiance level could be calculated with fair-to-good accuracy.

Although the equations above are derived for un isolated rectangular image, it is hypothesized that they also apply to the detection of bar and sine wave patterns on the premise that for pattern detection, we must detect

the presence of a bar. However, the threshold signal-to-noise ratio required to detect a bar in the presence of a number of bars may differ from that needed to detect an isolated bar on a uniform background.

For reasons that will become apparent as we progress, the dimensions of the bar in the bar pattern will be given in terms of the reciprocal distances N_V, N_H where

$$N_H = Y/\Delta y$$

$$N_V = Y/n_V \Delta y \cdot \tag{78}$$

In the above, Y is the total picture height, Δy is the linear dimension of the bar width and n_V is the bar height-to-width ratio. Then, the bar image area relative to the total effective photocathode area is equal to

$$\left(\frac{a}{A}\right) = \frac{n_V \Delta y^2}{\alpha Y^2}$$

$$= \frac{n_V}{\alpha N_H^2} , \tag{79}$$

where N_H is designated the patterns spatial frequency in "lines per picture height". With this result, Eq. (77) becomes

$$SNR_D = [2t \Delta f_V/\alpha]^{\frac{1}{2}} \frac{n_V^{\frac{1}{2}}}{N_H} \cdot SNR_V \tag{80}$$

81

3.2 Effect of Finite Apertures

In the perfect imaging sensor considered heretofore, a point image
on the photocathode is assumed to appear as a point image on the display.
In short, all images are transmitted through the sensor with perfect fidelity.
In real sensors, the images at the display may be distorted in amplitude,
shape, or phase (position), or all three. These distortions are due to
finite imaging apertures such as the objective lens, any fiber-optic face-
plates, geometrical defocusing, electron scanning beams, finite phosphor
particles, electrical bandwidth limitations, etc. The effect of these
apertures is to smear image detail in a manner analogous to the filtering
of electrical signals by electrical filter networks. This analogy can be
put to good use.

To illustrate the effect of apertures, consider the point source
object of Fig. 35(a). Due to diffraction, chromatic and geometric aberra-
tions, and imperfect focusing, the point will be imaged by the lens as a blur.
Similarly, a line source is imaged as a line-spread function as shown in
Fig. 35(b). The line-spread case corresponds most directly to the case
most commonly encountered in communications systems, wherein the signals
vary only in amplitude and time. Where an image is very long in one
dimension compared to the other, it can usually be considered a one-
dimensional image, varying only in intensity and a single spatial dimension.

In any event, we will, for the moment, consider an aperture to be
analogous to a linear electrical filter, except that it may be two-dimensional.
Where two dimensions are involved, we will assume that the two
dimensions are either independent (so that they can be treated separately)
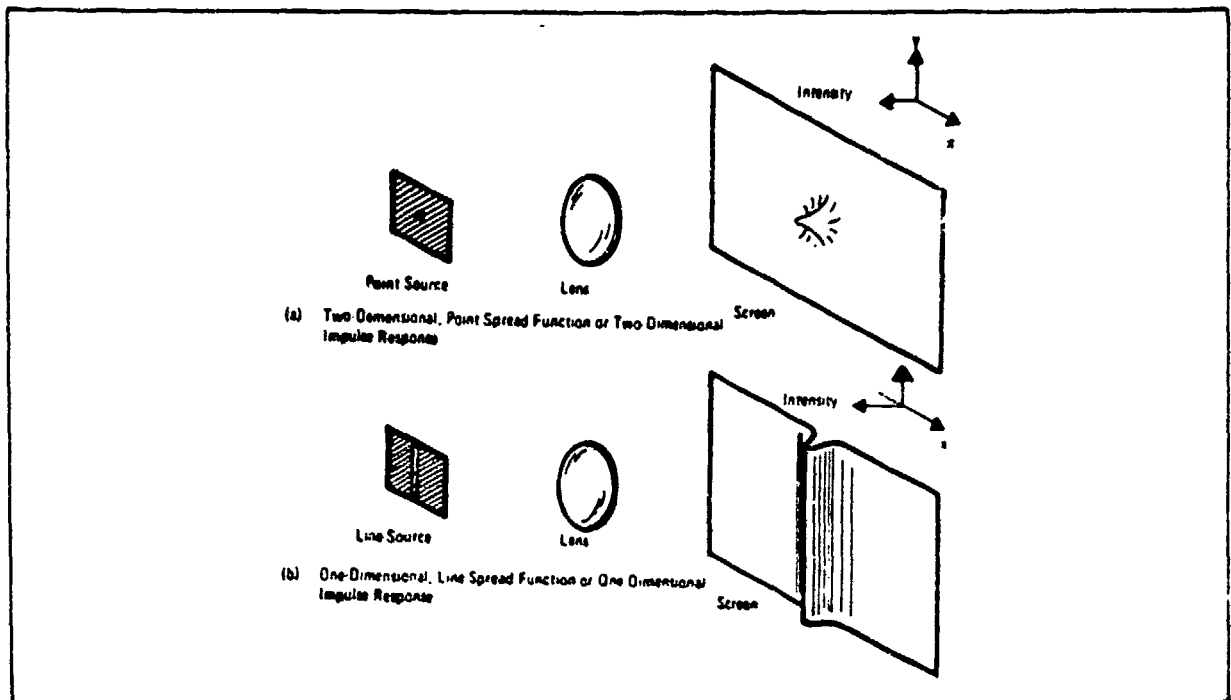
Fig. 35. Point Spread and Line Spread Impulse Responses

or that they possess radial symmetry (so that they become essentially one-dimensional in character). Many of the apertures that appear in nature are found to have a response to several input stimuli acting simultaneously that is identical to the sum of the responses that each stimuli would produce individually. A system of this type is a linear system. The property of linearity leads to considerable simplification in the mathematical description of such phenomena. In particular, it becomes possible to decompose complicated input signals to simpler signals for which the system response is known and then, to find the total response by summing the individual responses in linear combination. Furthermore, we can then use Fourier analysis in which signals are decomposed to sine and cosine waves. The Fourier transform of a function $f(x,y)$ of two independent variables

x and y is given by

$$F(\omega_x, \omega_y) = \mathscr{F}[f(xy)]$$

$$= \iint\limits_{-\infty}^{\infty} f(x,y) \exp[-j(\omega_x x + \omega_y y)]\, dx\, dy \qquad (81)$$

where $\mathscr{F}$ denotes the taking of the Fourier transform, j is the complex operator and ω_x and ω_y are referred to as spatial frequencies.* The transform as defined above is a complex valued function of two independent variables ω_x and ω_y. Given the function $F(\omega_x, \omega_y)$, the original spatial function $f(x,y)$ can be recovered through use of the inverse Fourier transforms ($\mathscr{F}^{-1}$) where

$$f(x,y) = \mathscr{F}^{-1}[F(\omega_x, \omega_y)]$$

$$= \frac{1}{4\pi^2} \iint\limits_{-\infty}^{\infty} F(\omega_x, \omega_y) \exp[j(\omega_x x + \omega_y y)]\, d\omega_x d\omega_y \qquad (82)$$

To be transformable, $f(x,y)$ must satisfy the existence conditions

      a. $f(x,y)$ must be absolutely integrable over the infinite x, y plane.

      b. $f(x,y)$ must have only a finite number of discontinuities and a finite number of maxima and minima in any finite rectangle.

      c. $f(x,y)$ must have no infinite discontinuities.

For real linear systems, transforms must exist. However, some of the idealized mathematical functions created to represent the waveforms of interest will not meet the existence theorems. Fortunately, it is possible, in many cases, to find meaningful transforms that do not strictly satisfy

---

* The spatial frequencies ω_x and ω_y are given by $\omega_x = 2\pi k_x$ and $\omega_y = 2\pi k_y$ where ω_x and ω_y are in radians per mm whereas k_x and k_y are in line pairs per mm.

the existence conditions, but that can be written as the limit of trans-formable functions. The limit of the transform of this new sequence is called the generalized Fourier transform, and these functions can be manip-ulated in the same manner as conventional transforms. The singularity function such as the Dirac delta function, the unit step, etc., are examples which are handled in this manner.

The Dirac delta function which is also known as the unit volume impulse or zero order singularity test function is designated as $\delta_o(x-x_1, y-y_1)$ and has the property of being infinite at $x = x_1$, and $y = y_1$, and zero everywhere else. Also,

$$\int_{-\infty}^{\infty} \delta_o(x-x_1, y-y_1) \, dx \, dy = 1.0 \tag{83}$$

and its Fourier transform is equal to 1.0. The Dirac delta function may be thought of as a point image of infinite amplitude, but finite volume in x, y space and a uniform distribution in spatial frequency space over all frequencies. This frequency distribution is sometimes referred to as a "white" spectrum.

The response of any sensor aperture, be it the lens, photosurface, electron beam or whatever, to the Dirac delta function is designated $r_o(x,y)$ in the space domain and $R_o(\omega_x, \omega_y)$ in the spatial frequency domain. The function $r_o(x,y)$ is known as the aperture's impulse response or point spread function and $R_o(\omega_x, \omega_y)$ is known as the complex steady state frequency response. If either $r_o(x,y)$ or $R_o(\omega_x, \omega_y)$ are known, then the aperture's response to any test signal can be determined, i.e., these functions completely specify the parameters of the aperture.

85
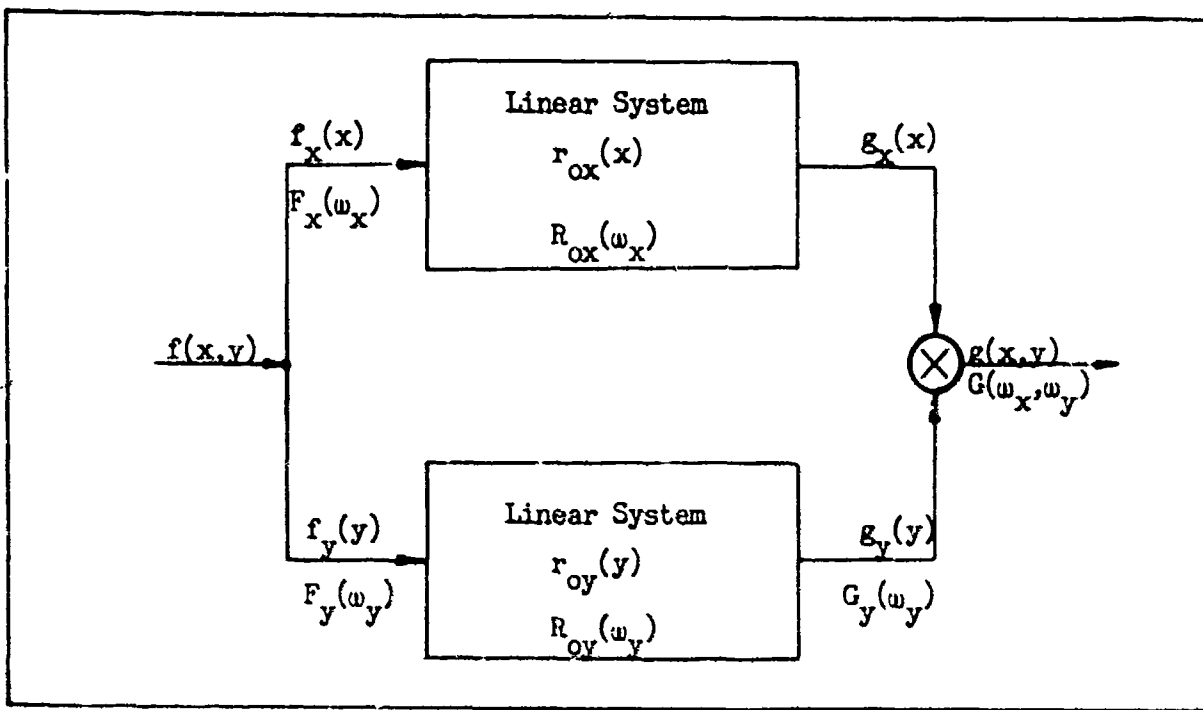
Fig. 36. Signal Processes in a Two-Dimensional System Whose Input Signals and Impulse Responses are Separable Functions of Two Independent Variables.

If the variables x and y are independent and separable we can then draw the block diagram of Fig. 36 to represent the signal processes. The assumption of separability permits us to write the arbitrary function $g(x,y)$ as,

$$g(x,y) = g_X(x) \cdot g_Y(y) \tag{84}$$

and its Fourier transform as,

$$\mathcal{F}\{g(x,y)\} = \mathcal{F}_x\{g(x)\} \cdot \mathcal{F}_y\{g(y)\} \tag{85}$$

Therefore, the transform is separable into a product of two factors, one a function of $f(x)$ only, the second, a function of $f(y)$ only. Thus, the

process of two-dimensional transformation simplifies to a succession of more readily calculated and manipulated one-dimensional transforms.

If ω_x and ω_y are independent variables, then $R_o(\omega_x,\omega_y) = R_o(\omega_x) \cdot R_o(\omega_y)$ and either may be measured through the use of sine wave patterns at the input. The output signal amplitude is then measured and a plot of these amplitudes (as the pattern frequency is varied) represents the magnitude of $|R_o(\omega_x)|$ or $|R_o(\omega_y)|$. Either term is also known as the modulation transfer function (MTF) when the output amplitudes are normalized to its magnitude at zero frequency. In general,

$$R_o(\omega) = |R_o(\omega)| \exp [j \emptyset (\omega)] \qquad (86)$$

Where $\emptyset (\omega)$ represents a phase or position shift and has been designated by the International Commission for Optics (ICO) as the phase transfer function (PTF). The ICO also refers to $R_o(\omega)$, the complex steady state response as the optical transfer function (OTF) which seems only partially appropriate to sensors. The ICO recommends changing the word function to curve when referring to curves representing the functions. Also for specific values of the function at a given frequency, the word function is replaced by factor, e.g., the modulation transfer factor.

MTF is also synonomous with sine wave amplitude response. In the testing of sensors, sine wave amplitude response can be directly measured although the machinery required can be quite complex and costly. Thus, in current practice, it is more usual to employ bar patterns in making tests. The quantity measured is then the square wave amplitude response $R_{SQ}(\omega)$.

If $R_o(\omega)$ is known, then $R_{SQ}(\omega)$ can be determined directly from

$$R_{SQ}(\omega) = Sq(\omega) \cdot R_o(\omega) \tag{87}$$

where $Sq(\omega)$ is the Fourier spectrum of a square wave wavetrain. However, the inverse operation

$$R_o(\omega) \neq \frac{R_{SQ}(\omega)}{Sq(\omega)} \tag{88}$$

cannot be performed because $Sq(\omega)$ is not a well behaved analytic function, but approximations are available[15].

The statement of linearity implies that the system response to any stimulus can be described by the solution to some appropriate set of simultaneous linear differential equations of constant coefficients. The restriction to constant coefficients rules out consideration of linear systems with time or space-varying parameters, but it permits us to apply the principal of super-position.

In general, the linear systems we will deal with are considered to be space and time invariant (sometimes called isoplanatic). By this, it is meant that the system impulse response $r_o(x_1,y_1,\xi,\eta)$ depends only on the distances $(x_1-\xi)$, $(y_1-\eta)$ in which case,

$$r_o(x_1,y_1,\xi,\eta) = r_o(x-\xi, y-\eta). \tag{89}$$

In the case of an imaging system, it is said to be space invariant if the image of a point source changes only in position, but not in functional

88

form, as the image moves about the image plane. In a television sensor, this would imply that corner resolution is the same as center resolution. This is seldom the case, but for analytical purposes, we can divide the image plane into small areas (or isoplanatic patches) within which the system is spatially invariant.

In order to illustrate the effect of finite apertures on image detection, assume that the aperture of concern is one dimensional and that its response $r_0(x)$ to a unit area impulse $\delta_0(x)$ is equal to

$$r_0(x) = \exp{(-x^2/2\alpha^2)}/(2\pi\alpha^2)^{\frac{1}{2}} \tag{90}$$

This equation is known as the Guassian error curve and in form is identical to that used for the normal probability density function. It is also a good approximation to the line spread function of many real optical apertures. This function is plotted in dimensionless coordinates in Fig. 37 . We define the equivalent duration of the impulse response as a rectangle of height equal to $r_0(o)$ and area equal to that under the impulse curve which is given by

$$D_0 = [\int_{-\infty}^{\infty} r_0(x) \; dx]/r_0(o)$$

$$= [2 \pi \alpha^2]^{\frac{1}{2}} \tag{91}$$

This equivalent duration is shown in Fig. 37.

The Fourier transform of the Guassian curve impulse response is itself an error curve, i.e.,

89
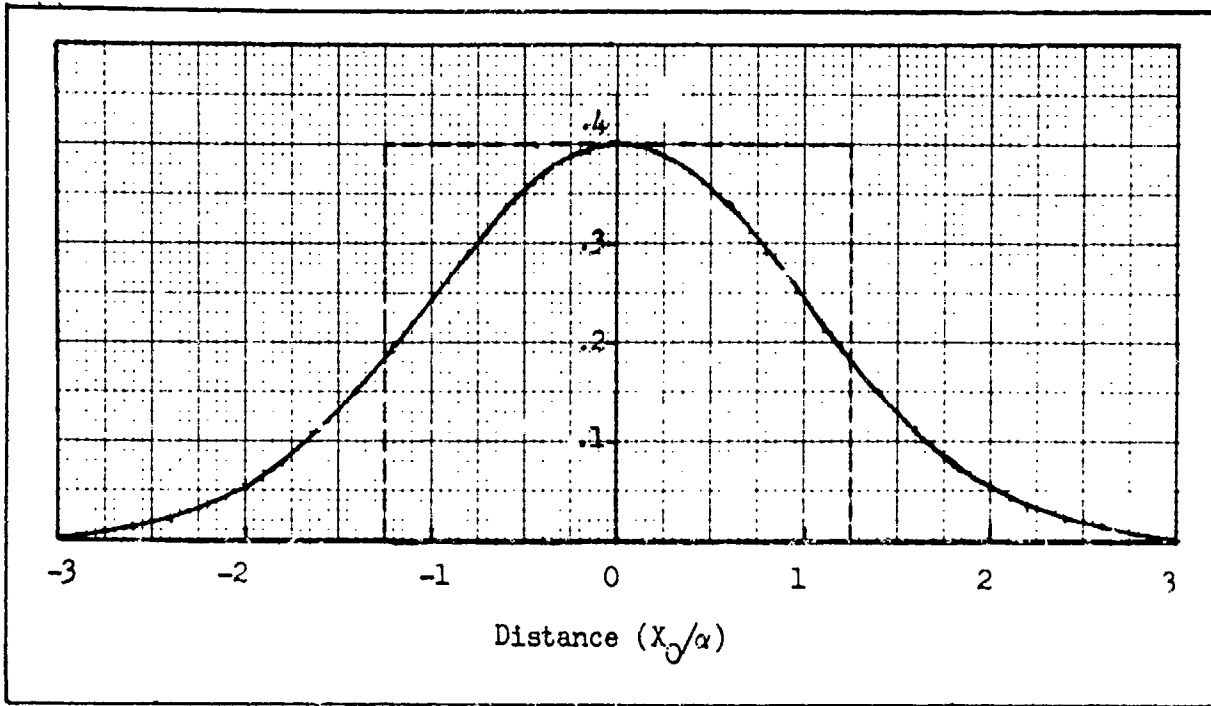
Fig. 37.   Impulse Response of the Error Curves Aperture and
its Equivalent Duration in Dimensionless Coordinates

$$|R_o(\omega)| = \exp(-\alpha^2\omega^2/2) .\tag{92}$$

The error curve frequency response is characterized by zero phase shift so
that the output image is in correct 1:1 spatial correspondence with that
at the input at all frequencies. Then $|R_o(\omega)|$ becomes $R_o(\omega)$ and in
principle, we have sufficient information, knowing either, to find the
apertures response to any input. The error curve frequency response is
shown in Fig. 38 in dimensionless coordinates.

The equivalent bandwidth of the error curve response (not to be
confused with noise equivalent bandwidth to be defined), is defined to be
equal to the width of a rectangle with the same area as the error curve
frequency response. Numerically,

90
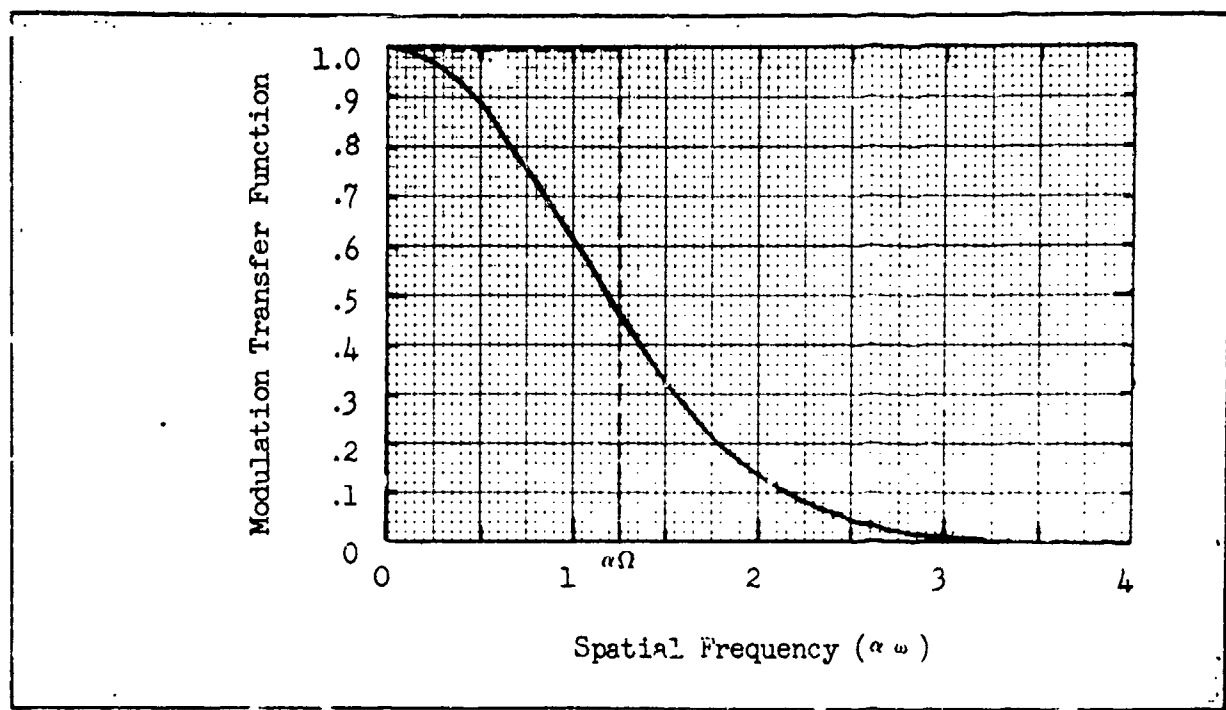
Fig. 38.   Modulation Transfer Function for an Error Curve
            Aperture and its Equivalent Bandwidth in Dimensionless
            Coordinates.

$$\alpha\Omega = (\pi/2)^{\frac{1}{2}} \tag{93}$$

which is also shown in Fig. 38. Comparing Eqs. (91 and 93),

$$D_o = \tau/\Omega \tag{94}$$

Thus, the wider the equivalent bandwidth, the narrower the equivalent
impulse duration and conversely. This is the well-known reciprocal spreading
effect between the space and frequency domain. Also, as the input pulse is
decreased to zero width the equivalent output pulse width decreases only to
that of the equivalent duration of the impulse response and no further.

91

The input impulse is of unit area by definition. The area of the output pulse is also unity as can be seen from Eqs. (90 and 91), i.e.,

$$D_o \cdot r_o(o) = (2\pi\alpha^2)^{\frac{1}{2}} / (2\pi\alpha^2)^{\frac{1}{2}} = 1.0 \qquad (95)$$

This result might have been foreseen because the error curve "filter" is dissipationless. This is often true of sensor apertures.

The unit step function $\delta_{-1}(x)$ is perhaps the second most useful singularity test signal. It is defined by

$$\delta_{-1}(x) = \begin{cases} 0, & x < 0 \\ 1, & x > 0 \end{cases} \qquad (96)$$

and also,

$$\delta_{-1}(x) = \int_{-\infty}^{x} \delta_o(x) \, dx \qquad (97)$$

Similarly, the unit step response of an aperture is given by $r_{-1}(x)$ and can be obtained from

$$r_{-1}(x) = \int_{-\infty}^{x} r_o(x) \, dx \qquad (98)$$

For the error curve aperture

$$r_{-1}(x) = \frac{1}{2} + \frac{1}{2} \operatorname{erf} \frac{x}{(2\alpha^2)^{\frac{1}{2}}} \qquad (99)$$

92
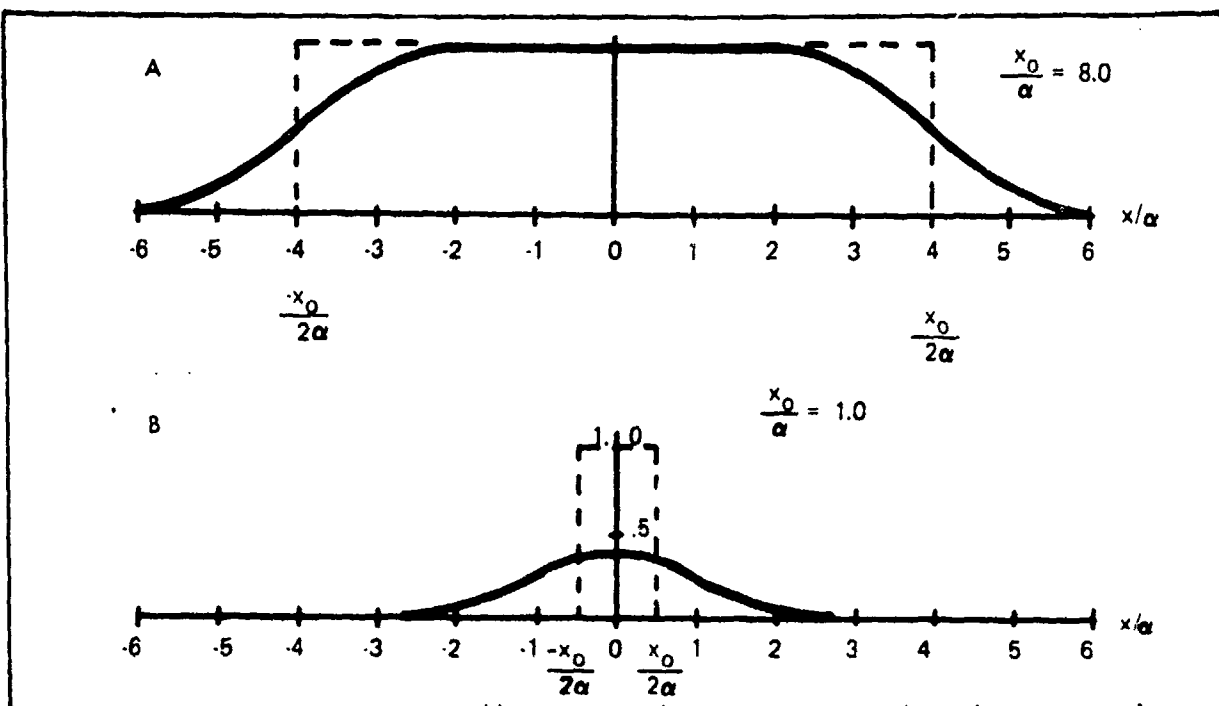
Fig. 39.   Output Pulse (-) for an Error Curve Filter as the Width
of a Unit Amplitude Rectangular Input Pulse (---) Varies

In optical tests the unit step test is similar to the knife edge test.
Suppose next, that the input pulse is a unit area rectangle of width x_0/α.
By superposition, this input can be considered to be described by two
unit-step inputs shifted by $\pm\, x_0/2\alpha$. For this input, the output becomes

$$g(x) = \left[1/2\ \mathrm{erf} \left[\frac{x + x_0/2}{(2\,\alpha^2)^{1/2}} \right] - 1/2\ \mathrm{erf} \left[\frac{x - x_0/2}{(2\,\alpha^2)^{1/2}} \right] \right] \qquad (100)$$

The effect of the error curve aperture on the unit amplitude input pulse
is shown for two cases in Fig. 39. In (a), the effect of the aperture
on a wide input pulse is to merely round its corners. On a narrow input
pulse as shown in (b), the aperture rounds the corners and reduces the
signal amplitude. However, as we have previously noted, area under the
output pulse curve is identical to that under the input.

93

In the elementary detection model, the display signal-to-noise ratio is assumed to be proportional to image area for images of not too large an angular extent, i.e.,

$$SNR_D = [2t(\frac{a}{A})]^{\frac{1}{2}} \frac{2 C_M i_{av}}{(2 e i_{av})^{\frac{1}{2}}} \quad . \tag{101}$$

This equation implies that the eye extends its spatial integration limits to the extent required to fully integrate the signal. As we have observed, a dissapationless aperture, or filter, acting on an aperiodic image alters the image's energy distribution, or volume in the case of a two-dimensional image, under its waveshape. Thus, if the elementary model is used, the conclusion might be that the image's detectability is unchanged but this is not what we would intuitively expect.

Schade[8] proposes the following solution to the dilemma. Suppose the aperture to be infinite such that the object is imaged with perfect fidelity and suppose further that the object's image is of area a_o. Next, suppose the object is imaged by a real lens which enlarges the objects image to a new area, a_L. If the real lens is dissipationless* then it is true that

$$\Delta H_o a_o = \Delta H_L a_L \quad , \tag{102}$$

---

* Ignoring transmission losses which are spatially independent.

94

where ΔH_0 and ΔH_L are the incremental irradiances for the infinite and real apertures respectively. If both irradiances are equally photoconverted, then

$$\Delta i_0 a_0 = \Delta i_L a_L \quad . \tag{103}$$

The SNR_D equation using Eq. 103 becomes

$$SNR_D = [\frac{2t}{eA}]^{\frac{1}{2}} \frac{\Delta i_L a_L}{(2 a_L i_{av})^{\frac{1}{2}}}$$

$$= [\frac{2t}{eA}]^{\frac{1}{2}} \frac{\Delta i_0 a_0}{(2 a_L i_{av})^{\frac{1}{2}}} \tag{104}$$

That is, the signal remains unchanged but because $a_L > a_0$, the noise increases. Observe that the lens aperture did not increase the noise, it merely increased the image area. However, the photoconversion process is noisy and the enlarged image area includes more of the noise. This process is illustrated in Fig. 40 wherein an object's image of width x_0 with an infinite aperture becomes effectively of width $(x_0^2 + \delta_L^2)$ after passing through a real aperture. The quantity δ_L is the noise equivalent impulse diameter to be defined below.

To determine the increase in image dimensions, suppose the test object irradiance is a function $k f(x,y)$ where k is the amplitude of the function at $x,y = 0,0$. Let the area $a_0 = \iint f^2(x,y) \, dx \, dy$ before including the aperture effects. Suppose next that the irradiance function after including the aperture effects is $g(x,y)$ neglecting any constant gains. Then the area, a_L, will be

95
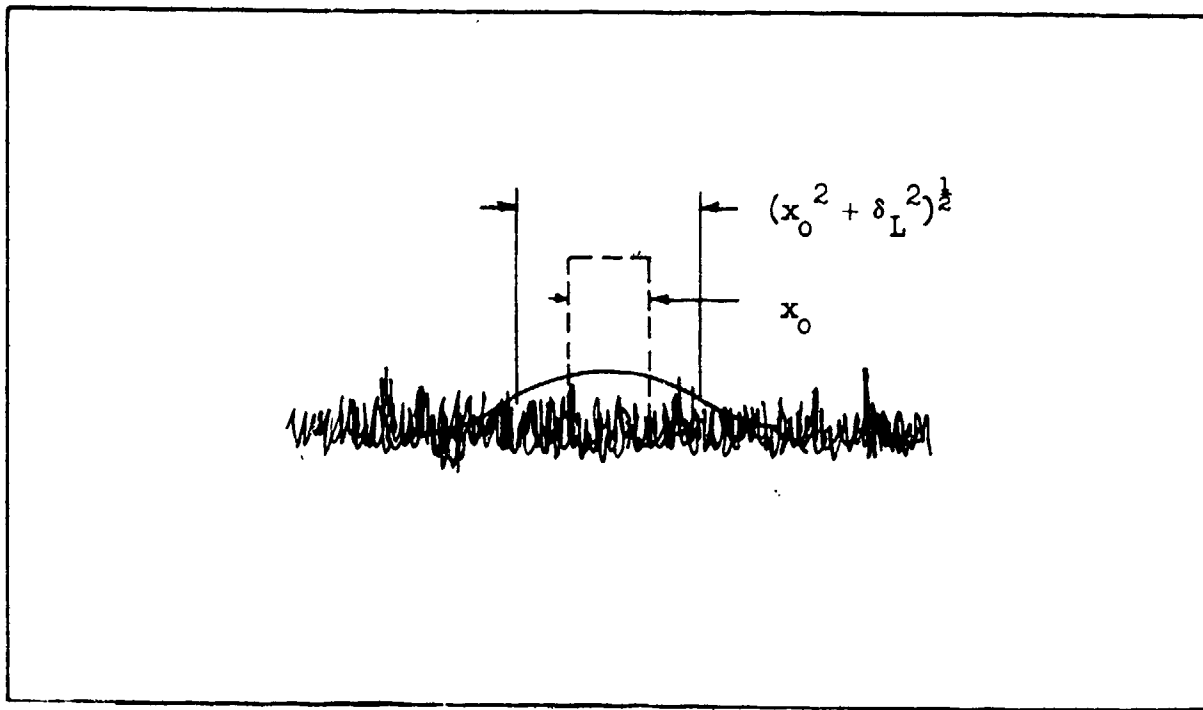
Fig. 40. Noise Increase Process due to Increase of Effective Image Size After Passing through a Finite Aperture Prior to Point of Noise Insertion.

$$a_L = \frac{a_o^2}{\displaystyle\iint_{-\infty}^{\infty} g^2(x,y)\, dx\, dy} \tag{105}$$

The area a_L is designated the noise equivalent sampling area. Also, note that by application of the Fourier Energy Theorem that

$$a_L = \frac{a_o^2}{\displaystyle\iint_{0}^{\infty} G^2(N_x, N_y)\, dN_x\, dN_y} \tag{106}$$

where $G(N_x, N_y)$ is the Fourier transform of $g(x,y)$ when N is a spatial frequency as given by Eq. 45. When the test object

96

is rectangular of dimensions, x_o, y_o, and of uniform amplitude, Schade gives the following useful approximation

$$a_L \cong x_o \ y_o \ (1 + \frac{\delta_L^2}{x_o^2})^{\frac{1}{2}} \ . \ (1 + \frac{\delta_L^2}{y_o^2})^{\frac{1}{2}} \tag{107}$$

where δ_L is the noise equivalent impulse diameter of the aperture assuming the apertures point spread functions are equal, independent and separable in the two dimensions x,y. Numerically,

$$\delta_L = \frac{1}{N_{eL}} = \frac{1}{\int_o^\infty |R_{oL}(N)|^2 \ dN} \tag{108}$$

where $|R_{oL}|$ is the apertures MTF. The quantity N_e has been designated the noise equivalent passband by Schade. With these equations, the SNR_D may be written as

$$SNR_D = \left[\frac{2t}{eA} \cdot \frac{x_o \ y_o}{[1 + (\delta_L/x_o)^2]^{\frac{1}{2}} \cdot [1 + (\delta_L/y_o)^2]^{\frac{1}{2}}} \right]^{\frac{1}{2}} \frac{\lrcorner i_o}{(2 i_{ave})^{\frac{1}{2}}} \tag{109}$$

It should be observed that an MTF prior to the point of a noise generation or insertion, is more serious than an MTF following such noise insertion since in the latter case, the noise is reduced from a white to a finite spectrum.

To account for a finite noise spectrum, we will define a function which is the factor by which an SNR_D computed for a white noise spectrum must be increased to correct for a finite noise spectrum. To illustrate the

processes involved, suppose the image is passed through the lens as above and then passed through a second aperture of MTF, $|R_{o_2}(N)|$, prior to photoconversion. Then, the SNR_D would be

$$SNR_D = \left[\frac{2t}{eA} \frac{x_o y_o}{\left[1+(\delta_L/x_o)^2+(\delta_n/x_o)^2\right]^{\frac{1}{2}}\left[1+(\delta_L/y_o)^2+(\delta_n/y_o)^2\right]^{\frac{1}{2}}}\right]^{\frac{1}{2}} \frac{\Delta i_o}{(2 i_{ave})^{\frac{1}{2}}} \quad (110)$$

where δ_n is the equivalent impulse diameter for the second aperture. If the second MTF followed the phototransducer rather than preceding it, then we must correct for the fact that the photoelectron noise is filtered. The correction factors ζ_x and ζ_y are

$$\zeta_x = \frac{\left[1+(\delta_L/x_o)^2+(\delta_n/x_o)^2\right]^{\frac{1}{2}}}{\left[1+(\delta_L/x_o)^2\right]^{\frac{1}{2}}}$$

$$\zeta_y = \frac{\left[1+(\delta_L/y_o)^2+(\delta_n/y_o)^2\right]^{\frac{1}{2}}}{\left[1+(\delta_L/y_o)^2\right]^{\frac{1}{2}}} \quad (111)$$

Multiplying the right side of Eq. (110) by $\zeta_x \cdot \zeta_y$, we obtain

$$SNR_D = \left[\frac{2t}{eA} \frac{x_o y_o}{\frac{1+(\delta_L/x_o)^2}{\left[1+(\delta_L/x_o)^2+(\delta_n/x_o)^2\right]^{\frac{1}{2}}} \cdot \frac{1+(\delta_L/y_o)^2}{\left[1+(\delta_L/y_o)^2+(\delta_n/y_o)^2\right]^{\frac{1}{2}}}}\right]^{\frac{1}{2}} \frac{\Delta i_o}{(2 i_{ave})^{\frac{1}{2}}} \quad (112)$$

This result can be extended to include any number of apertures in cascade.

98

We turn next to the effect of apertures on periodic test patterns which are aperiodic in the direction along the individual bars and periodic across the bars. The effect of the apertures along the bars may be taken into account by the methods already described although, for bars of large length to width ratio, the effect along the bars can be neglected since it is small relative to the effect in the periodic direction. In the following, the effects along the bars will be neglected. In the aperiodic case, the apertures increased the distance over which the eye integrates such that the eye includes more noise leaving the signal unchanged.

In the periodic direction, the integration width presumably remains unchanged by the apertures while the mean signal amplitude decreases. The new mean amplitude proposed by Schade is given by the square wave flux response defined by

$$R_{SF}(N) = \frac{3}{\pi^2} \sum_{k=1}^{\infty} \frac{1}{k^2} \ R_o(kN)$$

$$k = 1, 3, 5, \cdots$$

(113)

where $R_o(kN)$ represents the values of the sensor's complex steady state frequency response at frequencies kN. This new measure is made necessary, according to Schade because the square wave amplitude response bears no fixed relationship to the average value of flux in the half waves of the variational flux as in the case with sine waves but instead, depends on the harmonic components of the waveform. The notion of the square wave flux response is illustrated in Fig. 41 and the relationships between the square wave flux response, the sine wave response and the square wave amplitude responses are illustrated in Fig. 42. Note that if N_L is the

99
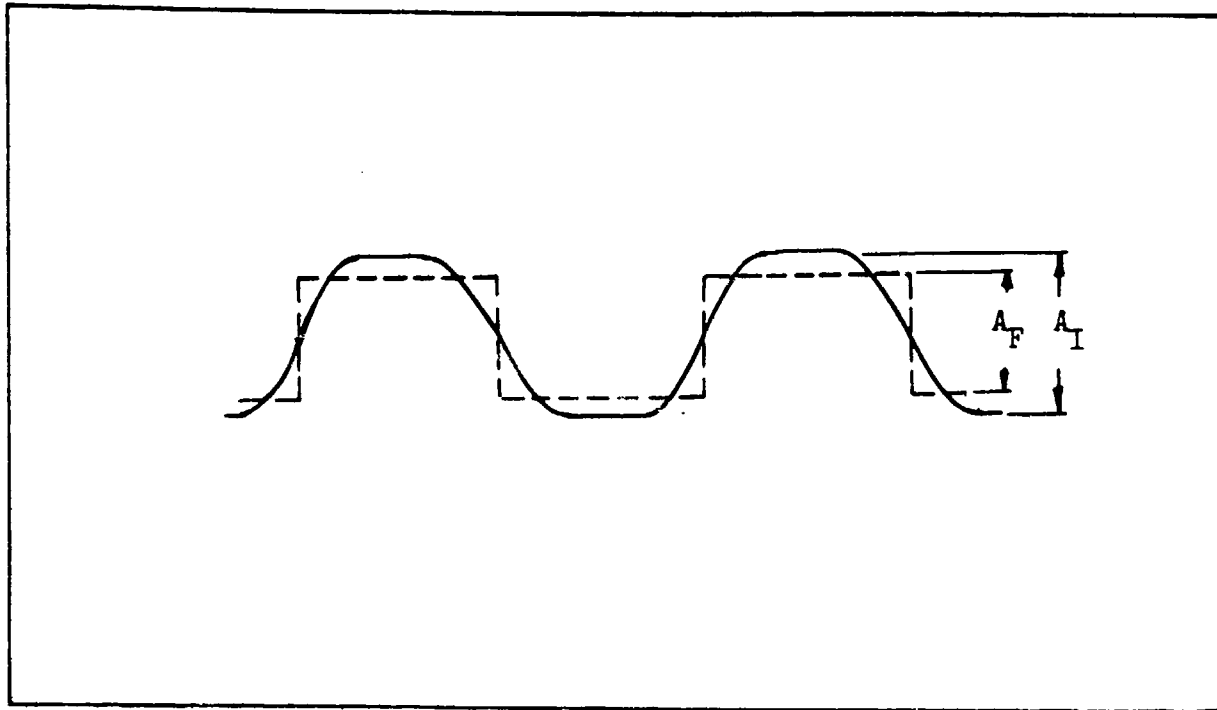
Fig. 41. Actual Image Amplitude, A_I, and Waveshape (———) Compared to Equivalent Square Wave Flux Amplitude, A_F, and Waveshape (- - -).
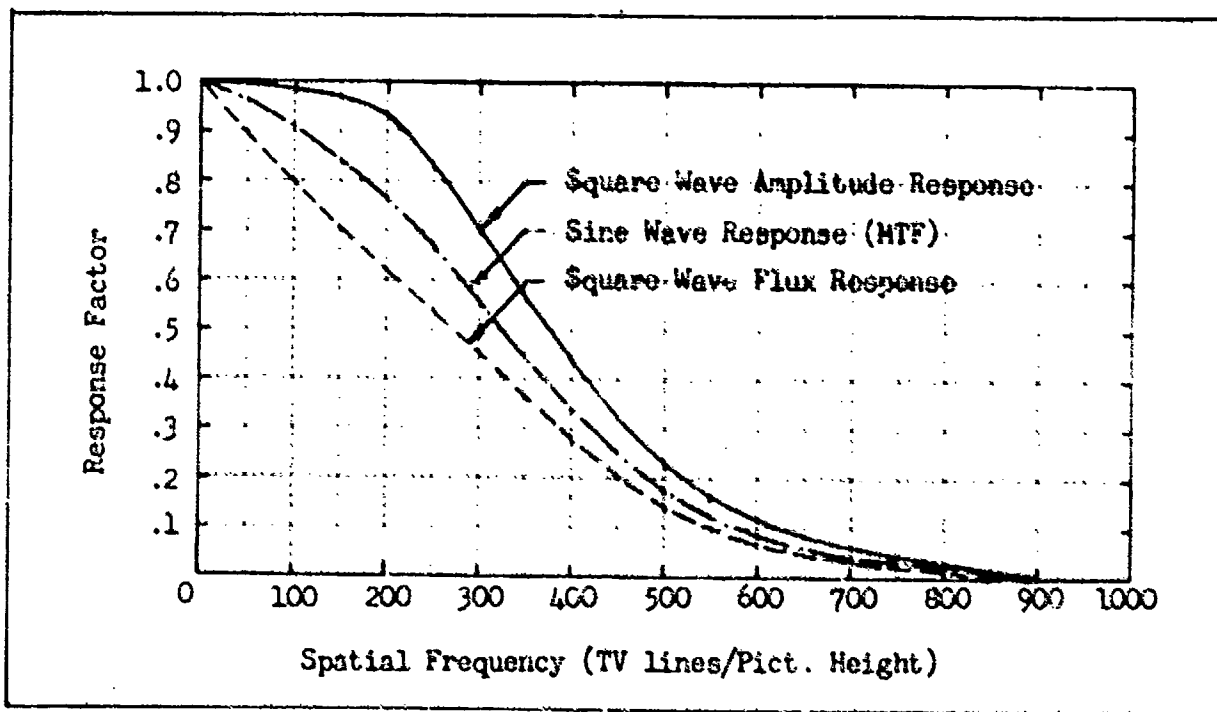
Fig. 42. Relationship Between Various Sensor Response Factors for an Assumed MTF.

100

line number at which the MTF is approximately zero, then at values of $N \geq \frac{N_L}{3}$, the square wave flux is given by

$$R_{SF}(N) = \frac{8}{\pi^2} R_o(N) \quad \text{for } N \geq \frac{N_L}{3} \tag{114}$$

Let the width, W, of a single bar be written as $N = 1/W$ where W is measured in units of picture heights. Then the SNR_D equation, written in terms of the new mean amplitude (but ignoring the effect along the bars) becomes

$$SNR_D = [\frac{2 t n_v}{\alpha N}]^{\frac{1}{2}} \cdot \frac{R_{SF}(N)}{N^{\frac{1}{2}}} \cdot \frac{\Delta i_o}{(2 e i_{ave})^{\frac{1}{2}}} \tag{115}$$

In the above, it is assumed that the aperture preceded the point of noise insertion (the signal is degraded leaving noise unchanged) and also that the effect of the apertures along the bar length may be neglected.

If, on the other hand, the aperture follows the point of noise insertion, it becomes necessary to include the noise filtering effect which is done by defining a factor β,

$$\beta = N_n/N$$
$$= \frac{\int_o^N |(R_k \cdot R_L --- R_{out})|^2 \, dN}{N}, \tag{116}$$

where $R_k \cdot R_L --- R_{out}$ are all the MTF's following the point of noise insertion. Also, note that the effect of β on SNR_D is as follows

$$SNR_D = [\frac{2 t n_v}{\alpha N}]^{\frac{1}{2}} \cdot \frac{R_{SF}(N)}{(\beta N)^{\frac{1}{2}}} \frac{\Delta i_o}{(2 e i_{ave})^{\frac{1}{2}}} \tag{117}$$

101

In the above, $R_{SF}(N)$ includes the MTF of the lens and the input photocathode since it precedes the point of noise insertion but β does not. If a system generated noise is added (such as preamplifier noise, I_p), its effect can be included as follows

$$SNR_D = [\frac{2\ t\ n_v}{\alpha}]^{\frac{1}{2}} \cdot \frac{R_{SF}(N)}{N} \cdot \frac{G\ \Delta\ i_o}{[2\beta G^2 ei_{ave} + I_p^2/\Delta f_V]^{\frac{1}{2}}} \qquad (118)$$

where G is the system gain preceding the point of preamp noise insertion and Δf_V is the noise equivalent video bandwidth. In terms of average signal current, i_{ave}, and the contrast, C_M, we have

$$SNR_D = [\frac{2\ t\ n_v}{\alpha}]^{\frac{1}{2}} \frac{R_{SF}(N)}{N} \frac{G\ 2\ C_M\ i_{ave}}{[2\beta G^2 ei_{ave} + I_p^2/\Delta f_V]^{\frac{1}{2}}} \qquad (119)$$

It should be observed that under certain conditions, aperture correction or compensation may be of benefit. The loss in signal amplitude due to the lens cannot be compensated since it occured prior to noise insertion but the losses due to the apertures which follow can be partially compensated through appropriate correcting networks. The extent of the correction which can be made depends upon the phase shift generated by the correcting network and upon the magnitude of any noises inserted between the aperture and the correcting network. Thus, aperture correction will be much more effective in the photoelectron noise limited case of Eq. (117) than in the case of Eq. (118) where preamp noise is a factor. In particular, the preamp noise generally is an increasing function of frequency such that aperture correction may increase noise at a faster rate than the signal improves.

Classification of Discrimination Level	Meaning
Detection	An object is present.
Orientation	The object is approximately symmetrical or unsymmetrical and its orientation may be discerned.
Recognition	The class to which the object belongs may be discerned (e.g., tank, truck, man, etc.).
Identification	The target can be described to the limit of the observer's knowledge (e.g., T-34 tank, friendly jeep, etc.).

Fig. 43. Levels of Object Discrimination.

3.3 Levels of Object Discrimination vs SNR_D

At very long range, a scene object may appear only as a blob. By moving ever closer, the observer first begins to discern its shape, than becomes able to classify it and finally to identify it positively. Johnson[7], has arbitrarily divided these levels of object discrimination into 4 categories which are shown in Fig. 43.

It is readily evident that a higher degree of visual acuity is needed to identify an object as opposed to just detecting it. To obtain a quantitative feel for the problem, Johnson performed a series of experiments using electro-optical sensors. In these experiments, an attempt was made to correlate the detectability of a bar pattern of a given spatial frequency with the level of object discrimination. The procedure was to increase the object range until it was just barely detected (or recognized, etc.).

103
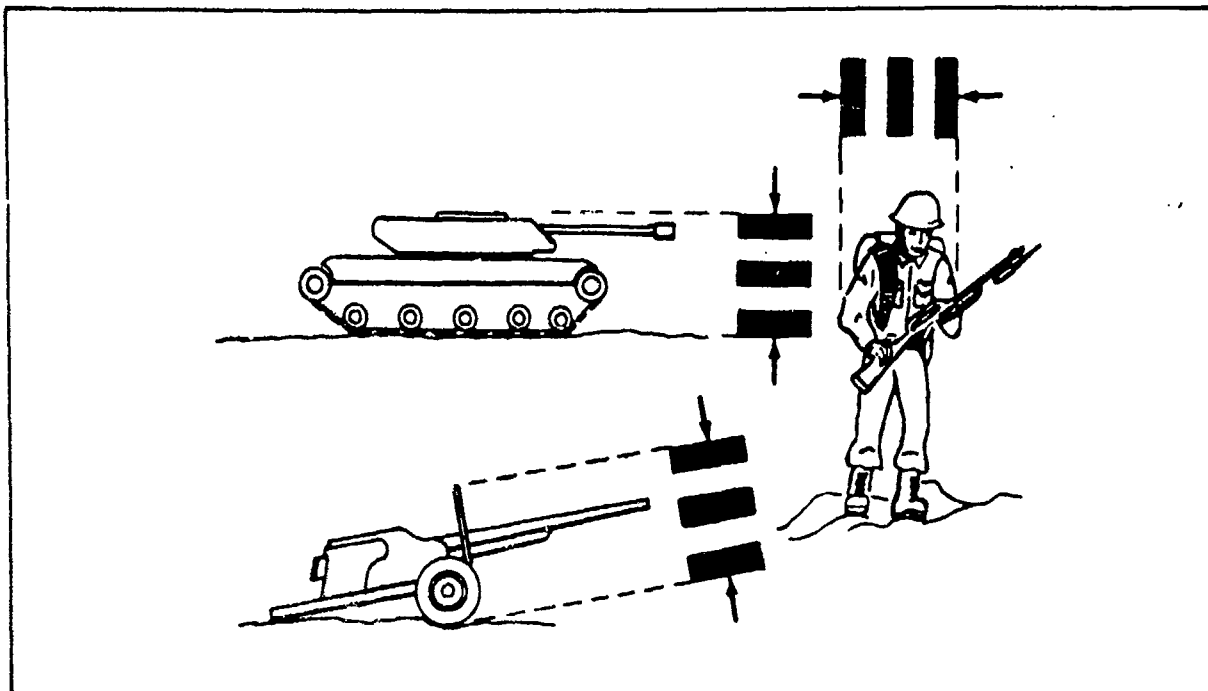
Fig. 44.   For the Number of Lines per Miminum Object Dimension, Count Both
            Black and White Bars Individually.

Then a bar pattern was placed in the field of view and its spatial frequency

was increased until it could barely be resolved at the equivalent range.   The

spatial frequency of the pattern was specified in terms of the number of

lines in the pattern subtended by the objects minimum dimension as illustrated

in Fig. 44   where the object in each case subtends 5 lines.

        Johnson's results, as tabulated in Fig. 45   are not unexpected.

If the observer could only just resolve a coarse pattern corresponding to

2 bars per minimum object dimension, the level of object discrimination

was limited to detection.   With higher acuity, a bar pattern of higher

spatial frequency could be discerned and the level of object discrimination

increased in turn.   This table has been widely used and misused by systems

designers from the time of their publication to the present.   The misuse

stems from the neglect of additional requirements imposed by Johnson, to wit,

Discrimination Level		Resolution per Minimum Target Dimension (TV Lines)*
Detection	2	+1.0 / -0.5
Orientation	2.8	+0.8 / -0.4
Recognition	8.0	+1.6 / -1.4
Identification	12.8	+3.2 / -2.8

* Plus and minus values taken from the maximum spread in the data from Johnson's Table I.

Fig. 45. Johnson's Criteria for the Resolution Required per Minimum Object Dimension for Various Levels of Discrimination. Adapted from the Image Intensifier Symposium, Ft. Belvoir, Va., Oct. 1958, AD220160.

that the "signal-to-noise" ratio and image contrast must also be sufficient.

However, it was not too clear how these quantities were to be measured and

calculated and thus, the further requirements were neglected in many cases.

However, many competent designers did use the sensor's threshold resolution

vs scene irradiance curves in estimating the level of discrimination. Since

the threshold curves do contain image signal-to-noise as a factor in their

measurement, estimates made on this basis turn out to be reasonable if not

precise.

Most sensors are characterized by an absolute limiting resolution.

If the sensor sensitivity at a given scene irradiance level and object

contrast is sufficient to realize the limiting resolution and if this level

of scene resolution is not sufficient to perform the desired discrimination

task, further increases in scene irradiance level will be to no avail.

The only solution is to move closer. On the other hand, if the resolution were sufficient at a given irradiance level, a decrease in scene irradiance level could cause the sensor/operator combination's acuity to fall below the level required for the wanted level of object discrimination.

In the above, we have inferred that image signal-to-noise ratio, image contrast and sensor/observer resolution are independent and separable quantities, whereas, in fact, these quantities are functionally related, i. e., the image signal-to-noise ratio is proportional to the image size, contrast, irradiance level, sensor sensitivity, etc. Viewed in this light, Johnson's requirements reduce to one, namely, that an object should be discriminated at the desired level, if its signal-to-noise ratio at the output of the observer's retina after processing and interpretation by the brain is sufficient. Obviously, the signal-to-noise ratio as defined in this manner, is not directly measurable but as will be seen, can be indirectly measured through psychophysical experimentation.

The quantitative models developed in this report, are based on simple test images such as rectangles or bar patterns for which, an image size or "resolution" can be precisely defined. Through psychophysical experiments, the threshold signal-to-noise ratios, as calculated on the basis of image geometry, measured electrical quantities and estimated psychophysical parameters are determined. While the test images are of simple geometry, it is hypothesized that these images and the requirements for their discrimination can be correlated with the discrimination of more complex imagery as encountered in a real world scene. Such correlation does appear to exist as will be discussed below.

Detection is the lowest level of object discrimination since it

usually implies only that an object of undeterminable shape has been sighted in the field of view. In some cases, shape need not be known if other clues are available. For example, a series of regularly spaced and moving blobs on a road may be interpreted as vehicular traffic. On the other hand, a single stationary blob on a road may be the shadow of a tree, a puddle, a truck or any other number of objects. While a blob on a road has a reasonable probability of being a vehicle, the same blob in a field or among even a sparse forest can be almost anything. Thus, there are obviously many degrees of discrimination even within a discrimination level. A single criterion such as that based on resolution and signal-to-noise ratio is unlikely to be sufficient to cover every case. Rather, a number of cases must be considered, and subclasses formed.

As we noted before, the results obtained by Johnson have been widely used. The basic notion that higher levels of sensor resolution are needed to obtain higher levels of object discrimination is certainly sound. The concept gains even greater appeal when formulated in the form of a signal-to-noise ratio which includes resolution as a parameter in its determination. For this purpose, we hypothesized that the Johnson resolution criteria is essentially correct. Then, psychophysical experiments were performed using photographic images of real objects (vehicles). A signal-to-noise ratio was analytically associated with these images as described in Section 4.3. In the experiments, the probabilities of correct recognition and identification were then determined as the images' signal-to-noise ratios were varied.

Next, the photographic real world objects were replaced by bar

patterns with bar lengths equal to the length of the vehicle and of spacing
equal to approximately 1/8 and 1/13 the vehicles minimum dimensions. Then,
the probability of resolving the bar pattern was determined as a function
of signal-to-noise ratio. The result was that the signal-to-noise ratio
required to resolve the 8-bar pattern was very similar to the
signal-to-noise ratio needed to recognize the vehicle* and the signal-to-
noise ratio for the 13-bar target was very similar to the signal-to-
noise ratio needed for vehicle identification. The correspondence obtained
for the case where the vehicle was imaged against a uniform background and
when the object is imaged amid clutter as indicated in Fig. 46 but the
difference in either case is not large. In the Fig. 46, the factor k_d gives
the value by which the objects minimum dimension should be divided to obtain
the value of threshold signal-to-noise ratio noted. Alternatively, the SNR_D
could be held constant and k_d could be increased for the clutter case.

The Johnson criteria is based on achieving a certain level of
resolution in one dimension but resolution of the same order in the other
dimension is implied. This could be a shortcoming of the technique if the
sensor resolution is widely different in the two dimensions. A partial
solution might be to estimate the range with the longitudinal axis in one
direction and in a direction at 90° to it. Then range might be estimated
as the square root of the ranges determined in the mutually perpendicular
directions.

---

* When the calculations are made as in Section 4.3.

Discrimination Level	Background	k_d Lines per Minimum Dimension	Threshold SNR_D Line Number			
			100	300	500	700
Recognition	Uniform	8	4.8	2.9	2.5	2.5
	Clutter	8	6.4	3.9	3.4	3.4
Identification	Uniform	13	5.8	3.6	3.0	3.0

Fig. 46   Best Estimate of Threshold Signal-to-Noise Ratio for Recognition and Identification of Images in terms of an Equivalent Bar Pattern.

3.4   Application of the Updated Model to Sensor Prediction

In the previous sections, we have associated a signal-to-noise ratio with an image and we have shown how the image signal-to-noise ratio at the output of a sensor can be calculated. Through the psychophysical experimentation discussed in Section 4, the observer's signal-to-noise ratio requirements are determined for simple geometric test objects such as squares, rectangles and periodic test patterns and a limited number of vehicular objects as previously noted.

In the last two decades, it has become customary to compare sensors on the basis of an observer's ability to resolve periodic test patterns on the sensor's display as a function of the test patterns irradiance on the input photosurface. The resulting curves are known as the "limiting" or "threshold" resolution vs light level (or irradiance)

109
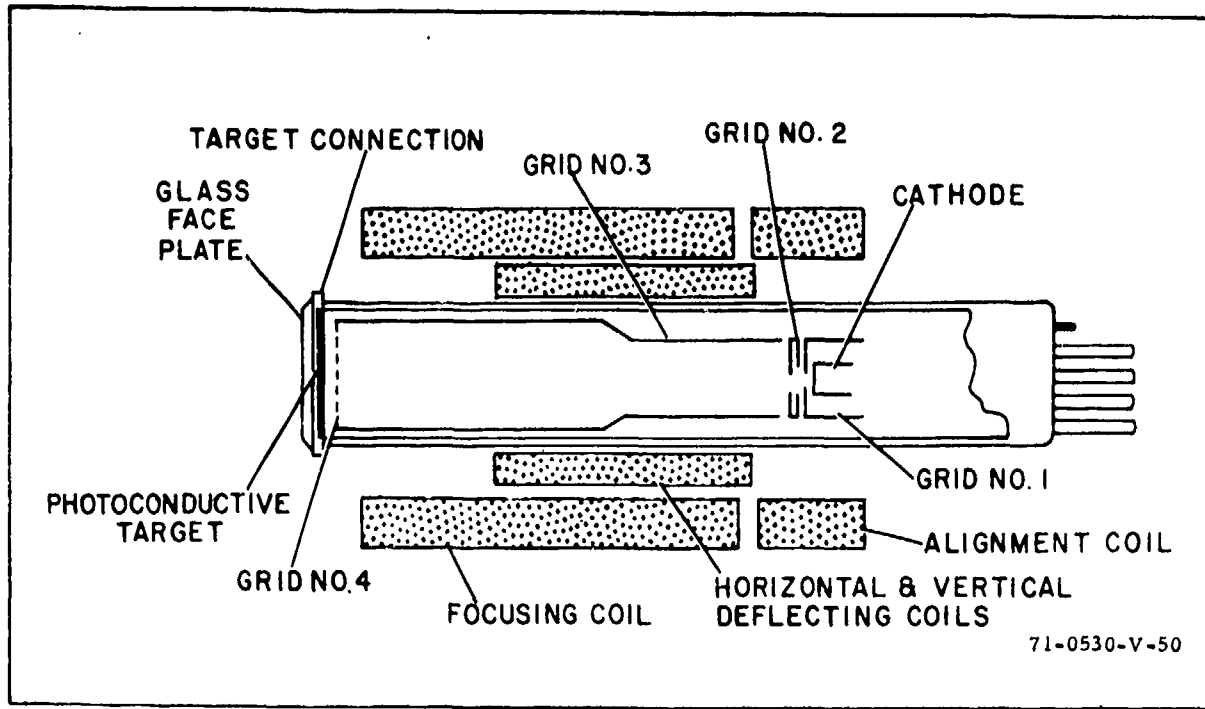
Fig. 47. Schematic of the Silicon Vidicon.

characteristic. As we will show by example, this characteristic can be computed directly with good results. Also, the threshold resolution has a direct correspondence with the detectability, recognizability or identifiability of "real world" objects as we will show in Section 4.

For the purposes of illustration, the limiting resolution characteristic will be calculated for three cameras, the silicon vidicon or Si V, the silicon-electron-bombardment induced response or SEBIR camera and the intensified-SEBIR or I-SEBIR camera. The principles of operation of these cameras have been discussed in some detail in Ref. 2. All of the TV pickup tubes used in the above cameras employ a signal storage target consisting of a matrix of silicon diodes. In the case of the Si V, the silicon target also serves as a photoconductive photon-to-electron transducer as shown in the Si V schematic of Fig. 47. The spectral response

110
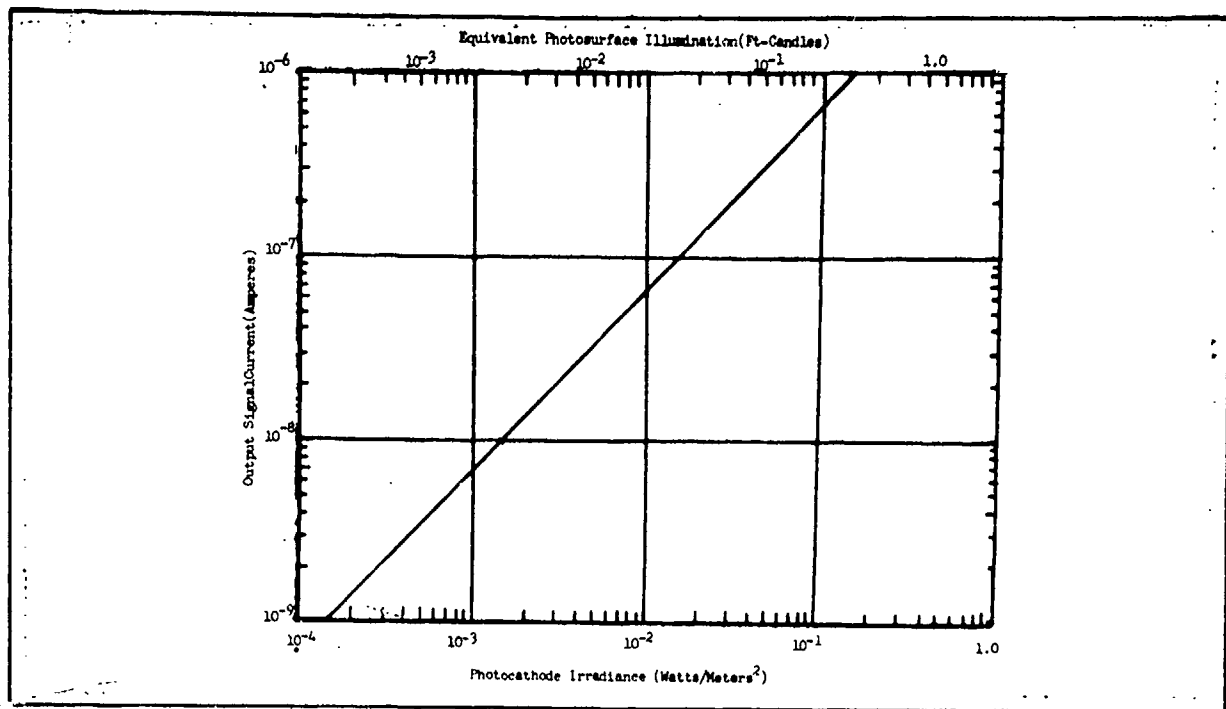
Fig. 48. Signal Output Current vs Photosurface Irradiance for the
16 mm Silicon Vidicon (2870°K Source).

of the photoconductor is as shown in Fig. 19.

For the specific radiation or light source such as a tungsten
lamp operated at 2854° K, we can write the photosurface current as

$$I_T = \sigma_T \, A \, H_T / e_v \, e_h \tag{120}$$

where σ_T is the specific responsivity of the photosurface to the tungsten
source, the irradiance H_T, A is the effective photosurface area and $e_v \, e_h$ are
the vertical and horizontal scan efficiencies respectively. The output
signal current vs photosurface irradiance characteristic is as shown in
Fig. 48 for a photosurface of 16 mm diameter, picture aspect ratio of
4 x 3 so that the effective photosurface area is 12.9 x 9.6 mm and a
photosurface responsivity of 45 mA/Watt. The modulation transfer and square

111
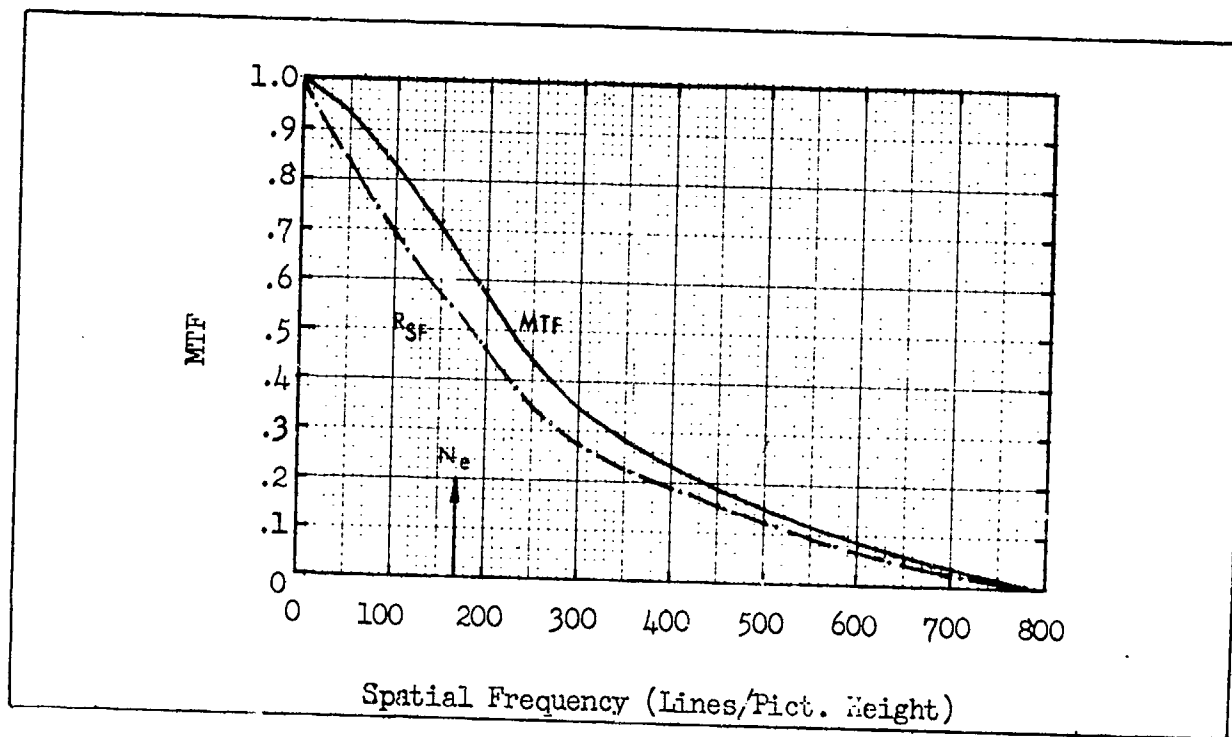
Fig. 49. Modulation Transfer Function, Square Wave Flux Function and Noise Equivalent Bandwidth vs Spatial Frequency for the 16 mm Silicon Vidicon.

wave flux functions are shown in Fig. 49 along with the noise equivalent bandwidth. The noise equivalent bandwidth is not particularly significant for the Si V since it is preamp rather than photoelectron noise limited. For a preamp noise limited sensor, the SNR_D equation for a bar pattern is written as

$$SNR_D = \left[\frac{2\,n_v\,t}{\alpha}\right]^{\frac{1}{2}} \cdot \frac{R_{SF}\,(N)}{N} \cdot \frac{2\,C_H\,i_{av}/e_v\,e_h}{Ip/(\Delta f_v)^{\frac{1}{2}}} \tag{121}$$

where $i_{av} = \sigma_T\,A\,H_{T-av}$ and Ip is the rms preamplifier noise*. Because of

_____

* Assumed to be of uniform spectral density, i.e., "white".

112
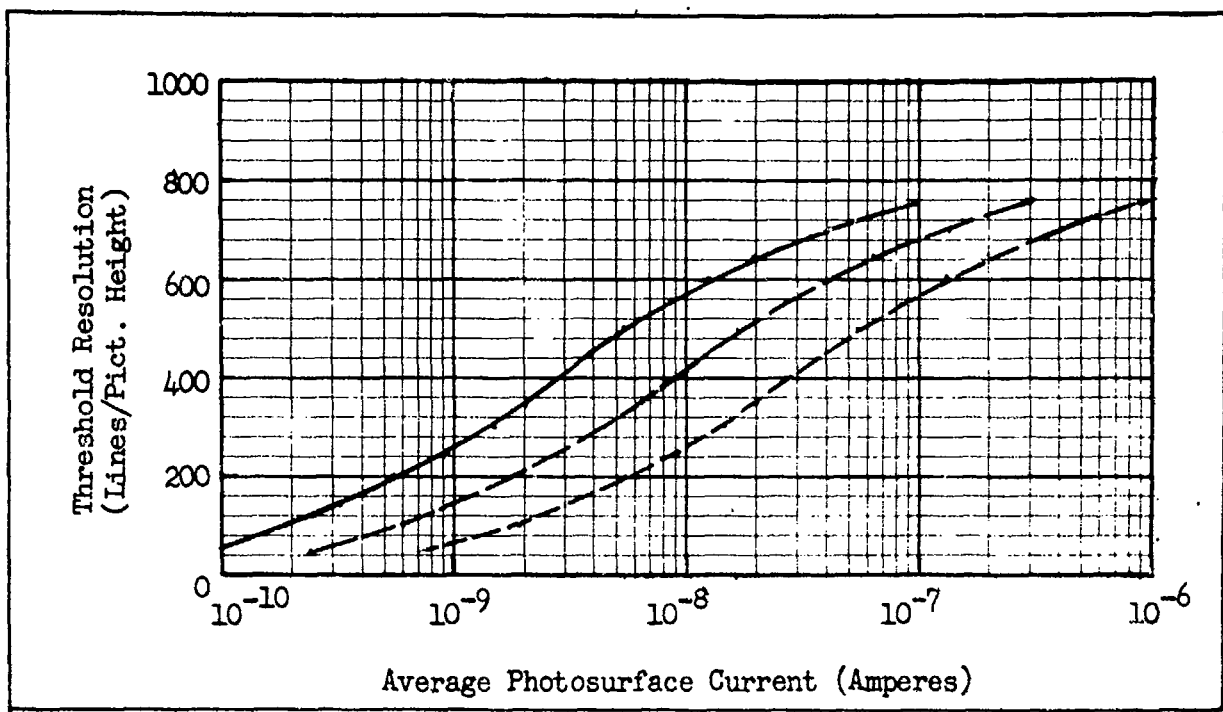
Fig. 50. Threshold Resolution vs Average Photosurface Current for the 16 mm Silicon Vidicon with Input Image Modulation Contrast of (——) 100%, (—— ——) 31.6%, and (- - -) 10%. Bar Height-to-Width Ratio is 5.0.

simplicity of Eq. (121), we can obtain the threshold resolution vs photo-current (or scene irradiance) directly by setting the SNR_D equal to the threshold value SNR_{DT} and solving for i_{av} as follows

$$i_{av-min} = [\frac{\alpha}{2\ n_v\ t\ \Delta f_V}]^{\frac{1}{2}} \cdot \frac{SNR_{DT}}{2}\ \frac{N}{R_{SF}\ (N)} \cdot \frac{e_v\ e_h\ Ip}{C_M} \quad (122)$$

Note that when SNR_D is set equal to SNR_{DT}, i_{av} becomes the threshold current i_{av-min}. The above equation is numerically evaluated using $SNR_{DT} = 2.4$ corresponding to an optimum viewing distance, $\alpha = 4/3$, $n_v = 5$, $e_v\ e_h = 0.79$, $\Delta f_V = 6 \times 10^6$ Hz and Ip $= 3 \times 10^{-9}$ Amp. The result, is plotted as threshold resolution vs average input photosurface current in Fig. 50 for three values of image modulation contrast. These same curves are replotted as threshold resolution vs image irradiance and illuminance in Fig. 51 using a value of

113
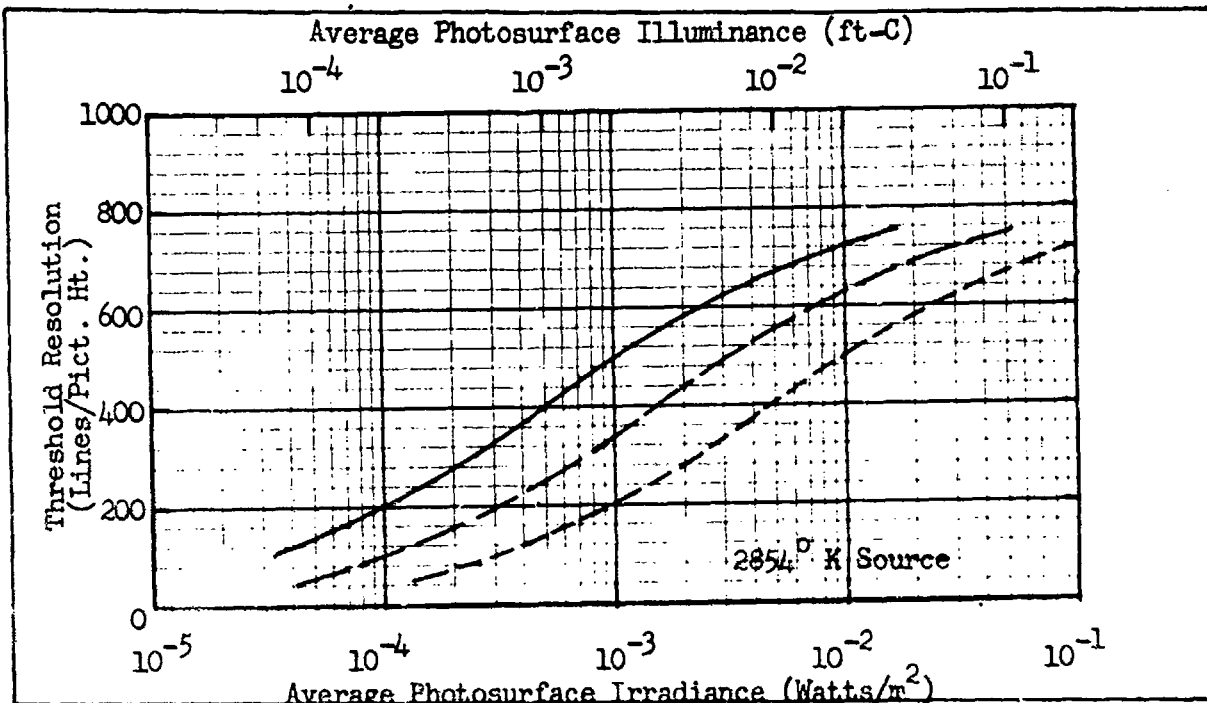
Fig. 51. Threshold Resolution vs Average Photosurface Irradiance and
Illuminance for the 16 mm Silicon Vidicon at Image Modulation
Contrasts of (———) 100%, (— —) 31.6%, and (- - - -) 10%.
Bar Height-to-Width Ratio is 5.0.

45 mA/W for the specific test source responsivity. The illuminance scale is

obtained by noting that for a 2854° K source, Watts/m² = ft-candles/2 as

previously noted in Ref. 2.

While the SEBIR camera is intermediate in sensitivity between

the Si V and the I-SEBIR, the I-SEBIR will be considered next because it

is simpler to analyze since, like the Si V, only one noise source is

significant. In the case of the Si V, the photoconverted signal is not

amplified prior to the preamp so that preamp noise dominates. In the

I-SEBIR, the signal gain within the camera tube is so high that photoelectron

noise generated in the input photocathode dominates. The I-SEBIR is shown

schematically in Fig. 52. The input photocathode of the intensifier converts

a photon image to a photoelectron image which is accelerated to a phosphor

which recreates a visible image of greater radiance due both to the
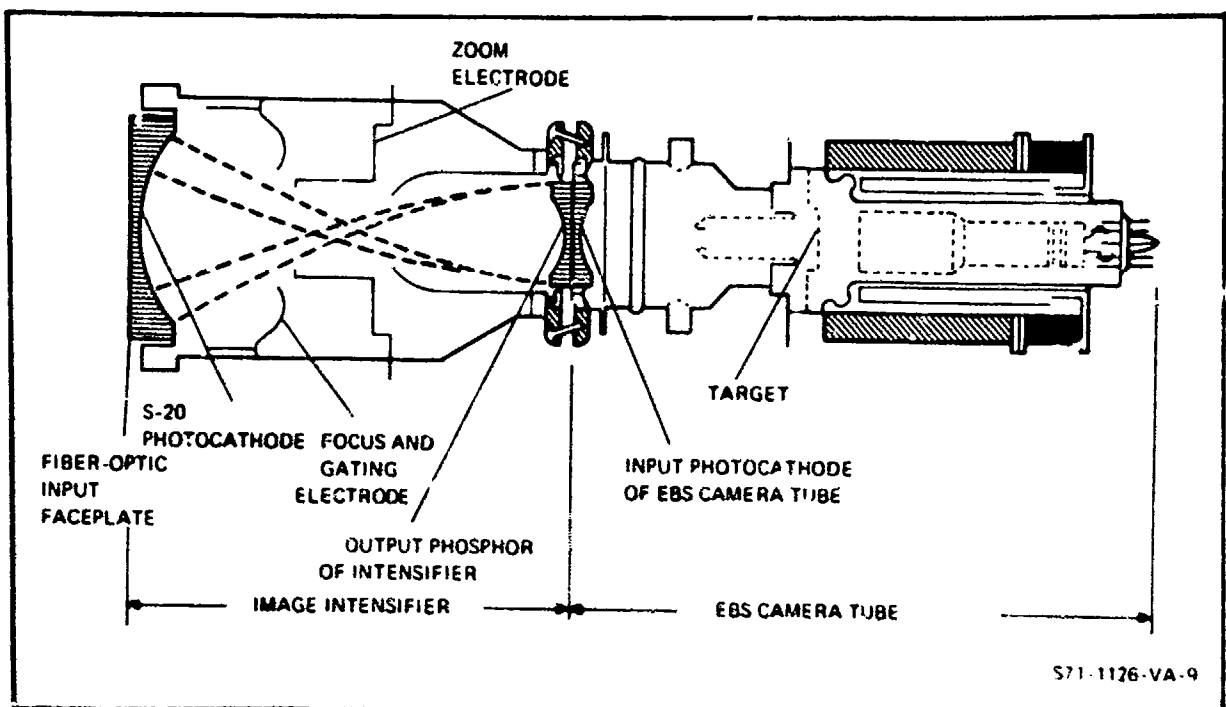
Fig. 52. Schematic of the Intensified Electron-Bombarded-Silicon
Television Pickup Tube with Electronic Viewfield Zoom Capability.

accelerating voltage and phosphor and to any image minification between the
input photosurface and phosphor. The minification gain is proportional
to the area of the intensifier photocathode and its phosphor.

The amplified image is transferred via fiber optics to a
second photocathode which once again creates a photoelectron image. The
net signal gain due to phosphor and photocathode is about 20 - 40 when the
intensifier is operated at maximum voltage. The new photoelectron image
generated by the SEBIR's photosurface is accelerated to the SEBIR's
silicon diode matrix target where the image is greatly amplified by an
amount up to 2000 and then stored for subsequent read-out by the scanning
electron beam. The SNR_D equation for the SEBIR and I-SEBIR cameras is
given by

$$SNR_D = \left[\frac{2\,n_v\,t}{\alpha}\right]^{\frac{1}{2}} \frac{R_{SF}\,(N)}{N} \frac{2\,C_M\,G\,i_{av}/e_v\,e_h}{\left[\frac{2\,e\,G^2\,\beta\,i_{av}}{(e_v\,e_h)^2} + \frac{Ip^2}{\Delta f_V}\right]^{\frac{1}{2}}} \quad . \qquad (123)$$

Since the gain G obtainable from the intensifier/SEBIR photocathode can be very large, the preamplifier noise can be safely neglected so that Eq. (123) simplifies to

$$SNR_D = \left[\frac{2\,n_v\,t}{\alpha}\right]^{\frac{1}{2}} \frac{R_{SF}\,(N)}{N} \cdot \frac{C_M}{1} \cdot \left[\frac{2\,i_{av}}{e\,\beta}\right]^{\frac{1}{2}} \quad . \qquad (124)$$

As in the case of the Si V, this equation is quite simple and can be solved for i_{av} which becomes i_{av-min} for $SNR_D = SNR_{DT}$ as follows

$$i_{av-min} = \frac{SNR_{DT}^2}{C_M^2} \cdot \frac{\alpha}{2\,n_v\,t} \cdot \frac{e\,\beta}{2}\left[\frac{N}{R_{SF}\,(N)}\right]^2 \qquad (125)$$

The signal current vs photosurface irradiance curves are shown for various SEBIR and I-SEBIR cameras in Fig. 53. The modulation transfer, square wave flux and finite-noise-bandwidth correction functions are shown for an I-SEBIR with an intensifier of 80, 40 or 25 mm photocathode, 25 mm phosphor and a SEBIR with a 25 mm photocathode and a 16 mm target in Fig. 54. The same quantities are shown for an I-SEBIR with an intensifier of 80 or 40 mm photocathode, 40 mm phosphor and a SEBIR of 40 mm photocathode and 25 mm target in Fig. 55. The threshold resolution vs average input photocathode current is plotted for the I-SEBIR with 16 mm photocathode
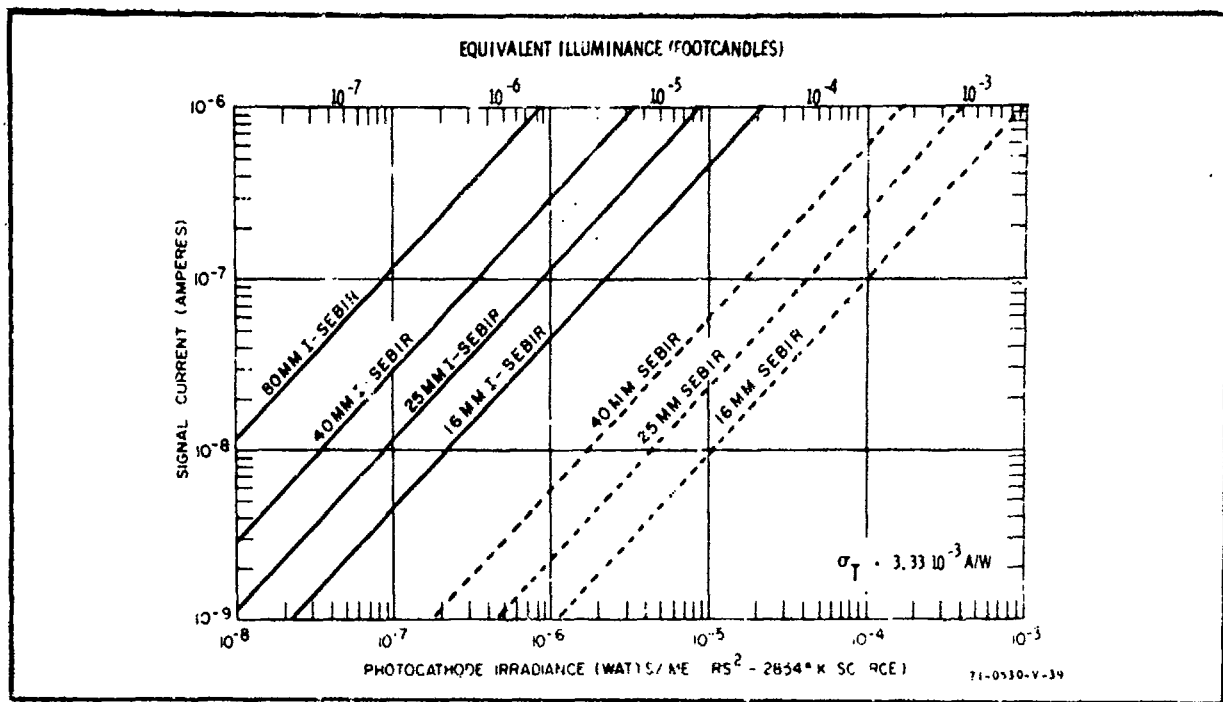
Fig. 53. Signal Current Versus Photocathode Irradiance Characteristic for the Silicon-EBIR and Intensifier-Silicon-ERIR Cameras for Various Input Photocathode Diameters
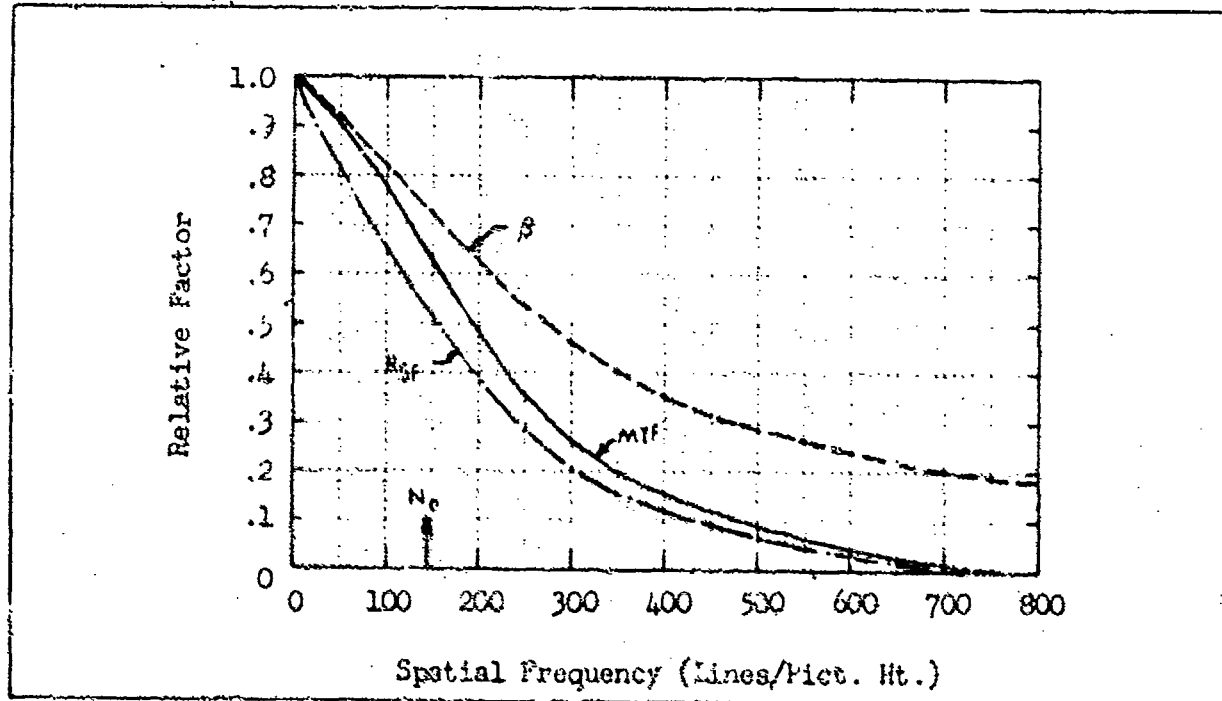
Fig. 54. Modulation Transfer Function, Finite-Noise-Bandwidth Correction Function, β, Square Wave Flux Function, R_{SF} and Noise Equivalent Bandwidth, N_e, for the 80/25, 40/25 and 25/25 mm I-SEBIR with 16 mm Target.
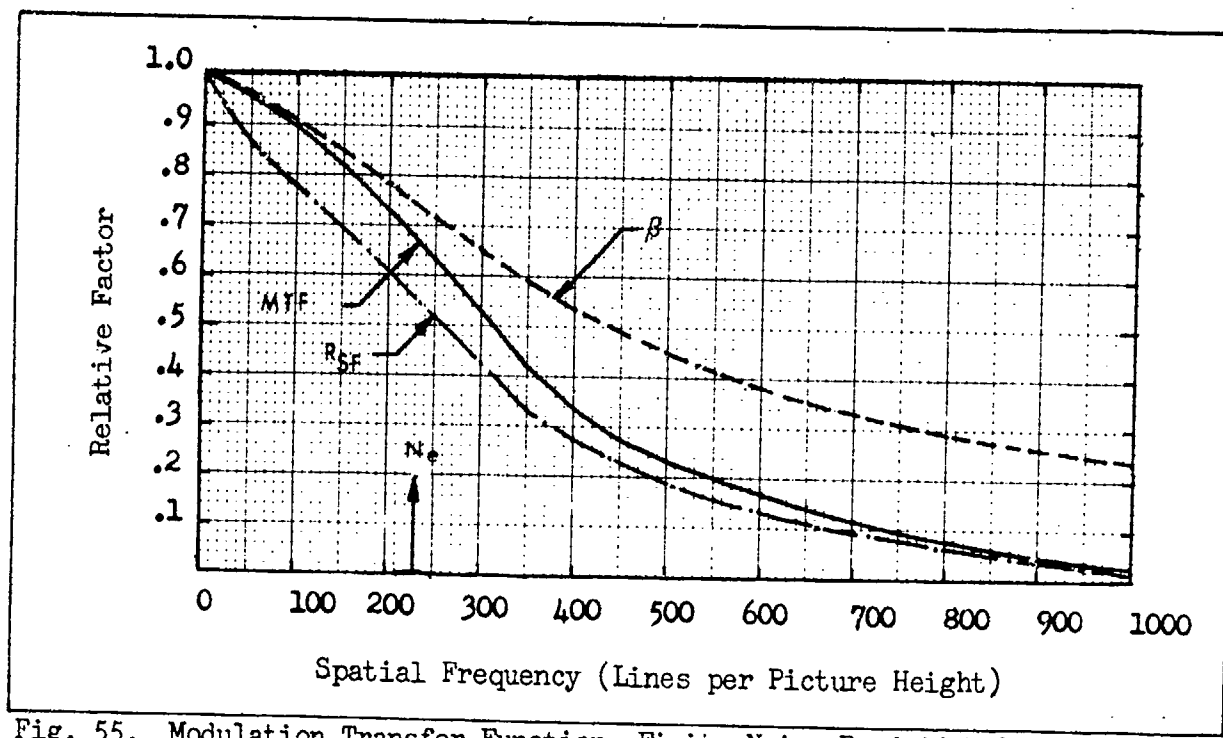
Fig. 55. Modulation Transfer Function, Finite Noise Bandwidth Correction Function β and Square Wave Flux Function, R_{SF}, and Noise Equivalent Bandwidth, N_e, for the 80/40 and 40/40 mm I-SEBIR with 25 mm Target.

in Fig. 56 and for the I-SEBIR with 25 mm photocathode in Fig. 57. For the latter case, we plot the threshold resolution vs average photocathode irradiance for two photosurface diameters and two image modulation contrast in Fig. 58. The photocathode sensitivity for these calculations was taken to be 4.5 mA/W and the picture aspect ratio is 4/3.

The SEBIR camera tube is shown schematically in Fig. 59. The MTF, R_{SF}, β and Ne for the SEBIR camera with 16 mm target is shown in Fig. 60 and with a 25 mm target in Fig. 61. The SNR_D is calculated for the 25 mm target case using Eq. (123) and numerical values of 1890 for the SEBIR target gain, 6×10^{-9} Amperes for the rms preamp noise, an 8×10^6 Hz video bandwidth and an image modulation contrast of unity. The result is plotted in Fig. 62. While the observer's signal-to-noise ratio requirement for any given image is approximately a constant for any bar pattern spatial

118
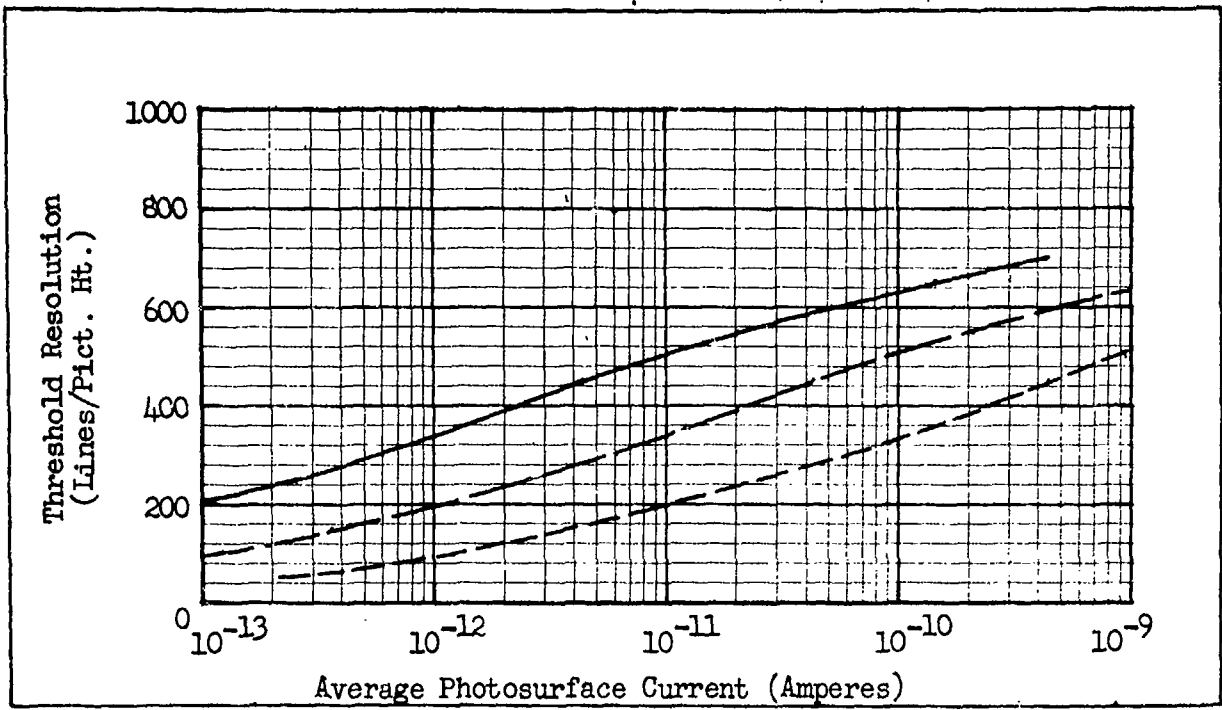
Fig. 56. Threshold Resolution vs Average Photocathode Current for the
80/25, 40/25, and 25/25 mm I-SEBIR with 16 mm Target at
Image Modulation Contrasts of (———) 100%, (— —) 31.6%, and
(- - - -) 10%. Bar Height-to-Width Ratio is 5.0.
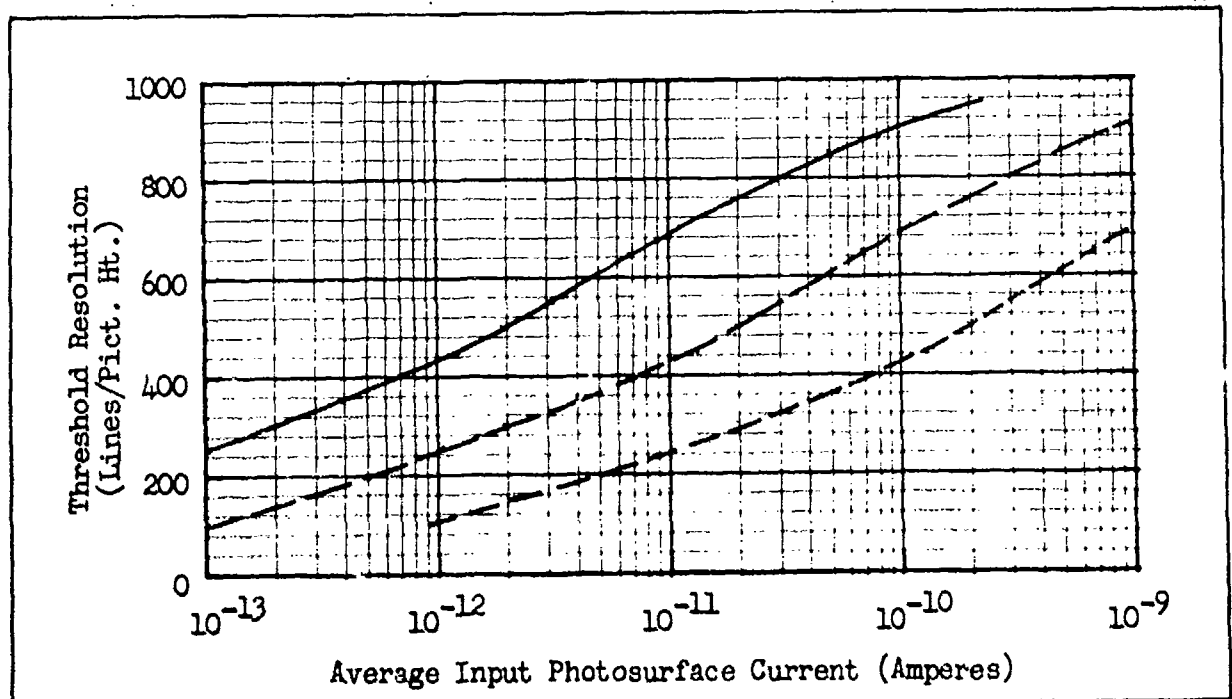
Fig. 57. Threshold Resolution vs Average Photocathode Current for the
80/40 and 40/40 mm I-SEBIR with 25 mm Target at Image Modulation
Contrasts of (———) 100%, (— —) 31.6% and (- - -) 10%. Bar
Height-to-Width Ratio is 5.0.

119
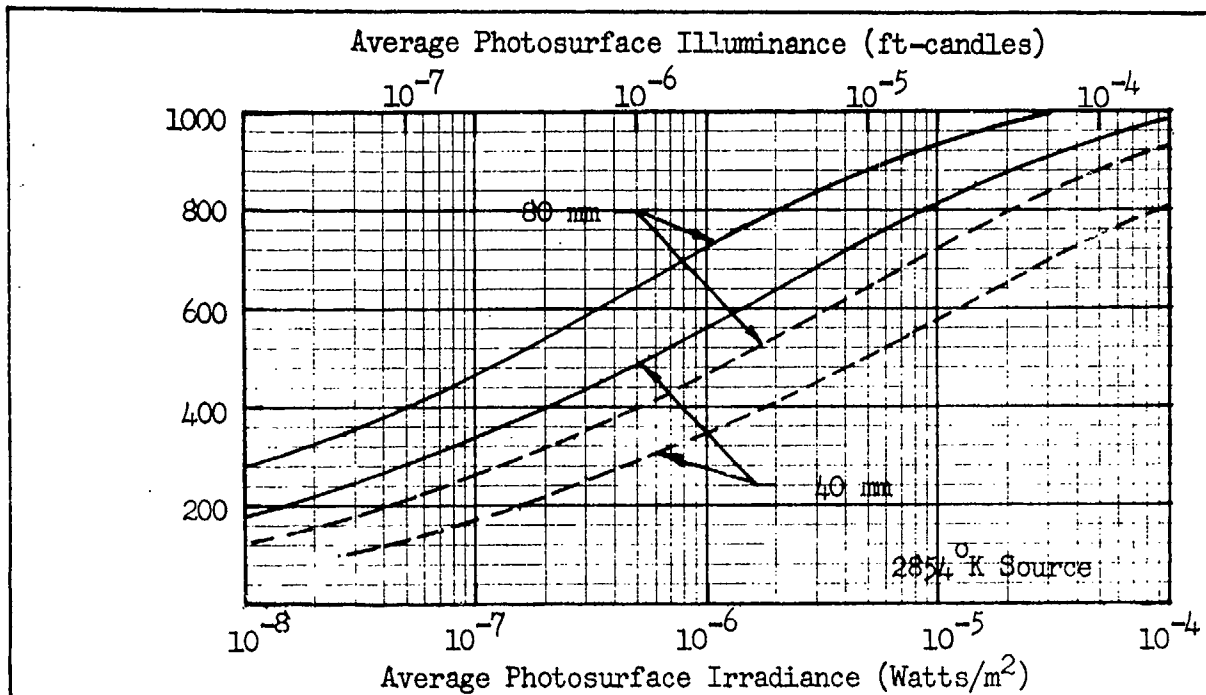
Fig. 58 Threshold Resolution vs Average Photosurface Irradiance or
Illuminance for the 80/40 and 40/40 mm I-SEBIR with 25 mm Target.
Image Modulation Contrast is (———) 100% and (- - -) 31.6% and
Bar Height-to-Width Ratio is 5.

frequency or image modulation contrast, it is mathematically convenient

to assume that the observer's SNR_{DT} increases with reduced contrast, i.e.,

$$SNR_{DT}' = \frac{SNR_{DT} (C_M = 1)}{C_M} \qquad (126)$$

In actual fact, the effect of reduced image contrast is to reduce signal,

not increase observer SNR_D requirements; but handling the effect of contrast

reduction as a signal reduction would greatly complicate the drawing of

Fig. 62. Threshold resolution vs average signal current values are obtained

by noting the intersection of the SNR_{DT}' curves with the SNR_D curves in Fig.

62 and the result is plotted in Fig. 63. The threshold resolution vs

photocathode irradiance and illuminance characteristic is plotted in Fig. 64.

120
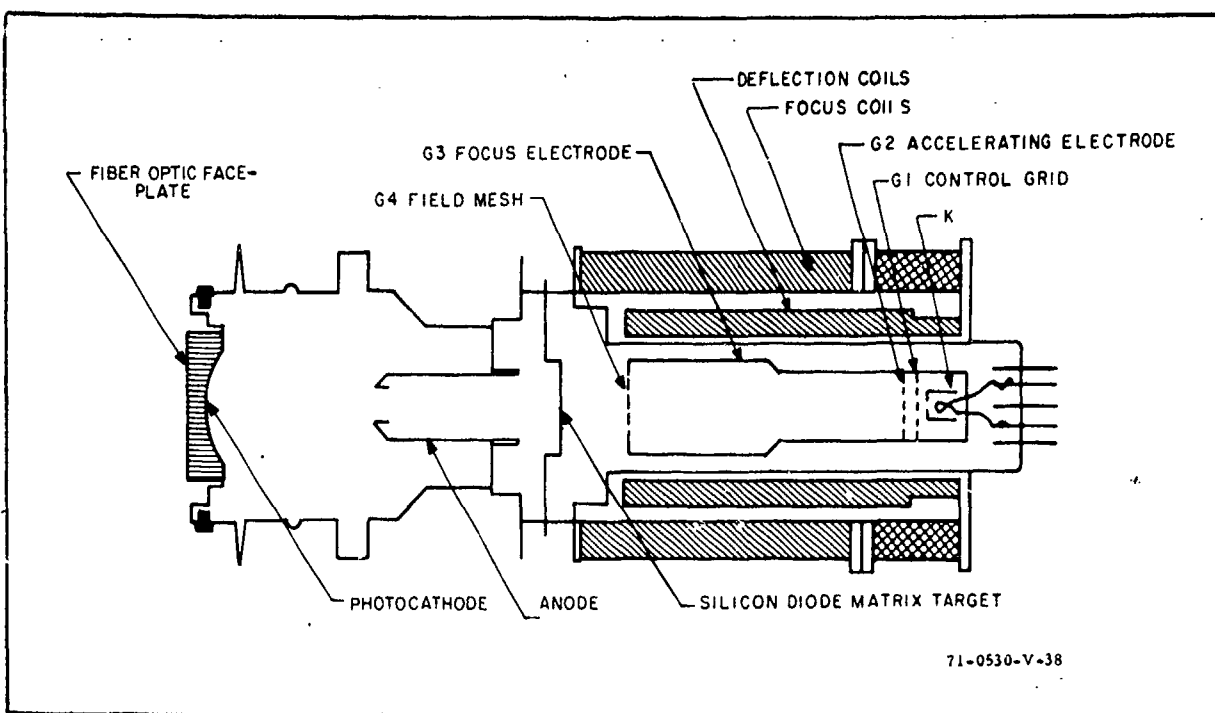
Fig. 59. Cross Section of a SEBIR Camera Tube.
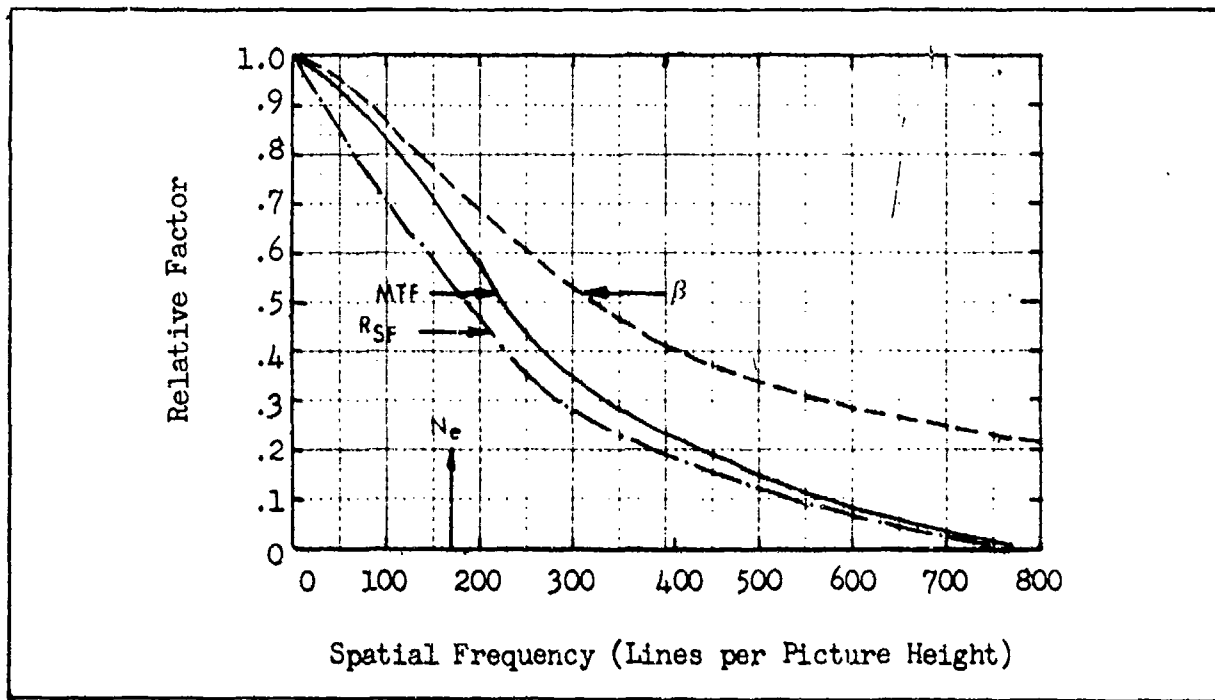
Fig. 60. Modulation Transfer, Square Wave Flux and Finite-Noise Band-
width Correction Functions for the SEBIR Camera Tube with
16 mm Target. N_e is the Noise Equivalent Bandwidth.

121
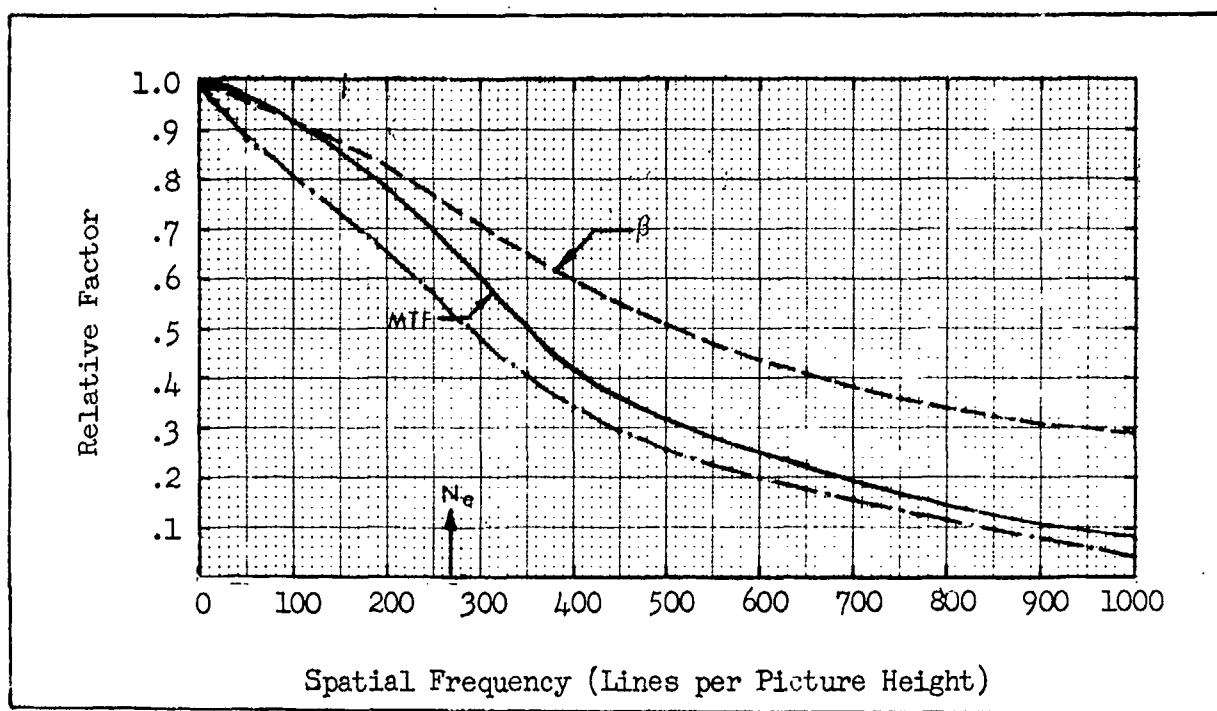
Fig. 61 Modulation Transfer, Finite Noise Bandwidth and Square Wave Flux
Functions for the SEBIR Camera Tube with 25 mm Target N_e is the
Noise Equivalent Bandwidth.

3.5 Summary of the Model Update Program

In this section, a new analytical model has been constructed
incorporating methods proposed by Schade. The primary purpose of
incorporating Schade's techniques is to obtain greater general acceptance
of the basic model. The elementary model used is almost identical to that
proposed in Ref. 2 but the new model treats the effects of apertures in a
somewhat different manner. While the numerical results using the new model
are almost identical to those obtained using the previous model, there are
conceptual differences. One difference which favored the older model is
that the older model weighted noise at the signal frequency more heavily.
That is, it was felt that noise at the signal frequency is more disturbing
than noise at other frequencies and this notion has been experimentally
noted by other workers. The effect is not a large one, however, and need
not be cause for undue concern. Further efforts in this area are needed.

122
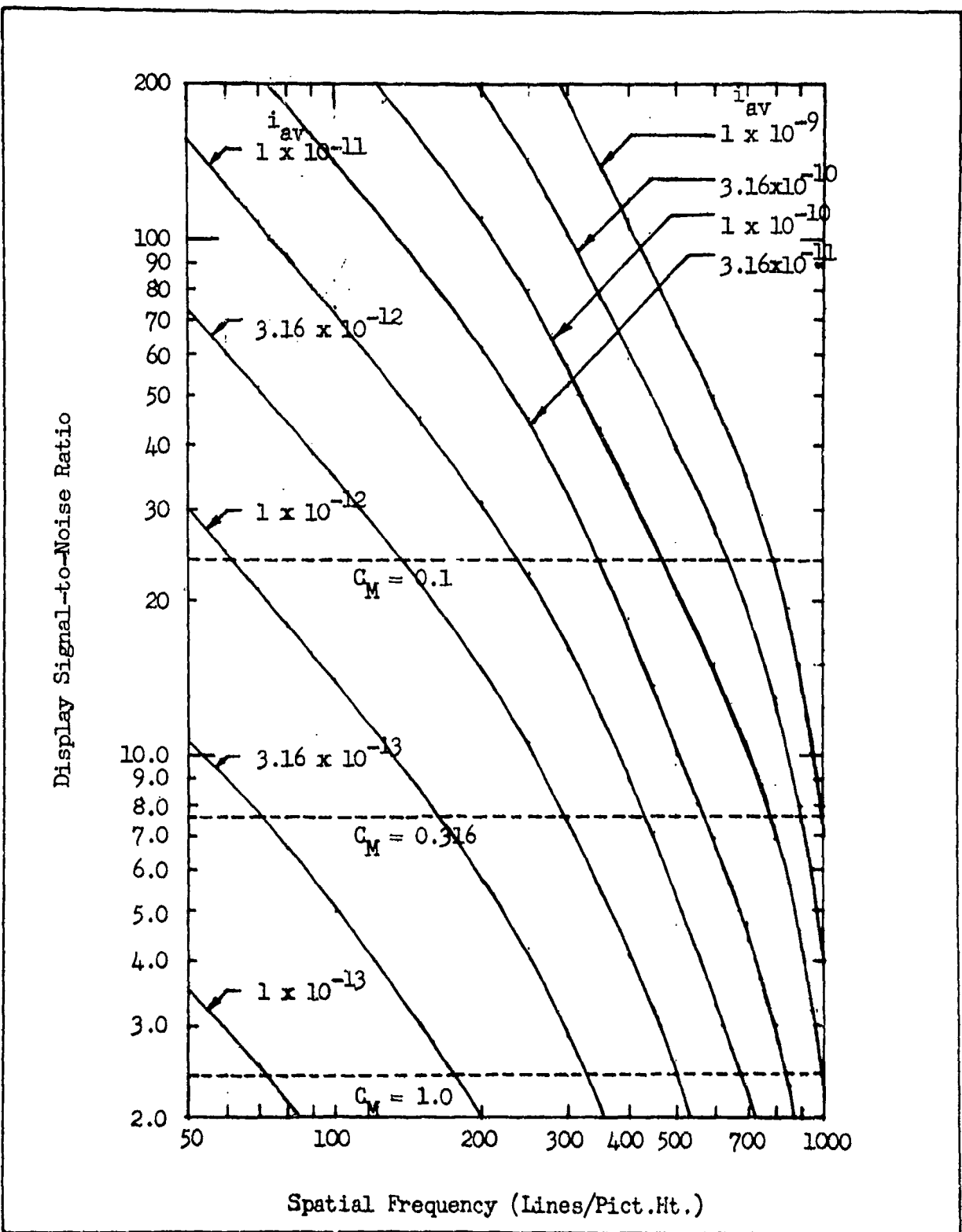
Fig. 62 Display Signal-to-Noise Ratio (————) Obtainable From the SEBIR
with 25 mm Target at Various Photocurrents vs that (- - -)
Required by the Observer at Various Image Contrasts as a Function
of Bar Pattern Spatial Frequency.

123
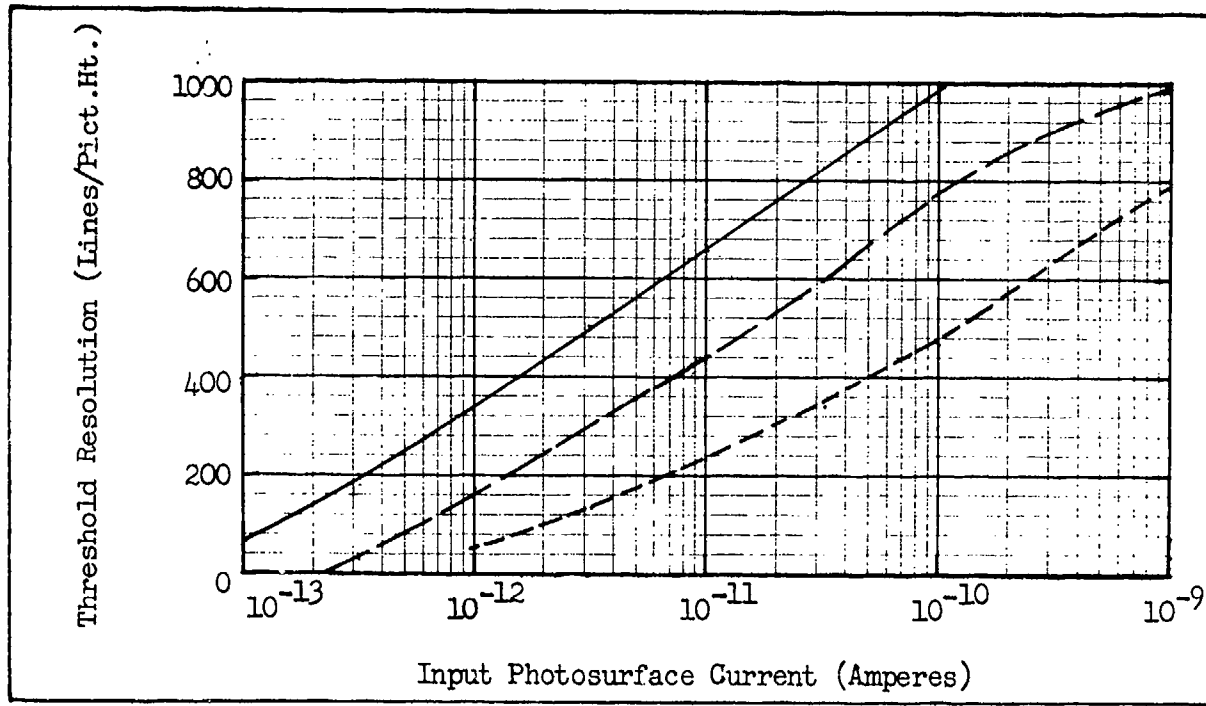
Fig. 63   Threshold Resolution vs Input Photosurface Current for the SEBIR·
with 25 mm Target for Image Contrasts of (———) 100%, (—— ——)
31.6%, and (- - -) 10%.   Bar Length-to-Width Ratio = 5.

The updated model shows considerable improvement over that
previously used in that observer signal thresholds have been more intensively
investigated and extended to more complicated imaging situations, i.e.,
to higher levels of object discrimination.   The major shortcoming still
present is that the updated model only applies to stationary images whereas
in practice some scene motion will nearly always be the case.   Considerable
effort has been expended in this program to treat the effects of image
motion as will be seen in the discussion of Section 5.   However, we do not
yet feel confident of our analytical approach and we will defer incorporation
of image motion effects into the model to the follow-on program.

While we have indicated some confidence in the analytical pre-
diction models, it must be recognized that the art of sensory system
prediction is still in an early stage.   The major first order effects, save
motion, have been investigated but a large variety of second order effects
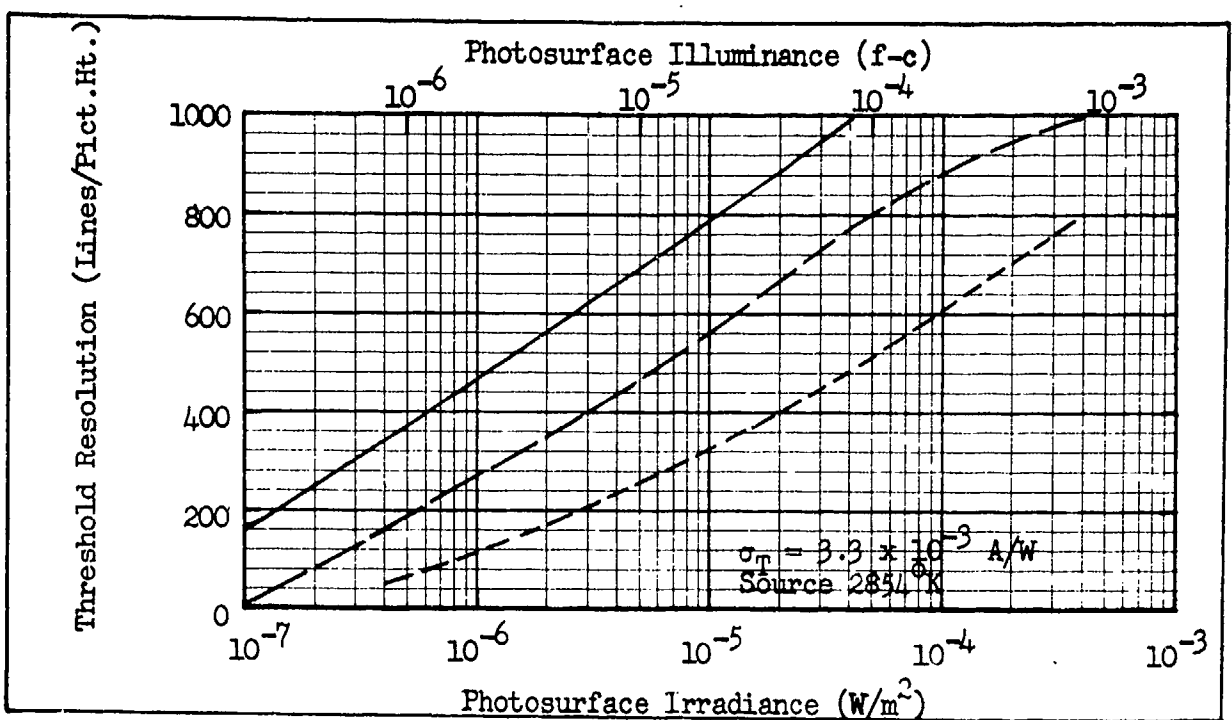
Fig. 64   Threshold Resolution vs Input Photosurface Irradiance and
Illuminance for the SEBIR with 40 mm Photosurface and 25 mm Target
for Image Contrasts of (———) 100%, (— —) 31.6% and (- - -)
10% Bar Height-to-Width Ratio is 5.

remain as problem areas. For example, the treatment of sensor apertures,

while basically sound, has not been experimentally verified. The filtering

effects of apertures on image sharpness, for example, is largely unknown

as is the effect of non-white noise spectra whether due to apertures or

to psychophysical phenomena. The interaction between the observer and the

sensor display needs considerable further effort. In recent flight and

field tests, the degrading effects of atmosphere on image sharpness are

becoming more evident and need further consideration. As we progress toward

greater refinement of the model, more emphasis must be placed on second

order effects but these effects will prove much more difficult to resolve.

Considerably more care must be exercised in the areas of instrumentation,

experimentation, data analysis and interpretation. Even with greater care,

the tangible results to be expected will be fewer than we have experienced

in these early efforts.

4.0 Psychophysical Experimentation

The analytical model used in predicting sensor and sensory system performance has been derived and discussed in Sections 2 and 3. In these analyses, the procedure was to calculate the signal-to-noise ratio of an image provided by the sensor at the display. Then this signal-to-noise ratio was compared with the observer's needs to determine the image's threshold detection, recognition or identification range. In this section, the observer's needs are investigated through psychophysical experimentation and the results are reported. The test images used in the experiments were of three general types, simple geometric shapes such as squares and rectangles, periodic images such as bar patterns and, so-called "real world" objects such as vehicles. In the latter case, both uniform and varigated backgrounds were employed.

4.1 Stationary Aperiodic Images

The aperiodic images used were simple squares and rectangles for which, the display signal-to-noise ratio has been derived in Section 3 in the form of Eq. (77) repeated below

$$SNR_D = [2t\Delta f_V \ (a/A)]^{\frac{1}{2}} \cdot SNR_V \ , \tag{127}$$

which holds if the test images are large relative to the point spread functions of the sensory system and if the noise is of substantially uniform spectrum over the video bandwidth Δf_V. The experimental setup we have used to perform the experiments is as shown in Fig. 65 . In this experiment, a signal pulse of rectangular waveshape but variable duration is electronically generated and mixed with band-limited white noise of Guassian distribution.

127
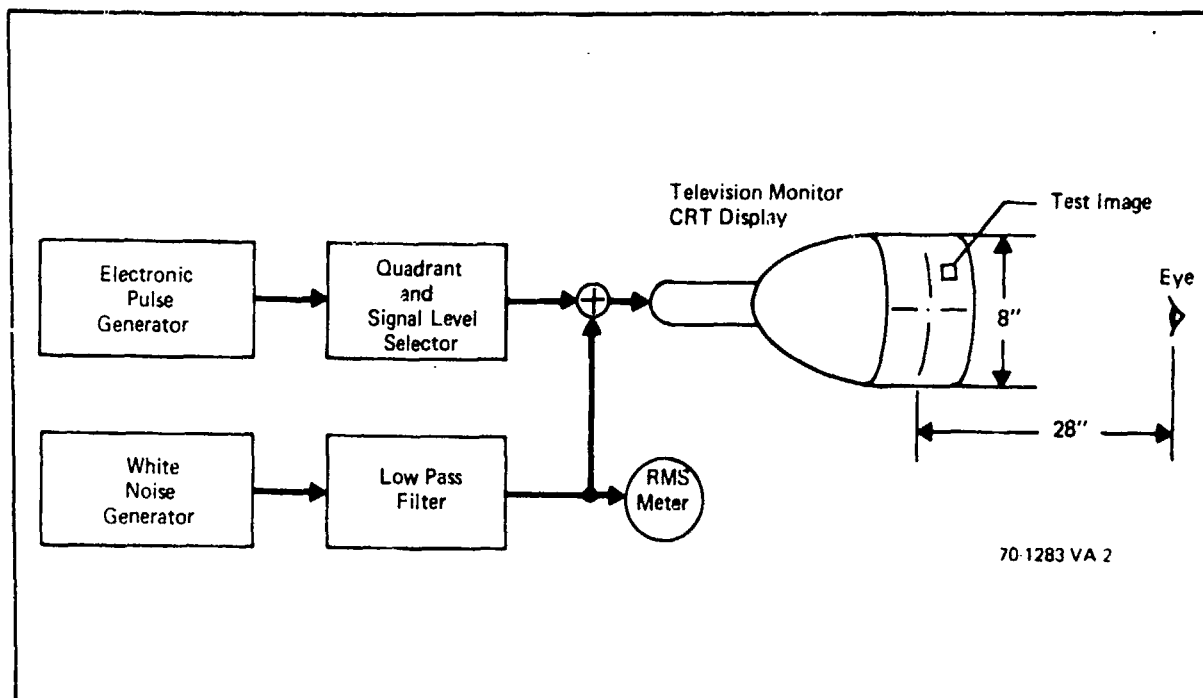
Fig. 65   The Display Signal-to-Noise Ratio Experiment.

The spatial image displayed on the cathode ray tube (CRT) display is a
rectangle which can appear in any of four quadrants (but always in the same
position in the quadrant selected). The observer is asked to specify the
quadrant in which the image is located as the video signal-to-noise ratio
and the image locations are randomly located. The observer is asked to
specify the image location whether he could see it or not. The probability
of detection, determined in this manner, was than corrected for chance using
the formula

$$P_d = (P_o - P_c)/(1 - P_c) , \tag{128}$$

where P_d is the corrected probability, P_o is the raw probability data and
P_c is the probability due to chance (0.25 in the case cited). Two noise

128

bandwidths were used, 7.1 and 12.5 MHz and the observation times per trial were usually 10 seconds. The observer distance from the 8" high picture displayed was 28" unless otherwise specified and the display background luminance was usually 0.2 - 0.3 or 1 ft-Lambert. The television monitor was operated at 30 frames per second with a 525 line scan in the vertical. The precise experimental conditions for each experiment are given in Fig. 66.

For the rectangle experiments, it was found to be convenient to define the image size in terms of the dimensions of a single scan line. Thus, we define the quantities L_x and L_y as

$$L_x L_y = (490)^2 \cdot \alpha (a/A) , \tag{129}$$

where 490 is the number of active lines in a conventional 525 line television display and α is the width-to-height picture aspect ratio of the total effective picture on the CRT. Combining Eqs. (127) and (129), we have

$$SNR_D = (1/490) \cdot (2 L_x L_y t \Delta f_V/\alpha)^{\frac{1}{2}} \cdot SNR_V \tag{130}$$

This is the equation used to calculate the SNR_D for the rectangular images used in the experimental program reported below. The numerical values used were $t = 0.1$ sec and $\alpha = 4/3$.

For the first experiment, (Experiment No. 1, See Fig. 66) we hypothesized that the SNR_D required to detect a stationary rectangular image of variable length would be a constant (for liminal perception, we mean 50% probability of detection), independent of the image's area. To test this

Exp No.	NOTES* Test Images	(1) $\frac{D_V}{D_H}$	(2) B_D ft.-L	(3) Δf_V MHz	(4) $\frac{Time}{Trial}$ (SEC)	(5) No. of Trials	No. of Observers	Fig. No.
1	Long Thin Rectangle	3.5	0.2-0.3	7.1	10	800	5	67, 68
2	Large Rectangles	3.5	1.0	12.5	10	800	5	69, 70
3	Small to Medium Squares	3.5	0.2-0.3	7.1	10	800	5	71, 72
4	Medium to Large Squares	3.5	1.0	12.5	10	1200	5	73, 74
5	Medium to Large Squares	7.0	1.0	12.5	10	700	3	77

NOTES

* (1) Display Viewing Distance to Height Ratio

(2) Display Brightness (ft-Lamberts)

(3) Noise Equivalent Bandwidth (MHz)

(4) Time Allowed for Observer Response

(5) Total Trials per Experiment

Fig. 66 Experimental Conditions for the Aperiodic Images.

130
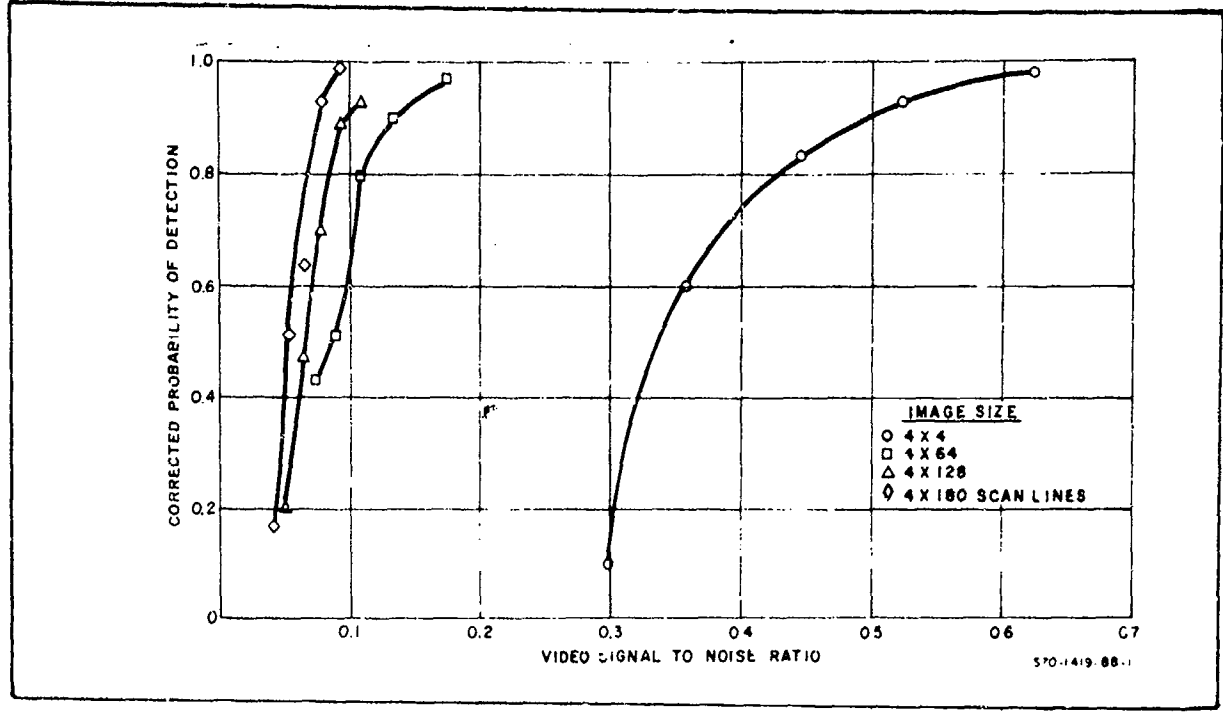
Fig. 67 Probability of Detection vs Video Signal-to-Noise Ratio
required for Rectangular Images of size ○ 4 x 4, □ 4 x 64,
△ 4 x 128, and ◇ 4 x 180 Scan Lines. Televised Images at
30 frames per second $D_V/D_H = 3.5$.

notion, we measured probability of detection vs SNR_V and SNR_D for

rectangles of size 4 x 4, 4 x 64, 4 x 128 and 4 x 180 scan lines. The

results, plotted in the form of probability of detection vs video SNR are

shown in Fig. 67   where it is seen that the larger the image length*, the

smaller the SNR_V required for a given level of probability. When the

probability of detection is plotted vs the display signal-to-noise ratio

as calculated using Eq. (130) and shown in Fig. 68 , the data collapses to

a single curve confirming the original hypothesis. Observe that the angular

extent of the test images relative to the observer's eye varied from 0.13° x

0.13° for the smallest rectangle to 0.13° x 6.02° for the largest rectangle.

This experiment infers that the eye can integrate over very large angles

---

* In this experiment, the longitudinal axis of the rectangle was horizontal.

131
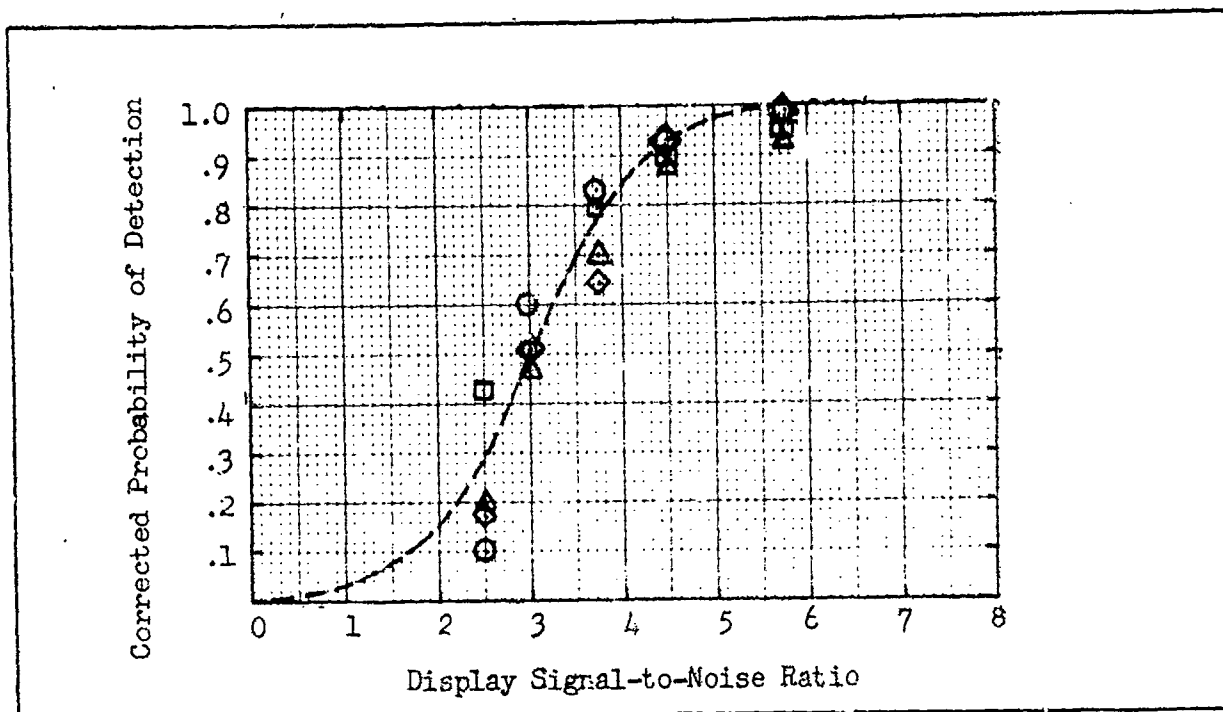
Fig. 68 Corrected Probability of Detection vs SNR_D required for Rectangular Images of Size $\circ$ 4 x 4, $\square$ 4 x 64, $\triangle$ 4 x 128, and $\diamondsuit$ 4 x 180 Scan Lines. Televised Images at 30 frames per second and 525 Scan Lines. $D_V/D_H = 3.5$.

in space; angles which are much larger than were previously thought to be the case. A review of the literature indicates that the eye's ability to spatially integrate with high effectiveness is limited to considerably smaller angles – perhaps $\frac{1}{2}$ to 1°.

Two possible explanations were advanced. One is that the imagery displayed on a CRT is a "flying spot" of very high intensity and that the eye is a differentiator. Thus, in viewing televised imagery, the eye differentiates the signal line by line and thus recovers all of the signal. The second thought was that the eye is more sensitive to edges than to areas (the Mach effect) and that the test image is nearly "all edge" since it is a long thin rectangle.

A second experiment was performed using a rectangle of length 4 scan lines or angular subtense 3.2° and of variable widths of 4, 8, 16
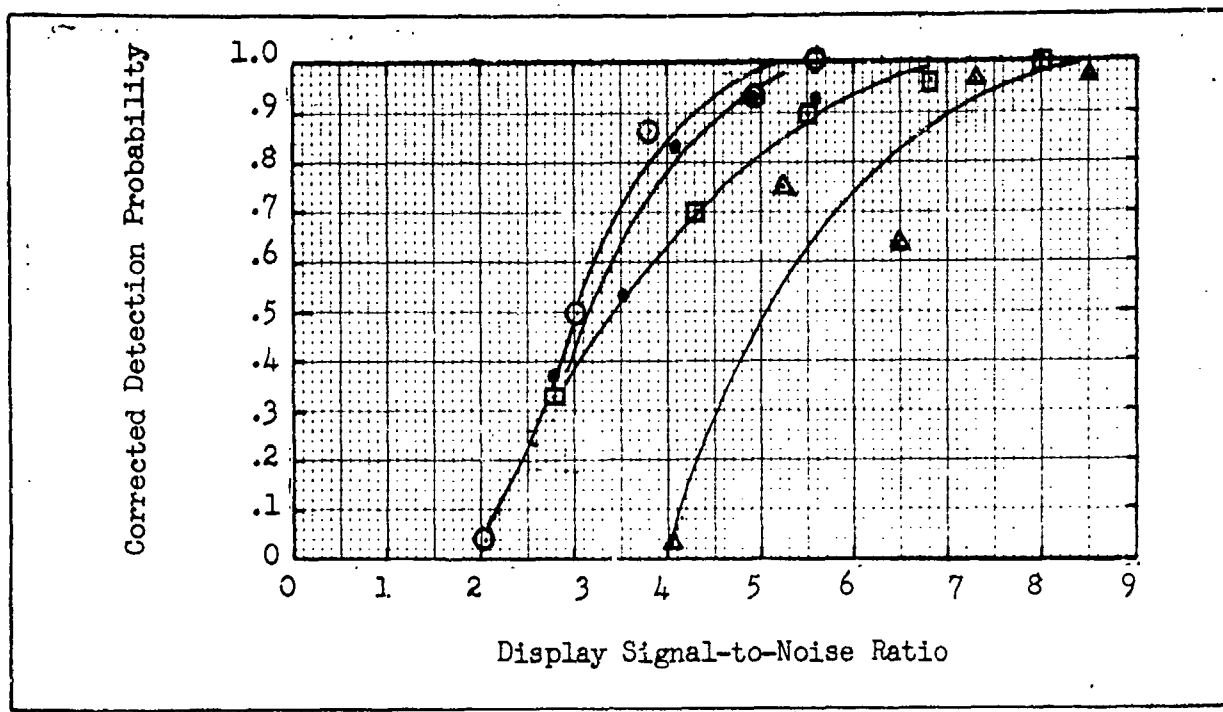
Fig. 69   Probability of Detection vs Display Signal-to-Noise
Ratio for a Rectangle of Height 96 Scan Lines and
Widths • 4, ○ 8, ☐ 16 and △ 32 Scan Lines. Televised
Imagery at 30 Frames/Sec, 525 lines. $D_V/D_H = 3.5$.

and 32 scan lines corresponding to angular subtenses of 0.13°, 0.267°,
0.534° and 1.07° relative to the observer. The corrected probability of
detection for this case is shown for the various rectangles in Fig. 69
and a plot of the thresholds as a function of image size is shown in Fig. 70.
For narrow long rectangles, the same threshold value of SNR_D is obtained
as was obtained for narrow rectangles of various lengths (Fig. 70) and
we conclude that for narrow widths (angular substance of up to about $.5^{\circ}$)
that the eye fully integrates the whole area of the rectangle but for wider
rectangles of angular subtense larger than 0.5°, the eye is apparently
less efficient in utilizing image area. The reduced ability of the eye
in integrating disks and squares of angular extent larger than 0.5° has
also been noted in the literature. It is therefore of interest to perform
additional experiments to establish the integration limits for squares.

133
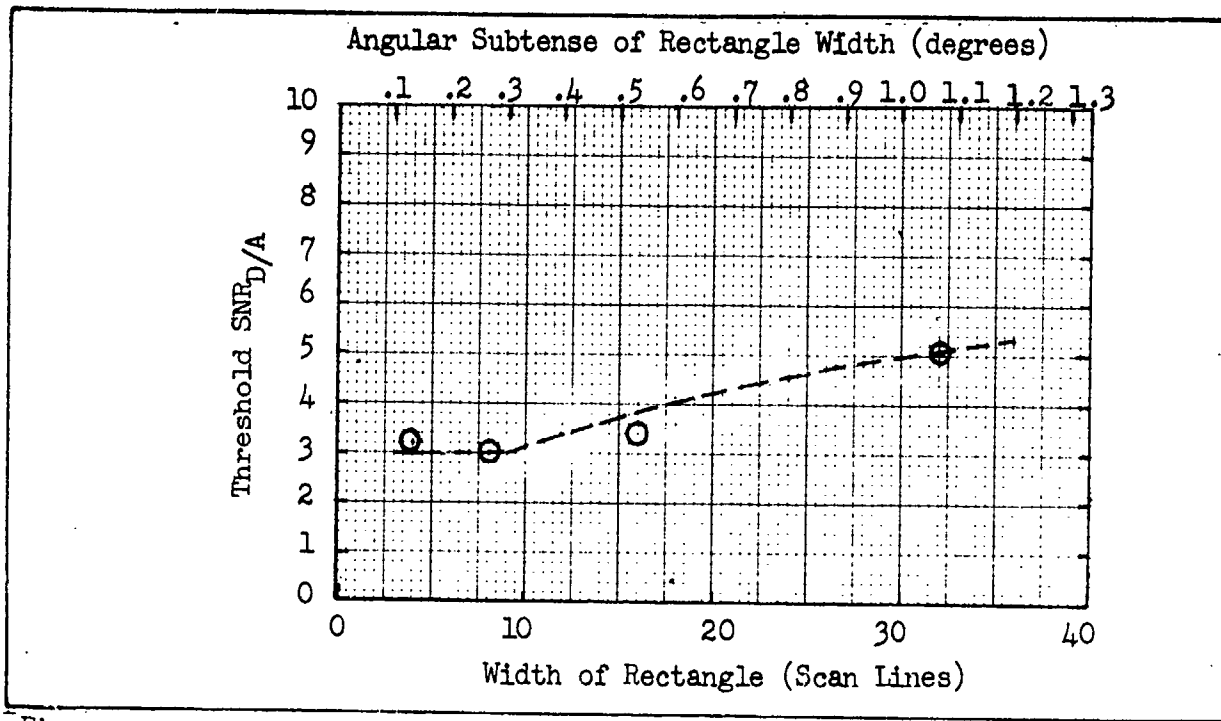
Fig. 70 Threshold SNR_D as a Function of the Linear and Angular Extent of a Rectangle of Height 96 Scan Lines (3.2^O) and Variable Width 4, 8, 16 and 32 Scan Lines (0.013^O, 0.267^O, 0.534^O and 1.07^O). Dashed Curve is Theoretical. Televised Imagery at 30 Frames/Second and 525 Scan Lines $D_V/D_H = 3.5$.

In the first square experiment, square images were used of size 2 x 2, 4 x 4, 8 x 8 and 16 x 16 scan lines for which the probability of detection vs SNR_D are as plotted in Fig. 71 . The best estimate of SNR_D thresholds were as noted in Fig. 72 . A statistical analysis for the 4 x 4, 8 x 8 and 16 x 16 scan line images indicated that image size was not significant but that size is significant when the 2 x 2 line data is included. However, the increase in SNR_D thresholds has been consistently noted for the 2 x 2 and 16 x 16 line images in other experiments and had these other data been included in the analysis, significance would probably have been found for the 16 x 16 rectangle as well, that is, it was likely that the rise in SNR_D indicated for the 16 x 16 square is real, and not due to random error.

To further investigate, experiments were performed using squares of larger angular extent with the results shown in Figs. 73 and 74 .

134
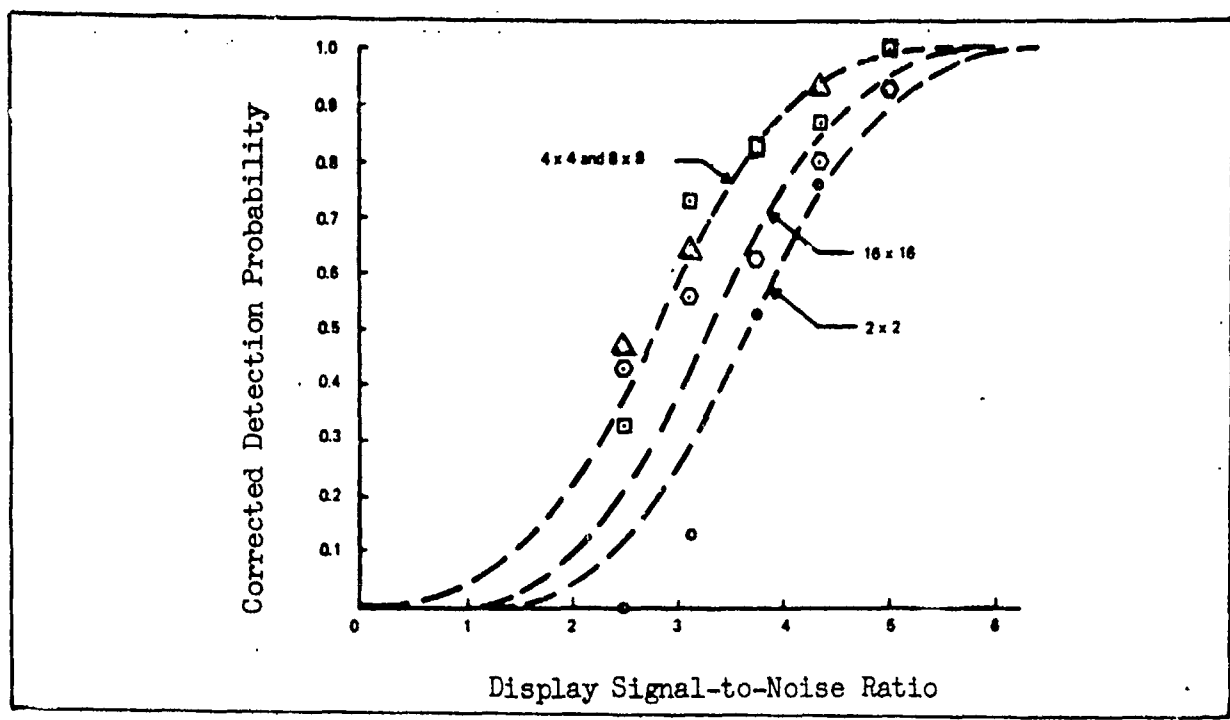
Fig. 71   Probability of Detection vs Display Signal-to-Noise
Ratio for Square Images of Size O 2 x 2, □ 4 x 4,
△8 x 8 and O 16 x 16 Scan Lines. Televised Images
at 30 frames/second and 525 Scan Lines. $D_V/H = 3.5$.

Image Size (Scan Lines)	Threshold SNR_D	Angular Subtense Relative to Observer's Eye
2 x 2	3.7	.065°
4 x 4	2.8	.013°
8 x 8	2.8	.267°
16 x 16	3.3	.534°

Fig. 72   Threshold Display Signal-to-Noise Ratio vs Image Size for
Various Square Images.

135
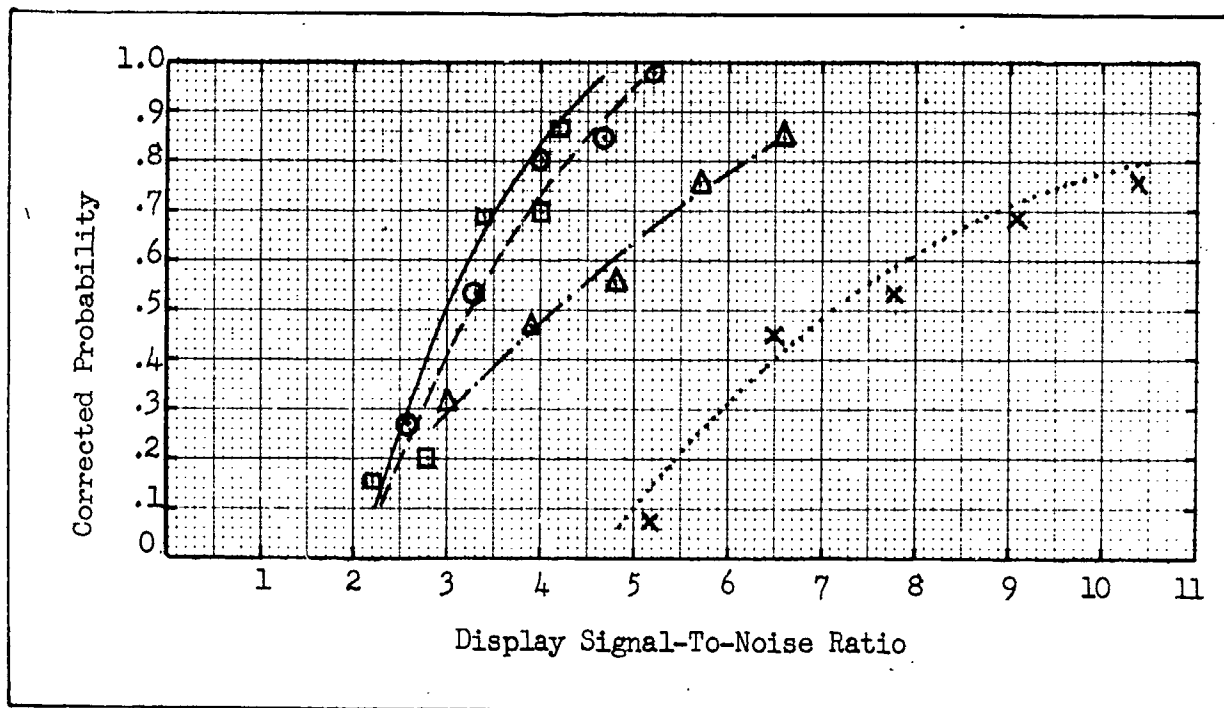
Fig. 73   Corrected Probability of Detection vs SNR_D required
for Square Images of Size □ 8 x 8, 0 16 x 16,
△ 32 x 32 and x 64 x 64 Scan Lines. Televised
Images at 30 frames per second and 525 Scan Lines. $D_V/D_H = 3.5$.

These data were taken using a wider noise spectrum (12.5 MHz as opposed to

7.1 MHz previously) and with a brighter display background (1 f.L. vs 0.2

f.L. previously). The increase in video noise bandwidth and display

brightness was not expected to change the SNR_D thresholds and did not.

The thresholds did increase for the larger angular sizes, however, being

about 2.5 times larger for the squares of 2^O angular subtense than for

squares of subtense less than 0.5^O.

Thus, for both rectangles and squares we found as a result

that the eye is efficient in integrating the full image area only up to

angular subtenses of about 0.5^O*.

---

* When the angular subtense is greater than 0.5^O in two dimensions.
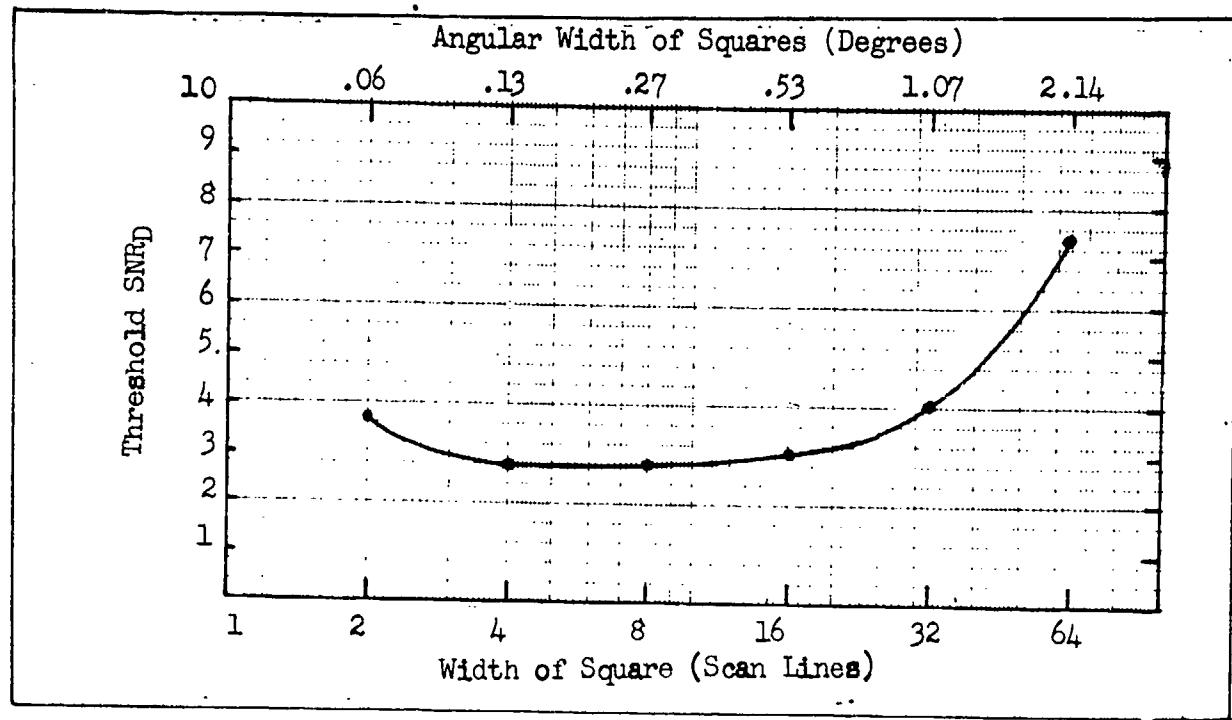
Fig. 74   Threshold SNR$_D$ required to detect Square Images of
           Various Size and Angular Extent. Televised Images
           at 30 frames/second, 525 Scan Line Raster. $D_V/D_H = 3.5$.

As a possible explanation for the observed increases in threshold,
we hypothesized that the eye actually integrates signal from an area around
the perimeter of the area rather than the total area. This is indicated
by the geometry of Fig. 75   . Let the angular extent of the test image
rectangle be θ_x by θ_y relative to the observer's eye. Assume that the eye
integrates the total area of the image if both $\theta_x < 2\,\alpha_x$ and $\theta_y < 2\,\alpha_y$, i.e.,

$$SNR_D \approx (\theta_x \cdot \theta_y)^{\frac{1}{2}} ,\qquad\qquad (131)$$

and for larger rectangles, our trial expression is

$$SNR_D \approx \left[(\theta_x \cdot \theta_y) - (\theta_x - 2\alpha_x) \cdot (\theta_y - 2\alpha_y)\right]^{\frac{1}{2}}$$

137
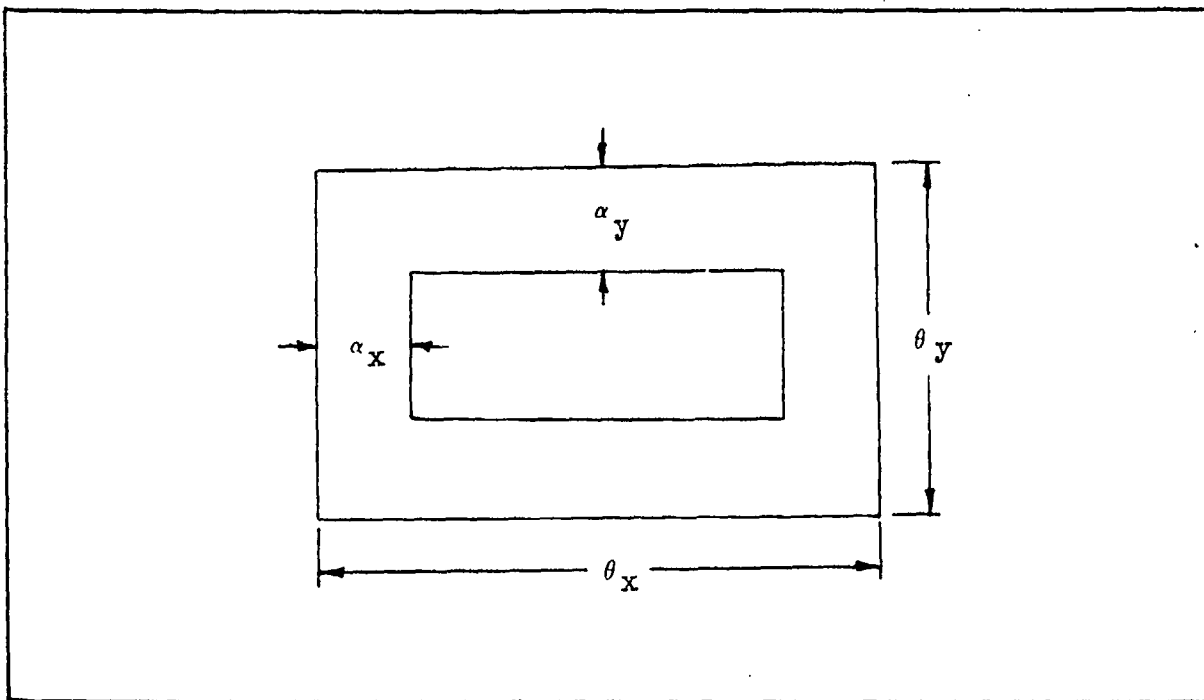
Fig. 75 Geometry for the Display Signal-to-Noise Ratio Analysis
for Rectangles of Large Angular Extent.

$$\approx \ [2\theta_x\alpha_y + 2\theta_y\alpha_x - 4\alpha_x\alpha_y]^{\frac{1}{2}} \tag{132}$$

provided that both θ_x and θ_y are larger than $2\alpha_x$ and $2\alpha_y$ respectively.

For squares, if $\alpha_x = \alpha_y = \alpha$ and $\theta_x = \theta_y = \theta$

$$SNR_D \ \approx \theta, \ \theta \leq 2\alpha \tag{133}$$

and

$$SNR_D \ \approx 2 \ [\alpha\theta - \alpha^2]^{\frac{1}{2}} \ , \ \theta \overset{>}{=} 2\alpha \tag{134}$$

For comparison purposes, we form the ratio of thresholds

$$\frac{SNR_D \ \text{(Threshold Calculated on total area bases)}}{SNR_D \ \text{(Threshold Calculated on perimeter area basis)}} \tag{135}$$

138
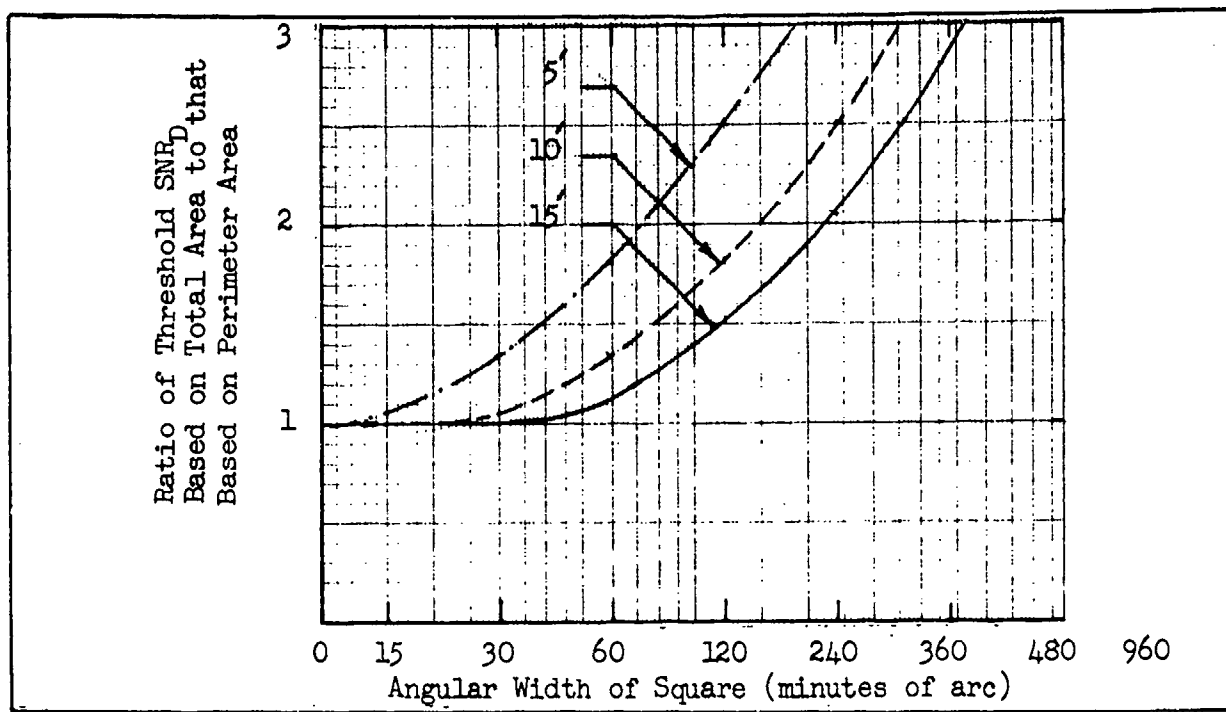
Fig. 76   Ratio of Threshold Display Signal-to-Noise Ratio Computed for
Squares on the Basis of Total Area to that Calculated on the Basis of
Perimeter Area vs the Square's Angular Width Relative to the Observer's
Eye for Three Values of Perimeter Area Integration Angles.

These ratios are plotted in Fig. 76   for three values of α; 5, 10 and

15 minutes of arc. It is seen from comparing Figs. 74 and 76

that the shapes of the curves are similar and that the computed 10' curve of

Fig. 76   would give a good fit to the measured data of Fig. 74 .

        If the perimeter area concept is to have any merit, then we should

be able to offset the increase in threshold that was noted by increase in

the objects angular extent by simply increasing the observer-to-display

viewing distance. Hence, an experiment was performed in which the observer's

viewing distance was increased from 28" to 56". As shown in Fig. 77   , the

expected effect did occur. Thus, the premise that the eye integrates only

around the perimenter, though not proven, is at least, made plausible.

        Before proceeding, we observe that the probability model used to

139
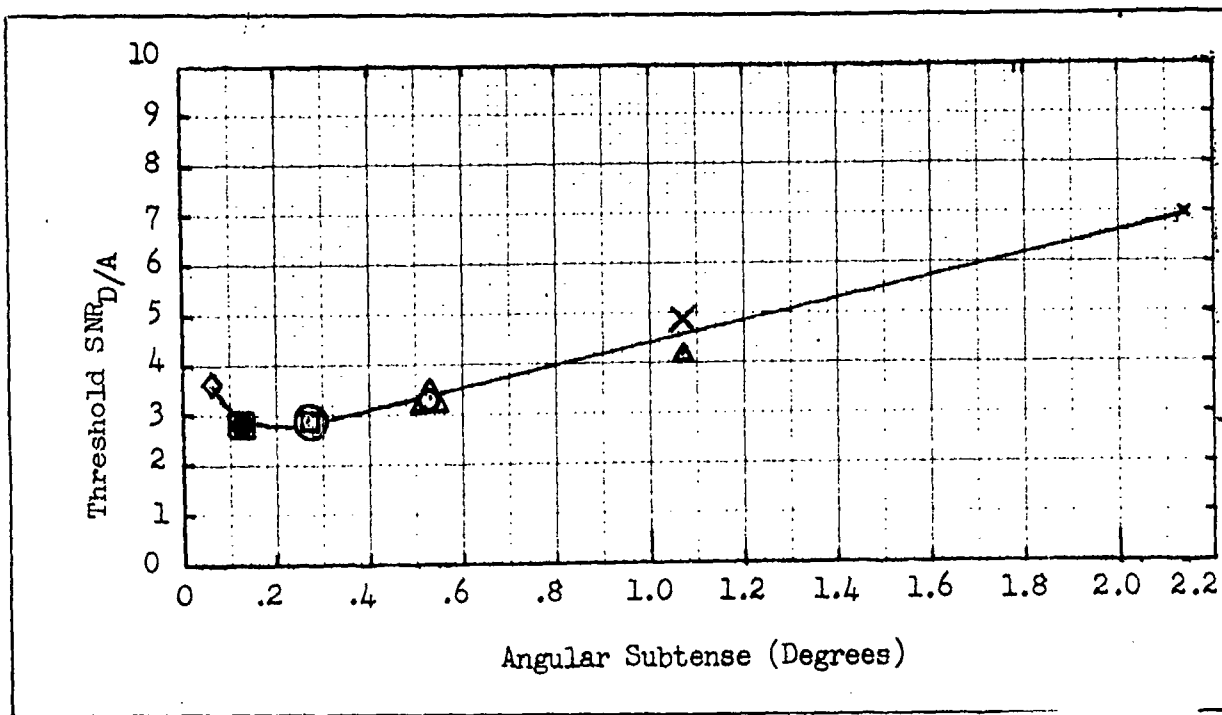
Fig. 77   Threshold Display Signal-to-Noise Ratio required to detect
Square Images as a Function of Their Angular Size for Two Viewing
Distances, 28" and 56", Image Size on Display is ◇2, ● 4, □ 8, 0 16,
△32, X64 Scan Lines on a side. Large Symbols at 56", Small at 28",
Televised Images at 30 Frames/Second, 525 Lines Scan. $D_V/D_H = 3.5$ and 7.0.

fit the experimental points of Fig. 68   are based on a model originally

suggested by Legault (3). In this model, it is assumed that the mean

number of photoelectrons within the sampling area and period has become

sufficiently large so that the Guassian or normal probability distribution

law given by

$$f_Z(z) = \exp[-z^2/2]/(2\pi)^{\frac{1}{2}} , \tag{136}$$

becomes a good approximation to the Poisson distribution law, which

actually represents the signal and noise processes. In the above, Z is a

random variable which is numerically equal to

$$Z = SNR_D - SNR_{DT} , \tag{137}$$

140

where SNR_{DT} is the threshold display signal-to-noise ratio which is generally regarded to be that needed to obtain a detection probability of 0.5. The random variable Z is of unit mean and variance. Other values of probability are obtained from the formula

$$P_d \ (-\infty < Z < z_2) \ = \ \frac{1}{2\pi^{\frac{1}{2}}} \int_{-\infty}^{z_2} \exp \ (-z^2/2) \ dz \qquad (138)$$

which cannot be integrated in closed form but is widely available in standard mathematical tables.

4.2 Stationary Periodic Images

The periodic test images used were primarily bar patterns of various height-to-width ratios, spatial frequencies and numbers of bars in the pattern. The experimental setup of Fig. 78 was used to perform the necessary psychophysical experiments. Test images are projected on the faceplate of a high resolution $1\frac{1}{2}$" vidicon operated at highlight video signal-to-noise ratios of 50:1 or better. The camera and TV monitor were operated at 25 frames/second with 875 scanning lines (825 active). Band-limited white noise of Guassian distribution was mixed with the camera generated signal. Both the signals and noise were passed through identical filters (noise equivalent bandwidth of 12.5 MHz) prior to mixing in the monitor. The monitor luminance was approximately 1 ft. Lambert unless otherwise specified. The displayed picture height was 8" and, unless otherwise stated, the observer-display distance was 28".

For the first series of experiments, the test images were bar patterns of various spatial frequencies and bar height-to-width ratios. The observer was required to state whether or not the pattern displayed was

141
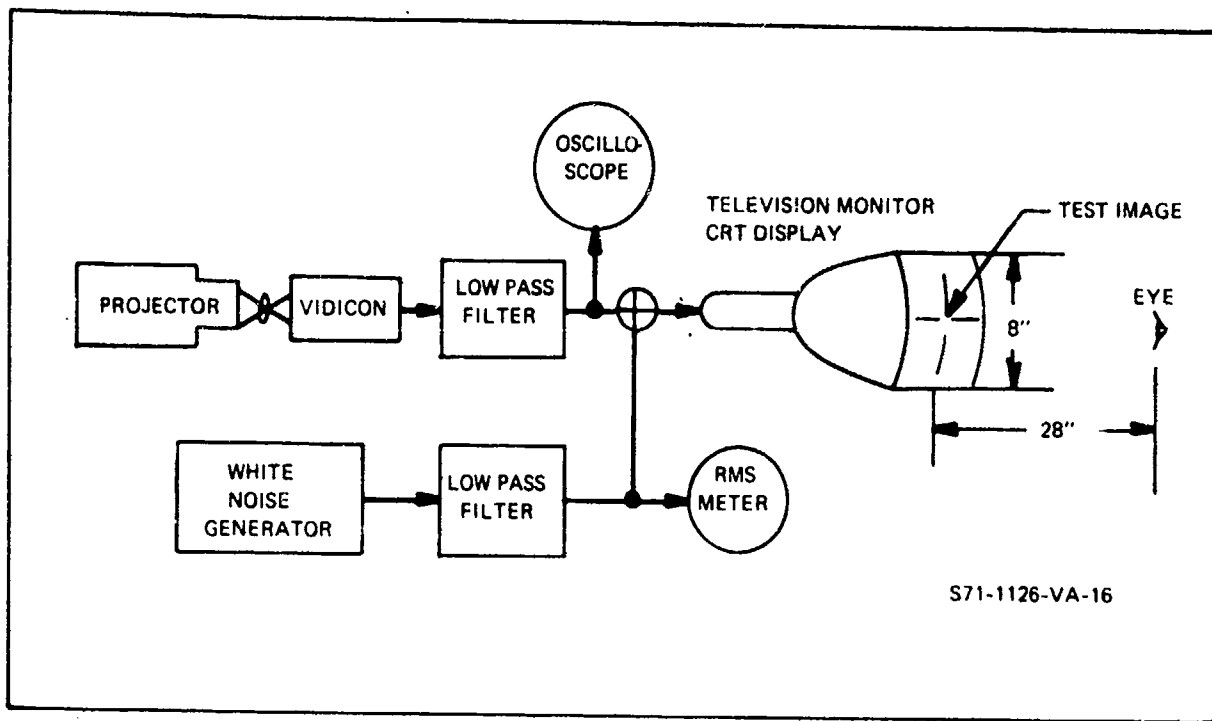
Fig. 78   Experimental Set-up for Television Camera Generated Imagery.

resolvable as the images SNR_D were randomly varied. Chance was not involved since the patterns were always present on the display. The experimental constants for the various experiments are given in Fig. 79 . The purpose of the first series of experiments was to determine the effect of bar height to width ratio on the bar pattern detectability with the results shown in Figs. 80, 81 and 82 . At low spatial frequencies of 104 lines/ picture height, the threshold signal-to-noise ratio SNR_{DT} is seen to increase slightly with bar height-to-width ratio (Fig. 80), while at the highest spatial frequency of 396 lines per picture height, the SNR_{DT} required is very nearly independent of bar height-to-width ratio as shown in Fig. 82 . By threshold SNR, it is implied that 50% of the total number of patterns displayed are resolved (or "barely discerned"). The SNR_{DT} values are summarized in Fig. 83 as a function of spatial frequency and are seen to

142

Exp No.	Test Images	1 $\frac{D_V}{D_H}$	2 B_D Ft-L	3 Δf_V MHz	No. of Obsvrs	4 No. of Trials	5 Response Forced	Figure Numbers
	NOTES*							
1	Bar Patterns, Various n_V & N	3.5	1.0	12.5	5	2,350	NO	80, 81, 82
2	Bar Patterns, Various N	3.5	1.0	12.5	5	460	NO	86, 87
3	Bar Patterns, Horizontal	3.5	1.0	12.5	1	280	YES	88
4	Bar Patterns, Various D_V/D_H	1.75 / 3.5 / 7.0	1.0	12.5	14	2,476	NO	89
5	Bar Patterns, Variable D_V/D_H	Optimum	1.0	12.5	5	1,210	NO	90

* NOTES:

1. Display Viewing Distance to Height Ratio
2. Display Brightness (Ft-L)
3. Noise Equivalent Bandwidth (MHz)
4. Total Trials/Experiment, 10 seconds per trial
5. In YES to Forced Response – Observer Picks Pattern of Highest Spatial Frequency Visible

Fig. 79   Test Conditions for the Psychophysical Experiments.

143
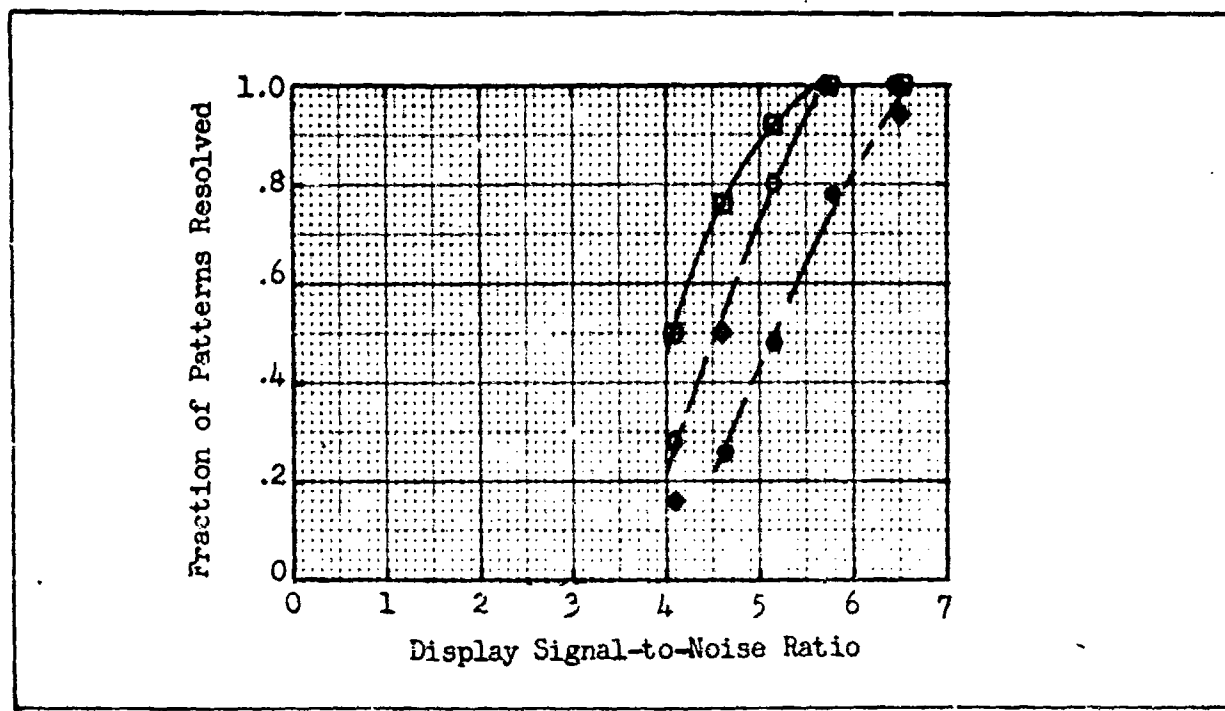
Fig. 80   Fraction of Bar Patterns Resolved vs. Display Signal-to-Noise
Ratio for a 104 Line Bar Pattern of Bar Length to Width Ratio
▢ 5:1, ○ 10:1, ● 20:1 Televised Images at 25 Frames/Sec,
875 Scan Lines, $D_V/D_H = 3.5$.
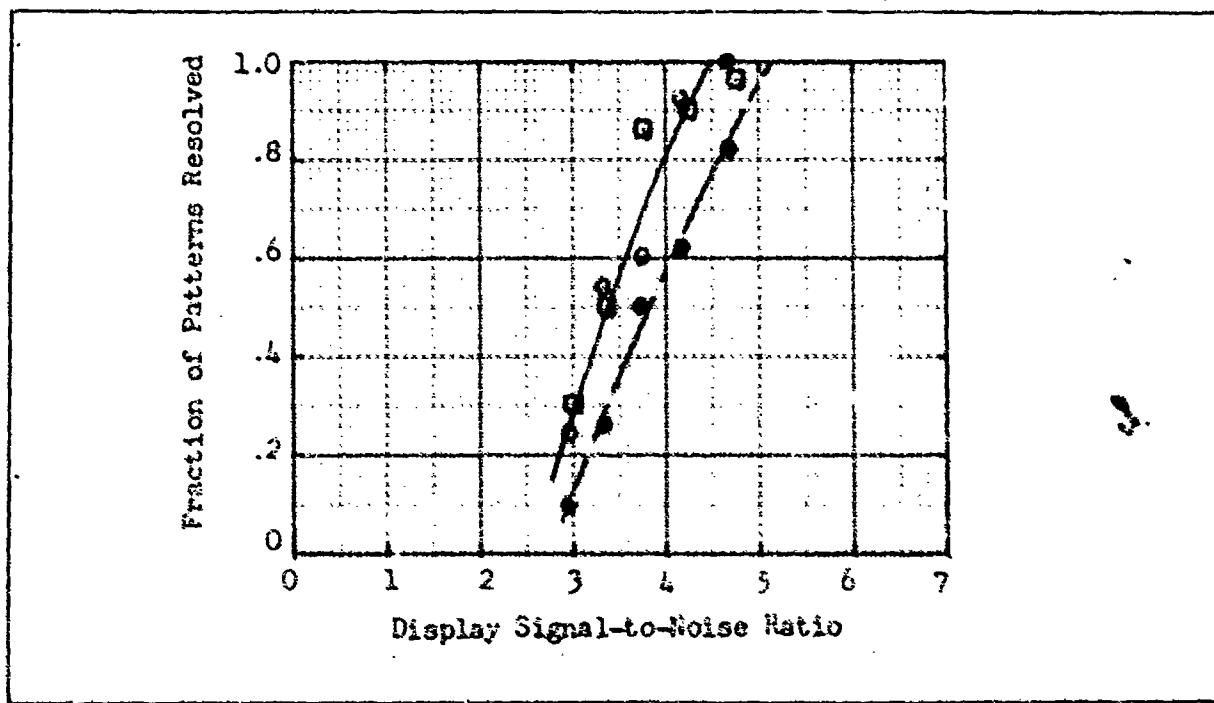
Fig. 81   Fraction of Bar Patterns Resolved vs. Display Signal-to-Noise
Ratio for a 200 Line Bar Pattern of Bar Length to Width Ratio
▢ 5:1, ○ 10:1, ● 20:1 Televised Images at 25 Frames/Sec,
875 Scan Lines, $D_V/D_H = 3.5$
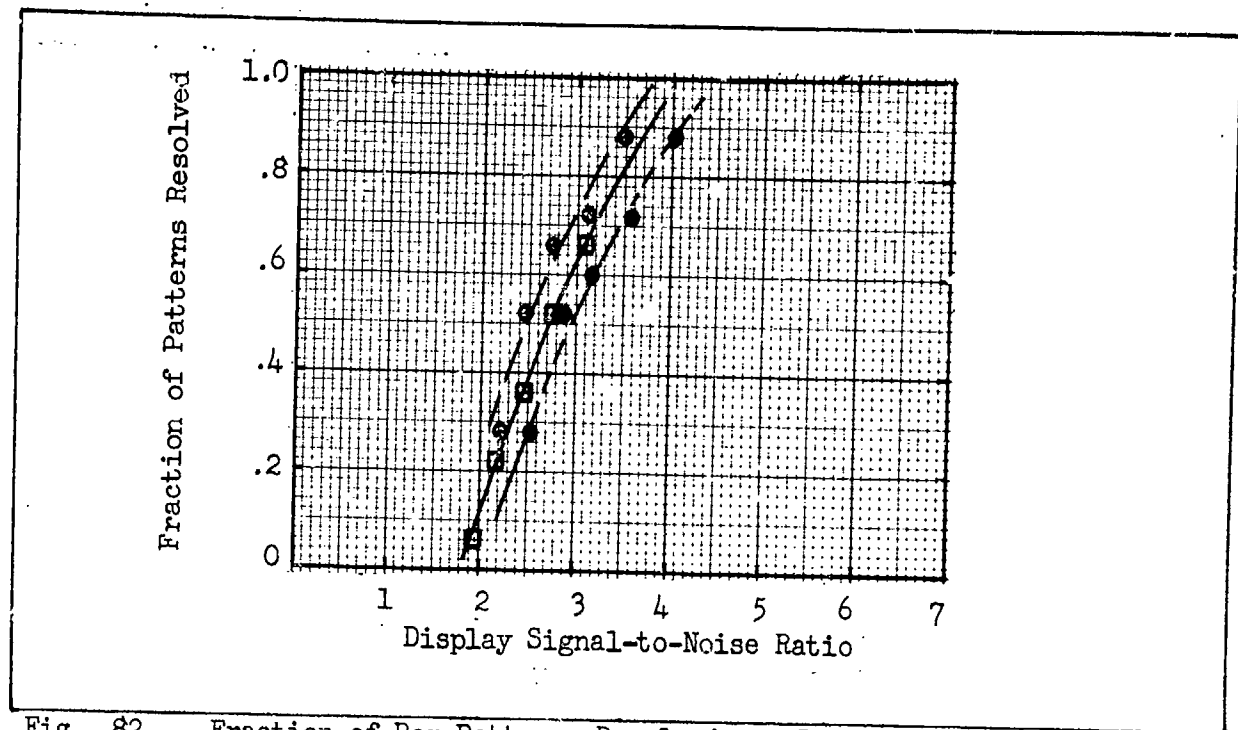
Fig. 82   Fraction of Bar Patterns Resolved vs. Display Signal-to-Noise
Ratio for a 396 Line Bar Pattern of Length-to-Width Ratio
□ 5:1, ○ 10:1, ● 20:1 Televised Images at 25 Frames/Sec.
875 Scan Lines, $D_V/D_H = 3.5$.
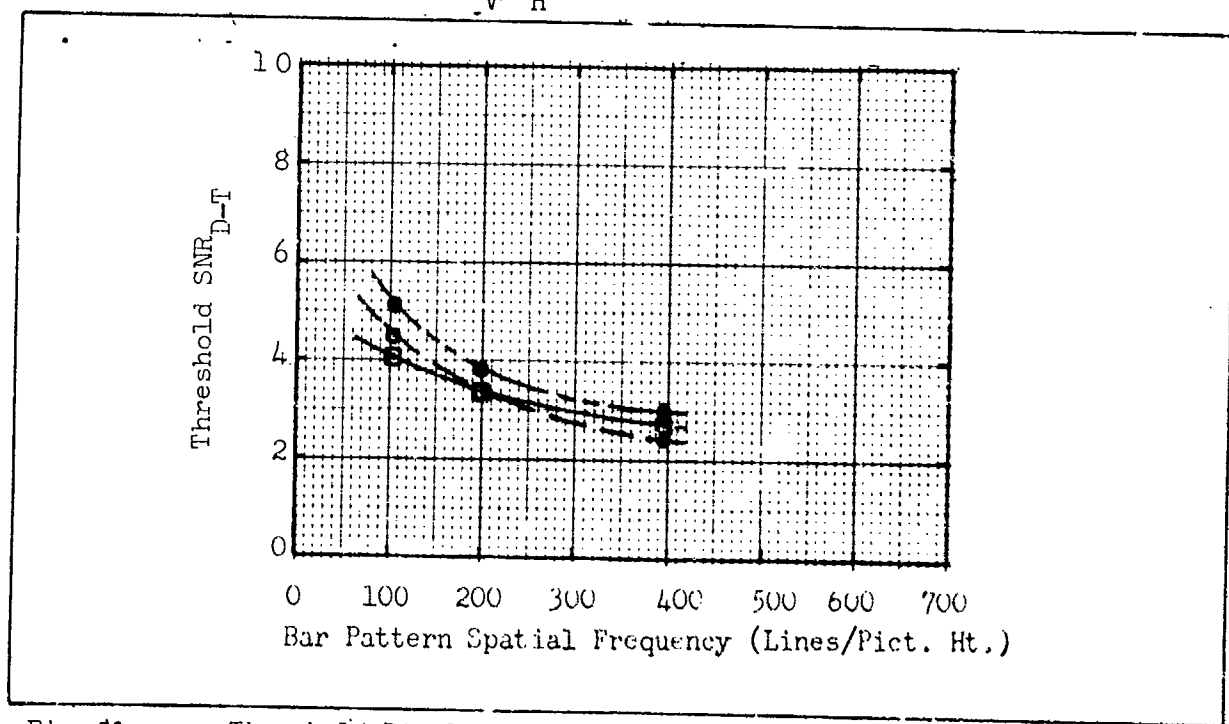
Fig. 83   Threshold Display-Signal-to-Noise Ratio vs. Bar Pattern
Spatial Frequency for Three Bar Length-to-Width Ratios of
□ 5:1, ○ 10:1, ● 20:1 Televised Images at 25 Frames/Second,
875 Scan Lines, $D_V/D_H = 3.5$

decrease slowly with line number for all of the patterns. Also, note that the number of bars in the various patterns were varied. For the 5:1 pattern, 5 bars were used; for the 10:1, 9 bars and for the 20:1, 17 bars. Length-to-width ratio and SNR were randomly varied. In these experiments, the angular subtense of a single bar in the pattern was as shown in Fig. 84.

Recall from Section 3 that SNR_D is calculated on the basis of the total area of a bar. Specifically, the Eq. (121) of Section 3, slightly modified is

$$SNR_D = [\frac{2tn_v \Lambda f_v}{\alpha}]^{\frac{1}{2}} \frac{R_{SF}(N)}{N} (\frac{\Delta i}{I_n}) , \qquad (139)$$

was used. In the above, Δi is the peak-to-peak signal current for a broad area pattern (unity modulation transfer function) and I_n is the rms noise that is added to the camera generated image. Real cameras, of course, have a response that is a function of frequency and the value of Δi in the video channel for square wave inputs becomes Δi_{p-p}, the peak-to-peak value of the video signal when the frequency effects are included, that is, we have

$$\Delta i_{p-p} = \Delta i \ R_{SQ}(N) \qquad (140)$$

Combining Eqs. (139) and (140), we have that Eq. (139) becomes

$$SNR_D = [\frac{2tn_v \Delta f_v}{\alpha}]^{\frac{1}{2}} (\frac{1}{N}) \frac{R_{SF}(N)}{R_{SQ}(N)} \frac{\Delta i_{p-p}}{I_n} \qquad (141)$$

where $R_{SF}(N)$ is the value of the flux factor at N, $R_{SQ}(N)$ is the value of the square wave response at N and Δi_{p-p} the value of the peak-to-peak signal

146

Bar Pattern Spatial Freq. (Lines/Pict. Ht.)	Angular Subtense in the Horizontal (degrees)	Angular Subtense in the Vertical for Bar Length to Width Ratios of		
		5	10	20
104	0.157°	0.785°	1.57°	3.14°
200	0.0818°	0.409°	0.818°	1.636°
396	0.0413°	0.2065°	0.413°	0.826°

Fig. 84   Angular Subtense of a Bar in Each Experiment Relative to the Observer as a Function of the Bar Length to Width Ratio.

corresponding to N as measured in the output of the video channel. For calculation purposes, t, the integration time of the eye is taken to be 0.1 sec and α, the picture aspect ratio is 4/3.   At low spatial frequencies the displayed images approach a square wave while at high spatial frequencies, above about 500 lines/picture height, the displayed images were nearly pure sine waves. In Fig. 85, the value of modulation transfer function, square wave response and flux factor are shown for the vidicon.

To further confirm the fall-off in thresholds at the higher spatial frequencies, a second series of experiments were performed using bar patterns with bars of 5:1 height-to-width ratio. A number of bar patterns of various spatial frequencies were displayed at the same time and the observer was asked to indicate the pattern of highest frequency that was
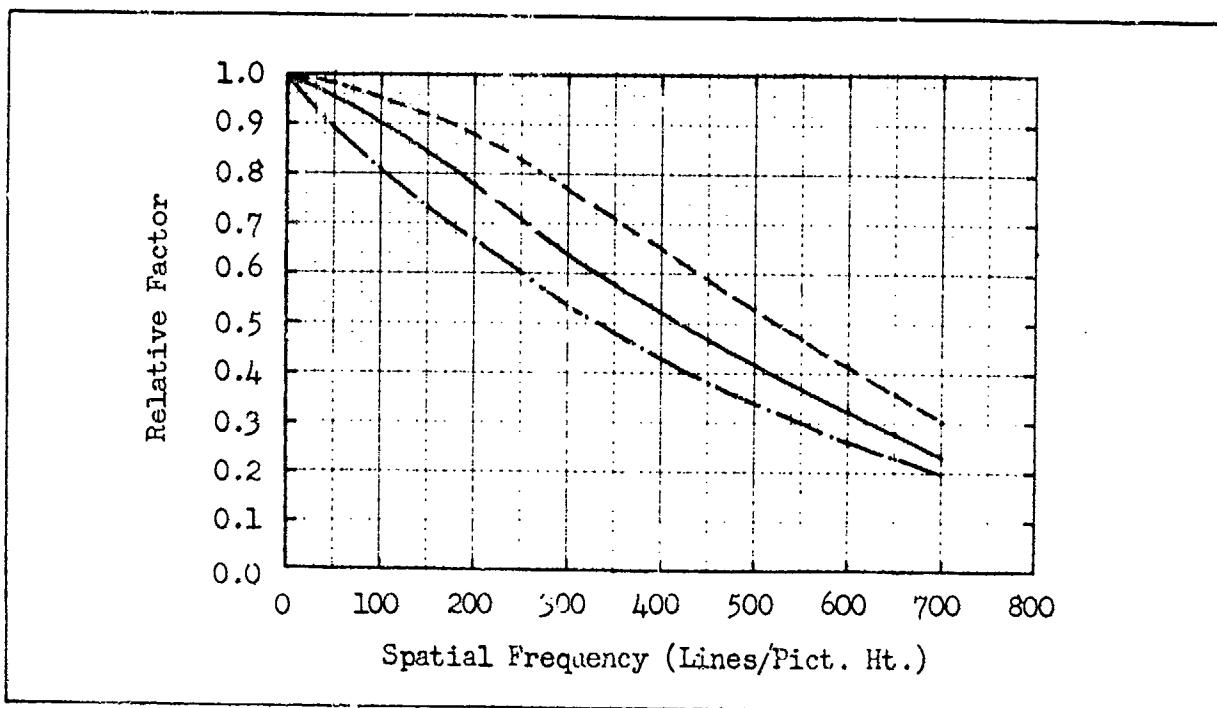
Fig. 85   Square Wave Amplitude (- - -), Modulation Transfer (———), and
Square Wave Flux (—·—) Functions for the $1\frac{1}{2}$" Vidicon used in
Bar Pattern and Real World Object Experiments.

barely visible as the signal-to-noise ratio was systematically varied from

high levels to low levels and the reverse in steps of 1 db. The fraction

of patterns resolved by this "method of limits" are plotted in Fig. 86   as

a function of Display Signal-to-Noise ratio and the thresholds determined are

plotted in Fig. 87 . Also plotted are the results determined in the

previous experiment. As can be seen, the "method of limits" gives the same

values for the thresholds and do confirm the fall-off in threshold with

spatial frequency. The method of limits is used in measuring the limiting

resolution of real camera tubes and this method of test thus appears to be

appropriate.

In the above experiments, the bar patterns were vertically

oriented with their longitudinal axes perpendicular to the direction of

scan. The results with the axes horizontal are shown in Fig. 88 . One
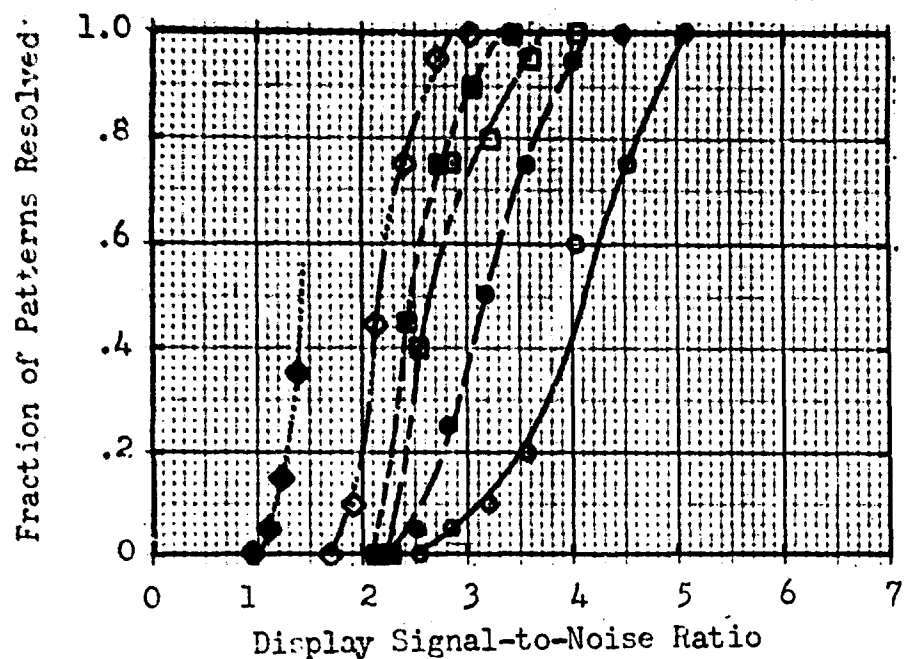
Fig. 86   Fraction of Bar Patterns Resolved vs. Display Signal-to-Noise
Ratio for Bar Patterns of Spatial Frequency ○ 104, ● 200, ◻ 329,
◼ 396, ◇ 482 and ◆ 635 Lines per Picture Height. Bar Height-to-
Width Ratio was 5 in All Cases. Televised Images at 25 Frames/
Sec, 875 Scan Lines, $D_V/D_H = 3.5$
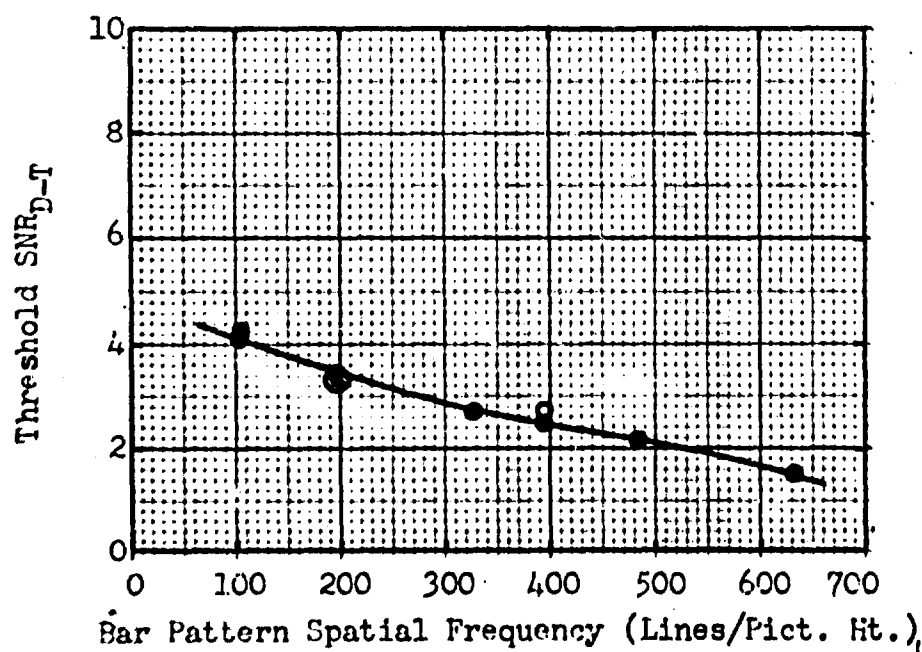
Fig. 87   Threshold Display Signal-to-Noise Ratio vs. Bar Pattern Spatial
Frequency obtained using Two Different Experimental Techniques;
● Method of Limits,   ○ Method of Random SNR Variation.
Televised Images at 25 Frames/Sec, 875 Scan Lines, $D_V/D_H = 3.5$.
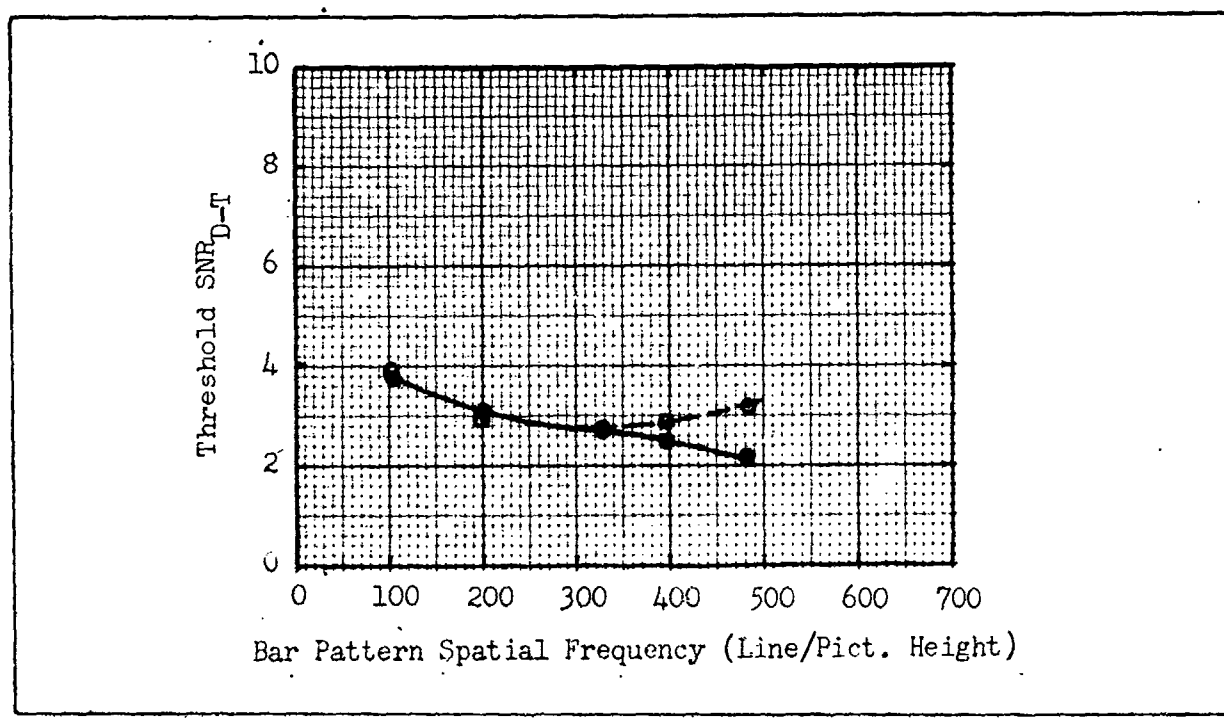
Fig. 88   Threshold Display Signal-to-Noise Ratio required to recognize
          the Presence of, ○ Horizontally Oriented and, ● Vertically
          Oriented Bar Patterns vs. Bar Pattern Spatial Frequency. Televised
          Images at 25 Frames/Sec., 875 Scan Lines, D_V/D_H = 3.5. Bar
          Height-to-Width Ratio was 5.

observer was used for the experiment. Also shown in Fig. 88 are the

results for vertical bars for the same observer (virtually, the same results

as those shown in Fig. 87). As can be seen, the orientation is immaterial

at the low spatial frequencies but the thresholds for the high spatial

frequencies increase with horizontal bars. Indeed, the 635 line pattern

could only be seen with no noise added to the signal.

        In the next bar pattern experiment, viewing distance was varied

in discrete steps from 14" to 28" to 56". The bars were vertically oriented.

The results are as shown in Fig. 89 . At the short distances, the low

pattern frequencies become less detectable while the reverse was true at

the long viewing distances. It is clear from Fig. 89 that, for a given line

number there is a viewing distance that minimizes threshold SNR_D. In the

final bar pattern experiment, the observer adjusted his position at each

150
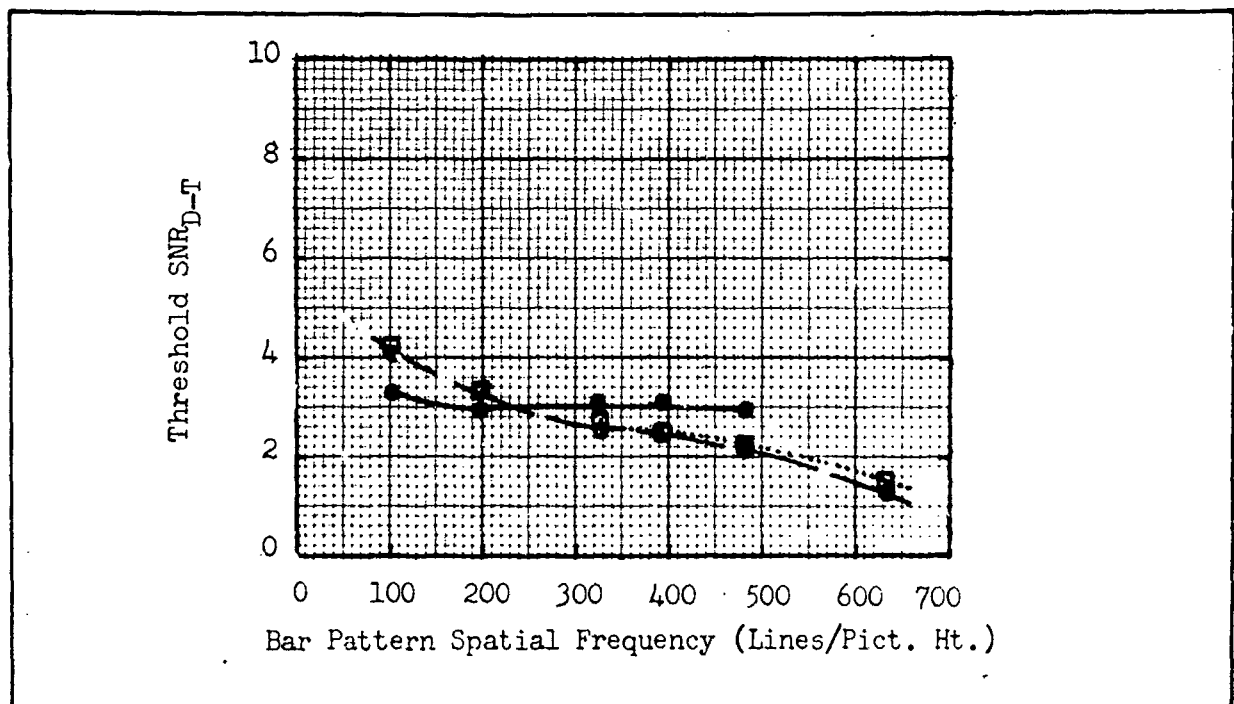
Fig. 89 Threshold Display Signal-to-Noise Ratio vs. Bar Pattern Spatial
Frequency for Display to Observer Viewing Distances of O 14",
□ 28" and ● 56". Televised Images at 25 Frames/Sec and 875
Scan Lines.

SNR_D value to enable him to see the highest line number possible for the

SNR_D value and the threshold values of SNR_D are shown in Fig. 90 . A

comparison of Figs. 89 and 90 shows that the optimum distances for low line

numbers are greater than 56" whereas for high line numbers, optimum distances

are approximately 14" from the 8" high display.

4.3 Levels of Discrimination

In the previous sections, various aspects of target detection were

discussed, and equations were derived for calculating the display signal-to-

noise ratio for detecting aperiodic laboratory targets such as squares and rec-

tangles as well as recognizing periodic patterns such as bar patterns. It was

shown that for a given detection probability that a specific value of display

signal-to-noise ratio was required and that this value was independent of

target size for aperiodic targets and was a slowly varying function of line

151
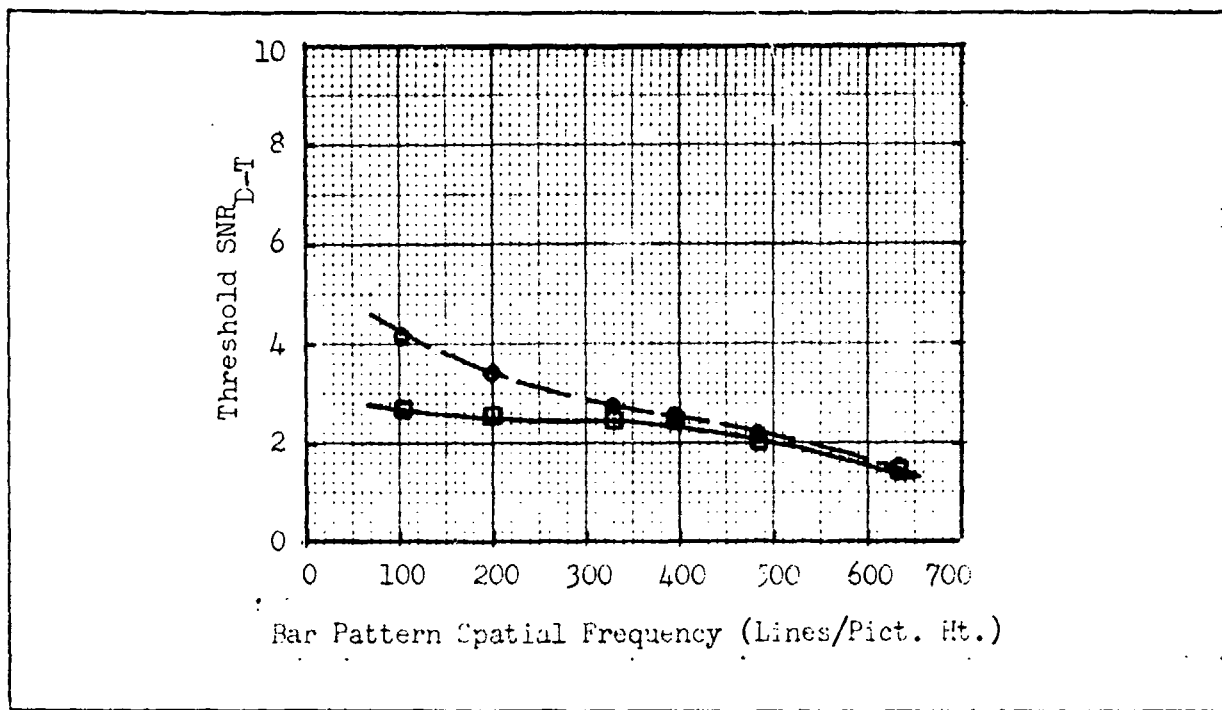
Fig. 90 Threshold Display Signal-to-Noise Ratio vs. Bar Pattern
Spatial Frequency for □ Optimum Viewing Distance and O 28"
Viewing Distance for One Observer.

number for periodic patterns. To perform higher levels of target discrimina-
tion than detection, such as target recognition or identification, we would
intuitively expect that a greater target resolution would be needed since
greater target detail must be discerned. Target detail can be expressed
in terms of resolution lines through the target and in the work by Johnson,
a criterion has been set up which expresses image discrimination in terms of
the number of lines through the minimum target dimension. This criterion
has been widely used. (Johnson's original data was in line paris, but to
be consistent with our symbology, we will use lines.) Johnson also
mentioned the parallel need for adequate signal-to-noise ratio but this
criteria was not often used.

Johnson has classified the levels of target discrimination as
detection, orientation, recognition and identification; and his definition

152

of each of these categories are discussed in Section 3.

In the above it is shown that there is a value of display signal-to-noise ratio which corresponds to bar pattern detection. By recognition it was meant that the observer can resolve the individual bars of the bar pattern. An interesting question is: is there a correspondence between bar pattern recognition and real target discrimination? Such a correspondence would be expected based on the results of Johnson, but the correspondence needs to be established for televised imagery together with the required signal-to-noise ratio values. Before proceeding to the results that were obtained using images of tactical targets, the reader should review the results that were obtained using bar patterns of 5:1, 10:1, and 20:1 length to width ratios (L/W ratios) shown in Fig. 83 .

4.4 Tactical Target Recognition

Two different classes of backgrounds were used for the recognition of tactical targets. The first background was a uniform white background and the second was a transparency of a real background. First, the uniform background case will be considered. The experimental setup is the same as that shown in Fig. 78 in which the transparency on a light box is imaged onto the photosurface of a high resolution $1\frac{1}{2}$" vidicon. Experimental conditions are detailed in Fig. 91 .

The transparencies used in this experiment were high quality photographs of models of vehicles amid white uniform backgrounds. The photographs were taken of the vehicles side aspect but at an angle of 45° to simulate a nadir to object aircraft angle of 45°. These photographs, shown in Fig. 92, included a tank, a van truck, a half track with a top mounted radar antenna and a tracked bulldozer with derrick. The areas of these various objects

Test Line*	Background	1 $\frac{D_V}{D_H}$	2 B_D ft-L	3 Δf_V MHz	4 $\frac{\text{Time}}{\text{Trial}}$ (sec.)	No. of Obsvr.	No. of Trials	Figure No.
Vehicle Recognition	Uniform	3.5	1.0	12.5	10	5	1,000	93
Bar Patterns	Uniform	3.5	1.0	12.5	–	5	872	94
Bar Patterns	Uniform	3.5	1.0	12.5	–	6	761	95
Vehicle Recognition	Road	3.5	1.0	12.5	10	8	800	97
Vehicle Recognition	Grass	3.5	1.0	12.5	10	8	800	98
Vehicle Recognition	Grass-Trees	3.5	1.0	12.5	10	8	800	99
Tank Identification	Uniform	3.5	1.0	12.5	10	5	1,250	101
Tank Identification	Uniform	3.5	1.0	12.5	10	5	1,250	102

NOTES:

* 1. Display Viewing Distance to Height Ratio.

  2. Display Brightness (ft-Lamberts).

  3. Noise Equivalent Bandwidth (MHz).

  4. Time Allowed for Observer Response.

Fig. 91 Conditions for the Recognition and Identification Experiments.
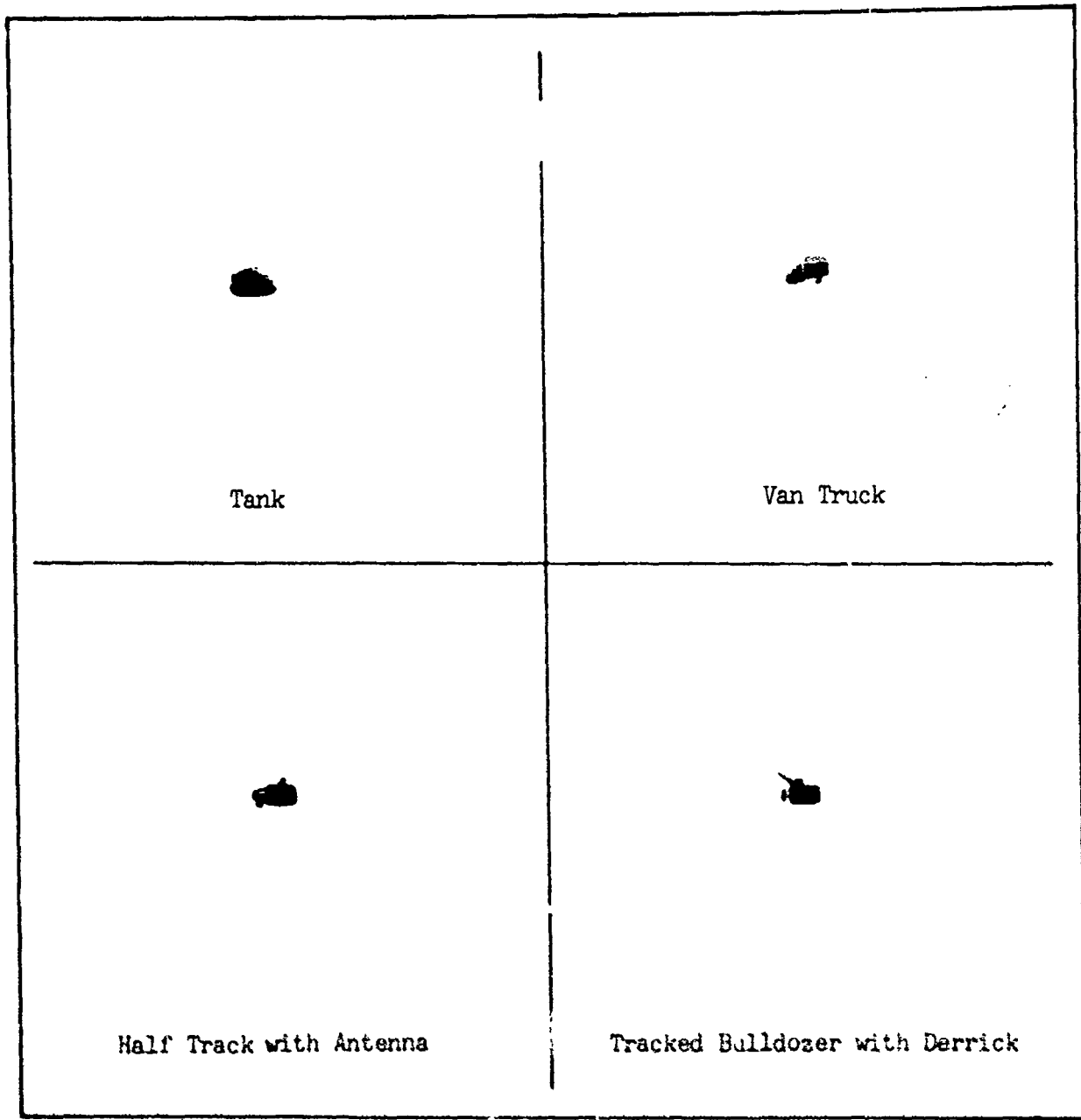
Fig. 92.   Photographs of Models Used for Recognition Experiments
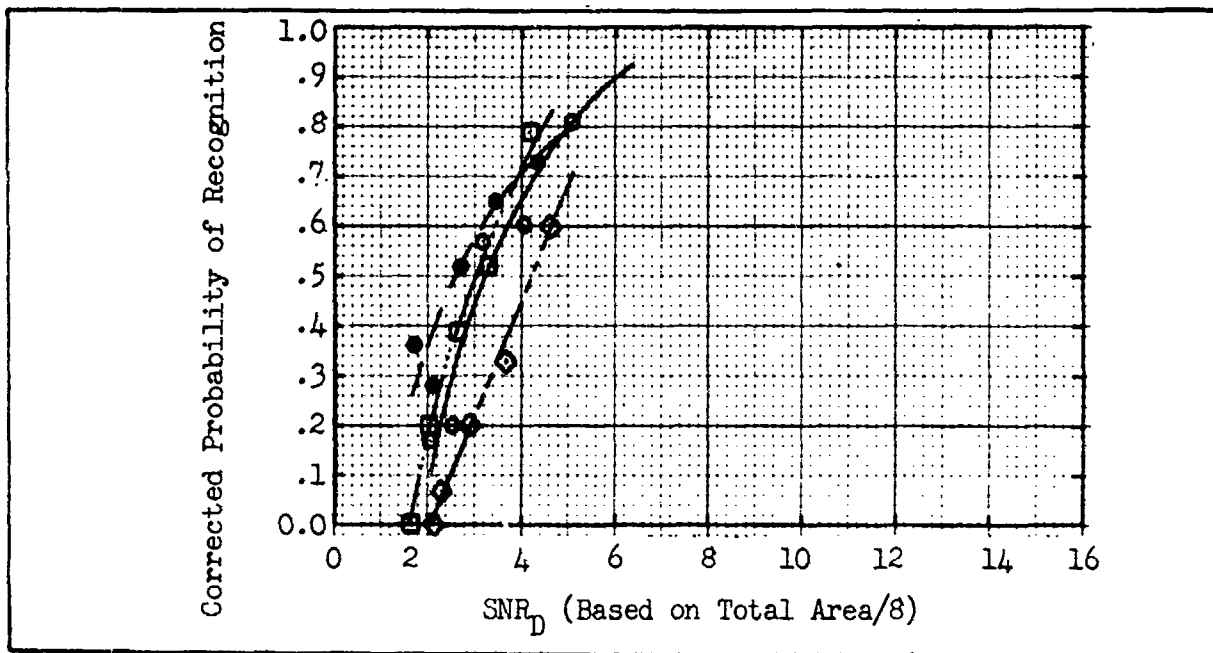
Fig. 93.   Probability of Recognition vs SNR_D for a ⊙ Tank, ◇ Radar Half Track, ⊡ Van Truck and ● Derrick Bulldozer. Uniform Background, Televised Imagery at 875 Lines, 25 frames/sec $D_V/D_H = 3.5$.

were adjusted to be approximately equal which, on the display were about $0.057 \ (in)^2$. The objects presented and the signal-to-noise ratios were randomly varied and the probabilities of recognition were determined. Chance was corrected for. SNR_D for the various images was calculated on the basis of the total image area divided by 8 and maximum peak-to-peak video signal-to-rms noise ratio. The maximum signal is specified because the images showed shades of grey. The angular subtenses of the displayed images relative to the observer were approximately 0.3 by 0.6 degrees. A total of 5 observers participated in the experiment and a total of 1,000 data points were taken.

In Fig. 93 , the results of the experiment are shown and it is seen that an average value of SNR_D of 3.3 is required to recognize the vertical target against the uniform background at the 50% level. Let us assume that we have a bar pattern of eight bars (Johnson's resolution

requirement for recognition) of total area equal to that of the
target image with the same SNR_D; that is, the value of SNR_D calculated
on the basis of the area of a single bar is 3.3. For the size target used
herein, the bar pattern spatial frequency would be 355 lines and bar length-
to-width ratio 16 (the target had a 2:1 length-to-width ratio) and from Fig.
83, it is seen that a value of SNR_{D-T} of about 2.9 is required to recognize
a square bar pattern consisting of bars of a 16:1 L/W ratio. Thus, to
within about 12%, the same value of SNR_{D-T} is required to recognize a
tactical target against a uniform background as is required to recognize
an 8-bar, bar pattern where the dimensions of a bar is W/8 x L. (L is the
average length and W is the average width of the image of the tactical target.)

The bar patterns used for the experiment which yielded the
results shown in Fig. 83 were approximately square whereas the
tactical targets that were used were of a 2:1 aspect so it was of interest to
do a bar pattern recognition experiment with bar patterns of 2:1 length-to-
width ratio. Two such experiments were performed, and the results of the
two experiments are shown in Figs. 94 and 95 . For each case the
background was black. The bar length-to-width ratio was 16 and the number of
bars was chosen so the pattern L/W ratio of the pattern was approximately 2:1.
The bar pattern spatial frequencies were 329, 396, 482, and 635 and there
were 7, 7, 9, and 11 bars in each bar pattern, respectively. From the
two Figs. (94 and 95) we have that the average value of SNR_{D-T} =
2.9 ' $\_$ 15%) which is the same value as that predicted from Fig. 83 and is
within 12% of that predicted from the uniform background recognition
experiment. There is, therefore, little error in using the results from
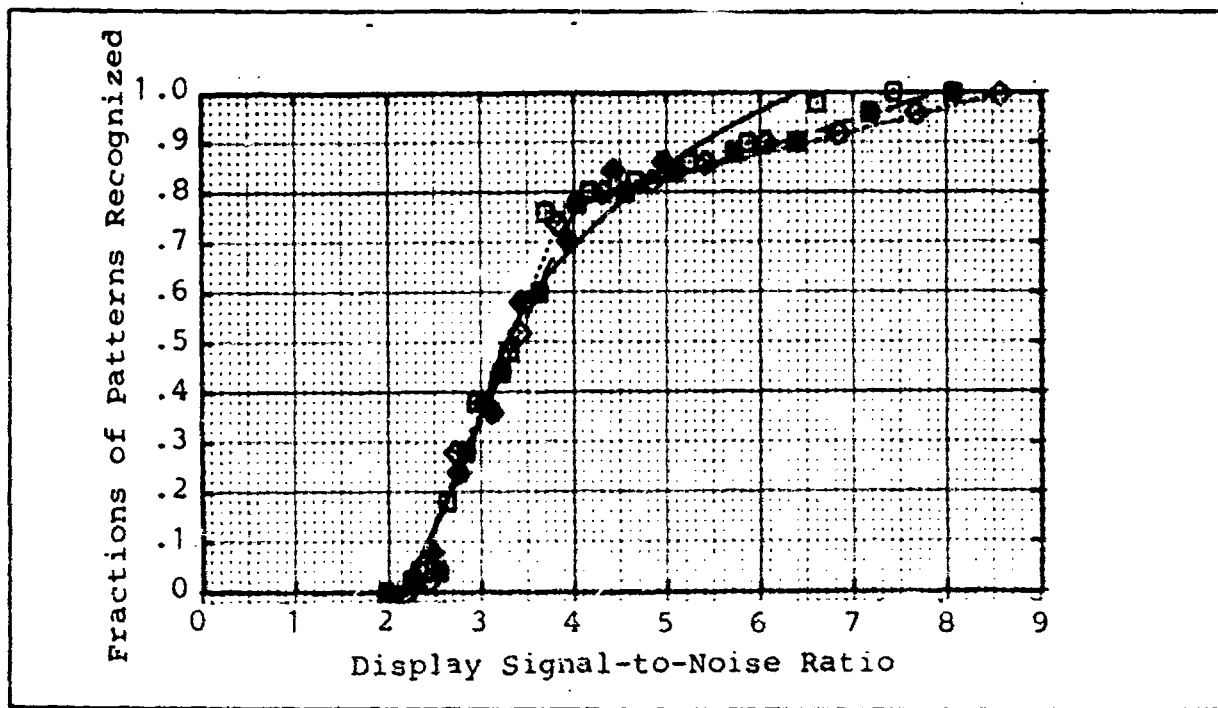
Fig. 94. Fractions of Bar Patterns Recognized vs SNR_D for Bar Patterns of Total Area Equal to the Average Area of "Real" Objects for $N = \square$ 329, 7 Bars, $\blacksquare$ 396, 7 Bars, $\lozenge$ N = 482, 9 Bars, $\blacklozenge$ N=635, 11 Bars. Televised Images at 875 Lines, 25 Frames/sec, D_V/D_H=3.5.
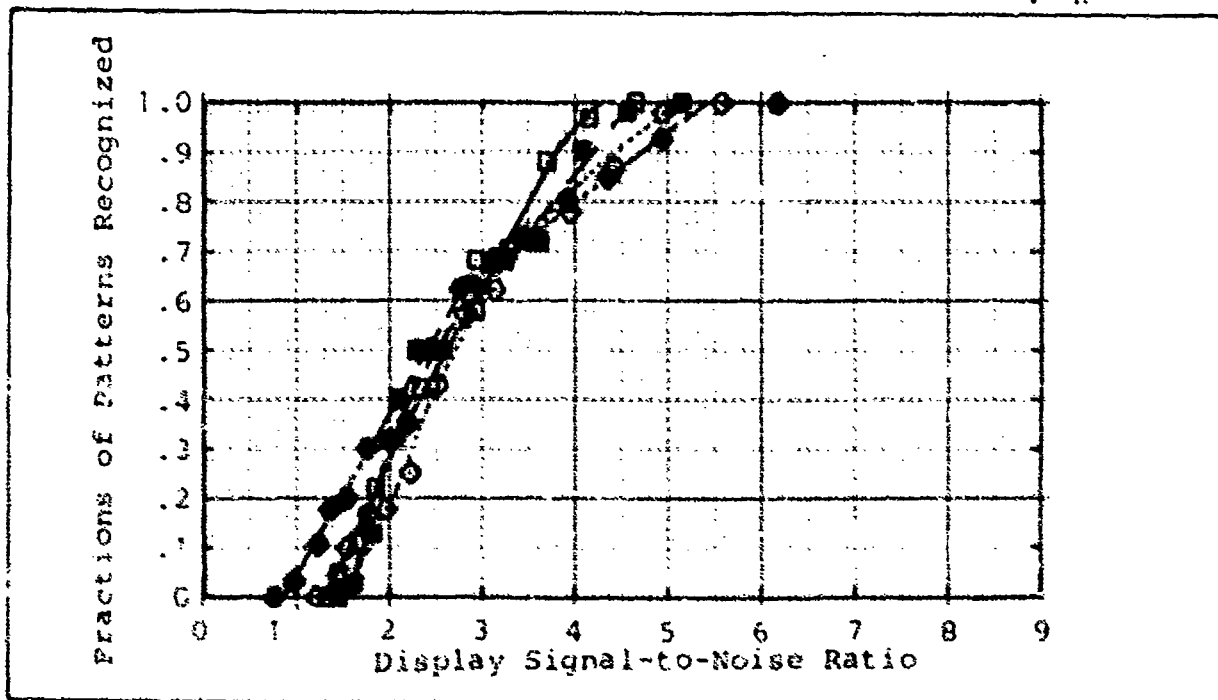
Fig. 95. Fractions of Bar Patterns Recognized vs SNR_D for Patterns of Area Equal to Average Real Object Area of $N^D = \square$ 329, 7 Bars; $\blacksquare$ 396, 7 Bars; $\lozenge$ 482, 9 Bars; $\blacklozenge$ 635, 11 Bars. TV Images, 875 Lines, 25 F/s, D_V/D_H = 3.5.

Fig. 83   for square wave bar patterns for bar patterns of 2:1 L/W ratio.

The second recognition experiment used a transparency with regions containing a road, a grassy field and grass among trees as the background and it is shown in Fig. 96. The target transparencies were the same ones used in the first recognition experiment discussed above. One of the vehicle transparencies was randomly chosen and placed over either the transparency of the road, the grassy field or the grass among trees. The choice of background was randomly chosen.

The signal-to-nois $t$io was also randomly varied so that each of the 12 vehicle-background combinations was shown at 5 different signal-to-noise ratios. A total of 60 different vehicle-background-SNR_D combinations were used. Eight observers viewed each combination 5 times and a total of 2,400 data points were taken. To calculate SNR_D, the maximum peak-to-peak video level was used as in the previous real vehicle experiments.

In Fig. 97, the results from the experiment with the road background are shown. The 50% threshold value of SNR_D is 3.8 which is only 15% higher than that previously measured with a uniform background.

In Fig. 98 , the results from the experiment with the grass background are shown. The 50% threshold value of SNR_D is 4.1, a value that is 25% higher than the uniform background case and 16% higher than that with the road background. In Fig. 99 , the results from the experiment with the grass between trees background are shown and the threshold value of SNR_D is 5.0. This value is 52% higher than that for the uniform background case, 31% higher than the road background case and 22% higher than the grass background case. From the above, it is seen that a somewhat higher SNR_D is
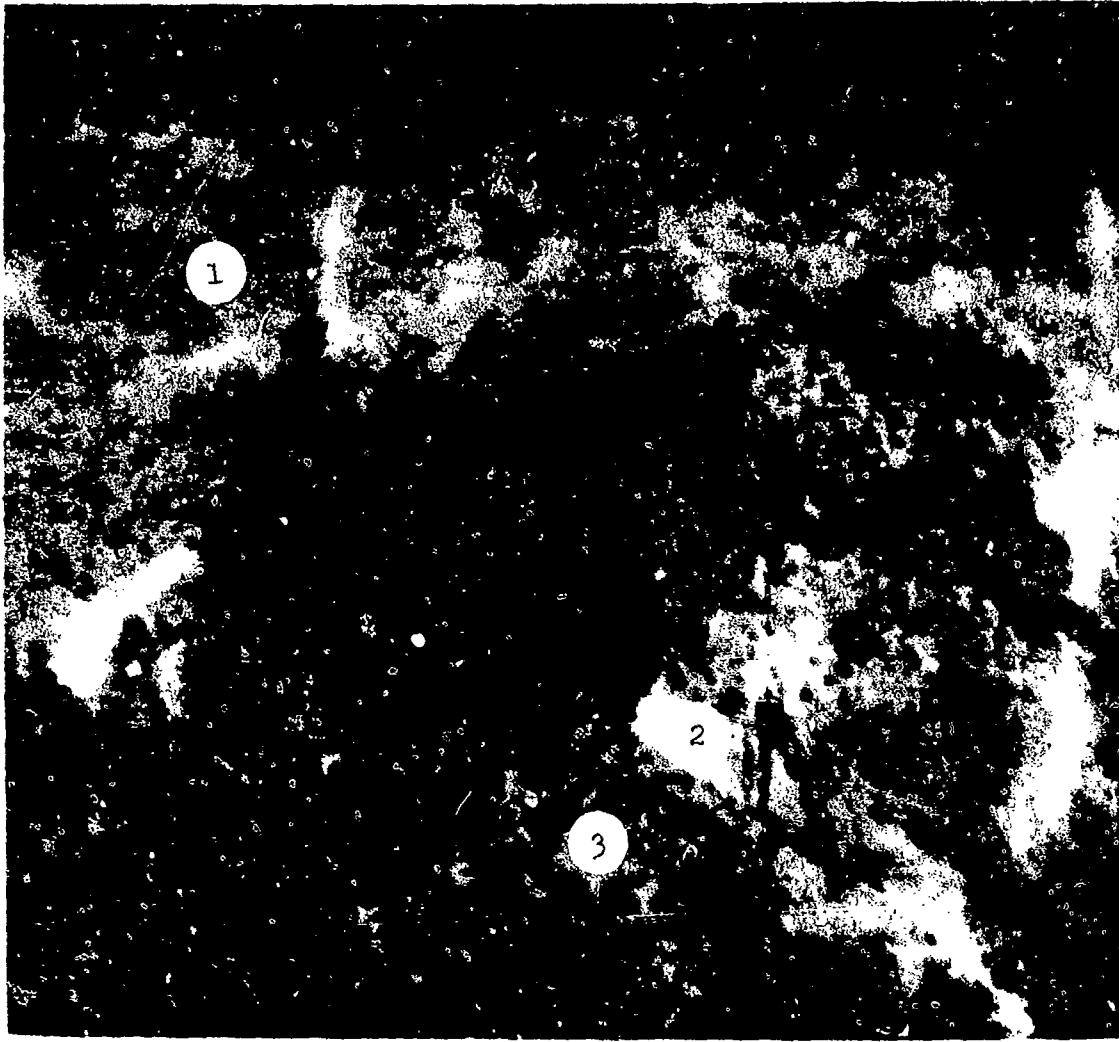
Fig. 96 Photograph of Real Background - #1 Grass #2 Road #3 Grass-
Trees Used for Recognition Experiments.
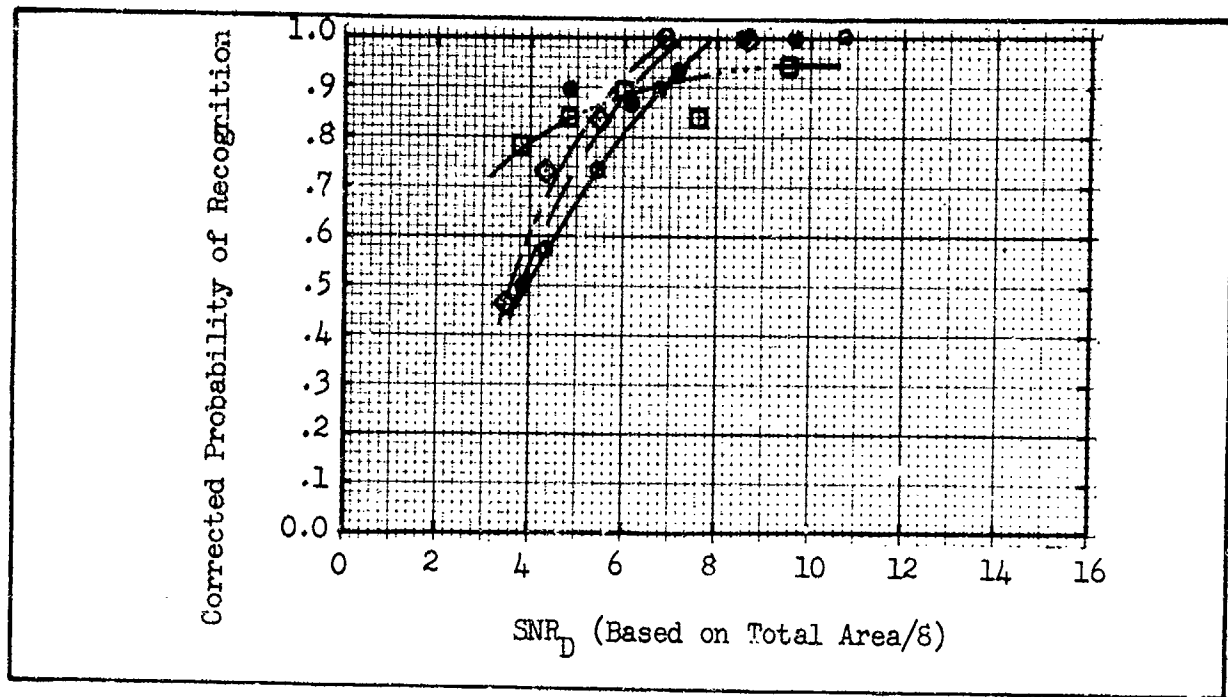
Fig. 97.   Probability of Recognition vs SNR$_D$ for a ○ Tank, ◇ Radar Half Track, □ Van Truck and ● Derrick Bulldozer.   Road Background Televised Imagery at 875 Lines, 25 frames/sec $D_V/D_H = 3.5$.
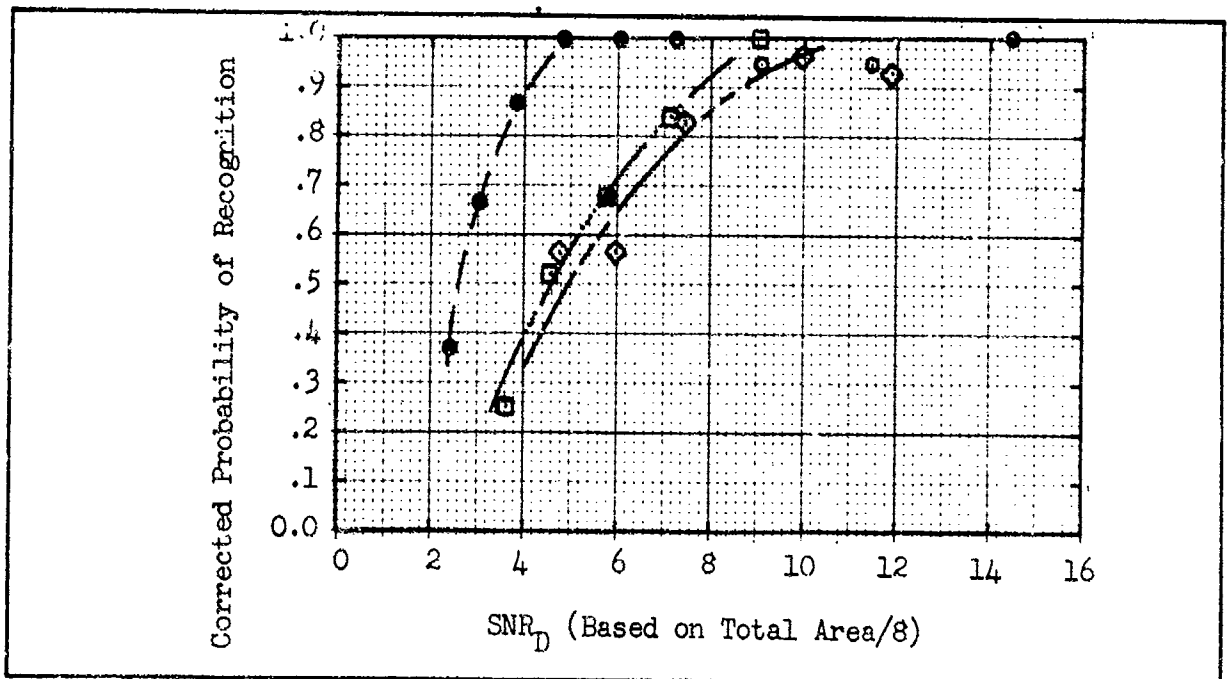
Fig. 98.   Probability of Recognition vs SNR$_D$ for a ○ Tank, ◇ Radar Half Track, □ Van Truck and ● Derrick Bulldozer, Grass Background, Televised Imagery at 875 Lines, 25 frames/sec $D_V/D_H = 3.5$.

161
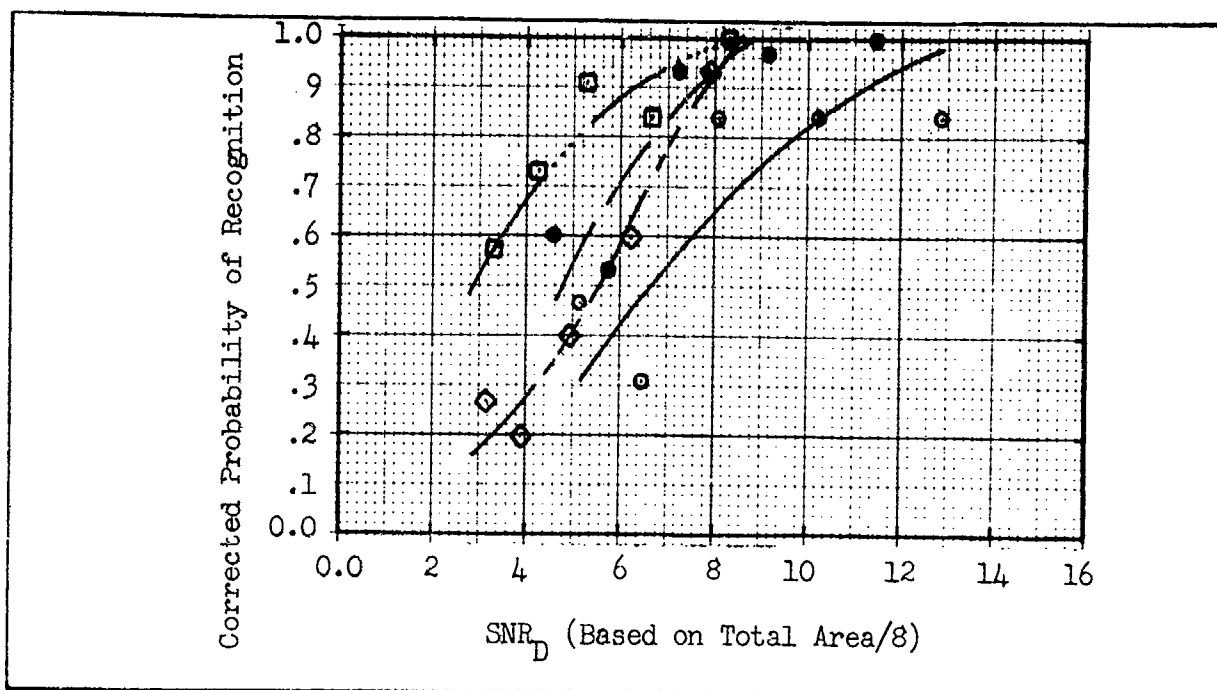
Fig. 99.   Probability of Recognition vs SNR_D for a ○ Tank, ◇ Radar Half Track, □ Van Truck and ● Derrick Bulldozer, Grass-Trees Background, Televised Imagery at 875 Lines, 25 frames/sec D_V/D_H=3.5

required at increased background complexity than is required in either the uniform background or road background cases.

4.5 Identification

Two different size images were used for this experiment. In each case the target was imaged against a uniform background. The images were high quality transparencies made from photographs of models of tanks. The photographs were taken side and top aspect at an angle of 45° to simulate a line-of-sight depression angle of 45° and are shown in Fig. 100. These models were of the American M47 Patton and M48, the British Centurion, the German Panther and the Russian Stalin. In the first experiment, the average image on the display was 0.9 in^2 and was approximately 1.3 x 2.6 degrees of angular extent at the observer's eye whereas in the second

M47

M48

Stalin
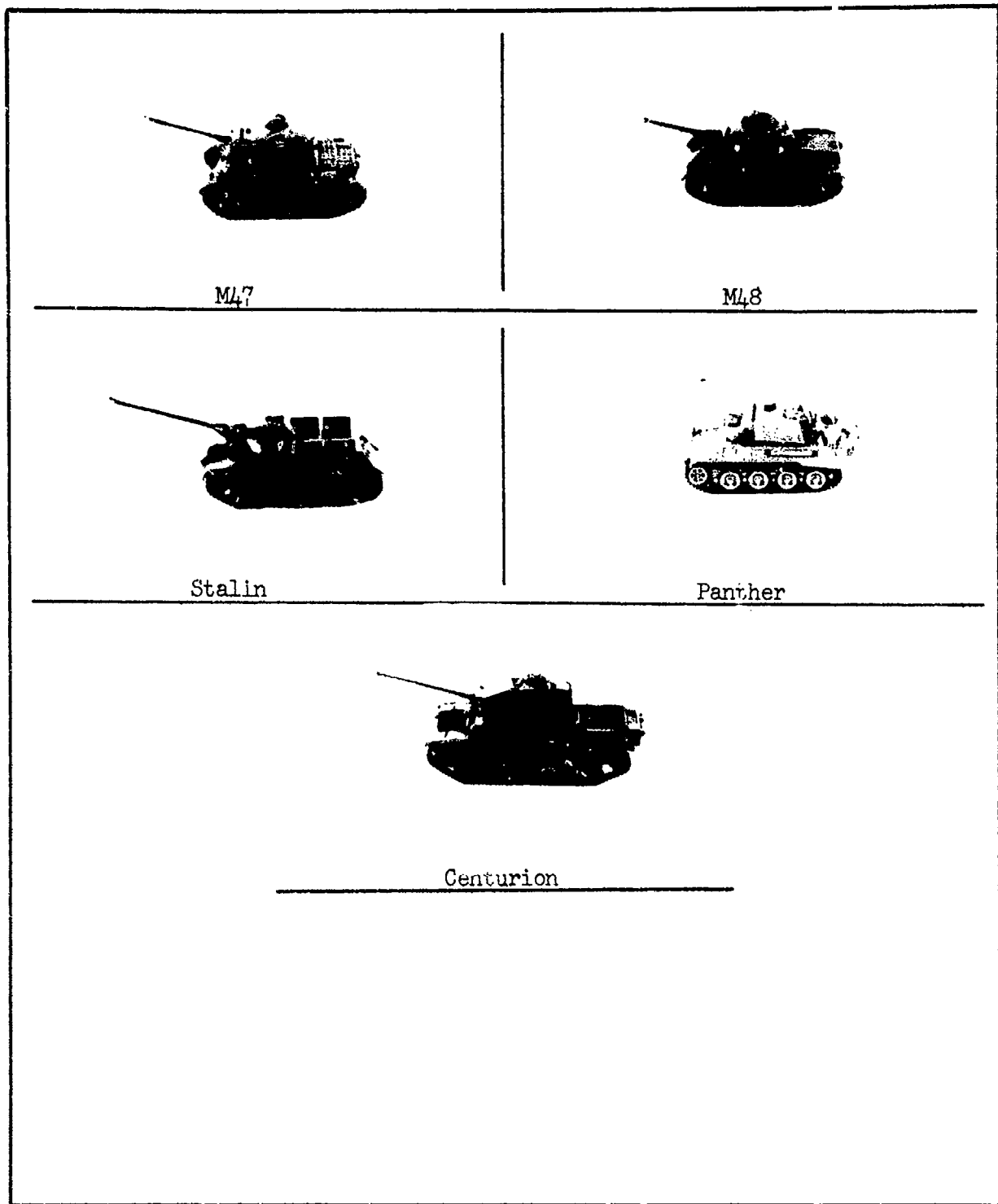
Panther

Centurion

Fig. 100   Photographs of Tank Models
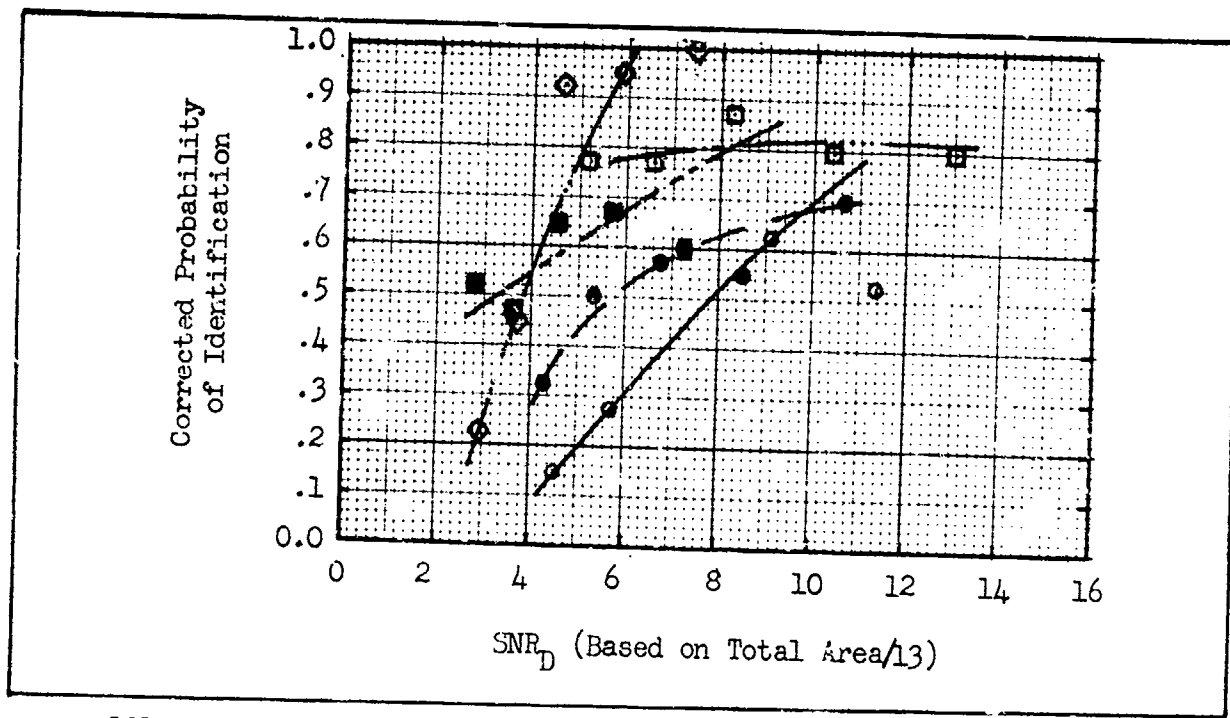
Fig. 101. Corrected Probability of Identification vs SNR_D for Tanks of $1.3°$ x $2.6°$ Angular Extent. ⬥M47, ● M48, ▢ Centurion, ■ Panther, ◇ Stalin—Against Uniform Background. Televised Imagery at 875 Lines, 25 frames/sec, $D_V/D_H = 3.5$.

experiment, the image was about 2.2 in^2 and the angular extent of the target was about 2 x 4 degrees. The object and signal-to-noise ratios were randomly varied and the probabilities of identification, corrected for chance, were determined. For the calculation of SNR_D, the total image area divided by 13 and the maximum peak-to-peak video signal-to-noise ratio was used. In each case, 5 observers were used and 1,250 data points were taken. In Fig. 101, the results from the first experiment are shown. From Fig. 101, we get that the average value of SNR_D is 5.2. The corresponding bar pattern of the same total area with 13 bars of 26:1 L/W ratio (N = 137) should have a $SNR_{D-T} = 5.2$. An estimate of 5.2 is obtained from Fig. 83 for SNR_{D-T} for a 23:1 bar L/W for N = 137, and we see that the estimated value is very reasonable.

Finally, in Fig. 102, the results from the second identification

164
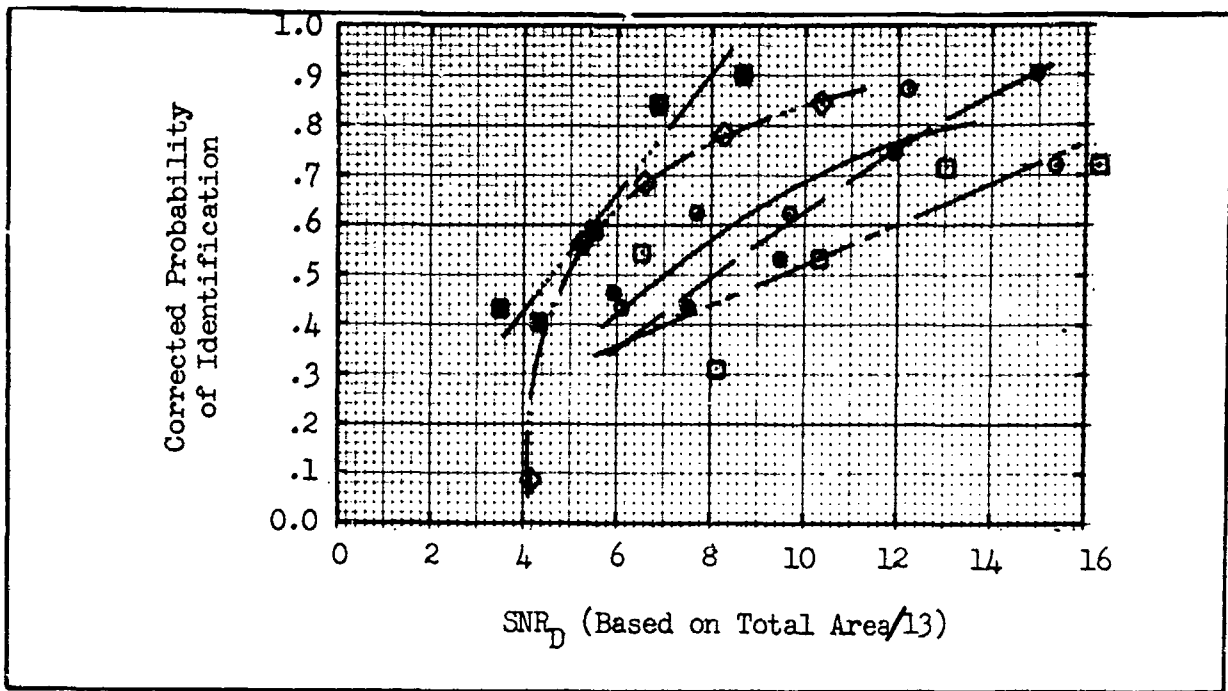
Fig. 102   Corrected Probability of Identification vs SNR_D for Tanks of 2^O x 4° Angular Extent. O M47, ● M48, □ Centurion, ▣ Panther, ◇ Stalin--Against Uniform Background. Televised Imagery at 875 Lines, 25 frames/sec, D_V/D_H = 3.5.

experiment are shown. The average value of SNR_D is 6.8. The corresponding bar pattern of the same total area with 13 bars of 26:1 L/W ratio (N = 101) should have a SNR_{D-T} = 6.8. An estimate of 5.8 is obtained from Fig. 83 and again, we see that the estimated value of SNR_{D-T} is reasonable.

4.6 Conclusions of the Recognition and Identification Experiments

We have seen that higher levels of target discrimination such as recognition and identification can be approximated by bar pattern resolution and SNR_D. Specifically, Johnson's resolution requirements for recognition or identification of an object together with the SNR_{D-T} values required to recognize a bar pattern of the same size as the target with the number of bars equal to Johnson's required resolution requirements yields a value of SNR_D that is the same as measured for the real target. Thus, real target recognition and identification can be equated to

165

bar pattern recognition. This correspondence significantly simplifies the analysis and synthesis of real tactical targets.

4.7 Noise due to the Retinal Photoconversion Process

In the analysis of sensor performance, it is normally assumed that operator performance is limited only by the image signal-to-noise ratio as established by the sensor. It was assumed that the primary effect of display luminance was in establishing the operator's visual acuity and that the luminance was adequate so as to insure that the operator was not acuity limited by light level. This is a reasonable assumption for many situations but cases can occur in which a fluctuation noise, generated in the observer's retinal photoconversion process due to the average display luminance can limit the detectability of images. Such a situation may occur where the scene high-light-to-low-light irradiance ratio is large and signal gain must be reduced due to display brightness or dynamic range limitations. In this situation, the small signals due to the scene may be so small that they cannot be seen in the presence of the fluctuation noise associated with the average monitor luminance. In the following, the results of some psycho-physical experiments directed toward determining the noise equivalence of the monitor luminance will be given. Then an example will be given on the impact on system performance.

To illustrate the possibility of this limitation, we will first consider the principle of display operation as shown in Fig. 103. Ordinarily, there are two controls used by the observer in adjusting the CRT's operating points. The first is the "brightness" control which adjusts the average level of display luminance. The second control is usually referred to as a contrast control but is actually a video gain control.

166

Cathode Ray Tube

Electron Beam

Background
Luminance β_o

Signal $\Delta\beta$

$G\ i_s$

Video Signal Input

Brightness
Control

Gain or Contrast
Control

Display Fluctuation Noise

$\Delta\beta\ \alpha\ G\ i_s$ As set by Contrast Control

β_o As set by Bright-
ness Control

Display Luminance

Distance Along Scan Line

71-0530-V-20
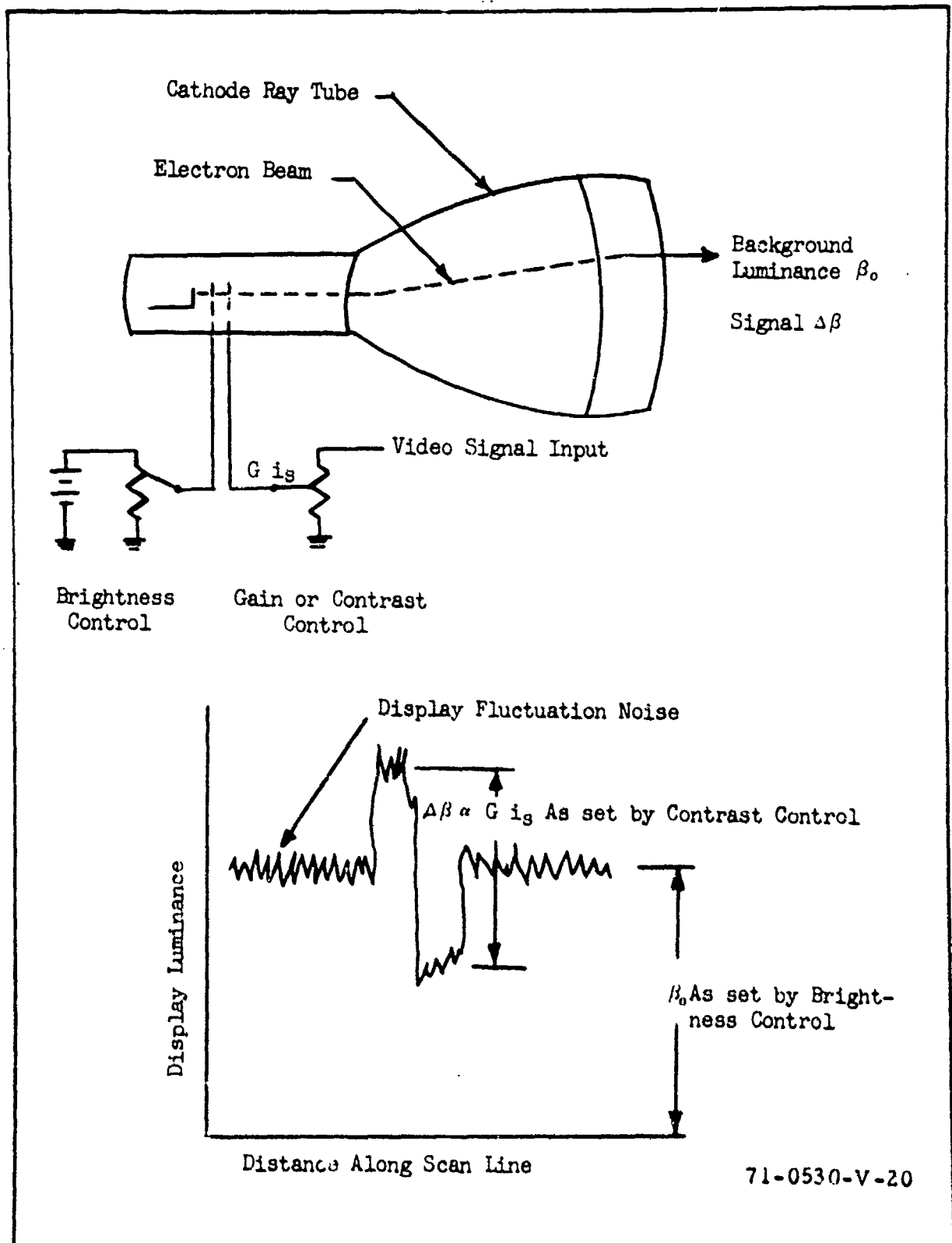
Fig. 103   Effect   Display Controls on Output Image Brightness
and Contrast

167

This is not a complete misnomer, however, since this control determines the swing of the display luminance about the steady state luminance and therefore increases or decreases the contrast of the displayed image. As was mentioned above, there is a retinal fluctuation noise associated with the display background brightness and if the video gain is sufficiently reduced, the signals which correspond to the low lights in the scene can fall below the level of the fluctuation noise. In this case, the observer will be said to be display-luminance-fluctuation-noise limited rather than sensor noise or photo-electron-noise-limited.

The conditions for the experiments which follow are given in Fig. 104. For the first two psychophysical experiments, the experimental setup shown in Fig. 65 was used. The displayed images were electronically generated squares. In the first experiment, the video gain of the monitor was equal to 15.5 and the target was a square 4 scan lines high. No noise was added in the video, the observer-monitor distance was 28 in. Four display luminance values were used, 0.2, 1.0, 5.0 and 10.0 ft-Lamberts and the monitor luminance was systematically varied from low to higher values. At each luminance value, the video signals were randomly varied between 5 values.

In Fig. 105, corrected probability versus video signal level is shown for the four values of monitor luminance. At a given probability, the higher the value of monitor luminance, the larger the video signal level must be. In the actual image of a scene, if the signal levels from other portions of the picture were not too high, the video gain could be increased to such a level that the influence of fluctuation noise from the monitor is negligible. However, this is not always possible because of the display's maximum luminance limitation and consequently the resulting retinal

168

Notes*		$\dfrac{D_V}{D_H}$ 1	B_D ft-L 2	Δf_V MHz 3	$\dfrac{\text{Time}}{\text{Trial}}$ 4	No. of Obsvrs.	No. of Trials	Fig. #'s
1	Squares – Static	3.5	0.2 to 10	7.1	10 sec	5	600	105
2	Squares – Static	3.5	0.2 to 10	7.1	10 sec	5	1000	106, 107
3	Bar Patterns – Static	3.5	10	12.5	Unlimited	4	2732	110, 111, 112
4	Squares – 20 sec/P.W.	3.5	.2	7.1	20 sec	5	600	115, 117
5	Squares – 5 sec/P.W.	3.5	.2	7.1	5 sec	5	600	116, 117
6	Bar Patterns – 20 sec/P. W.	3.5	1	12.5	20 sec	1	280	119

NOTES*

1. Display Viewing Distance to Height Ratio.

2. Average Display Luminance (ft-L).

3. Video Bandwidth.

4. Time Allowed for Observer to Make Response.

Fig. 104 Conditions for the Display Luminance and the Image Motion Experiments.

169
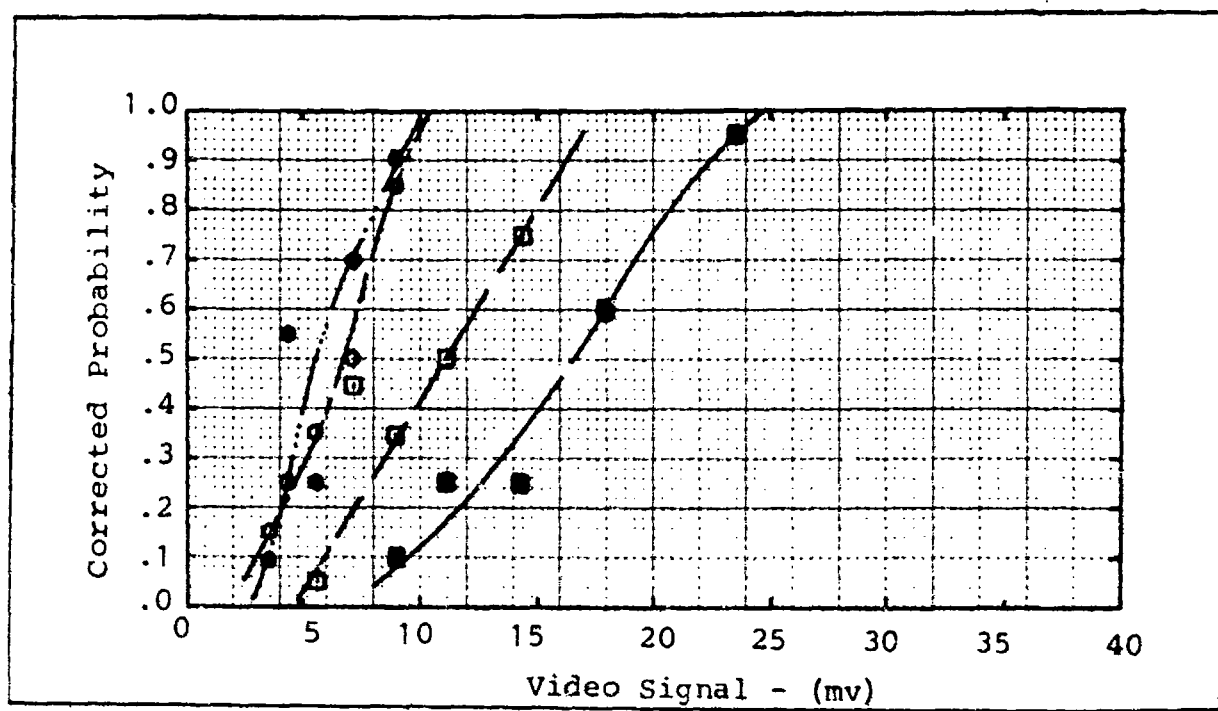
Fig.105 Influence of Monitor Luminance for a Square 4 Raster Lines High for Monitor Luminance Values of ○ .2,● 1,□ 5 and ■ 10 ft. Lambert No Noise at Input in Video. Televised Images at 30 frames/Second, 525 Scan Lines, $D_V/D_H = 3.5$ Video Gain = 15.5

photoconversion noise can be limiting as observed for the detection of squares above. In Fig. 106, the results of a similar experiment for a 8 raster line wide square are shown. The video gain was 5.5. The same trends noted in Fig. 105 are seen in Fig. 106 but the data is shifted in video level which is to be expected due to the different size target and different video gain level.

For the cases where the noise in the video is the dominant noise source, the display signal-to-noise ratio can be written as

$$SNR_D = \left(\frac{2\ a\ t\ \Delta f_V}{A}\right)^{\frac{1}{2}}\ \frac{S_V\ G_V}{N_V\ G_V} \quad , \tag{142}$$

where a is the area of the image on the display, A the area of the display, t the integration time of the eye, Δf_V the video bandwidth over which the rms

170
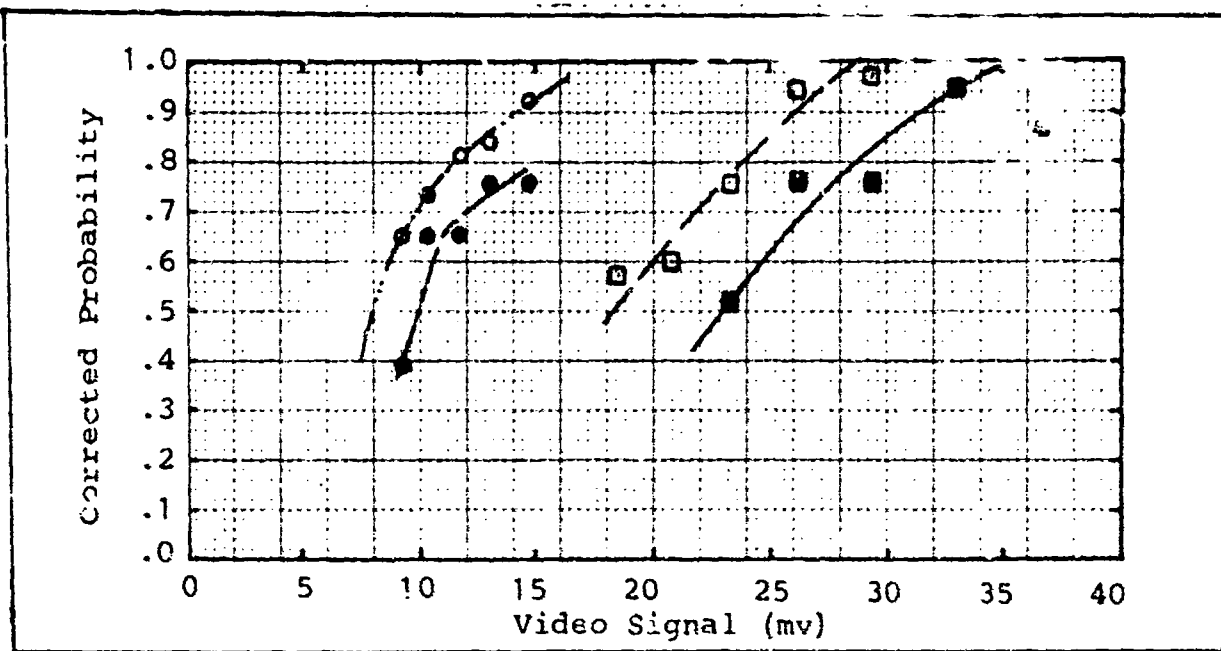
Fig. 106 Influence of Monitor Luminance for a Square 8 Raster Lines High for
Monitor Luminance Value of ◐.2, ● 1, ☐ 5 and ■ 10 ft. Lambert. No
Noise At input in Video. Televised Images at 30 frames/Second,
525 Scan Lines, $D_V/D_H = 3.5$ Video Gain = 5.5

value of noise, N_V is measured, S_V the peak-to-peak video signal and G_V the

gain of the monitor as measured between the input of the monitor and the

control grid of the cathode ray tube. Assume that in the absence of noise

in the video channel, that the retinal photoconversion noise associated with

the monitor luminance can be expressed as an equivalent electrical noise at

the grid of the monitor of value N_L over a bandwidth of Δf_V. By analogy to

Eq. (142), we have

$$SNR_D = (\frac{2at\ \Delta f_V}{A})^{\frac{1}{2}}\ \frac{S_V\ G_V}{N_L} \quad . \tag{143}$$

Using the threshold values of display signal-to-noise ratio from Fig. 74,

Eq. (143) can be solved with the experimental data from the above two

experiments for N_L, the noise equivalence of the monitor luminance. Doing

171
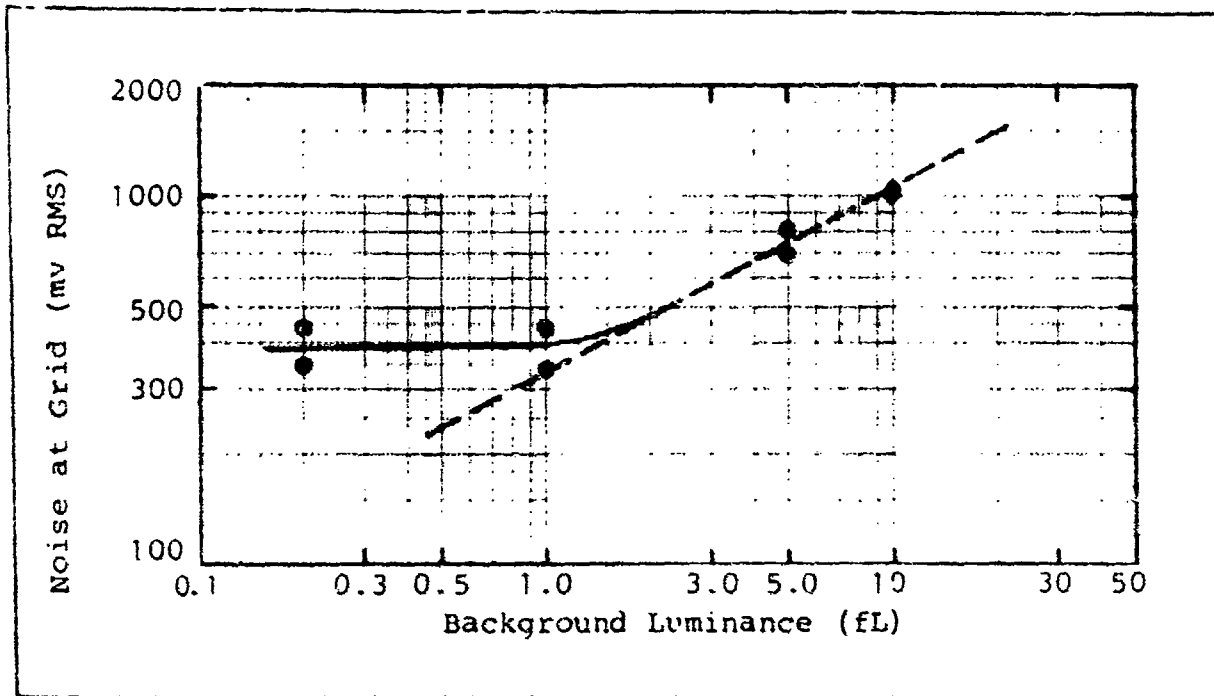
Fig. 107 Equivalent Noise at the Display Gri . as a Function of Average
Display Luminance for Display Gains of ◯ G = 15.5 with 4 x 4
Scan Line Image and ● G= 5.5 with 8 x 8 Scan Line Image. No
Additive Noise. TV Images, 525 Scan Lines, 30/sec. D_V/D_H=3.5.

this, one obtains the results shown in Fig. 107 which show that at low

luminance levels, N_L is a constant whereas at higher levels, N_L is pro-

portional to the square root of the monitor luminance, that is

$$N_L = K (B)^{\frac{1}{2}} ,$$

(144)

where K is a proportionality constant and B is the monitor luminance. In

Fig. 108 the noise equivalence of the monitor luminance is shown for a

number of display luminance, and gain values. At high monitor luminance

values, high monitor gain values must be used if the influence of the retinal

fluctuation noise associated with the monitor luminance is to be negligible.

It is reasonable to expect that the total noise at the control

grid of the CRT with video noise of N_V, rms is given by

EQUIVALENT Noise of Display (mv)	DISPLAY LUMINANCE (fL)							
	1.0	5	10	50	100	500	1,000	5,000
N_B at control grid of CRT	395	750	1,050	2,350	2,320	7,500	10,500	23,500
N_B/G at video input for G=10	39.5	75	105	235	332	750	1,050	2,350
N_B/G at video input for G=100	3.95	7.5	10.5	23.5	33.2	75	105	235

Fig. 108   Noise Equivalence of Retinal Photoconversion Noise at the Display Input.

$$N_T = (N_L^2 + N_V^2 G_V^2)^{\frac{1}{2}} , \tag{145}$$

and the display signal-to-noise ratio is given by

$$SNR_D = (\frac{2at\,\Delta f_V}{A})^{\frac{1}{2}} \frac{S_V\,G_V}{N_T} . \tag{146}$$

Using Eqs. (145 and 146), together with the data from Fig. 107, the curves shown in Fig. 109 can be made. The horizontal axis in Fig. 109 is $N_V\,G_V$ and the vertical axis is $S_V\,G_V\,(2at\,\Delta f_V/A)^{\frac{1}{2}}$. At low scene irradiance levels, the signal currents are low and the amount of photoelectron noise is small. This corresponds to low values of noise-gain in Fig. 106 if the value of monitor gain is low. Under these conditions, the required value of signal

173
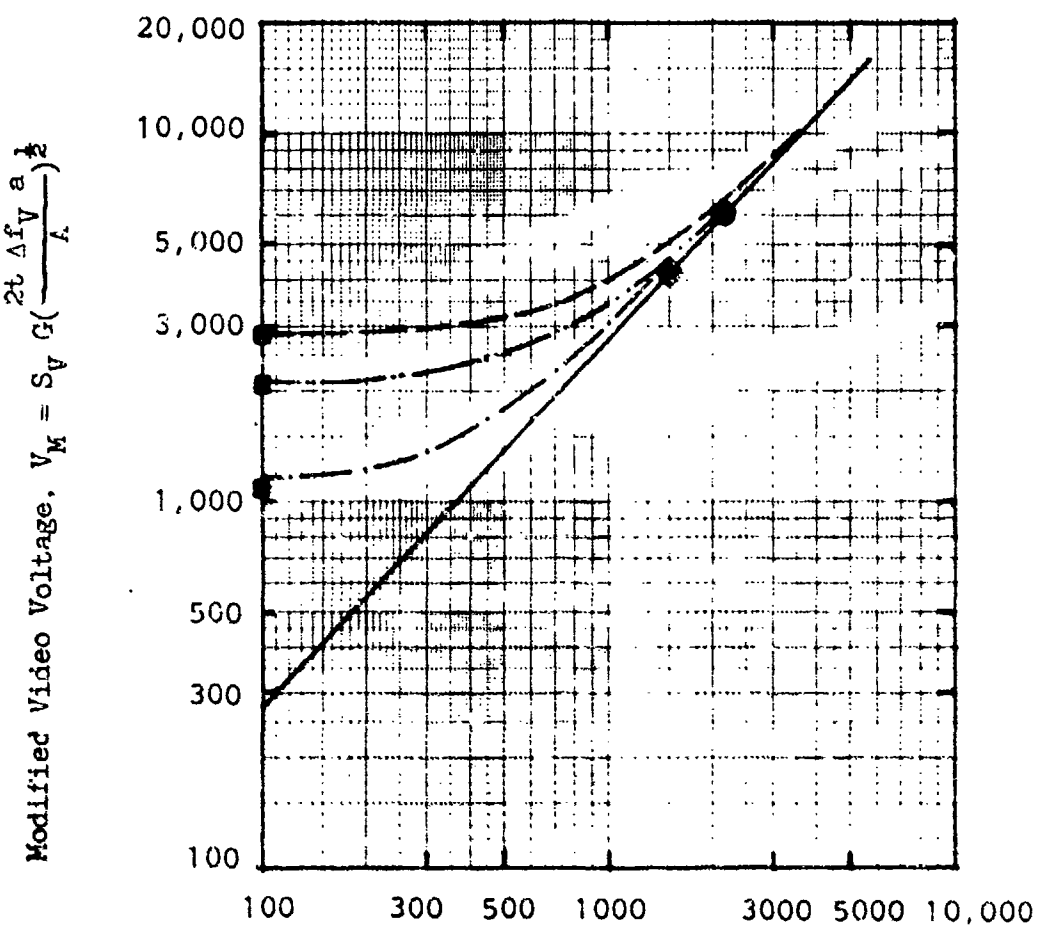
Fig. 109 Modified Video Voltage vs Product of Video Gain and Noise for
Monitor Luminances of (— —) 10 ft. L, (— ·· —) 5 ft. L.
and (— · —) 1 ft. L. Solid Curve ——— Assumes Monitor
Luminance Independence. Data Points ■ , No Noise in Video,
◆ 75 mV in Video, G = 15.5, Δf_V = 7.1 MHz corrected to 12.5 MHz,
● 400 mV in Video, G = 5.5, Δf_V = 12.5 MHz TV Images at 30/Sec,
525 Scan Lines, D_V/D_H = 3.5.
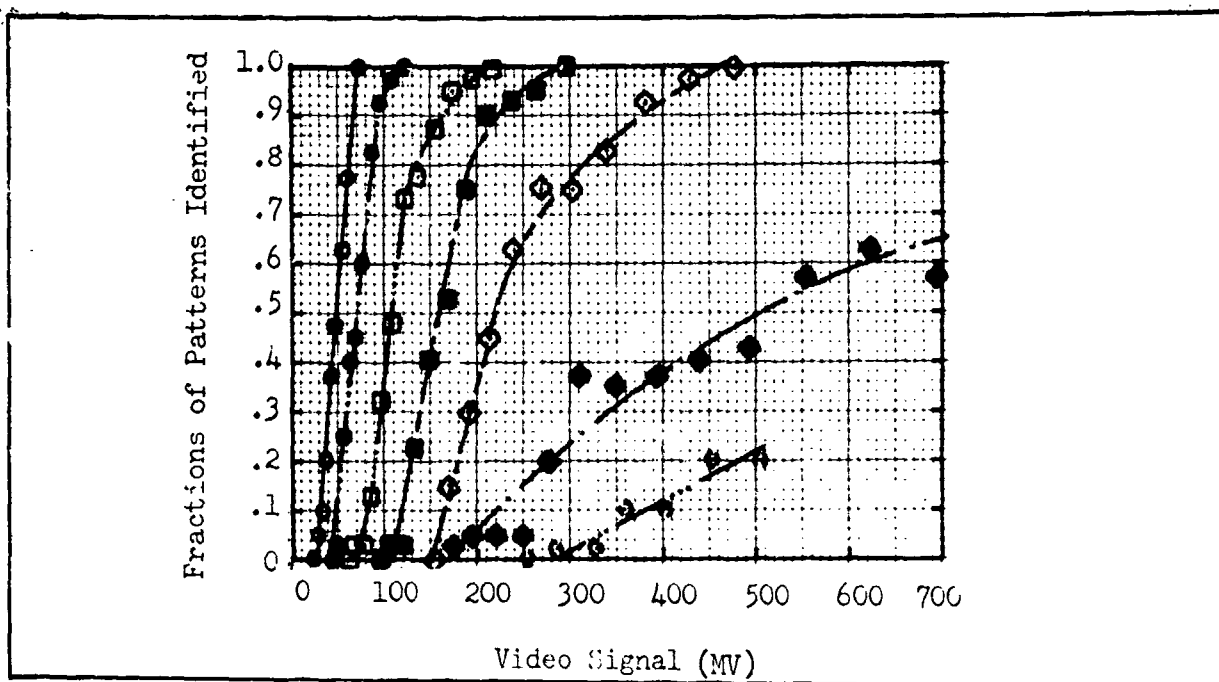
Fig. 110   Fraction of Patterns Recognized vs Video Signal as a
            Function of Spatial Frequency for a Monitor Gain
            of 2.3, N = ○ 104, ● 200, □ 329, ■ 396, ◇ 482,
            ◆ 635,   ○ 729.

to satisfy Eq. (146) must be much larger for high monitor luminance values

than at low ones. Indeed, factors of 10 or more increases in video signal

are required because of the fluctuation noise. This requirement can

severely limit system performance.

A third psychophysical experiment was performed using bar patterns

and the vidicon camera with the setup like Fig. 78. Two gain settings,

2.3 and 11 were used and 1426 and 1206 data points were taken respectively

at the two settings. Four observers were used at each gain setting. White

noise of 200 mv with a bandwidth of 12.5 MHz was added in the video. The

display luminance was 10 ft-Lamberts. The results of the experiments are

shown in Figs. 110 and 111. With a gain of 2.3, the noise equivalence of

the fluctuation noise associated with the monitor luminance should dominate

the video noise where as with a gain of 11, the video noise should dominate.
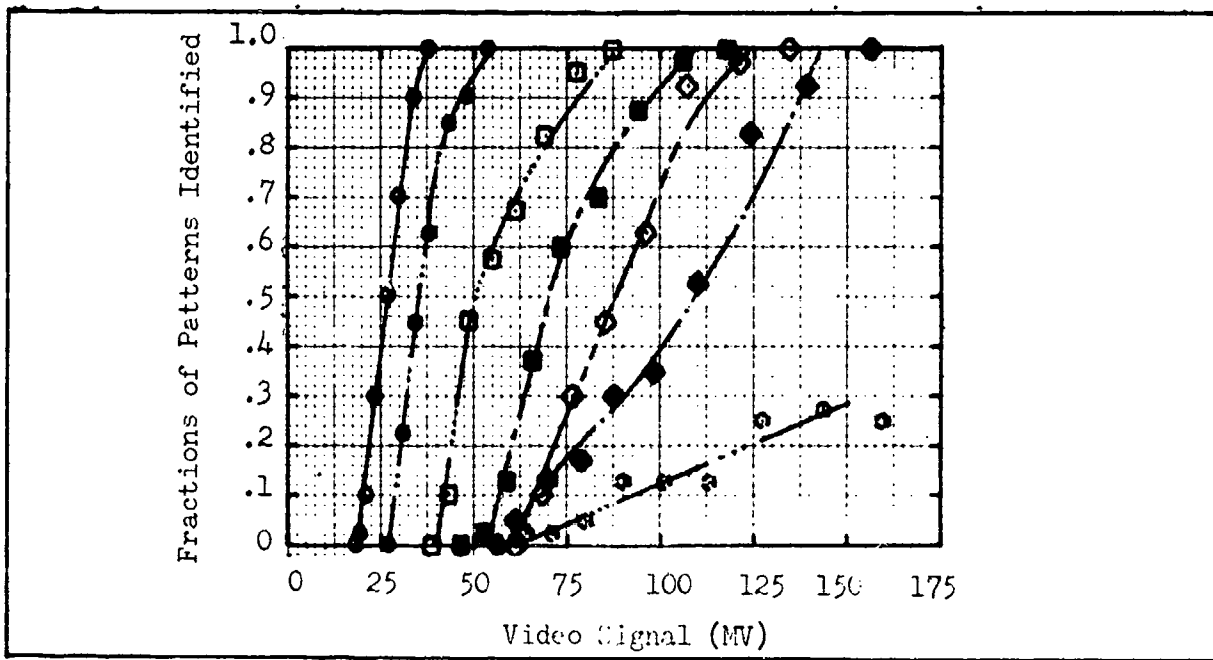
Fig. 111   Fractions of Patterns Recognized vs Video Signal as
                a Function of Spatial Frequency for a Montior Gain of
                11, N = ○ 104, ● 200, ◻ 329, ◼ 396, ◇ 482, ◆ 635, ◌ 729.

At a given probability, the electrical signal-to-noise ratio at the control
grid of the CRT, including both noise sources, should be equal for the two
cases. That is

$$\frac{S_{V1}\ G_{V1}}{(G_{V1}{}^2\ N_V{}^2 + N_L{}^2)^{\frac{1}{2}}} = \frac{S_{V2}\ G_{V2}}{(G_{V2}{}^2\ N_V{}^2 + N_L{}^2)^{\frac{1}{2}}} \tag{147}$$

where S_{V1} and S_{V2} are the measured video signals into the monitor corre-
sponding to gain G_{V1} and G_{V2} respectively, N_V is the video noise into the
monitor and N_L is the noise equivalence of the monitor luminance. Using
the results from Figs. 110 and 111 with Eq. (147), one can determine N_L
for different line numbers and the value of N_L is plotted vs N, line number,
in Fig. 112 using the 50% probability data from Figs. 109 and 110. Also

176
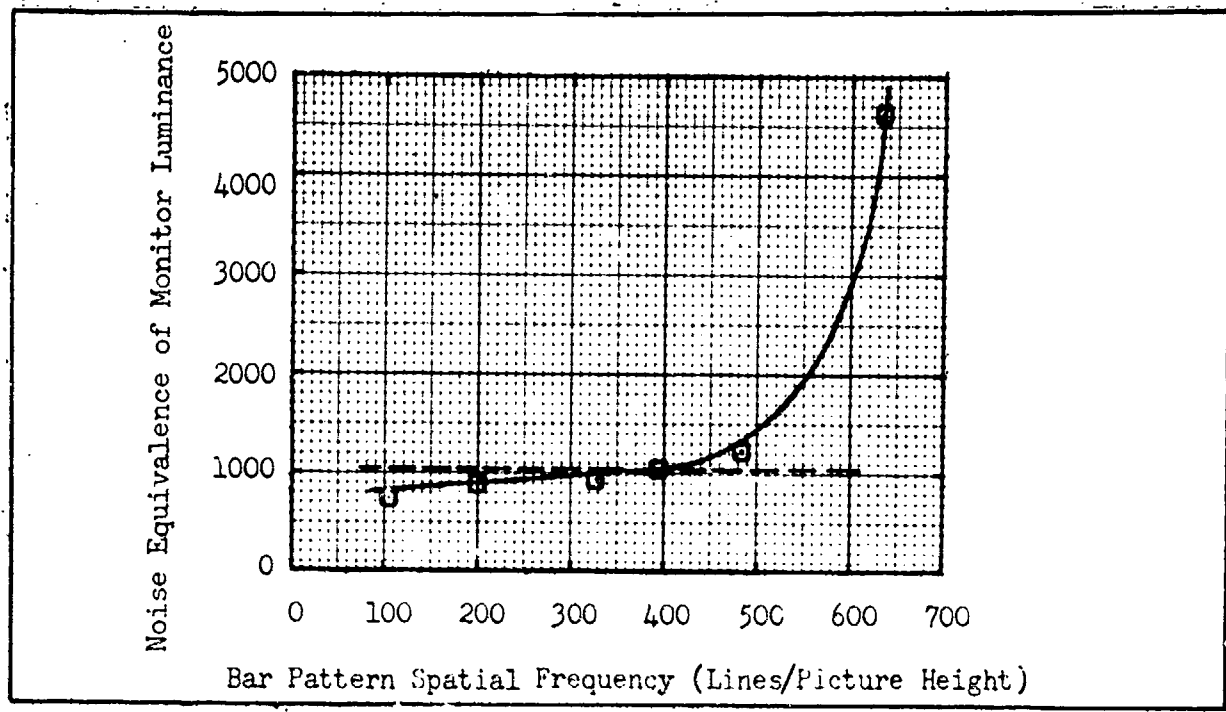
Fig. 112 Noise Equivalence of Luminance Fluctuation at Grid of Display
for 10 fL Monitor Luminance Level ▢ As a Function of Bar Pat-
tern Spatial Frequency —— Noise Equivalence as Determined
with Squares.

shown in Fig. 112 is the noise equivalence of 10 ft-Lamberts from Fig. 107

from the experiment with squares. There is a gradual rise in the noise

equivalence with bar frequency at all but the highest line number. After

the experiment, it was discovered that the black bars were nearly 67% larger

than the white bars for the 629 lines/picture height pattern and consequently

the estimate of N_L for the N = 629 should not be used. For the 5 values of N,

the average value of N_L is 970 which is only 8% lower than that determined

from the experiment with squares and, for the largest difference, (N = 104)

the value of N_L is only about 25% lower than the previously determined value.

As was shown most clearly in the experiment with squares, the

smallest incremented signal that can be seen increases as the gain decreases

or as the monitor luminance increases. This effect has been observed in

forward-looking infrared systems. In such systems, the minimum resolvable

177
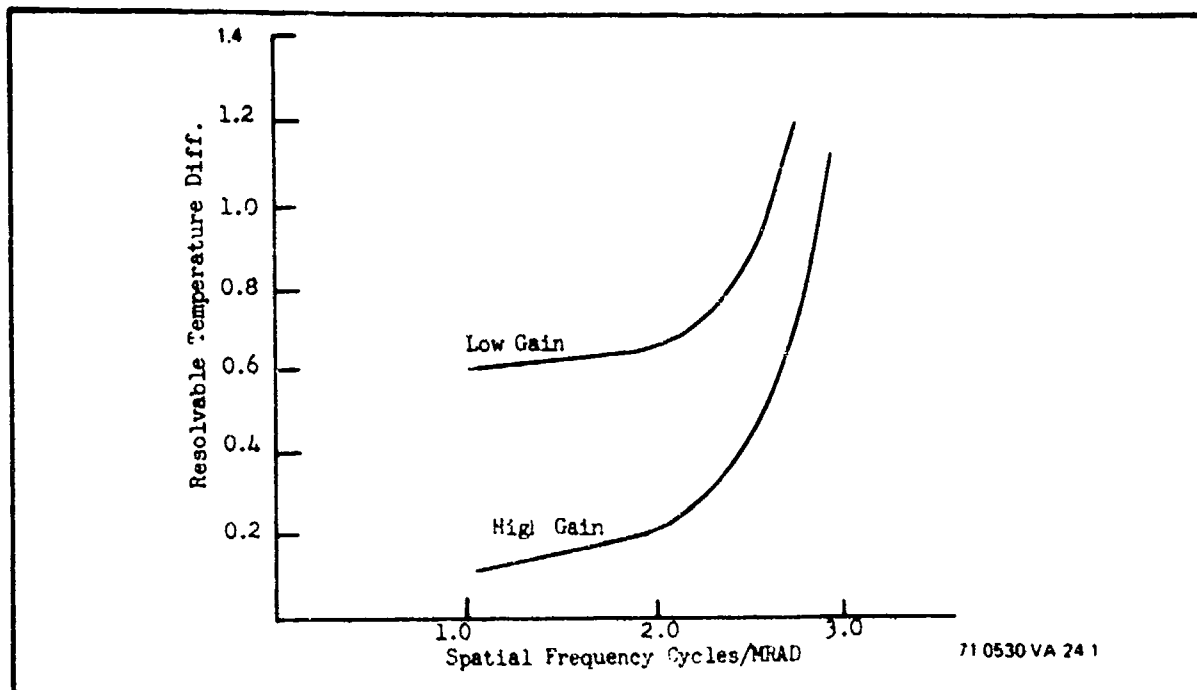
Fig. 113   Resolvable Temperature Difference for High and Low Gain
            CRT Contrast Control Settings

temperature difference as shown in Fig. 113 increases as gain is reduced.

The same effects are seen in LLLTV where video gain is reduced because of

bright lights in the field of view. In effect, the system sensitivity

is reduced and consequently, a higher irradiance level is required to

resolve a given line pattern than was required before the gain was reduced.

An example of the impact of inadequate gain on resolution vs light level

for LLLTV is shown in Fig. 114. The numbers used to calculate the low

gain case were taken from Fig. 109 and represent the relative effect of

loss of gain. Clearly, the system performance can be seriously limited

by the fluctuation noise if the monitor is bright and there is a large

scene high light to low light irradiance level.

4.8 Psychophysical Effects of Image Motion

        It has been observed that images in motion, when viewed on the

178
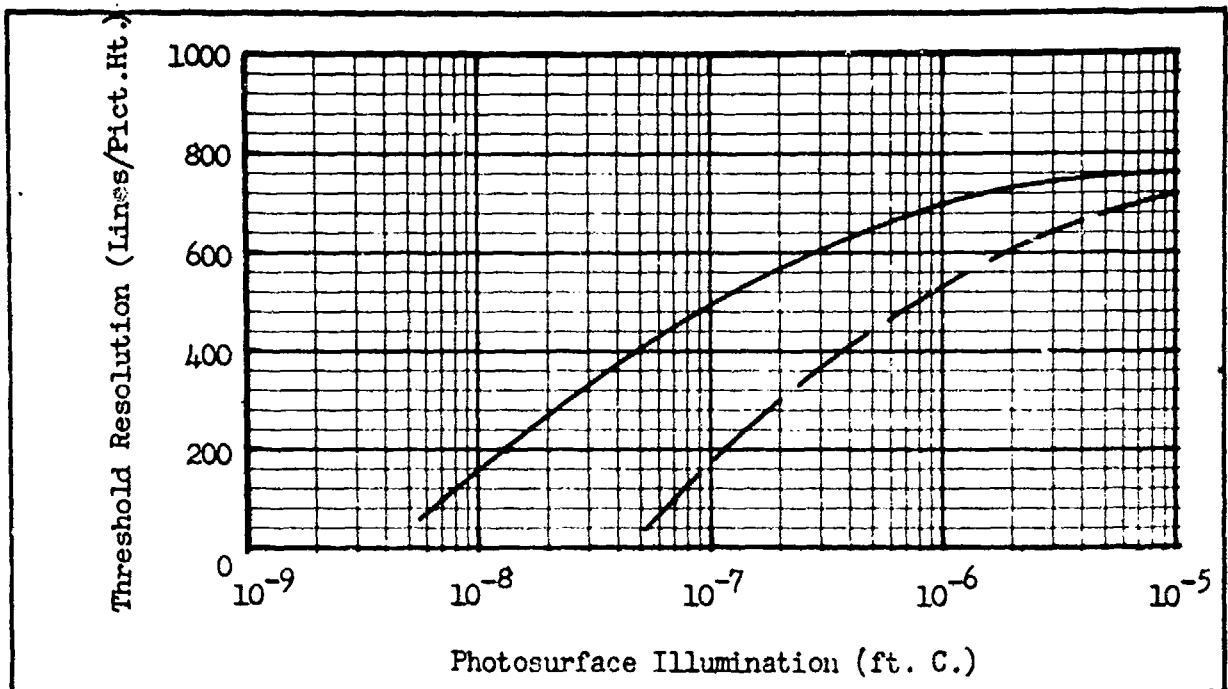
Fig. 114   Limiting Resolution vs Photosurface Illumination for 698DF
I-SEBIR ——— Measured Curve High Gain, —— —— Predicted
Curve Low Gain, High Monitor Brightness.

display of an electro-optical sensor's display are degraded. This

degradation can be due to the motion itself combined with storage mechanisms

within the sensor, psychophysical observer effects, and sensor time constants.

In this section, it proposed to investigate the psychophysical effects.

It is common experience that objects can be visually tracked at

rather high angular rates of speed. Data from the NASA Bioastronautics Data

Book,[16] for instance, shows that the eye can track at rates that are at least

as high as 120 degrees per sec. The data shows that at a given object

luminance that there is approximately a 3-fold increase in apparent object

size required (called the critical detail) for the same detectability if

the angular velocity is changed from 20 degrees per sec to 120 degrees per

sec. At 20 degrees per sec, the slopes of the curves are small and one

has the result that at small speeds the critical detail size is not very

179

different from that under static conditions.

For the 8-inch high display which was used for our psychophysical experiments which was 28 inches from the observer, the display width extends a visual angle of a little more than 20 degrees (21.6°) so a 20 degree per sec speed corresponds to a target speed of 1 sec per picture width; a very high speed for camera systems. Indeed, typical speeds used for testing camera systems are 5, 10, and 20 sec per picture width, which for the present case would correspond to 4, 2, and 1 degrees per sec; rates that are very slow indeed from a psychophysical viewpoint. For low light level television systems, it is reasonable to expect therefore that there should not be a large increase in the display signal-to-noise ratio required with image motion due to purely psychophysical effects at the speeds at which systems can operate. This remains to be demonstrated, however, and in the following the results of some experiments will be presented which tend to confirm this hypothesis.

In the first experiment, we electronically generate the moving images for the television display. In this case, the lag and frequency effects associated for camera tube generated imagery are absent. The television monitor itself exhibits lag and a frequency effect but these are negligible for the image sizes and pattern speeds which are used below. For the experiment, squares in motion were used as the test objects. The experimental setup is similar to that of Fig. 65 except that the square could appear in either the top, middle, or lower third of the displayed picture. The test motion was from left to right. Two image motion rates were used, 20 and 5 seconds per picture width (only 93% of the actual picture width was used). The effect of these speeds on detection probability
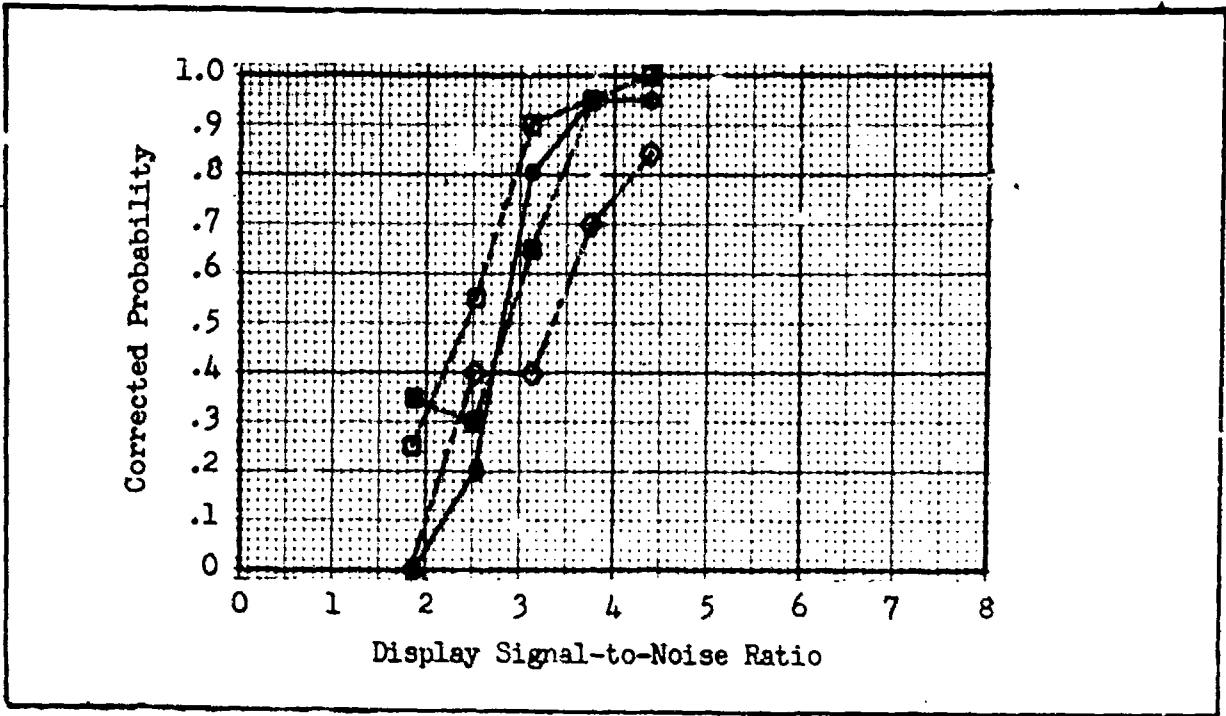
Fig. 115　Probability of Detection vs Display Signal-to-Noise Ratio for Square Images of Size ⦿ 2 x 2, ▢ 4 x 4, ▆ 8 x 8 and ◇ 16 x 16 Scan Lines Moving Across 93% of the Horizontal Field of View in 20 Seconds. Televised Images at 30 frames/sec. 525 Scan Lines $D_V/D_H = 3.5$.

is shown in Figs. 115 and 116. In Fig. 117, the threshold values of display signal-to-noise ratio are plotted as a function of square size for the static, 20 and 5 sec per picture width cases. For all but the smallest images, an image speed of 20 sec per picture width has virtually no effect on the required display signal-to-noise ratio; the threshold values of display signal-to-noise ratio are virtually the same as those for the static case. Motion apparently helped the detection of the smallest target; the required value of display signal-to-noise ratio was 24% lower with 20 sec/picture width than in the static case. With 5 sec/picture width motion, the average value of display signal-to-noise ratio is 26% higher than the static case for the larger square and is virtually the same as the static case for the small square. The experimental conditions for these motion experiments summarized in Fig. 104.

181
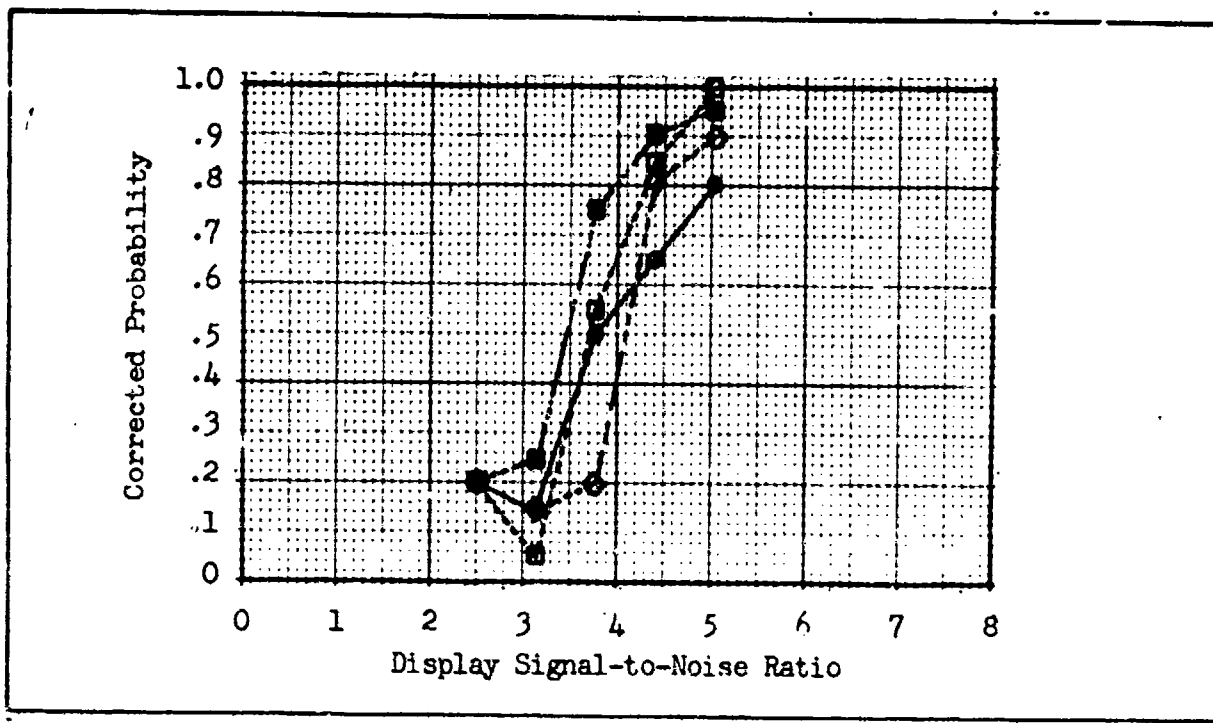
Fig. 116   Probability of Detection vs Display Signal-to-Noise Ratio for Square
Images of Size O 2 x 2, ☐ 4 x 4, ■ 6 x 8 and ◇ 16 x 16 Scan Lines
Moving Across 93% of the Horizontal Field of View in 5 Seconds.
Televised Images at 30 frames/sec. 525 Scan Lines $D_V/D_H = 3.5$.
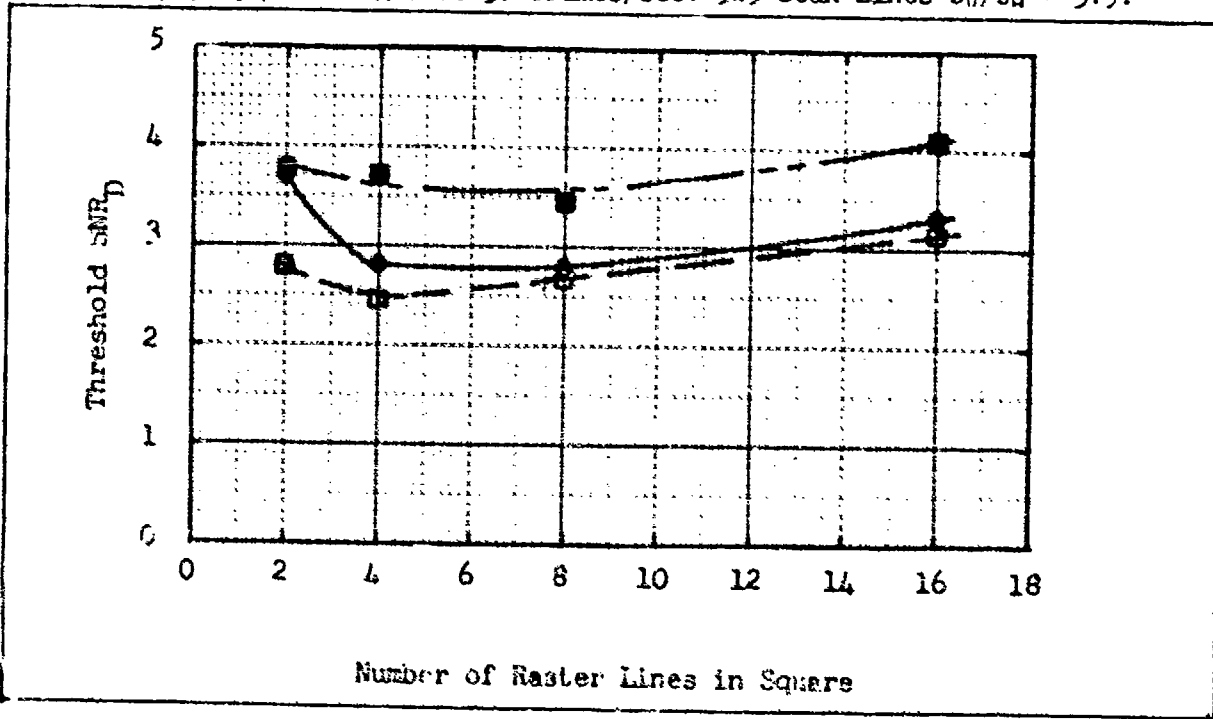
Fig. 117   Threshold $6NR_D$ vs Square Size in Raster Lines for, ☐ Stationary
Patterns, and Motions of, ○ 20 Sec. and ■ 5 Sec per Picture
Width.   Televised Images at 30/Sec, 525 Scan Lines and $D_V/D_H = 3.5$.

.2V/unit

1.0 μsec/unit
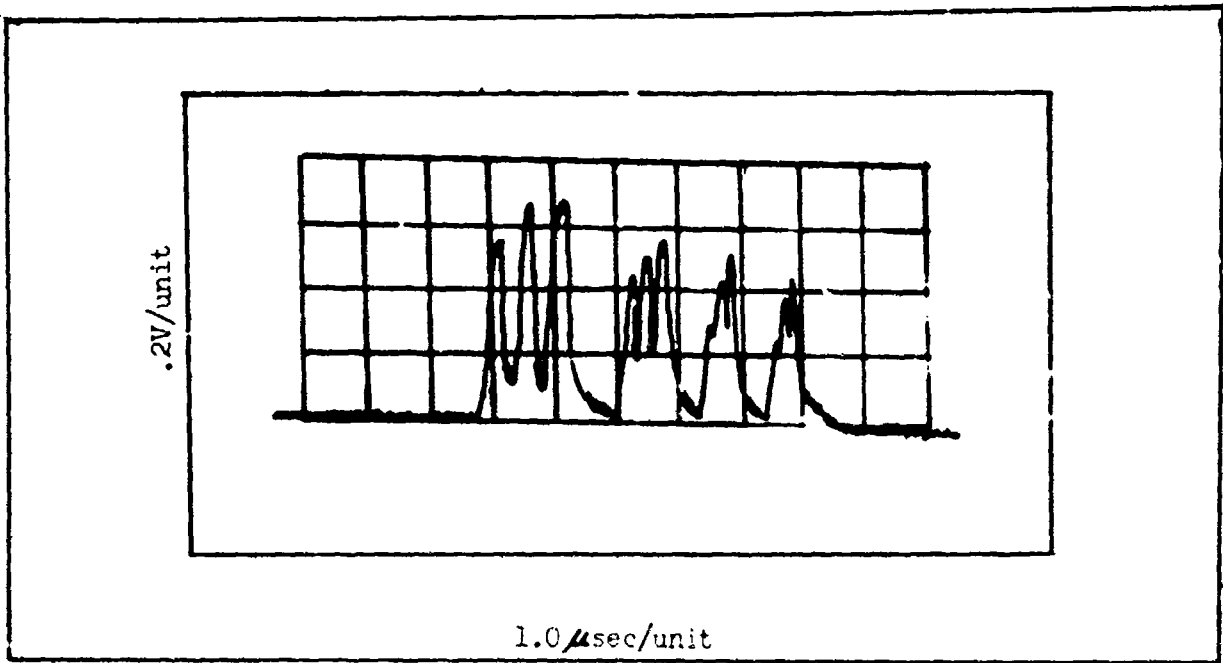
Fig. 118   A Trace of the Video Signals for Bar Pattern
Motion of 20 sec/Picture Width.

If bar patterns were used as the test objects instead of squares,
the results of the motion experiments would not be expected to be signifi-
cantly different from the above. Bar patterns could not be conveniently
generated by the electronics which were used above and consequently the
vidicon camera viewing transparencies of bar patterns was used for
generation of the images. The setup was similar to that shown in Fig. 78
except that the bar patterns could be moved at a rate of 20 sec per picture
width. The lag of the camera significantly influen is the signals. For
instance, in Fig. 118, an A-trace is shown of the signals and as is seen,
the peak-to-peak signal in the first bar of each bar pattern is significantly
less than that in the subsequent bars. For the calculation of display
signal-to-noise ratio, the average peak-to-peak signal in the three bars
was used. For the experiment, one observer was used and 280 data points

183
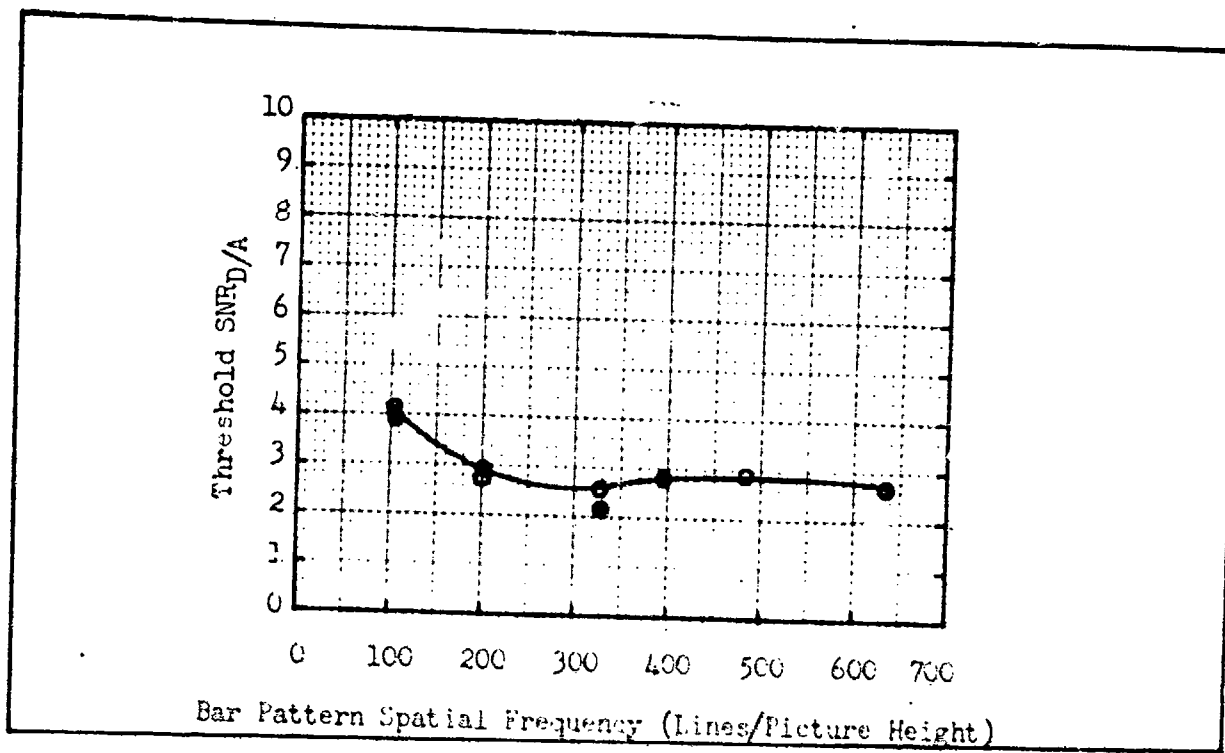
Fig. 119 Threshold Display Signal-to-Noise Ratio vs
Spatial Frequency of Bar Patterns — ● With 20
sec/p.w. Motion, ○ No Motion for Same Observer
as Motion Experiment.

were taken. The noise was 200 mv RMS "white" of 12.5 MHz bandwidth. The
display luminance was approximately 1 ft-Lambert. The results of the
experiment and the corresponding experiment with no motion for the same
observer are shown in Fig. 119 and it is seen that no difference between
the two cases is apparent.

The above results, although not complete, strongly suggest
that the purely psychophysical effects of image motion are rather small for
image motion rates encountered in real systems. To put the conclusion
another way, for values of image motion that the system can accommodate,
the psychophysical effects of the motion can be neglected in most cases.
This, of course, is implying that the system lag effects and pure motion
effects are such that with even moderate amounts of image motion that they
dominate. The following section will deal, in part, with camera lag effects
on the image motion.

5.0 Image Motion

In real time imaging systems incorporating image storage, it is imperative that the scene being viewed remain approximately stationary during the sensory systems exposure or integration period as will be shown. Stationary scenes are usually achieved by motion compensating and stabilizing the sensors sightline. Image motion is ordinarily a degrading effect but can be of aid in the specific case where a scene object is moving relative to its background in a way so as to distinguish it from background clutter. To be of most help, however, either the object or the background should be held stationary and hence both sightline stabilization and motion compensation are still needed. In the more usual case where the objects and backgrounds are both stationary, any sightline motion will be degrading due to the motion itself and due to sensor lag or response time effects.

The effects of image motion on system performance can be considered as three distinct mechanisms. The first is the interaction of image motion and signal storage time, the second is due to observer psychophysical effects and the third is the influence of sensor lag or response time. The psychophysical effects, which are generally small have been previously considered in Section 4.8. We note that the sensor lag effects are the most difficult mechanisms to model at this time.

5.1 Effects Due to Motion Only

In the following section, the emphasis will be on the degradation due to image motion alone. For this purpose, we will begin with

185

the flight geometry of Fig. 120. In this figure, an aircraft is assumed
to be in straight and level flight at altitude, H, and true ground velocity,
V, along the ground track. The sightline angle relative to the aircraft
is ψ which can be resolved to a depression angle component, β, and an
azimuth angle, α. The slant range to a flat earth is R. The angular
rate of change of the depression angle, $\dot{\beta}$, is desired. Referring to Fig. 120,
we have,

$$\frac{d\beta}{dt} = \frac{V_\beta}{R} = \frac{V_\beta \sin\beta}{H} = \frac{V_\alpha \sin^2\beta}{H} \, , \tag{148}$$

and

$$\frac{d\beta}{dt} = \frac{V}{H} \cos\alpha \sin^2\beta \, , \tag{149}$$

or

$$= \frac{V}{H} \cos\alpha \left(\frac{1 - \cos 2\beta}{2}\right) . \tag{150}$$

For the azimuth angle, α,

$$\frac{d\alpha}{dt} = \frac{V_x}{R_s} = \frac{V_x \sin\beta}{H} \, , \tag{151}$$

so that

$$\frac{d\alpha}{dt} = \frac{V}{H} \sin\alpha \sin\beta \, , \tag{152}$$

and for the sightline angle, ψ, since

$$\left(\frac{d\psi}{dt}\right)^2 = \left(\frac{d\alpha}{dt}\right)^2 + \left(\frac{d\beta}{dt}\right)^2 \, , \tag{153}$$

we have

$$\frac{d\psi}{dt} = \frac{V}{H} \sin\beta \left(1 - \cos^2\alpha \cos^2\beta\right)^{1/2} \, , \tag{154}$$

which has a maximum when β is 90° and the maximum is, of course, equal to
the V/H ratio. In a more usual viewing situation, β might be 30° and
$\alpha = 0^\circ$ but even here $\frac{d\psi}{dt}$ is 0.25 V/H. Thus, V/H, though it is a worst case

186
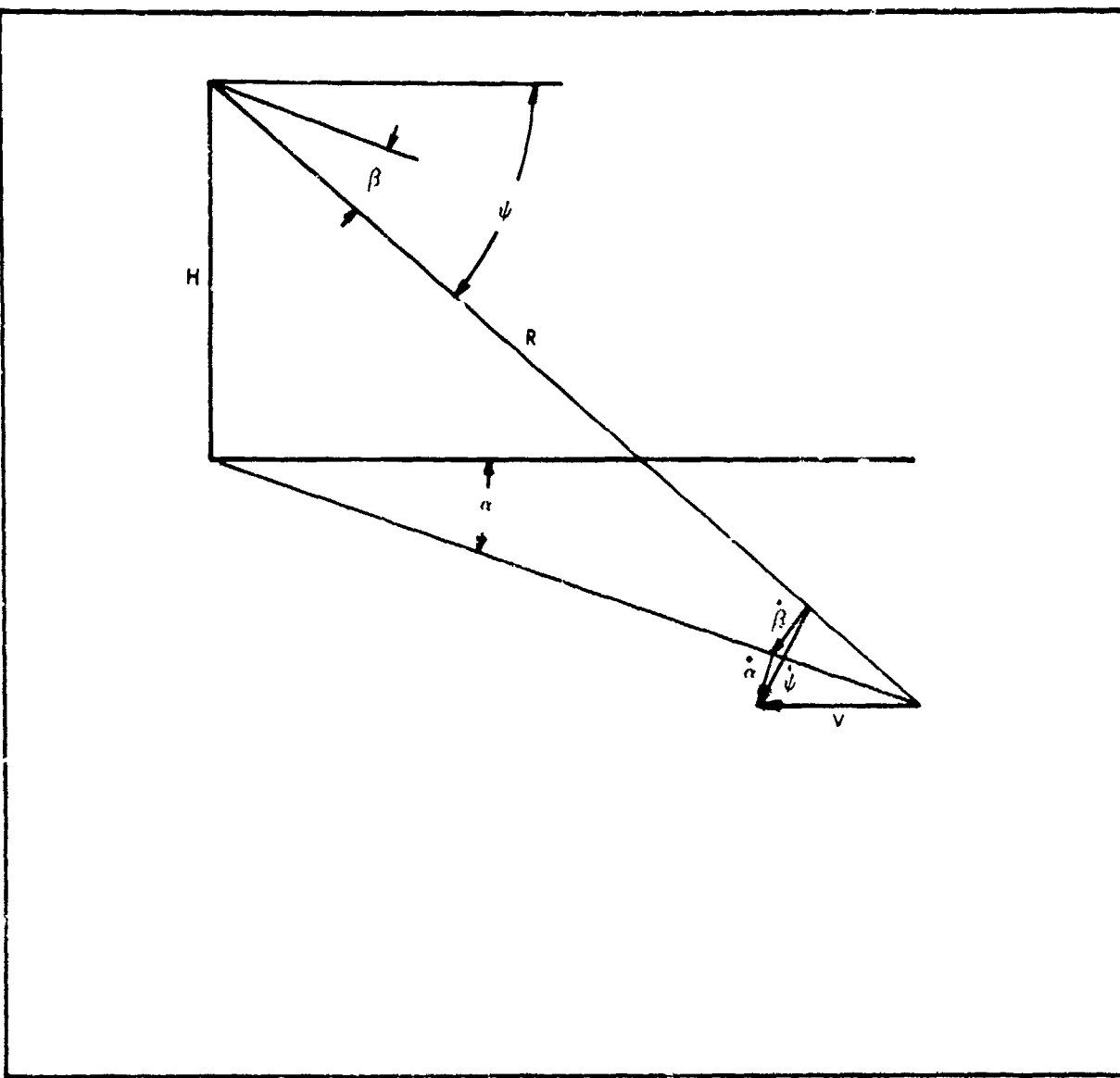
Fig. 120 Geometry for Scene Motion Analysis

estimate of the highest angular rates to be encountered, is not an unreasonable rate to design for.

Suppose it is desired to image a sine wave or bar pattern on the ground perpendicular to a sightline depressed at a fixed elevation angle, β. Let the angular subtense of one of the bars referenced to the sensor be $\Delta\psi$. If the sensor incorporates image storage for a frame time of t_f seconds, the pattern would completely disappear if the sightline moves a distance $2\Delta\psi$ in time t_f. Thus, to resolve the bar pattern,

$$\frac{d\psi}{dt} \leq \frac{2\Delta\psi}{t_f} \ . \tag{155}$$

For our worst case, $\frac{d\psi}{dt} = V/H$ and hence $2\Delta\psi/t_f > V/H$ or $V/H < 2\Delta\psi/t_f$. If $\Delta\psi = 0.1 \times 10^{-3}$ radians and $t_f = 1/30$ second, then $V/H \leq 6 \times 10^{-3}$ sec^{-1}. At an altitude of 6666 feet, V, the true ground speed would be limited to 24 kts which is obviously too slow for fixed wing aircraft. These V/H considerations are plotted in Fig. 121 for fixed depression angles of 90° and 30° for the equality of Eq. (155). A ground speed scale is also provided for an altitude of 6666 ft. It is seen that even with a 30° depression angle, that for resolution of the order of 0.1 mr, aircraft velocity is limited to less than 100 kts. Thus, high resolution systems must be image motion compensated for even modest V/H ratios.

It is readily seen that even with image motion compensation, that only one point in the image will be stationary — all other points will move at various rates. Assuming perfect compensation of the sightline and zero azimuth, the rate of change of images off the sightline will be
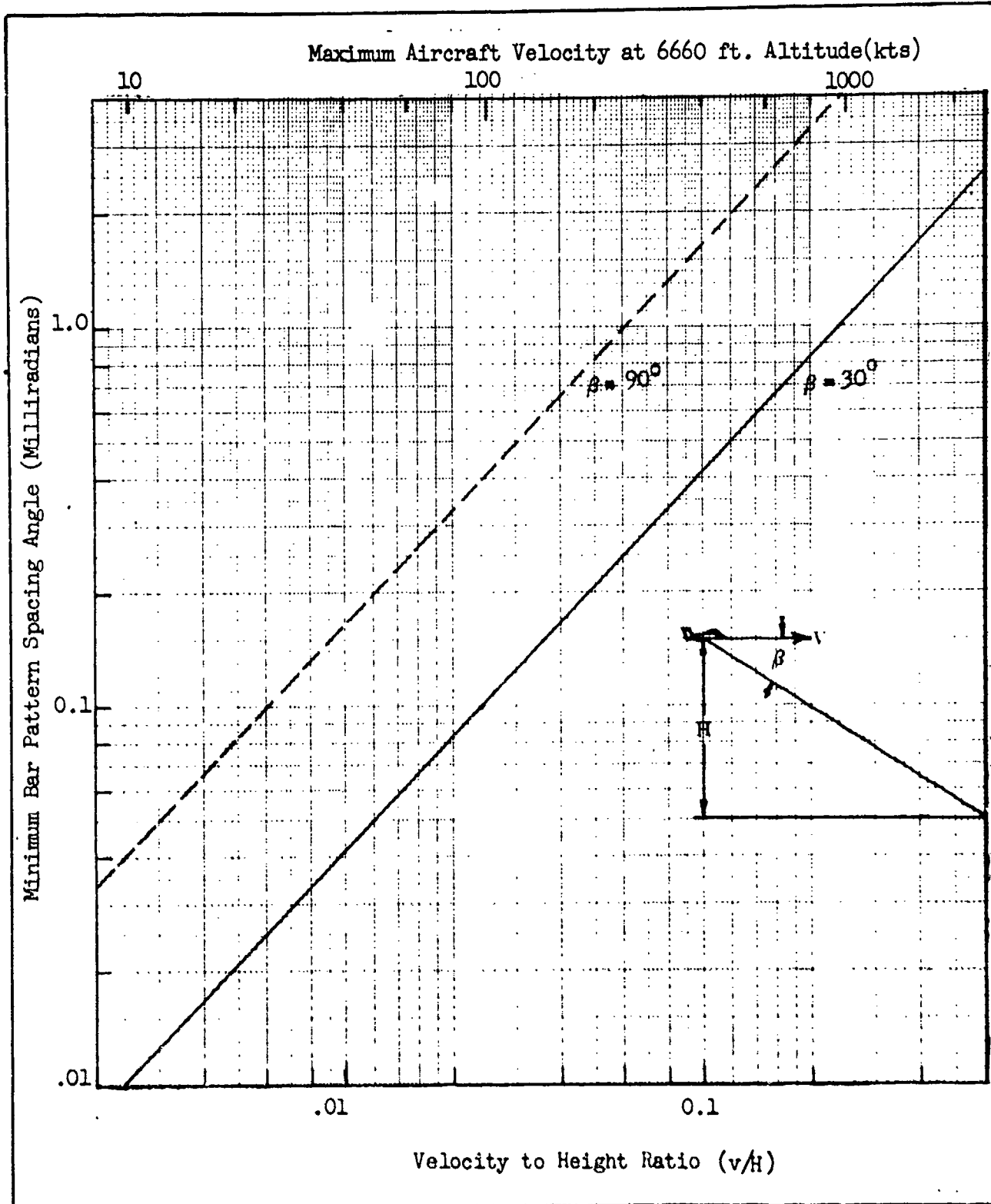
Fig. 121 Minimum Square Wave Bar Pattern Spacing Angle vs. v/h Ratio and Aircraft Velocity (for h = 6660 ft.) for a Fixed Sightline Depressed at 30° and 90° and at Zero Azimuth. Sensor Frame Time is 1/30 Second.

$$\frac{d\emptyset}{dt} = \frac{d (\beta + \Delta\beta)}{dt} - \frac{d\beta}{dt} \quad , \tag{156}$$

and using Eq. (150) for $\frac{d\beta}{dt}$ and $\frac{d (\beta + \Delta\beta)}{dt}$ for $\alpha = 0$, we have

$$\frac{d\emptyset}{dt} = \frac{V}{H} \quad 1/2 \left[-\cos 2\beta + \cos 2 (\beta + \Delta\beta) \right] ,$$

$$= \frac{V}{H} \quad 1/2 \left[-\cos 2\beta (1 - \cos 2\Delta\beta) + \sin 2\beta \sin 2\Delta\beta \right] . \tag{157}$$

The image point is at an angle $\Delta\beta$ from the sightline as shown in Fig. 122. The Eq. (157) has a maximum at $\beta = 45^{O}$ for which the equation becomes

$$\frac{d\emptyset}{dt} = \left(\frac{V}{H}\right) \frac{1}{2} \sin 2\Delta\beta . \tag{158}$$

As before, we assume that there is a bar pattern at the image point of bar width $\Delta\emptyset$. To resolve the pattern

$$\frac{d\emptyset}{dt} \leq \frac{2\Delta\emptyset}{t_f} \quad , \tag{159}$$

or, for the present case,

$$\frac{V}{H} \quad \frac{1}{2} \sin 2\Delta\beta \leq \frac{2\Delta\emptyset}{t_f} \quad , \tag{160}$$

and this equation has been plotted, in Fig. 122, as a function of V/H for

190
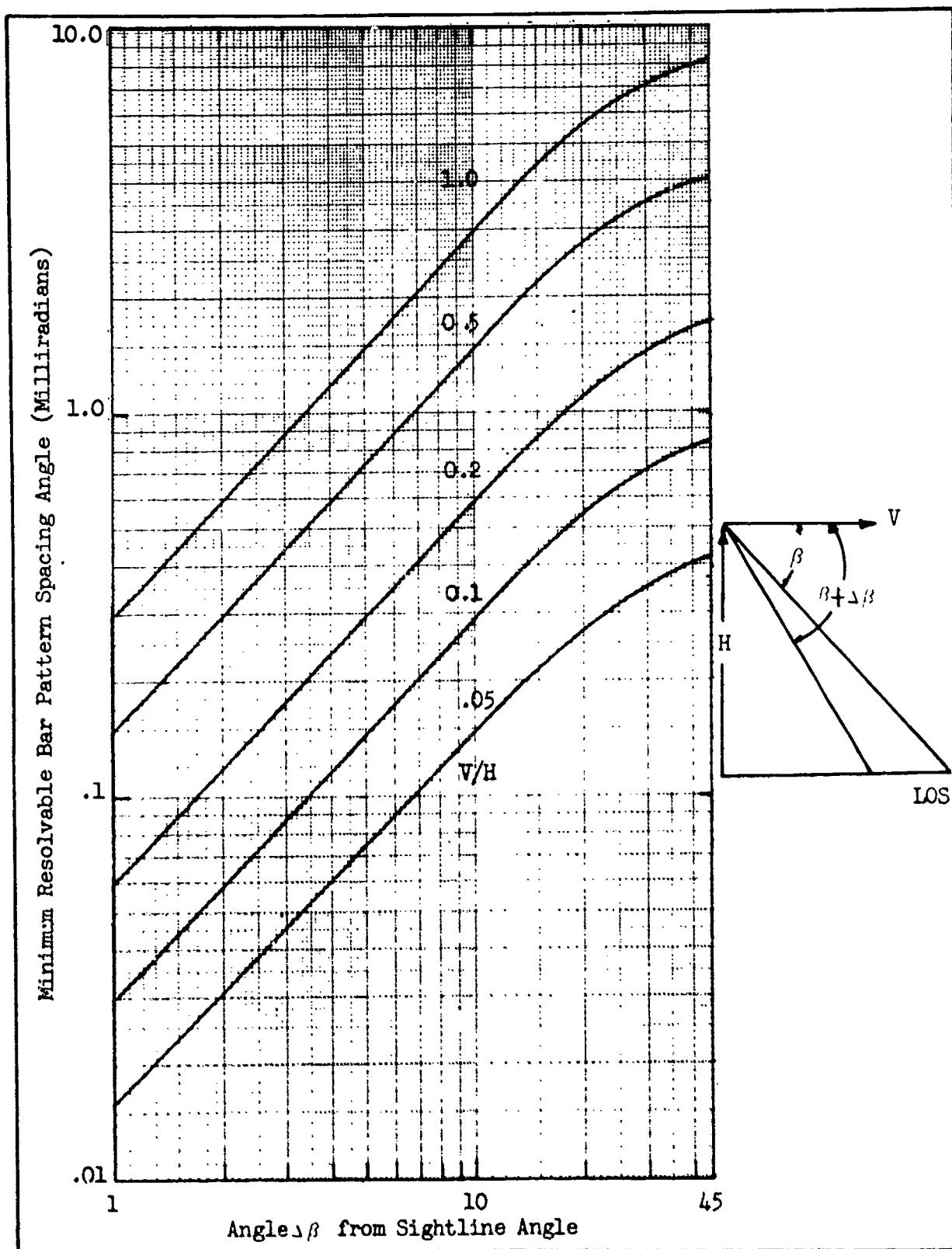
Fig. 122   Minimum Resolvable Square Wave Bar Pattern Spacing Angle vs Angle Off Image-Motion-Compensated Sightline for a Sightline at a 45° Depression Angle, a Sensor Frame Time of 1/30 Second and Various v/H Ratios.

191

the worst case where the equality holds. For the curve it was assumed that $t_f = 1/30$ second.

As can be seen, bar patterns spacings of 0.1 mr can be resolved only with low V/H ratios and then only for angles off the sightline of a few degrees. It is observed, however, that systems with 0.1 mr resolution seldom have fields-of-view larger than a few degrees in any event. The analysis above is quite approximate since no account was taken of the scene lengthening or foreshortening with change in β.

As an example of how the above would impact on a real system consider the following. Assume that an airplane is flying at an altitude of 6,660 ft. with a velocity of 454 miles/hr (V = 666 ft/sec). The V/H ratio is .1. Assume further that the field-of-view is 4° ($\Delta\beta = 2^\circ$) the downlook angle is 45°. From Fig. 122, we have that $\Delta\emptyset = .056 \times 10^{-3}$ rad which would correspond to a pattern line number of 746 lines per picture height for a 3 to 4 aspect field-of-view. In most cases, this would not limit the system too severely but if the altitude were lowered to 3,330 ft., then we find that $\Delta\emptyset$ becomes $.115 \times 10^{-3}$ rad or 372 lines per picture height. Clearly at lower altitudes the system is severely limited by motion. Using Eqs. (154, 155, 158, and 159), we can calculate the speed of a bar pattern through the field-of-view in units of seconds per picture width as follows. If θ is the height of the field-of-view in radians, the width is $4/3\,\theta$. For the fixed downlook case (not tracking), the velocity in seconds per picture width of the image of a bar pattern is given by

$$V_{PF} = \frac{(\frac{4}{3}\theta)}{(\frac{d\psi}{dt})} \quad , \tag{161}$$

where $\frac{d\psi}{dt}$ is given in Eq. (154). Similarly, when a ground point is tracked, and defining $\Delta\beta = (\frac{\theta}{4})$ we have that

$$V_{PT} = \frac{(\frac{4}{3}\theta)}{(\frac{d\phi}{dt})} \quad , \tag{162}$$

where $\frac{d\phi}{dt}$ is given by Eq. (158). The above equations have been solved for various values of field-of-views and V/H ratio and the results are plotted in Fig. 123. The smaller the field-of-view, the larger the differences in velocity for the two cases. For instance, for a 2° field-of-view and a 45° downlook angle, with a fixed downlook angle, the pattern would travel nearly 60 times faster than in the fixed point, ground track case.

It is seen from the above that to minimize the effects of motion one must track the ground. The smallest possible look down angle should be utilized and the smallest V/H ratio (highest altitude) is needed. One can't always satisfy these conditions and some loss, due to motion, will occur in the edges of the field-of-view for all systems.

The purpose of the above analysis was to show that image motion compensation is usually a necessity and that even with compensation, motion can be limiting to resolution. The resolution limits determined in the above are maximum since the limit criteria used was that value of resolution for which the signal current is zero. However, any motion whatsoever has a degrading effect at all spatial frequencies. As will be shown, these effects are best described in terms of a modulation transfer function.

The case to be considered will be that of linear motion of the field-of-view as shown in the geometry of Fig. 124. If the sensor's objective lens has a focal length, F_L, then the image moves at a rate

193
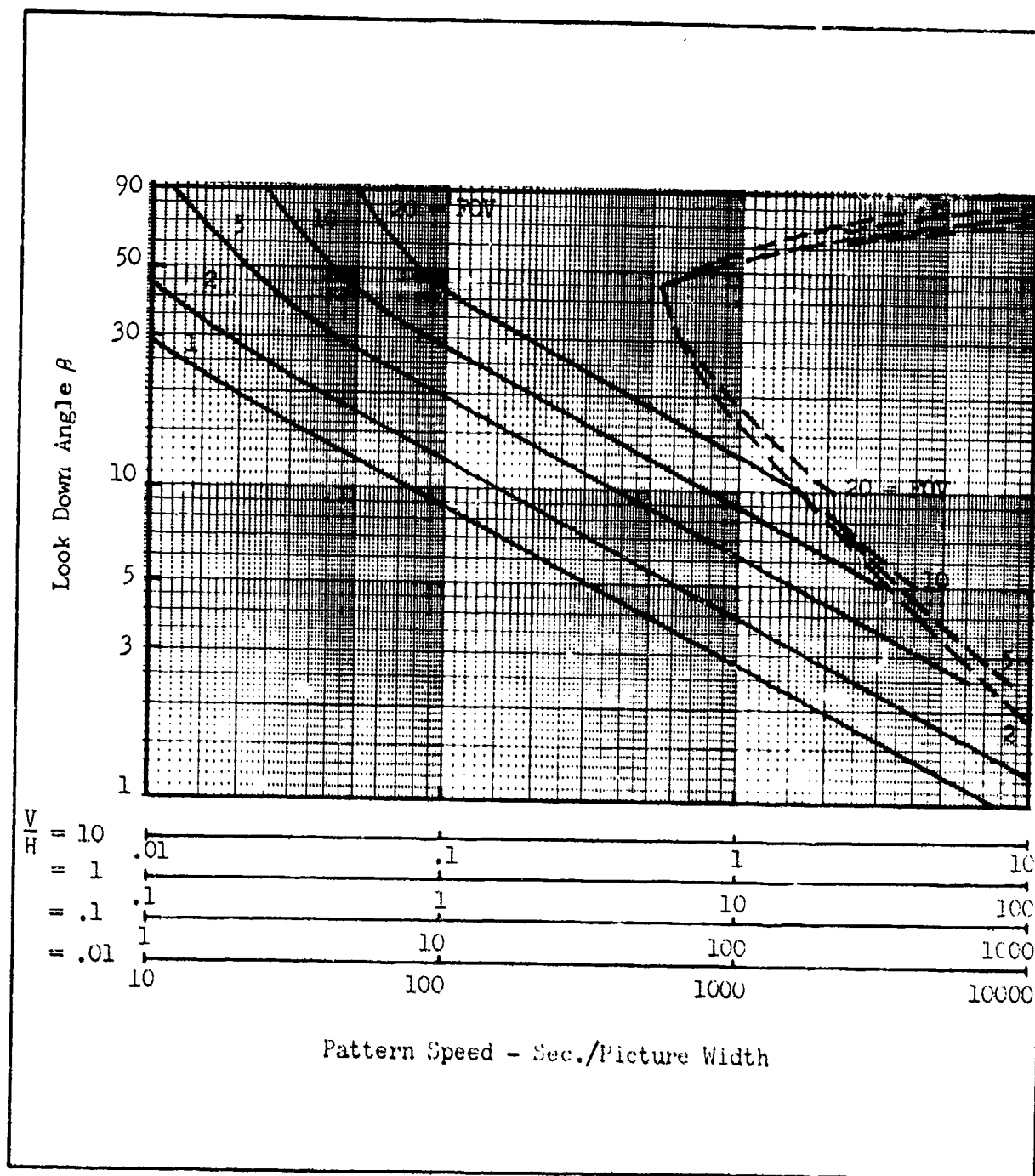
Fig. 123   Look Down Angle β, vs Pattern Speed for Various Fields of Views
———————— Fixed Down Look Angle, No Tracking ——— Fixed Ground
Point Tracking.   V/H = Velocity to Height Ratio.
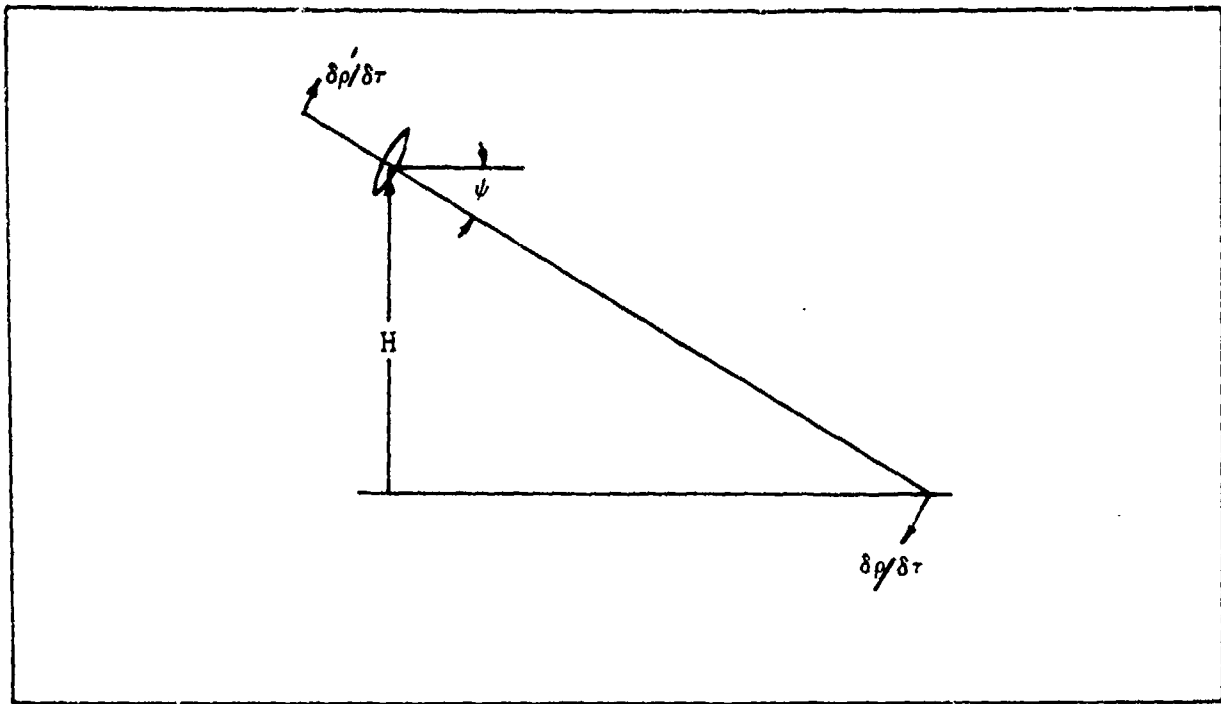
Fig. 124   Geometry for Image Motion Modulation Transfer Function
Analysis

d $\overset{\prime}{\rho}$/dt equal to

$$\frac{d \overset{\prime}{\rho}/dt}{F_L} = \frac{d \rho/dt}{R} \quad , \tag{163}$$

for a scene motion rate of d ρ/dt perpendicular to the sightline. But,
d ρ/dt, the velocity of the sightline vector is given by

$$(d \rho/dt) = \frac{Rd\psi}{dt} \quad , \tag{164}$$

so that

$$(d \overset{\prime}{\rho}/dt) = F_L \frac{d\psi}{dt} \quad , \tag{165}$$

195

where ψ is as shown in Fig. 124.

Now, suppose the image to be a line or impulse of strength J_o which is moving at a rate $d\rho/dt = v_i$. Let the sensor's storage time be t_f. Then the line image becomes smeared out into a rectangular image distribution of amplitude $J_o/v_i \, t_f$ and duration $\Delta\rho = v_i \, t_f$. If J_o is of unit area in the direction of motion, then the rectangular distribution becomes the line spread function due to motion and its Fourier transform becomes the complex steady state frequency response or optical transfer function whose magnitude is the MTF, i.e.,

$$R_o \, (k_p) \;=\; \frac{1}{v_i \, t_f} \int_{-v_i \, t_f/2}^{v_i \, t_f/2} \exp\,(-j\,2\pi\, k_p\, \rho)\; d\rho$$

$$=\; \frac{\sin \pi \, k_p \, v_i \, t_f}{\pi \, k_p \, v_i \, t_f}\;, \tag{166}$$

and

$$R_o \, (k_p) \;=\; \frac{\sin \pi k_p \, v_i \, t_f}{\pi k_p \, v_i \, t_f}\;, \tag{167}$$

where k_p is the spatial frequency in line pairs/mm if v_i is given in mm/sec. The above response has zeros at $k_p = p/v_i \, t_f$ where $p = 1, 2 \; \text{------}$. In terms of television resolution expressed in lines per picture height, N_T,

$$R_o \, (N_T) \;=\; \frac{\sin \,(\pi N_T \, v_i \, t_f/2Y)}{\pi N_T \, v_i \, t_f/2Y}\;, \tag{168}$$

for v_i given in mm/sec and Y is the picture height in mm. It is sometimes convenient to express the motion MTF in dimensionless form using the "cut-off" spatial frequency k_{pc} which is that frequency at which $R_o \, (k_p)$ first

196
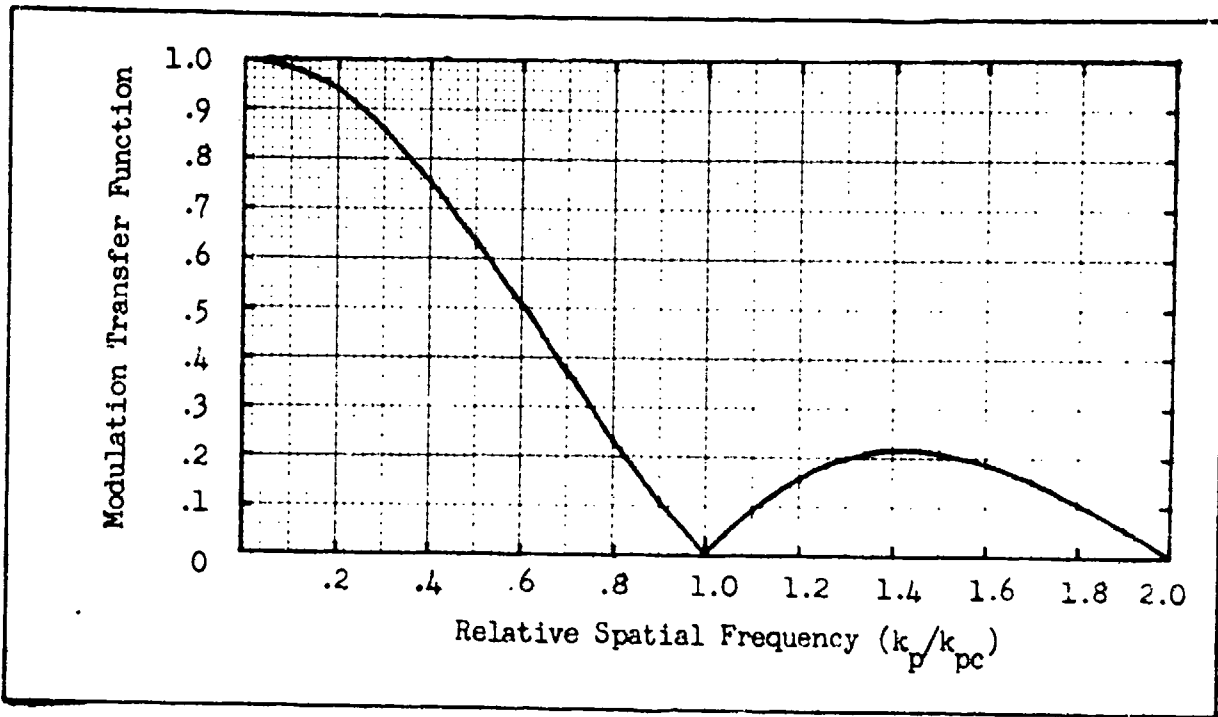
Fig. 125 Modulation Transfer Function Due to Linear Image Motion
vs Spatial Frequency Normalized to the Cut-Off Frequency, k_{pc}

goes to zero. Thus $k_{pc} = 1/v_i\, t_f$ and,

$$R_o\,(k_p) \;=\; \frac{\sin\,(\pi k_p/k_{pc})}{\pi k_p/k_{pc}} \quad , \tag{169}$$

which is plotted in Fig. 125.

It has become customary to measure the "dynamic resolution"
of many sensors. In the particular case of television cameras, one test
is to measure limiting or threshold resolution for bar patterns which are
in linear motion across the field-of-view. The motion is specified in terms
of the number of seconds, t_s, required for the test pattern to traverse the
picture width. For this case, the pattern velocity becomes

$$v_i \;=\; \frac{4Y}{3t_s} \quad \frac{\text{picture widths}}{\text{sec}} \quad , \tag{170}$$

197
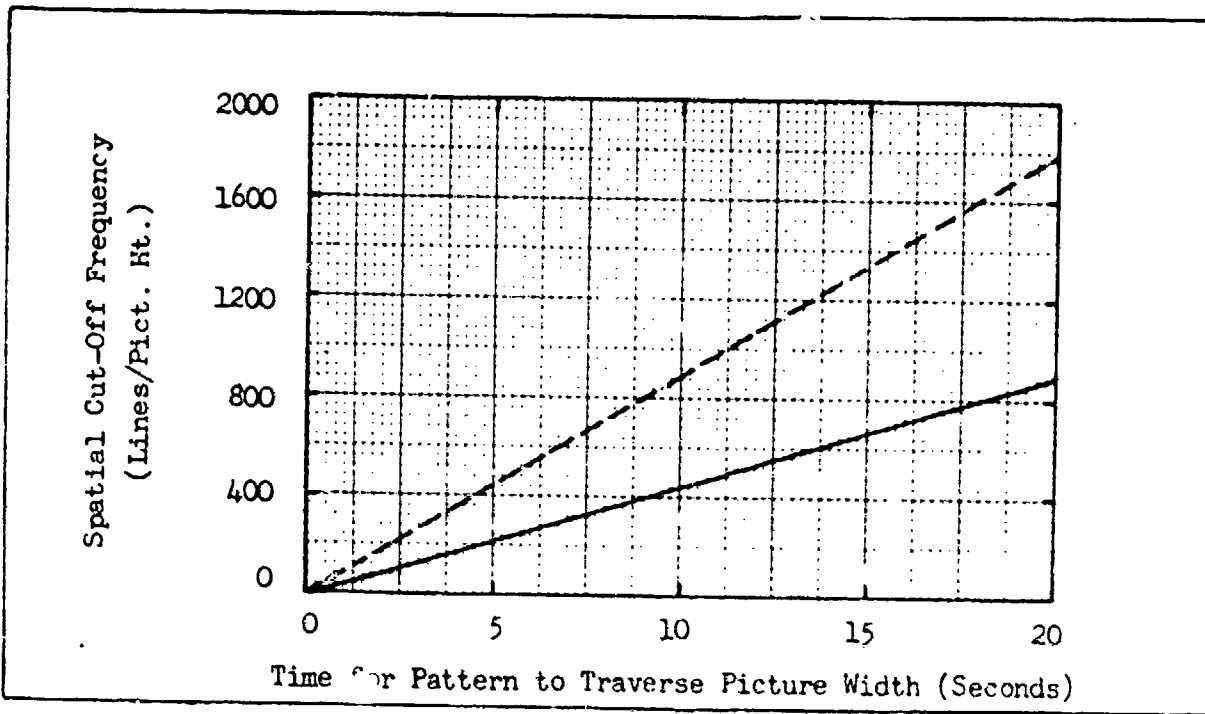
Fig. 126 Cut-Off Spatial Frequency vs Time For a Square Wave Pattern to Traverse Picture Width For Integration Times of (---) 1/60 Sec. and (——) 1/30 Sec.

and the cutoff frequency

$$N_{TC} = \frac{3}{2} \frac{t_s}{t_f} \frac{\text{lines}}{\text{picture height}} \quad , \tag{171}$$

which is plotted vs time t_s for two frame times of 1/60 and 1/30 second in Fig. 126. Using Eq. 171 in Eq. 168, the MTF due to motion for the two integration times can be calculated and the result of such a calculation is shown in Fig. 127. The two integration times are used because in an interlaced system such as TV, it is possible to erase both fields in a single scan such that the integration time is actually only 1/2 the frame time. It should be observed that patterns of higher spatial frequency than the cut-off frequency can be detected since the MTF due to motion

198
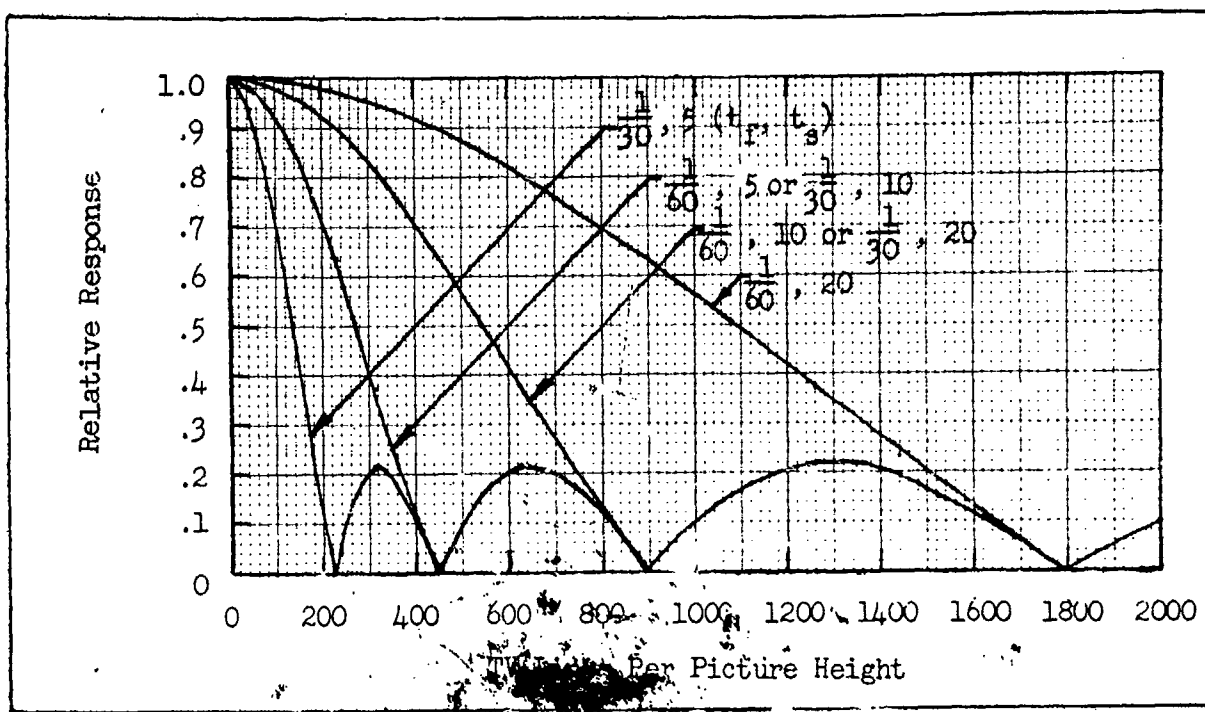
Fig. 127 Modulation Transfer Function for the 3 Most Commonly Used
Patterns Speeds for 1/60 sec and 1/30 sec Integration Times.

exists beyond the cut-off but response beyond these frequencies represents

false or spurious resolution. This process is sometimes called aliasing.

5.2 Introduction* to Camera Lag

With only a few exceptions, the performance characteristics of

camera tubes are generally specified in terms of results of static imaging

tests. With recognition of the fact that imaging of dynamic scenes results

in tube characteristics degraded from those achieved through static tests,

attempts to characterize dynamic performance in a simple way have led to

the specification of an image lag parameter. The lag parameter is a measure

---

* Sections 5.2 through 5.5 were performed at the Westinghouse Electronic
Tube Division, Elmira, New York.

of the degree of image retention when a spot of illumination, spatially fixed, is turned off and on. Basically, the parameter measures the deviation in performance of the particular camera tube from that exhibited by an ideal device.

The interpretation of the lag parameter depends upon its specific definition and method of measurement. Its real meaning however is achieved only through its association with actual dynamic performance after eliminating other degrading effects.

When measurements of limiting resolution as a function of the illumination of a camera tube sensing surface are carried out on moving resolution bar charts it is found that the tube sensitivity is less than that achieved when the measurements are made on a stationary bar chart. This particular type of measurement is very limited in meaning and involves several image degrading processes. Some of these are signal mixing, first scan read-out effect and the phenomenon of lag. Experiments of this type, while indicating tube sensitivity degradation at the illumination threshold for perception of given resolution specifications, do not indicate the performance to be expected at higher illumination levels.

It is the purpose of this section to summarize some preliminary investigations directed ultimately, toward achieving an understanding of the processes involved in dynamic imaging. More particularly the following sections deal with experiments in which the buildup and decay lag parameters are precisely defined and measured and the influence of moving resolution bar charts on tube sensitivity and amplitude response are assessed.

In the following section, the various pertinent phenomena influencing dynamic performance are discussed. This is followed in Section

200

5.4 by measurements made on a specific camera tube type while in Section 5.5, an attempt to calculate and relate some of the important processes to the experimentally observed results is made.

5.3 Phenomena Influencing Dynamic Performance

a) First Scan Readout Effect

This effect is not explicitly evaluated here, however, its existence should be noted. First scan or single scan readout of a charge storage target is generally manifested by a reduction in the target MTF compared to that achieved during repetitive and steady state operation. The extent of the MTF reduction is dependent on the target structure and is a result of the scanning electron beam, during first scan, sensing the potential distribution rather than the charge distribution stored in the target. Basically, the stored charge pattern produces a mirror image charge in the signal plate or other conducting electrode in proximity to it. This results in a broader potential distribution than would exist if the conducting electrode were absent. Once a steady state condition is established, the broadening due to the mirror image charge is compensated for and the MTF improves.

When a moving charge pattern is established in a storage target during dynamic imaging, a first scan condition will, to some extent, exist since various regions of the target will never have an apportunity to achieve a steady state condition.

The first scan readout effect has been discussed by several investigators[16-18] and Lowrance and Zucchino[19] have evaluated the effect for both the image isocon/orthicon and SEC type tubes. The image isocon/orthicon in particular shows very severe MTF reduction which may account

201

for their apparent great loss in sensitivity under dynamic imaging conditions.

b) Signal Mixing

Signal mixing is a process that occurs to the same extent in all charge storage targets, regardless of type, and is caused by the motion of the image across the storage target during the integration period. A bar chart imaged onto the photocathode of a camera tube results in a spatially distributed square wave charge distribution on the storage target. If the image is in motion, the charge distribution moves across the target and the charge built up during the integration time results in a stored charge distribution significantly different from the light pattern imaged on the photocathode. This process has been treated by Anderton and Beyer[20] and a family of curves generated relating relative contrast and resolution line number on the target for several rates of image motion. Fig. 128 shows such a chart generalized for any rate of image motion and adjusted to reflect an integration time of one frame (1/30 second) rather than one field (1/60 second) used by Anderton and Beyer.

c) The Phenomenon of Lag

The phenomenon of lag is a consequence of the inability of the camera tube read beam to completely neutralize the charge stored in a storage target during a single scan across a picture element. The incomplete neutralization of the stored charge results in the partial mixing of information from one frame to the next and may be manifested in image smear when viewing moving objects or, in the case of color television, lack of color purity.

Any quantitative specification of lag is dependent upon its precise definition and the method of measurement. For the purpose of this

202
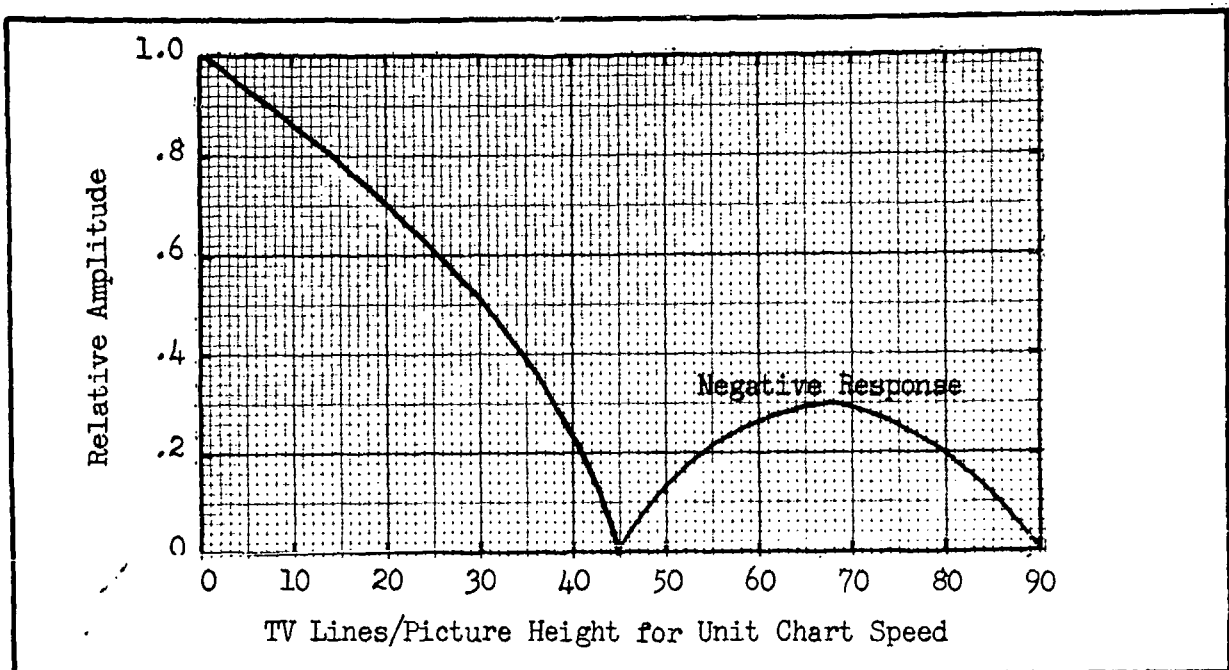
Fig. 128   Relative Response vs TV Lines/Picture Height for Unit
            Chart Speed - Multiply Abscissa by Chart Speed in Sec/
            Picture Width to Convert to TVL/PH.

report and the data to be presented later, two lag quantities, namely

buildup and decay lag are defined as follows. A small spot of light

is imaged onto the center of the input to the camera tube and the resulting

signal current as a series of pulses, one for each successive field, is

displayed on an oscilloscope. The occurrence of a pulse is mid-time between

the beginning and end of any field. This time is given a field designation.

At the same time during a vertical flyback the illumination is turned on.

The field prior to this is designated zero and that following the onset of

illumination is denoted one. Thus, the illumination is turned on mid-time

between the zero and first field readouts. This is shown in Fig. 129.

The light remains on for a sufficient number of fields to permit a steady

state to occur and then mid-time between two successive field readouts

the illumination is removed for an equal number of fields. In Fig. 129,

203
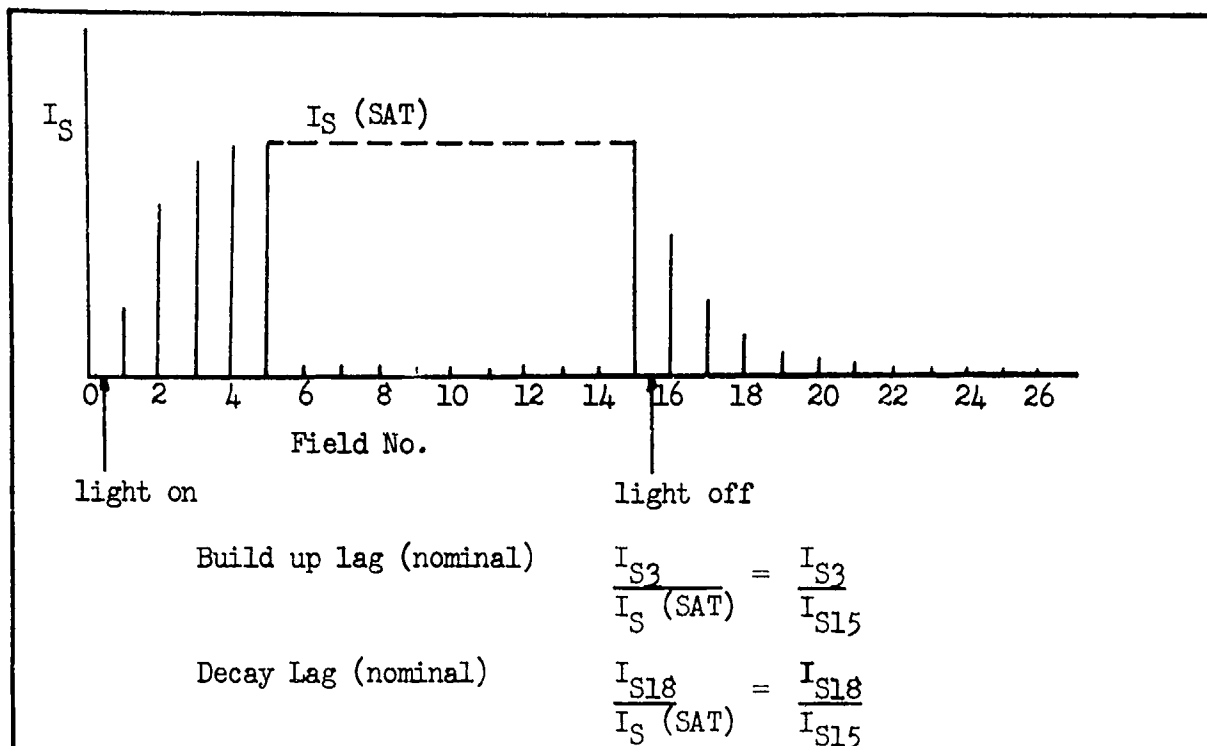
Fig. 129   Definition of Lag

the illumination was maintained for 15 fields. The nominal buildup lag

and decay lag parameters are defined as indicated on the figure. Unless

otherwise specified, this is the definition of lag used in this report.

If one considers an ideal target in which all the stored charge

in a picture element is neutralized in a single scan and a scan system

in which perfect interlace exists the signal buildup is 100% in the third

field and the signal decay is 100% (i.e., the signal current is zero) in

the eighteenth field which is the third field readout after the

illumination is removed.

Any third field signal current less than I_s (SAT) and any

eighteenth field signal current greater than zero indicates departure from

ideal performance. For the ideal target the stored target charge

dependence on the sequence described above is illustrated in Figs. 130 and
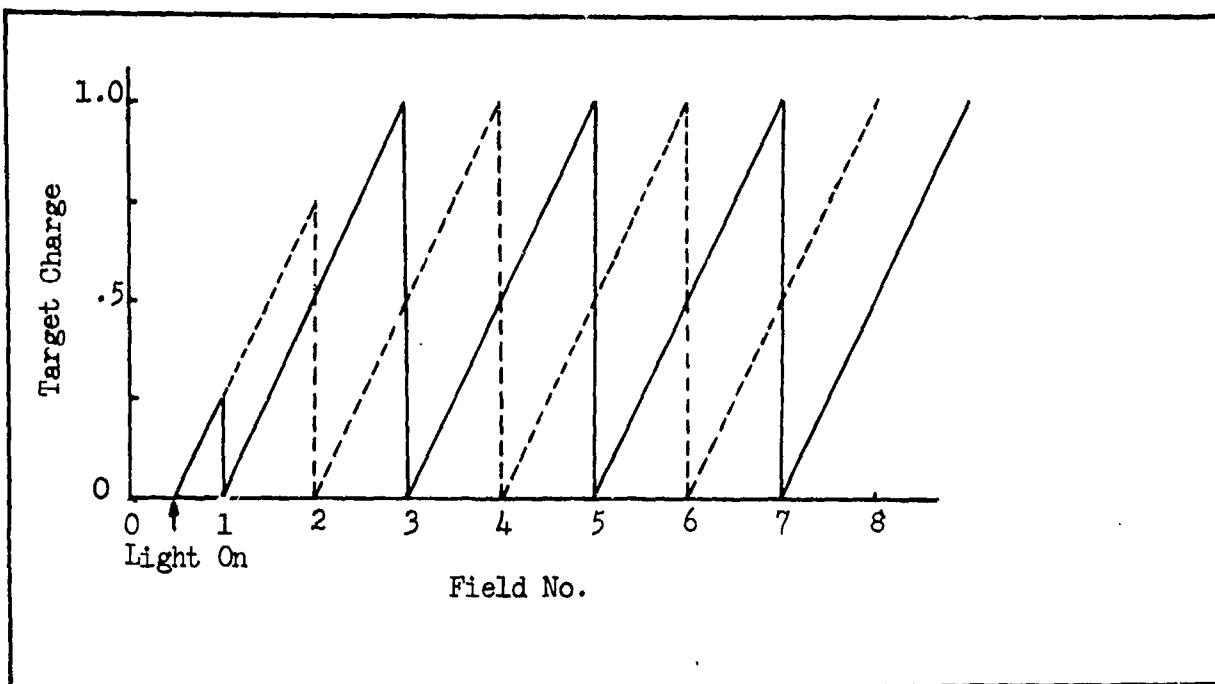
Fig. 130   Relative Charge Build Up - Ideal Target - Even Fields,
            -- Odd Fields Perfect Interlace

131.   For an ideal target, the number of fields required to achieve satura-
tion and complete decay are insensitive to the precise times at which the
illumination is turned on and off. In the case of real targets in which
the buildup lag is less than 100% and the decay lag is greater than zero
the precise timing of the illumination changes may be reflected in the value
of the nominal lag parameters.

        For a real target, assuming the sequences pictured in Fig. 129,
130 and 131 a relative charge buildup and decay diagram can be constructed.
This is shown in Fig. 132. During the steady state period a total charge
Q_T is accumulated and after a readout the charge is reduced to a residual
value Q_R. During the integration period, a charge Q_i is supplied to the
target during a single complete frame and Q_i is then the difference between
Q_T and Q_R which is the charge readout comprising the signal.   The relative
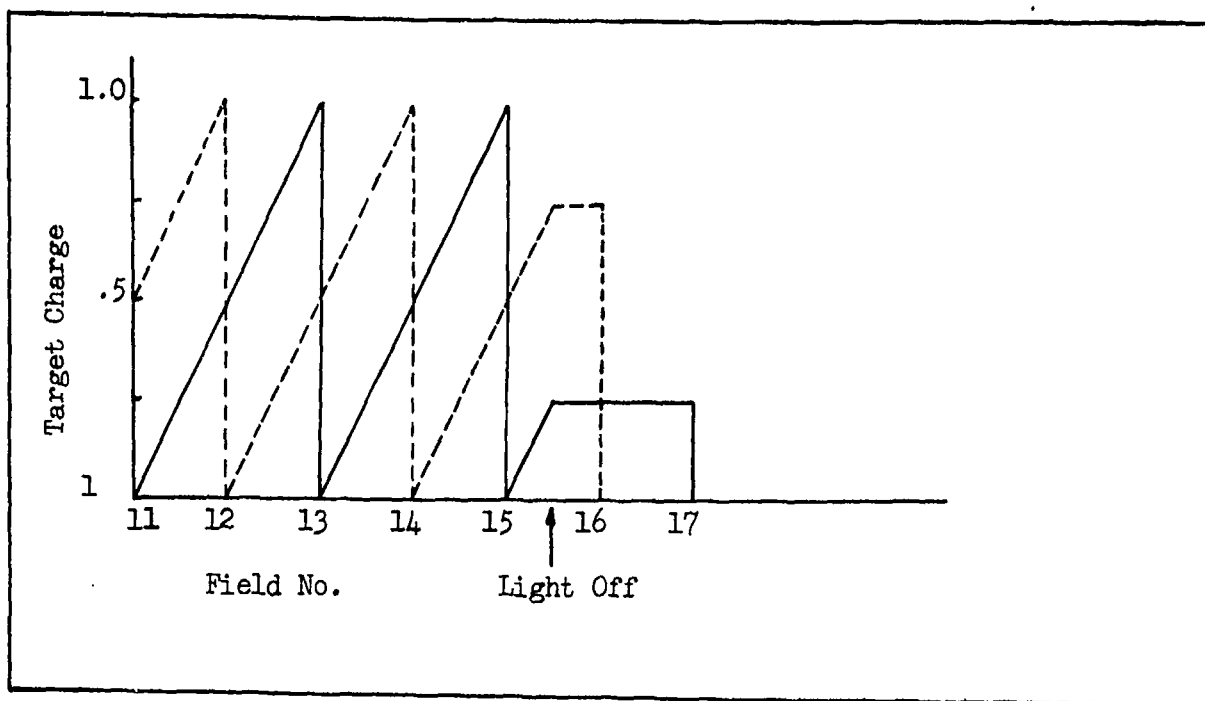
Fig. 131   Relative Charge Decay - Ideal Target - Even Field --
            Odd Field - Perfect Interlace.

magnitude of the residual charge Q_R with respect to Q_T is a function of the

detailed charge readout process which is reflected in the nominal lag

parameter. Although a nominal lag parameter can always be specified, the

precise nature of the buildup and decay transients will not be known unless

the details of the readout process are specified. One simple way of

specifying the readout process is to assume that for all readouts the

charge neutralized is a given fraction γ of the total charge on the target.

Such a specification turns out to characterize the performance of some

resistive sea type silicon diode array targets. Thus, if the steady

state _signal_ charge readout is γ Q_T where Q_T is the total charge, the

residual charge during steady state is $(1 - γ) Q_T$ and the decay lag, for

example is found to be $(4 - γ) (1 - γ)/4$. Similarly the buildup lag is

found to be $γ(5 - γ)/4$.

206
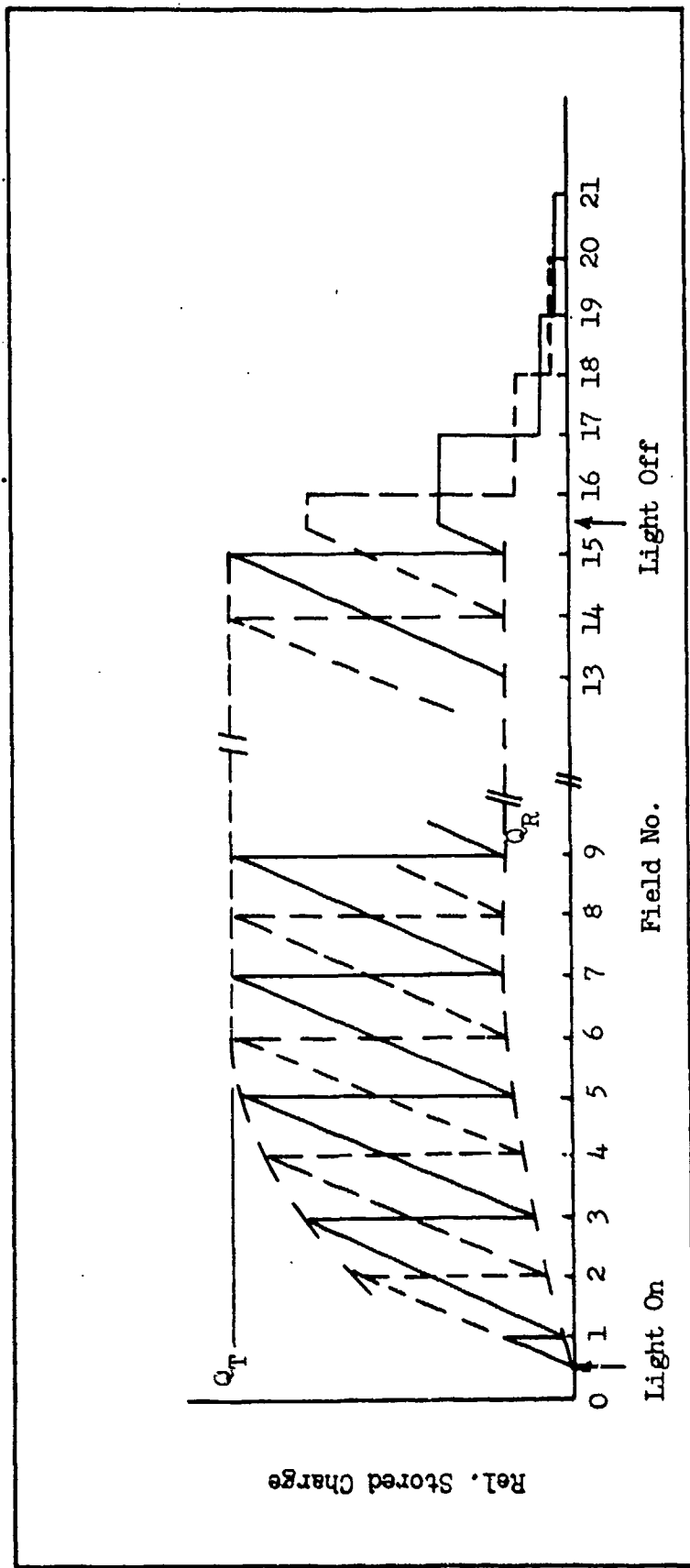
Fig. 132   Relative Charge Build Up and Decay for Real Target
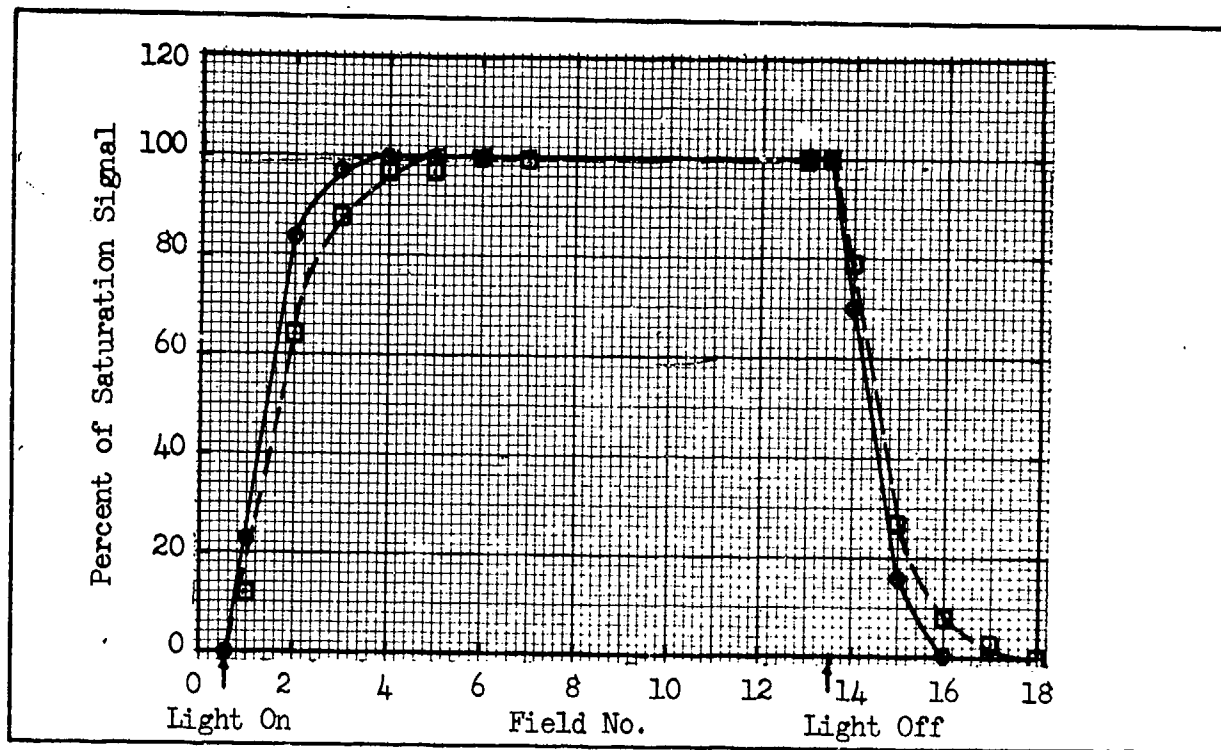
Fig. 133   Signal Build-Up and Decay - Deep Etch Target - WX31793
o 100 na V_T = 15V, ☐ 100 na V_T = 10V

For relating the lag phenomenon to dynamic imaging, the
details of the readout process should be specified, such as by specifying
γ if this specification is pertinent, or by some other parameter. Detailed
data on signal readout at each field serves this purpose.

Fig. 133 shows the signal buildup and decay for a WX-31793 type
tube employing an experimental Westinghouse deep etch target. The data
at a target voltage of 15 volts shows a characteristic very close to that
of an ideal target. In this case γ would be very close to 0.94. Fig. 134
shows a characteristic for a 25mm resistive sea silicon diode array
target. As in Fig. 133, Fig. 134 shows that the buildup and decay
processes are sensitive to the target bias voltage. For a bias of 15V, the
data is very closely approximated by a γ of 0.75.
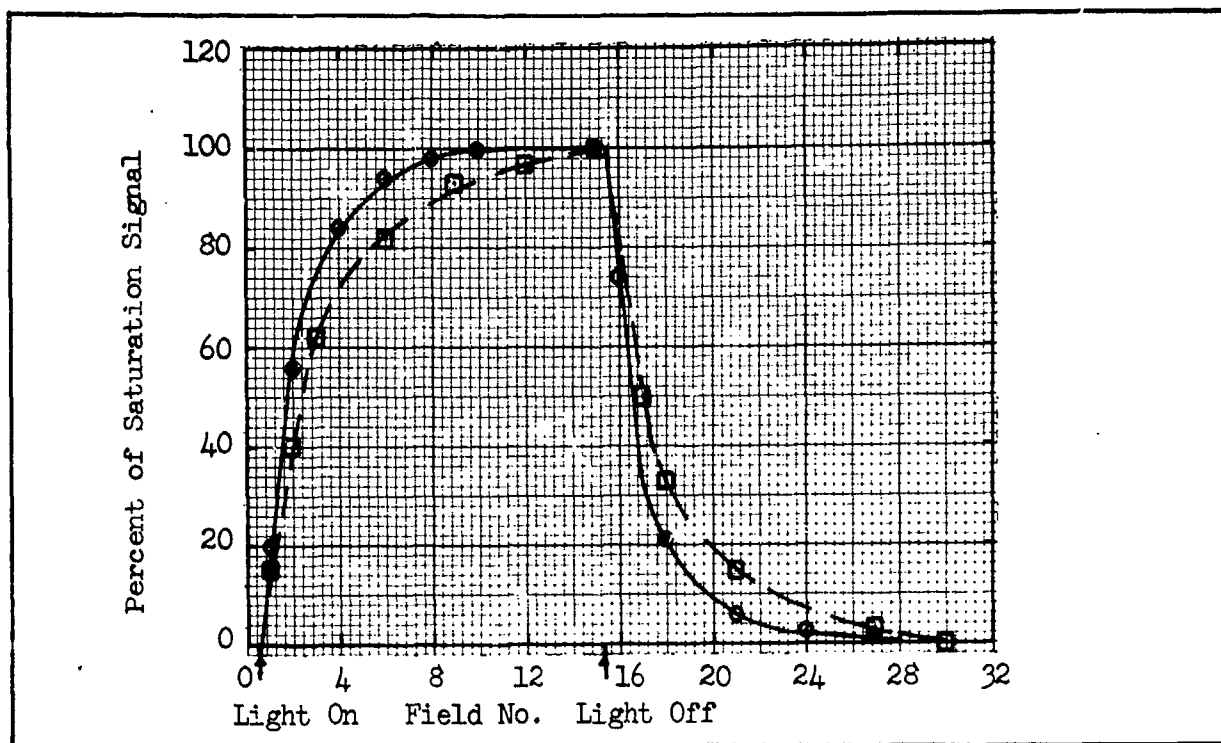
Fig. 134.   Signal Build-Up and Decay - WX31911
             o 100 na $V_T = 15V$, □ 100 na $V_T = 10V$

d) Specification of γ

The nature of the charge readout fraction γ is dependent upon
the specific type of charge storage target employed. As has already
been indicated this can be determined from the buildup and decay
measurements previously described. γ may be dependent upon the total
target charge at the time of readout in which case γ and both the
buildup and decay lag parameters are functions of the signal current. In
some cases, γ is essentially constant and is independent of the total
charge at the time of readout. Under these circumstances, the buildup
and decay lag parameters are essentially independent of the tube signal
current. This latter characteristic is exhibited to a considerable extent
by many silicon diode array resistive sea type targets and may be associated
with the potential division between the resistive sea capacitance (C_R)
and that of the silicon diode depletion region (C_d). The relation between γ

209

and the two capacitances is indicated in Appendix 1.

5.4 Static and Dynamic Resolution Measurements

a) Dynamic Imaging Measurements

Measurements were carried out using a Westinghouse WX-31841 type camera tube. This tube employs a 40 mm diameter photocathode of the multi-alkali type, a minifying diode electrostatic image section and a resistive sea type silicon diode array target of 25 mm active diameter with 2,000 diodes per linear inch. The gun employs magnetic focus and deflection. A read beam scan of 25 mm diagonal giving a raster of height to width ratio of 3:4 was employed.

b) Static Characteristics

The data given in Figs. 135 and 136 indicate the performance characteristics under static conditions. Measurements were made under standard TV scan conditions utilizing two interlaced fields per frame. The preamplifier noise was approximately 12 nA (rms) at a bandwidth of 12 MHz.

c) Dynamic Characteristics

Dynamic characteristics were obtained by measurements of buildup and decay lag, amplitude response dependence on motion of a moving resolution test chart and tube sensitivity dependence on rate of image motion.

d) Buildup and Decay Lag

Lag measurements were made as described above. The dependence of signal buildup and decay on steady state signal current and target voltage were assessed. The lag process proved to be essentially insensitive to the value of the steady state signal current but showed a significant dependence upon target bias voltage. This latter observation was anticipated and offers the opportunity to control the lag process over a

210

1. Photocathode Response (2879°K radiation).   95 μA/lumen.

2. Dark current with lens capped and a photocathode voltage of -10 kV.

Target bias (Volts)	I_d (na)
7.5	20.0
10.0	26.4
12.5	31.8
15.0	31.8
17.5	31.8
20.0	31.8

3. Signal current as a function of photocathode voltage at an illumination of 1.38×10^{-4} footcandles.

V_{pc} (kV)	I_s (nA)
10	135
8	70
6	23
4	0
3	0

4. Light transfer characteristics* taken with a photocathode voltage of -10 kV and target bias of +15 V.

Illumination (fc)	I_s (nA)
1×10^{-3}	985
5.2×10^{-4}	500
2.58×10^{-4}	255
1.38×10^{-4}	135
8.4×10^{-5}	80

5. Limiting resolution at a signal current of 400 nA and bandwidth of 12 MHz - 900 TVL/RH.

6. Static square wave amplitude response measurements made with the RCA P-200 chart at a bandwidth of 4 MHz, a signal current of 400 nA and a read beam adjusted to deliver a maximum signal current of 700 nA (See Fig. 136).

Fig. 135 Static Performance of the WX 31841 EBS Camera.
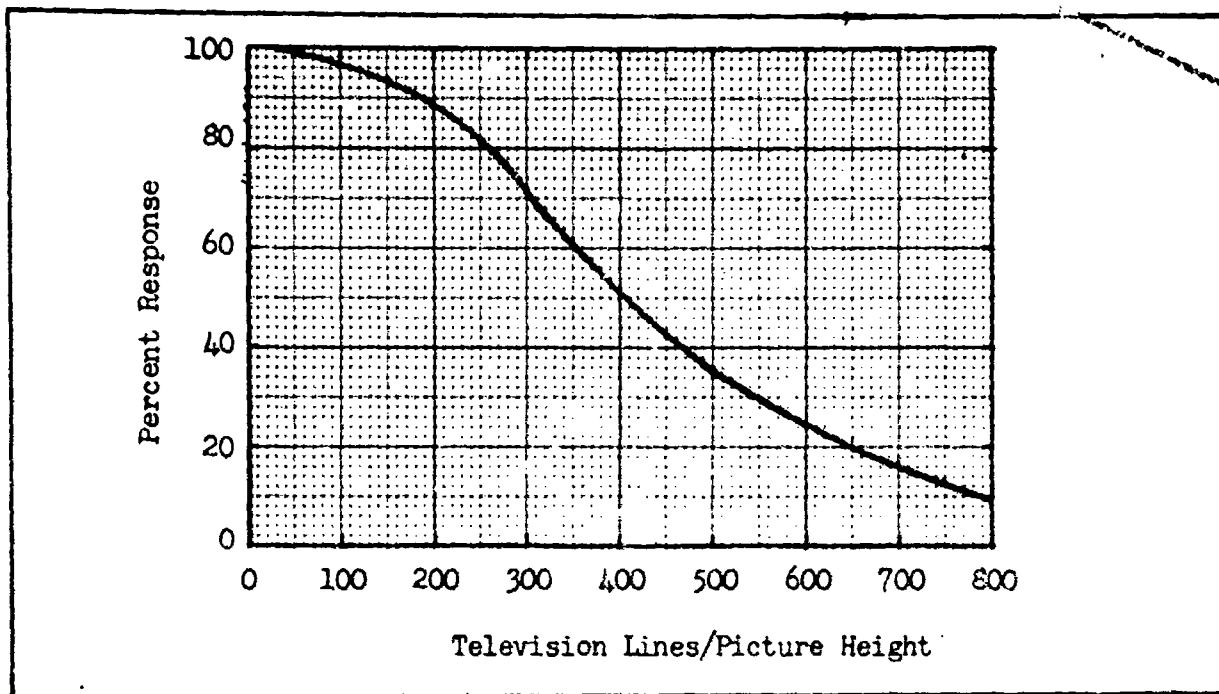
Fig. 136   Static Amplitude Response for WX 31841

wide range of lag values without altering the basic static sensitivity of
the tube.

Fig. 137 contains a summary of the buildup and decay characteristics
of this tube. The relative insensitivity of the nominal lag parameters to
signal current is apparent. The very marked dependence on target voltage
is obvious from the tabulated data.

Detailed signal buildup and decay data for the parameters indi-
cated in Fig. 137 as a function of signal readout field are tabulated in
Appendix 2.

e) Dynamic Amplitude Response

Dynamic amplitude response measurements were obtained by imaging
a slant burst pattern from an RCA P-200 resolution test chart onto the tube
photocathode. The pattern was affixed to a continuous transparent belt that

212

	BU	Decay	BU	Decay	BU	Decay	BU	Decay
7.5 V	54	49	43	49	52	43	57	46
10.0 V	66	38	54	37	62	32	66	37
12.5 V	74	29	66	29	74	26	72	29
15.0 V	80	26	72	26	76	21	74	23
20.0 V	86	20	77	20	83	17	80	20

Data taken on WX-31841 tube type.
Resistive sea type silicon diode array target
25mm diagonal 3 x 4 aspect ratio raster.

Target Bias I_s = 100 nA I_s = 200 nA I_s = 400 nA I_s = 600 nA

Fig. 137   Summary of Lag Characteristics for the WX 31841 EBS Camera.

could be run at various speeds across the field of view of the camera tube.
The pattern was illuminated from behind and the image adjusted to the proper
size. The illumination was adjusted to give a static signal current (in
excess of the dark current) of 400 nA.

The signal modulation was displayed on an oscilloscope and by
sampling the proper line bursts on the test pattern the percent modulation
was read directly from the oscilloscope presentation. When using this
chart a bandwidth of only 4 MHz is required. This results in a signi-
ficant decrease in noise thus offering the possibility of direct reading
from the ocislloscope for chart speeds as high as 2.5 seconds per
picture width.

Because of the test chart design it was found necessary to adjust
the chart speed for each resolution line number in order to obtain an

213
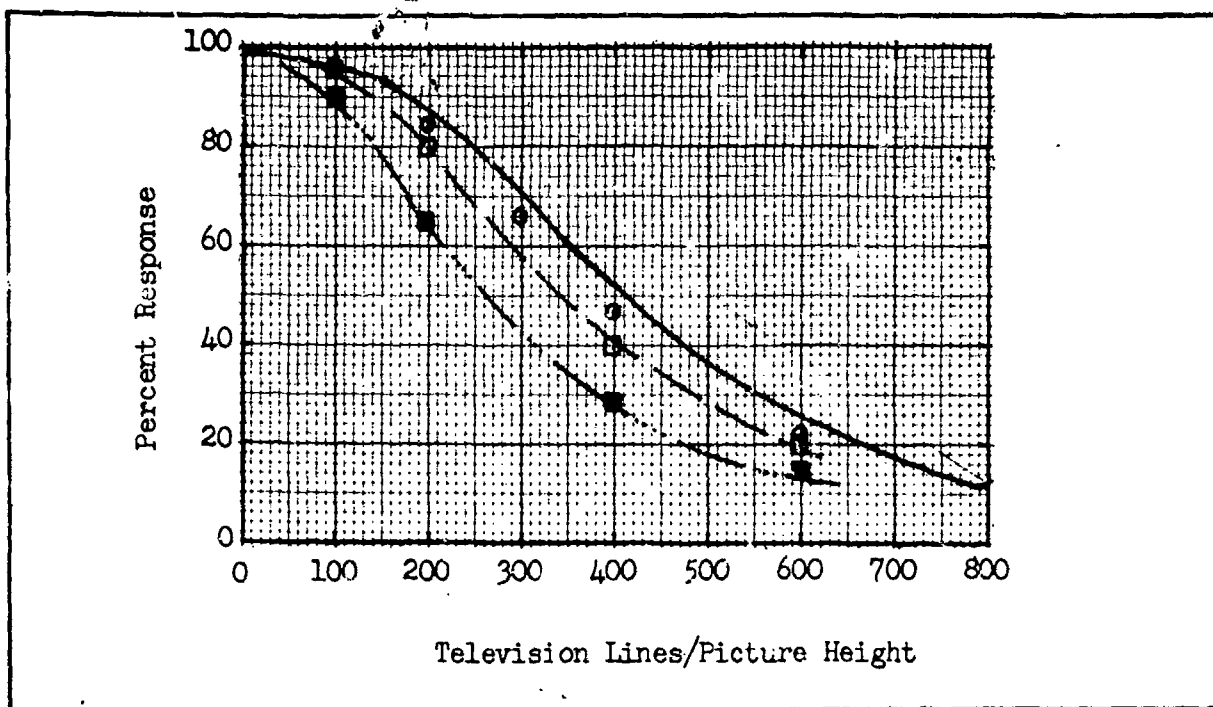
Fig. 138   Dynamic Amplitude Response for Pattern   Speed of 60 Second/
            Picture Width - o Signal Mix □ V_T = 20 V, ■ V_T = 7.5V for
            WX 31841   Solid Curve Static Case

equivalent single speed corresponding to that which would have been used

with a vertical bar chart. Chart speeds were employed that gave equivalent

vertical bar chart speeds of 60 sec/picture width, 20 sec/picture width and

10 sec/picture width. Measurements were made at target voltages of V_T = 7.5

volts. The corresponding lag characteristics are obtainable from Fig. 137

and Appendix 2. Response measurements were made for resolution line burst of

100, 200, 400 and 600 TVL Raster Height.

The influence of image motion on the amplitude response is

summarized in Figs. 138, 139, and 140. The data in the three figures give

the static response, the response at the indicated chart speed for the two

target bias values and data indicating the effect of signal mixing alone.

The latter points were calculated using the curve of Fig. 128 and multi-

plying these relative contrast values by the corresponding static ampli-

214
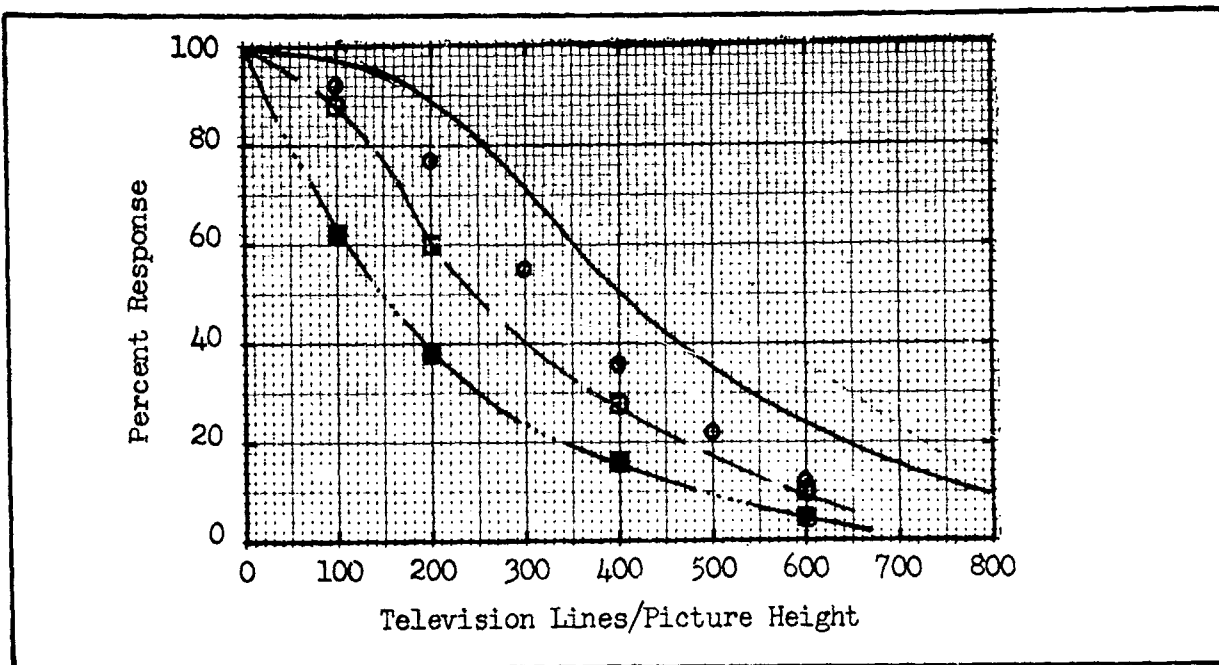
Fig. 139　Dynamic Amplitude Response for Pattern Speed of 20 Seconds/
Picture Width – o Signal Mixing, □ V_T = 20V, ■ V_T = 7.5 V
for WX 31841 – Solid Curve Static Case
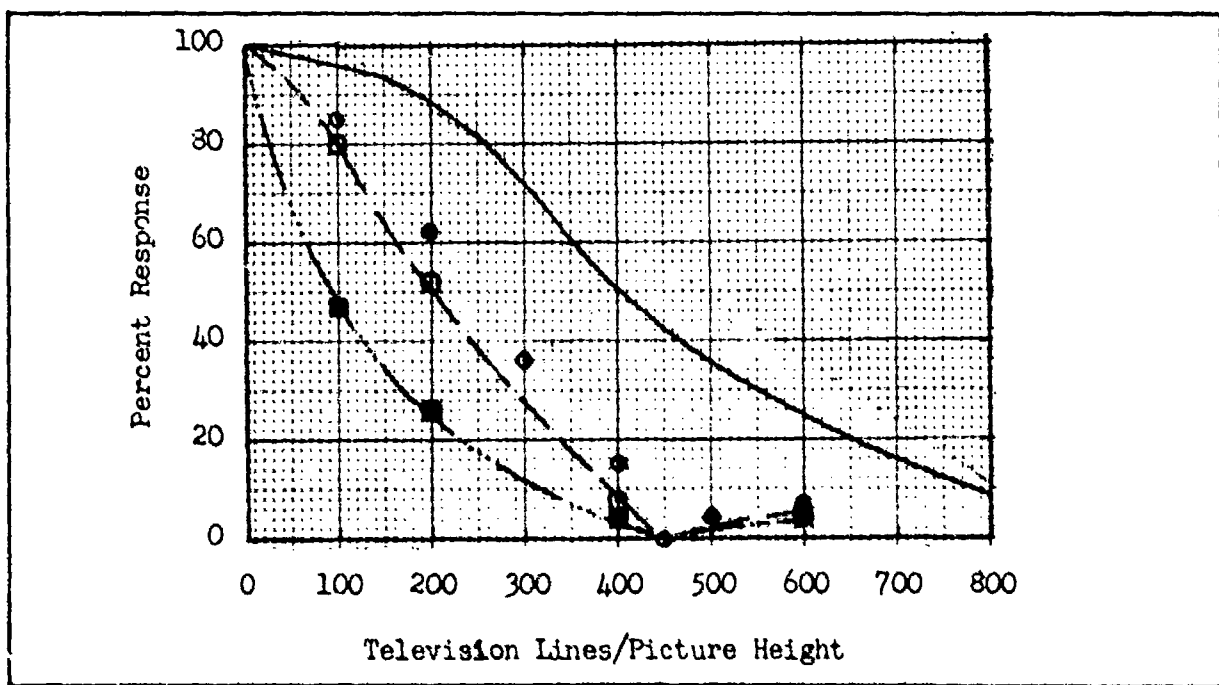
Fig. 140　Dynamic Amplitude Response for Pattern Speed of 10 Seconds/
Picture Width – o Signal Mixing, □ V_T = 20V, ■ V_T = 7.5V
for WX 31841 – Solid Curve Static Case

215

tude response values measured on the tube. This procedure is not
without some error as it involves multiplying together square wave responses.
It does, however, offer a fair assessment as to the degree of response
degradation due to the buildup and decay lag.

f) Dynamic Limiting Resolution

Similar to the measurement of dynamic amplitude response, measure-
ments were made of the tube dynamic sensitivity by imaging a 100% contrast
Westinghouse vertical bar resolution chart on the camera tube and determining
the minimum illumination required to permit perception of various resolution
line numbers. For these tests the tube was operated with target voltages
of 7.5 and 20 volts with the chart maintained stationary and also run at
speeds of 60, 20, 10 and 5 seconds per picture width. All measurements
were made with a photocathode potential of -10 kv and a video bandwidth
of 12 MHz. From the resulting data, curves of limiting resolution as a
function of photocathode illumination for the various rates of image
motion were generated. These are presented in Fig. 141 for a target
voltage of 20 volts and Fig. 142 for a target voltage of 7.5 volts.

For a resolution of 100 TVL/Raster height, the tube sensi-
tivity degradation between static conditions and motion at 5 sec/picture
width was only a factor of 6 for a target voltage of 20 volts and
for a target bias of 7.5 volts the degradation was approximately a factor
of 15.

The most surprising result was the large sensitivity loss for
the very slow image motion rate of 60 sec/picture width and its dependence
on the target voltage and consequently the target buildup and decay
lag. It is difficult to reconcile this loss in sensitivity with the

216
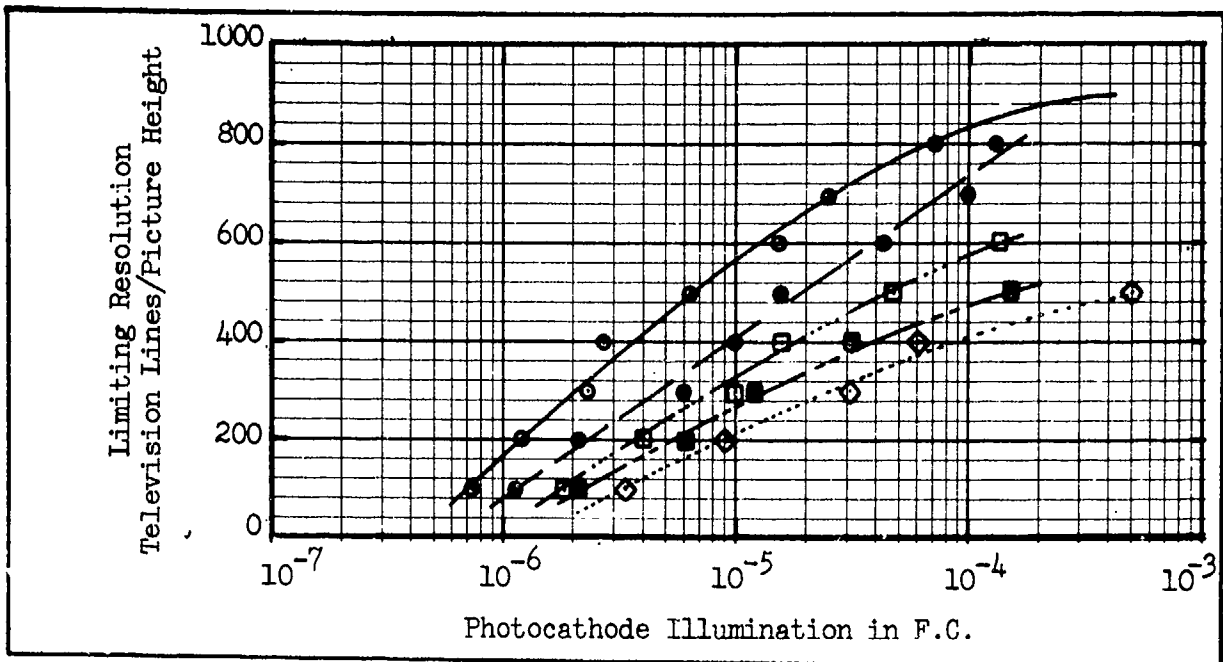
Fig. 141   Dynamic Sensitivity for 100% Contrast Pattern, V_T = 20 volts
o Static, ● 60 Sec/P.W., □ 20 Sec/P.W., ■ 10 Sec/P.W., ◇ 5
Sec/P.W., Bandwidth 12 MHz
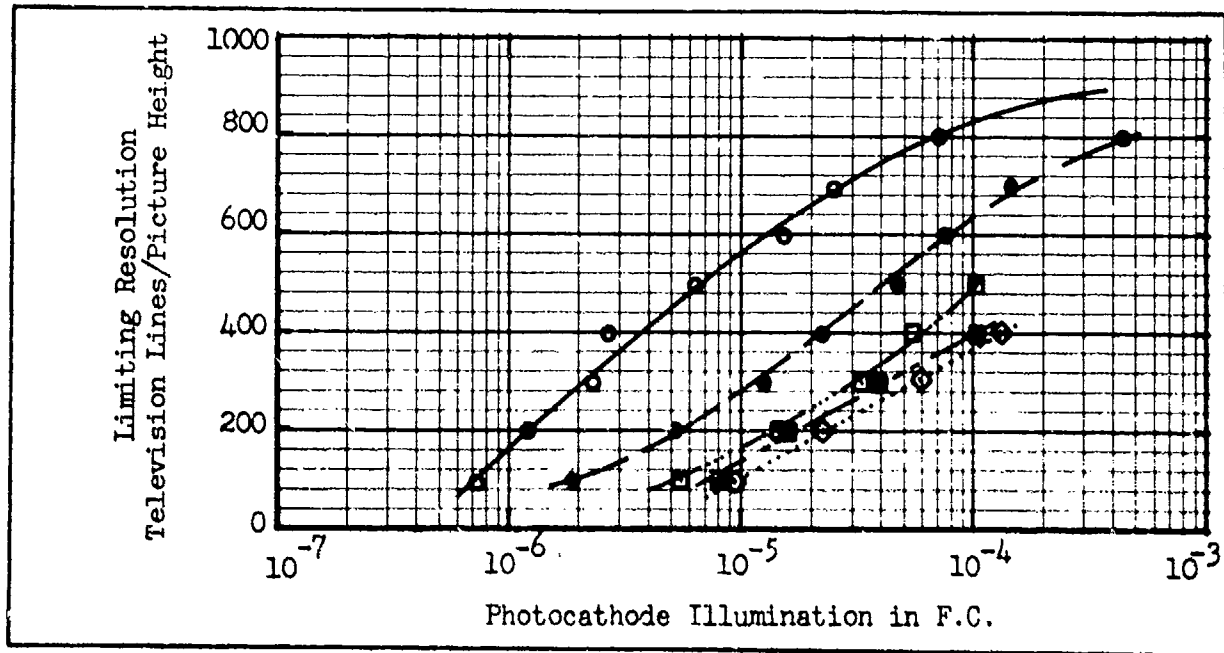
Fig. 142   Dynamic Sensitivity for 100% Contrast Pattern, V_T = 7.5 volts
o Static, ● 60 Sec/P.W., □ 20 Sec/P.W., ■ 10 Sec/P.W., ◇ 5
Sec/P.W., Bandwidth 12 MHz
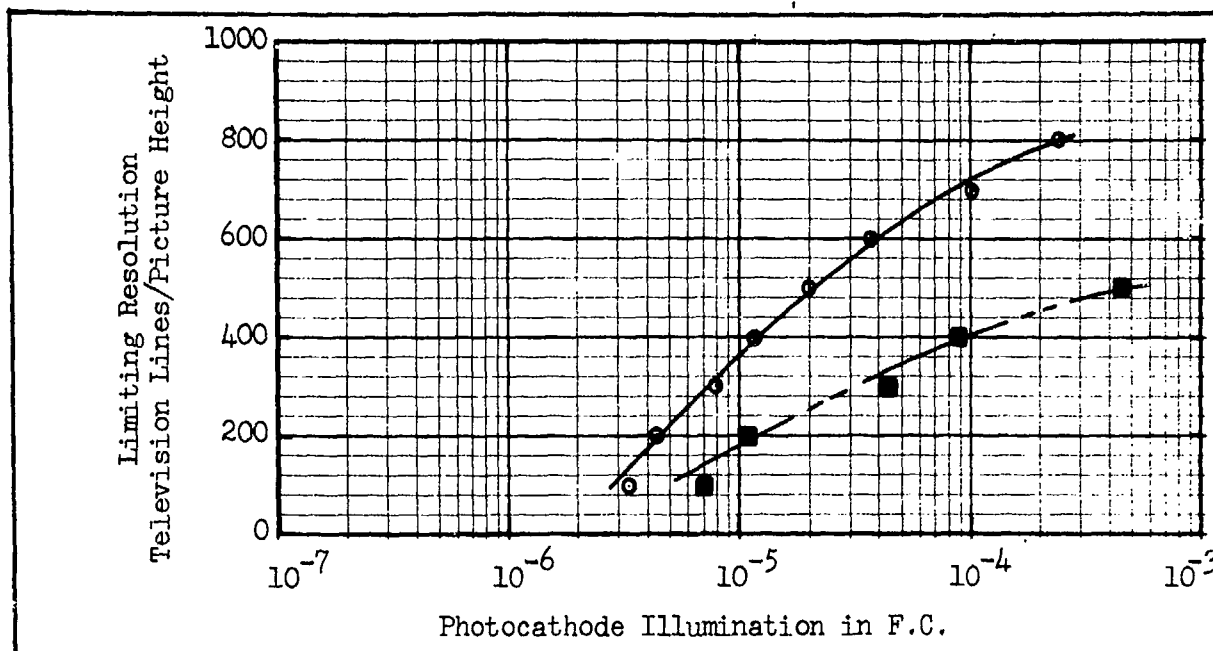
Fig. 143   Dynamic Sensitivity for 35% Contrast Pattern, V_T = 20 volts
o Static, ■ 10 Sec/P.W., Bandwidth 12 MHz

relative insensitivity of the amplitude response curves to the same rates
of image motion at identical target voltages.

Curves similar to those shown in Figs. 141 and 142 were generated
using 35% contrast patterns and are shown in Figs. 143 and 144. One image
speed was used, 10 seconds per picture width and the two target voltages
were used, 20 and 7.5 volts. With a low target lag (20 = V_T) the
amount of loss in sensitivity with motion is smaller for the 35% contrasts
case than that for a 100% contrast whereas for a high target lag (7.5 =
V_T) the amount of loss in sensitivity with motion is larger for 35% contrast
than that for a 100% contrast.

5.5   Discussion of Results

In the preceding measurements no attempt was made to separate
from the dynamic imaging process the influence of first scan readout.

218
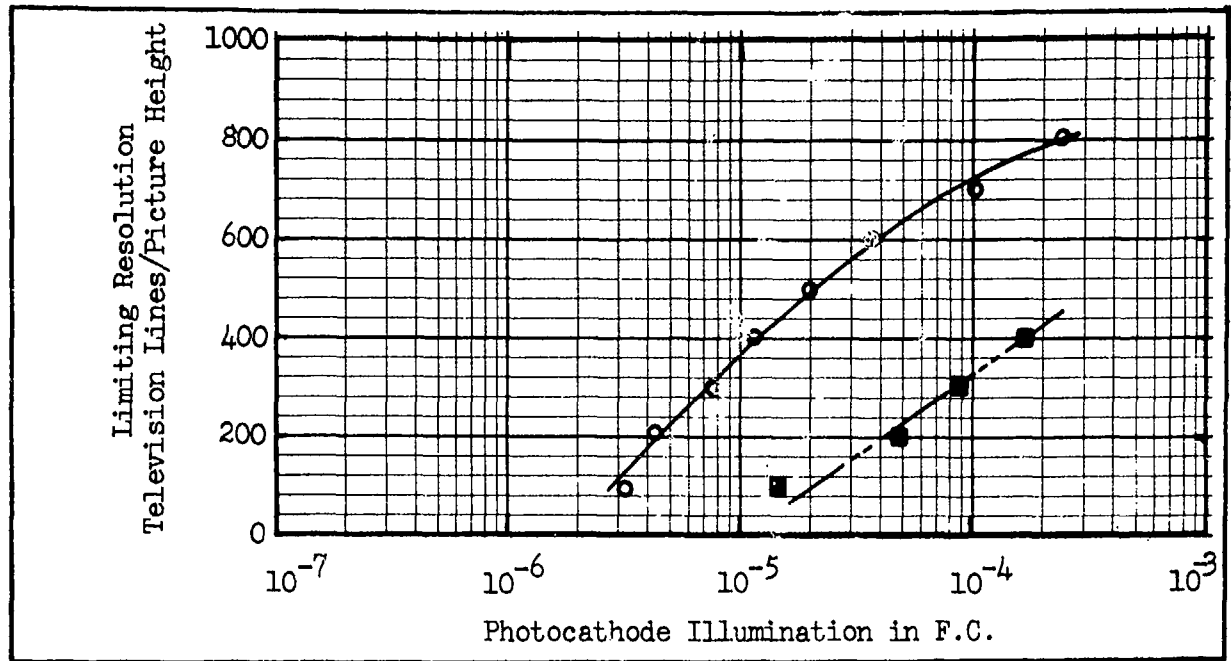
Fig. 144   Dynamic Sensitivity for 35% Contrast Pattern $V_T = 7.5$ volts
           O Static, ■ 10 Sec/P.W., Bandwidth 12 MHz

Performance degradation due to this effect is believed to be small as a

consequence of the high storage capacity of the silicon diode array

target. The diode depletion region depth is small, about 5 microns, and

the silicon dielectric constant high. The remaining factors leading

to degradation are signal mixing and lag.

        The influence of signal mixing is apparent from Figs. 138, 139,

and 140 where this contribution to degradation of performance is seen to

be very significant. In fact, the amplitude response data indicates

that for the lag obtained with a target voltage of 20 volts (i.e., buildup

lag about 83% and decay lag about 17%) the signal mixing effect is

severe and predominates at high line numbers. Lag figures such as these

indicate a target readout characteristic considerably different from that

of an ideal device. In spite of this, the effect of lag has not dis-

astrously affect the dynamic MTF of the tube. For the case of a 7.5 volt target bias where the buildup lag is about 52% and the decay lag 43% marked degradation beyond the effect of signal mixing is apparent.

The dynamic amplitude response curves obtained for an image motion of 10 sec per picture width exhibit a relatively flat tail between about 400 and 600 TVL per raster height. The existence of this very marked tail is a consequence of the influence of signal mixing. For the resolution line number of 450 TVL per raster height the response due to signal mixing falls to zero and for higher line numbers again increases. This is the region of negative contrast indicated on Fig. 128.

The dynamic sensitivity measurements in which the limiting resolution dependence on illumination was determined with image motion rate and lag (i.e., target voltage) as parameters show that for high lag the sensitivity is degraded by about a factor of 15 at 100 TVL per raster height while for low lag the loss of sensitivity is only a factor of about 6. These degradation values relate static performance with image motion at 5 sec per picture width.

At the very slow image motion rate of 60 seconds per picture a surprising loss in sensitivity is observed for even the low lag of approximately 80% buildup and 20% decay (i.e., $V_T = 20$ v). Examination of the corresponding amplitude response for 100 TVL does not immediately offer any direct clue concerning the cause of this effect.

One may assume that the integration period of the eye must be considered. Since this may be as high as 0.1 second serious signal mixing within the eye may occur. On the other hand if the eye automatically adjusts itself so that the image remains stationary on the retina no such

220

signal mixing occurs. In addition, in view of the fact that this observed effect is lag dependent, other causes must be sought.

For 60 seconds per picture width the modulation does not depart significantly at 100 TVL per raster height from 100% even for the high lag situation. For higher line numbers however, the MTF degradation does, at least in terms of percentage of the static value, indicate that some change in the video signal must be occurring even though the signal amplitude for 100 TVL does not decrease significantly. The effect that occurs is likely a distortion of the video signal with removal of sharp leading and trailing edges. Thus, if, for example, an observer focuses attention on the leading edge of a moving bar, the observer's ability to perceive the bar may be seriously impaired by any loss in edge sharpness.

Figs. 145 and 146 show a construction indicating the change in structure of a rectangular video profile to one with a slowly rising leading edge and slowly decaying trailing edge as a consequence of motion of a bar across the field-of-view. The particular patterns were developed for a rectangular bar corresponding in width to that of a 100 TVL per raster height bar and image motion at the rate of 60 seconds per picture width. Included in the construction were the effects of signal mixing and lag. Frames 1, 2 and 3 were calculated from the top configuration taking $\gamma = 0.75$ which corresponds roughly to a buildup lag of 80% and decay lag of 20%. The configurations shown in Fig. 146 were obtained as the 6th frame for a case in which $\gamma = 0.50$ which approximately corresponds to a buildup lag of 56% and decay lag of 44%.

The top configurations of Fig. 145 show the rectangular bar,

221
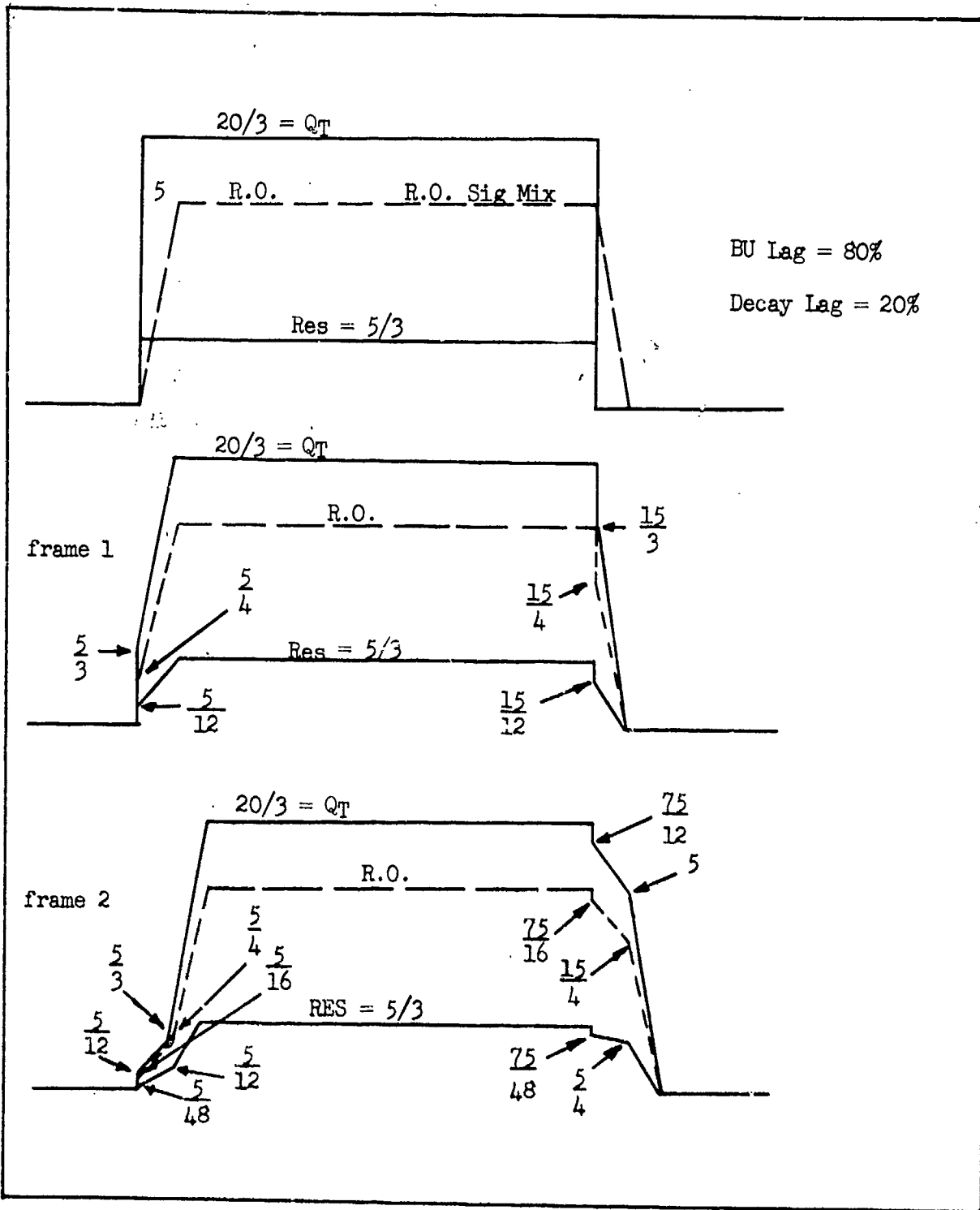
Fig. 145   Construction of Charge in Structure For Rectangular
Bar Corresponding to N = 100 for Motion of 60 Second/
Picture Width - Low Lag Case $\gamma = 3/4$
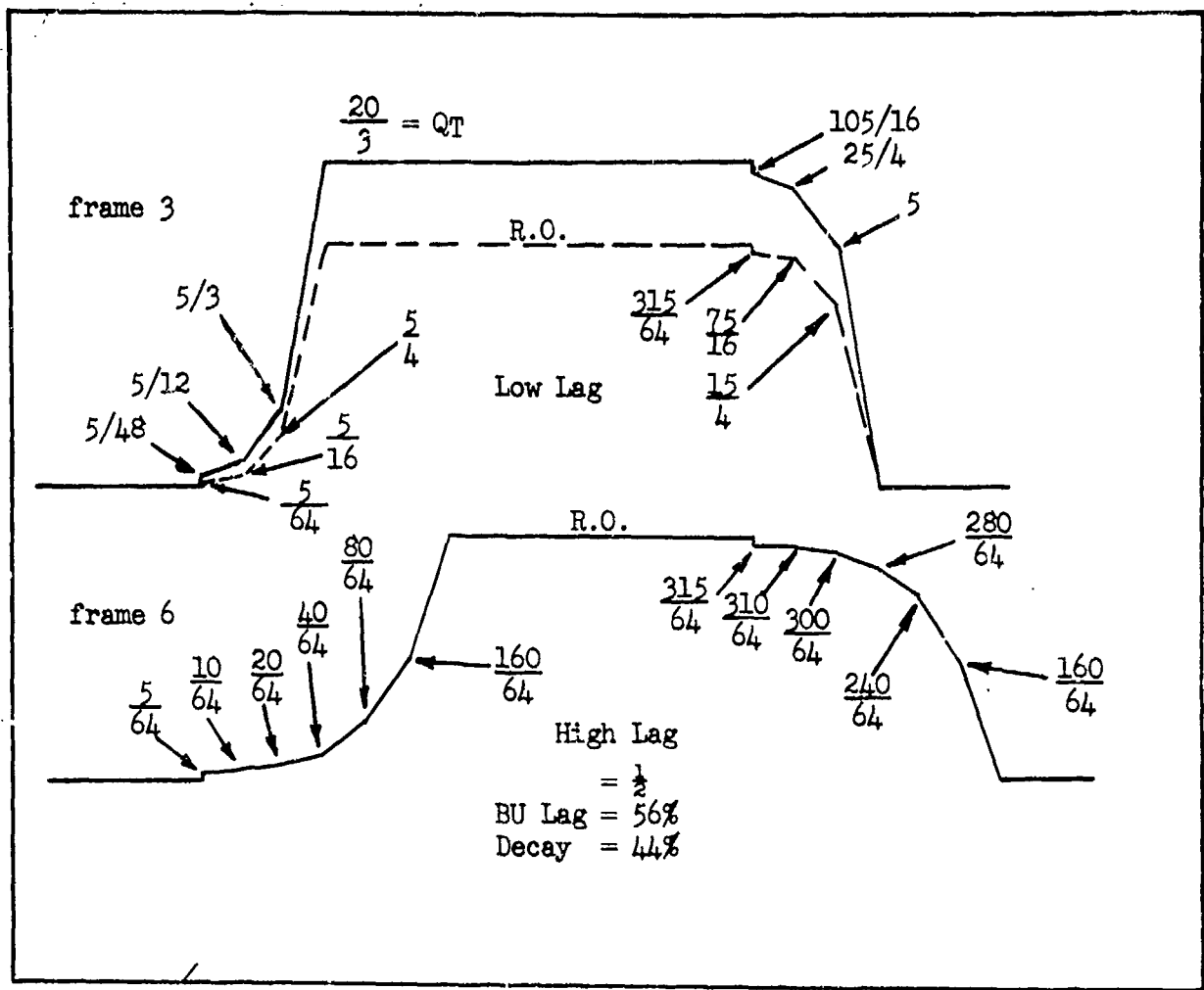
Fig. 146   Continuation of Construction of Charge in Structure for Rectangular Bar Corresponding to N = 100 for Motion of 60 Seconds/ Picture Width – Frame 3 Low Lag Case – Frame 6 – High Lag Case

during steady state, to have a total charge $Q_T = 20/3$. Readout is then

5 units (i.e., 20/3 x 0.75) leaving a residual charge indicated as

$R_{es} = 5/3$. If the chart were set in motion and signal mixing alone

occurred the broken line profile would occur. The configuration labeled

frame 1, Fig. 145, shows the configuration after 1 frame of motion

including buildup and decay lag along with signal mixing. For determining

the influence of lag, the broken line profile of frame 3 (i.e., low

lag), Fig. 146, should be compared with the profile indicated by frame 6

(i.e., high lag), Fig. 146. The reason for comparing two different frames

223

for the two cases arises from the fact that the trailing edges have both decayed to the same values, specifically indicated as 5/64 while the leading edges have risen to the same values 315/64. The magnitude of these values indicate that a steady state dynamic situation has approximately been achieved. For steady state to occur 3 frames are required for the low lag case and 6 for the high lag case with the indicated profiles resulting.

The construction indicated in Figs. 145 and 146 is readily carried out for broad bars and low rates of image motion. In principle, this method may be followed for high image motion rates and narrow bars although the procedure becomes extremely difficult and tedious. The process may be simplified however by considering the imaging of a bar pattern with a sinusoidal variation in illumination.

Assume a photoelectron current distribution due to an illuminated bar pattern falling on the photocathode to have the form

$$ J \; = \; 1 + \sin \frac{2\pi}{\lambda} \, (X - vt) $$

electrons per unit area per unit time. Here λ is the spatial wavelength of the bars. The bars are perpendicular to the position axis X. The rate of motion of the bars perpendicular to their length is given by their velocity v. The instantaneous time is given by t.

If one considers the charge readout process from the target to be characterized by a constant γ as previously discussed, the effects of signal mixing and lag may be incorporated into an expression describing the form of the video signal obtained from the target. Beginning with a situation in which the pattern is stationary and steady state prevailing, the signal readout charge to which the video signal is proportional is given

224

$$\gamma Q_{TN} = \gamma(1-\gamma)^{N-1} K + \sum_{n=1}^{N} \gamma(1-\gamma)^{n-1} T^{n-1}$$

$$+ \sum_{n=1}^{n=N} \gamma(1-\gamma)^{N-n} \frac{\lambda}{2\pi v} \cos \frac{2\pi}{\lambda}(x-vnT) - \cos \frac{2\pi}{\lambda} (x-v(n-1)T) \qquad (172)$$

where

Q_{TN} is the total charge after N frames

γ is the readout fraction

T is the frame period

λ is the spatial wavelength

x is the position coordinate

v is the velocity of motion of the image

$$K = (\frac{1-\gamma}{\gamma}) (1 + \sin \frac{2\pi X}{\lambda}) T$$

Using the above relations the spatial form of the target readout at a given time t may be determined. By choosing N sufficiently large a dynamic steady state condition may be examined. For smaller values of N the transient condition between initiation of the motion and the dynamic steady state is obtained.

If γ is taken as 1 the influence of signal mixing is obtained. If γ is other than unity its value, in part, determines the value of N for steady state. Thus, N should be chosen for steady state so that the

contribution from at least one term in the summation for which n is
sufficiently small may be neglected.

Due to computation errors this expression has not as yet been
completely evaluated. Development of the expression is indicated in
Appendix 3.

Preliminary data for evaluation of parameters influencing
dynamic imaging have been presented. These indicate as anticipated that
both signal mixing and buildup and decay lag influence dynamic imaging.
While both effects are degrading, the relative importance of them remains
to be more firmly established. The results suggest that for imaging of
bar patterns the signal amplitude for a given resolution line number is
not in itself sufficient for assessing the device performance. The entire
amplitude response curve must be considered. In addition to the amplitude,
the signal shape is of importance as this may influence the visual
perception capability of the observer.

The possibility of mathematically generating signal wave forms,
which include the effects of signal mixing and lag, for assessing
dynamic imaging performance have been indicated.

The material reported here is the result of an initial effort
toward investigation of the process of dynamic imaging. More extensive
experimentation is necessary, particularly with camera tubes employing a
variety of types of charge storage targets. The influence of the effect
of first scan readout on device performance which was not considered in
this preliminary study should be undertaken.

5.6   Some Comparative Dynamic Resolution Results

The above illustrates how important dynamic response characteristics

226
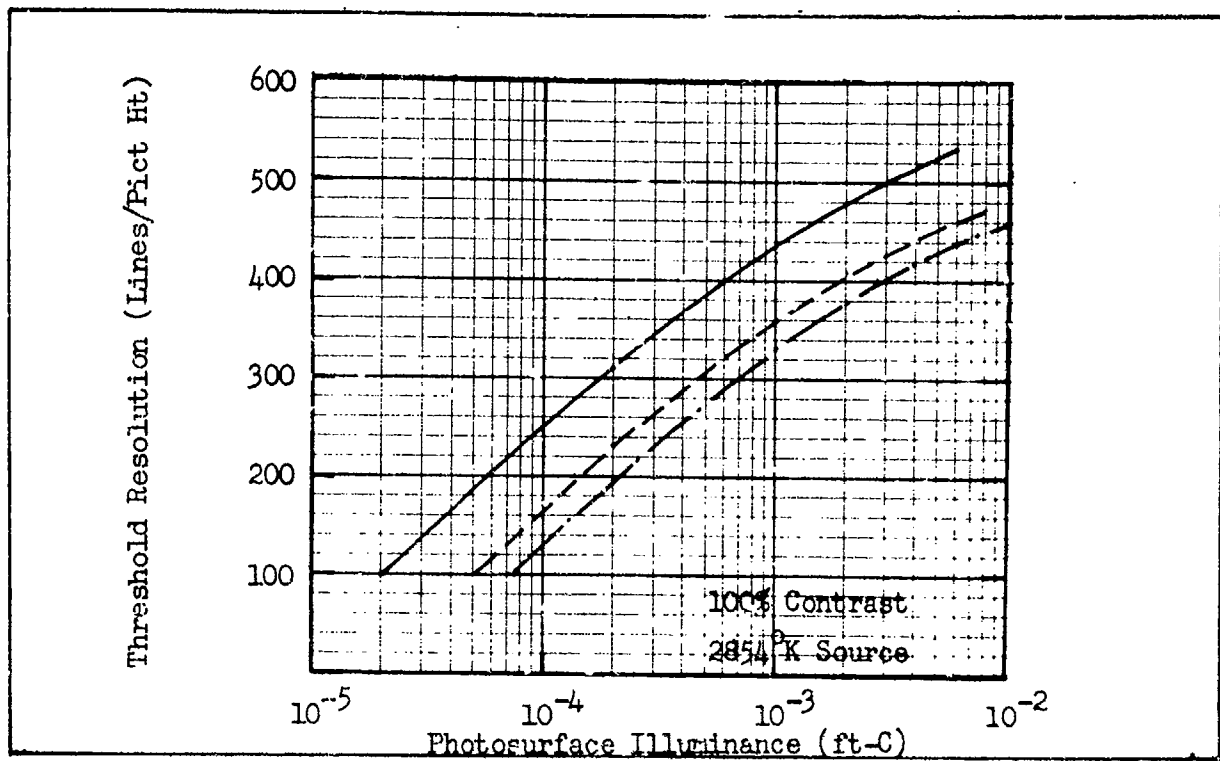
Fig. 147 Threshold Resolution vs Photosurface Illuminance for (———) Static
Bar Patterns and Patterns Moving at (— — —) 20 and (— · —) 10
seconds per Picture Width.   25 mm WX30691 SEC Camera. March 1968.

are. From the strong correlation between bar pattern resolution with tactical

image detection, recognition and identification we have that a system's

response to bar pattern motion should be a measure of system performance

under conditions which, to a varying degree, approximates actual

operational conditions. Unfortunately, very little dynamic resolution data

exists for the various cameras. In the following, some dynamic resolution

data is presented for the Secondary Electron Conduction, Electron Bombarded

Silicon, Image Isocon, and Intensifier Image Isocon cameras.

In Fig. 147, the dynamic resolution curves for the 25 mm

WX-30691 Secondary Electron Conduction camera are shown for image speeds

of 20 and 10 seconds per picture width for a 100% contrast pattern. The

loss in sensitivity, with image motion is nearly a constant for a given

amount of image motion. The average loss is a factor of about 4 for the 10

227
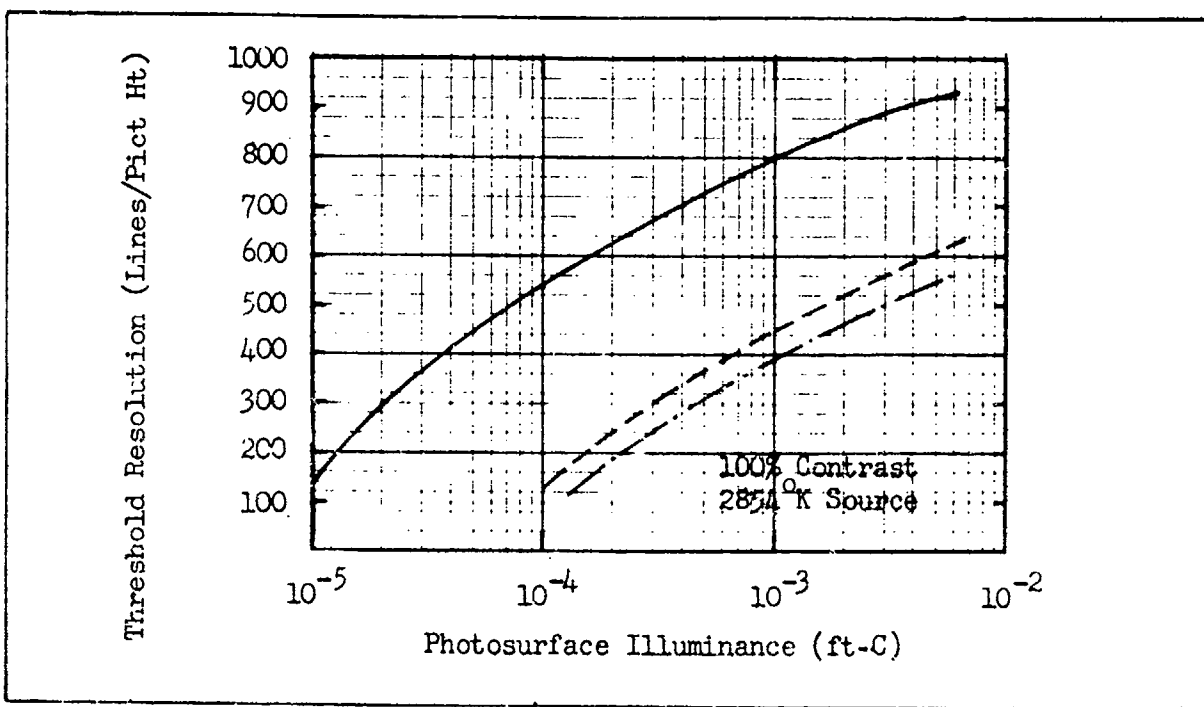
Fig. 148 Threshold Resolution vs Photosurface Illuminance for (———) Static
Bar Patterns and Patterns moving at (– – –) 25 and (— · —) 10
Seconds per Picture Width. RCA Data Sheet for 40 mm C21095C Image
Isocon, April 1970.

seconds per picture width and about 3 for the 20 seconds per picture width.

For the 40 mm C-21095C Image Isocon, the dynamic resolution
curves are as shown in Fig. 148. Again, the contrast of the pattern was
100%. The loss in sensitivity increases at the higher line numbers over
that at low line numbers, e.g., it is about 3 times larger at 600 lines
than at 150 lines. The average values of the loss in sensitivity are 30
and 18 for motion rates of 10 and 20 sec per picture width respectively.
Comparing the same resolution ranges for the Secondary Electron Conduction
and the Image Isocon, it is seen that the Image Isocon loses 5 times more
in sensitivity than the Secondary Electron Conduction camera. The results
for the intensifier version of the Image Isocon are shown in Fig. 149 with
a 40 mm intensifier added to the C-21095C Image Isocon. A comparison of
the curves for the Image Isocon and the Intensifier Image Isocon shows that

228
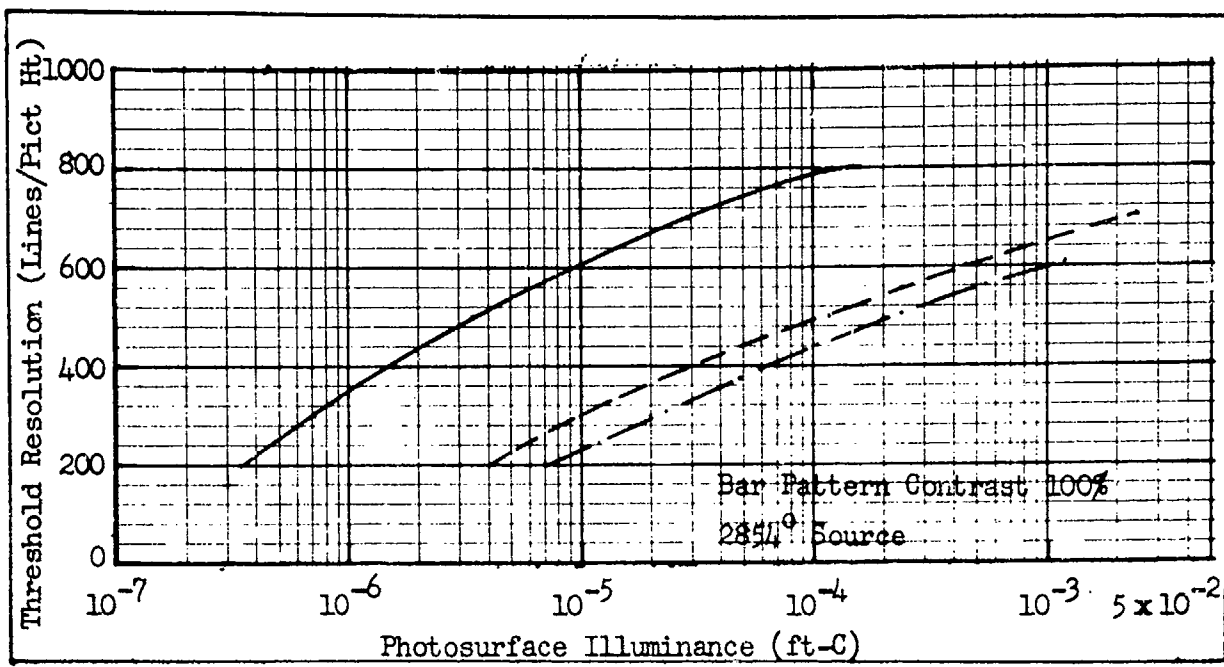
Fig. 149 Threshold Resolution vs Photosurface Illuminance for the 40 mm
Intensifier Image Isocon Type C21095C with (———) Static Bar
Patterns and Patterns Moving at 20 and 10 Seconds per Picture Width.
Naval Air Development Command Data of March 1970.

the addition of the intensifier does shift the dynamic resolution curves

for the Intensifier Image Isocon to approximately the same position as

that for the static Secondary Electron Conduction camera case.

In Fig. 150 the dynamic resolution curves for an Intensifier

Image Isocon with a 25% contrast pattern is shown. The larger line

numbers correspond to a larger loss in sensitivity. The average loss

in sensitivity is less, by a factor of 2, than that for the 100% contrast

pattern.

In Fig. 151, the 10 sec per picture width curve is shown, with

the static curve, with a 100% contrast pattern for the 40 mm WX-31911

Electron Bombarded Silicon camera. Comparing the same resolution range, we

229
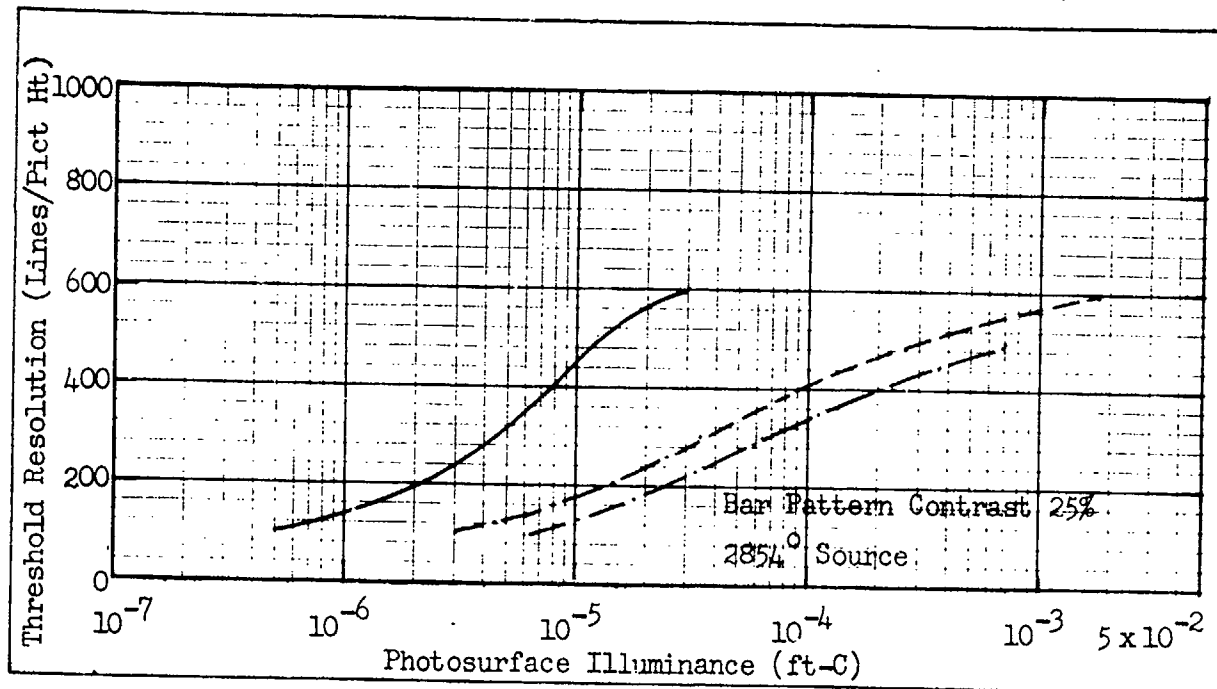
Fig. 150 Threshold Resolution vs Photosurface Illuminance for the 40 mm
Intensifier Image Isocon Type C21095C with (———) Static Bar
Patterns and Patterns Moving at 20 and 10 Seconds per Picture
Width. Naval Air Development Command Data of March 1970.
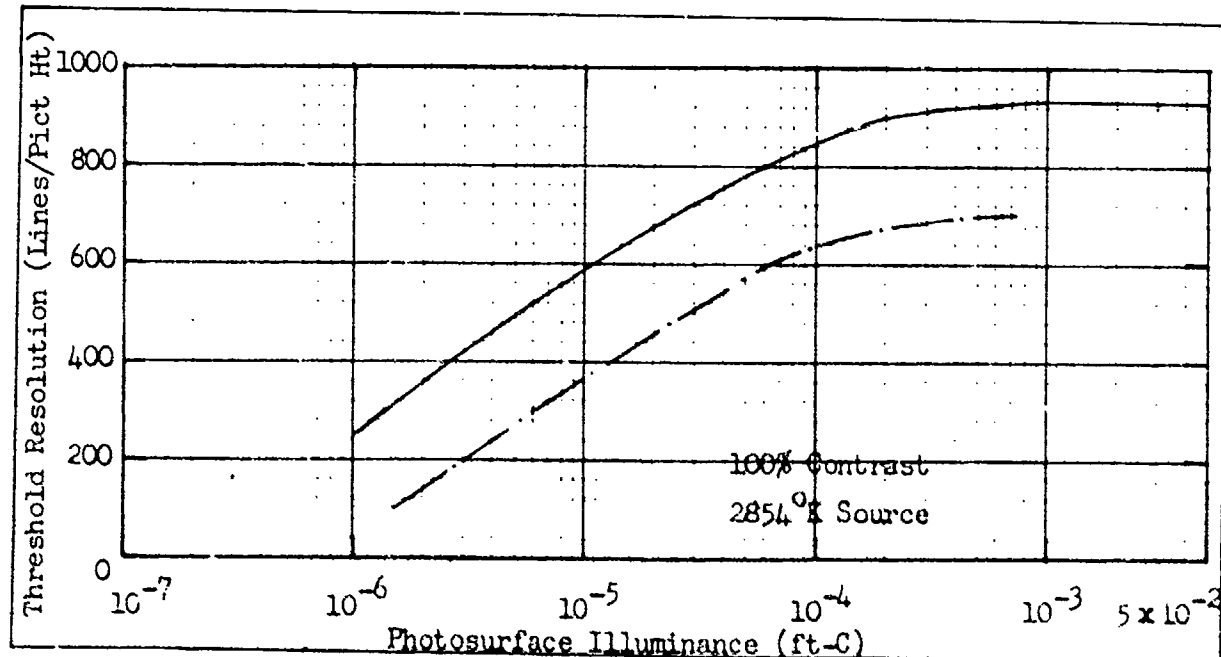
Fig. 151 Threshold Resolution vs Photosurface Illuminance for (———) Static
Bar Patterns and Patterns Moving at (— · —) 10 Seconds per
Picture Width. Westinghouse ETD Data of September 1971 for
the 40 mm WX 31911 Electron Bombarded Silicon Camera.

have that the Electron Bombarded Silicon camera exhibits a similar loss in resolution as the Secondary Electron Conduction camera but slightly higher (20%). A comparison of the corresponding curves for the Image Isocon shows that the Electron Bombarded Silicon camera is nearly a factor of 10 more sensitive for dynamic imaging at rates of 10 sec per picture width than is the Image Isocon.

In Fig. 152, NADC measurements for the 40/25 I-EBS camera with a 100% and 10% contrast pattern, for static, 25 and 10 seconds per picture width are shown. In Fig. 153, the corresponding curves are shown for a 25% contrast pattern. These were also measured by NADC.
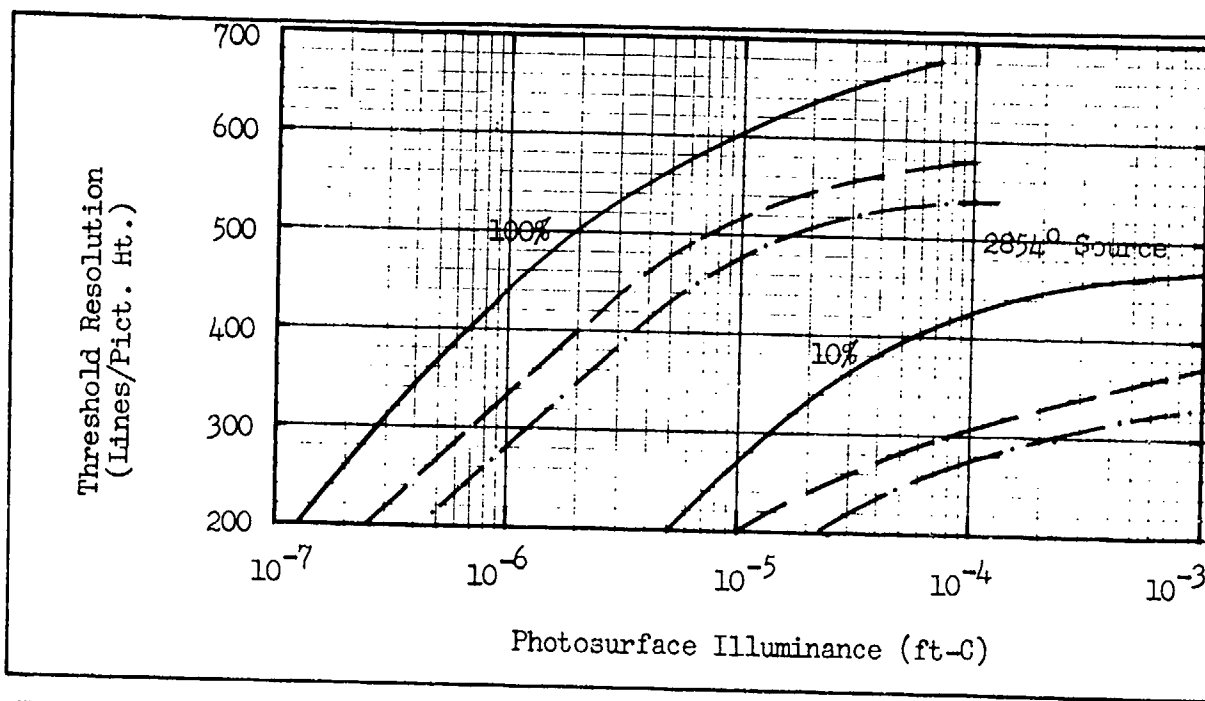
Fig. 152 Threshold Resolution vs Photosurface Illuminance for the 40/25 I-EBS Camera with 20 mm Target for Bar Pattern Motions of (———) 0, (— —) 25, (— · —) 10 Seconds per Picture Width. NADC Measurements – Curves on Left 100%, on Right 10% Contrast Patterns.
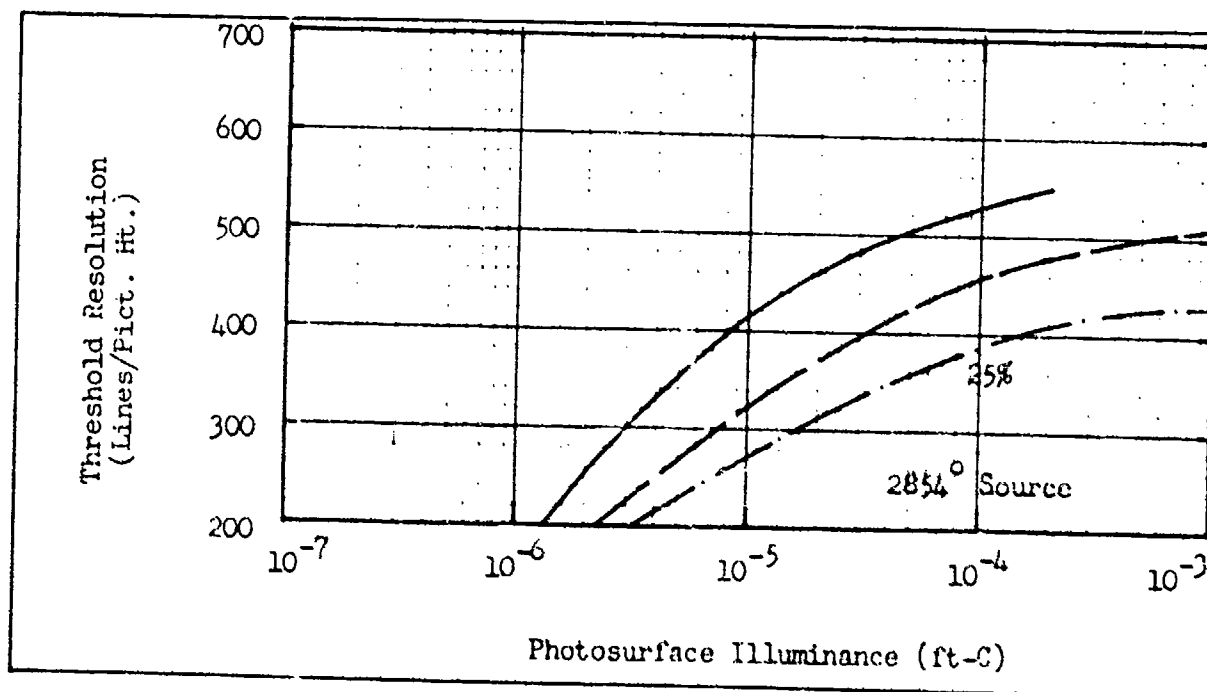
Fig. 153 Threshold Resolution vs Photosurface Illuminance for the 40/25 I-EBS Camera with 20 mm Target for Bar Pattern Motions of (———) 0, (— —) 25, (— · —) 10 Seconds per Picture Width. NADC Measurements – 25% Contrast Pattern.

6.0 System Performance Specifications

The purpose of this performance synthesis program is to develop analytical models for predicting the performance of observers augmented by electro-optical equipments in the visual tasks of detecting, recognizing and identifying scene objects at long range. Though considerable effort remains in the quest for more accurate models, the inroads made to the general problem are also considerable both in terms of developing and applying models and in gaining general acceptance for their use throughout the government and industry. We consider the gaining of general acceptance of the models to be of foremost importance since they may then be used in system procurement specifications.

By specifications, we do not mean physical details of the equipment such as the finish of parts, their vulnerability to fungus, the quality of construction, or the like. Though these features are important to the final product utilization, the concern here is with providing the procuring agency with some assurance that the equipment being proposed for a given mission will have some reasonable expectation of actually meeting the mission requirement.

Before beginning, we observe that human observers, of statistically varying capabilities, interests and motivations, are integral parts of electro-optical imaging systems and hence, it follows that performance predictions will also be statistical in nature. Thus, any system performance specification must be accompanied by some statement regarding the level of probability desired.

6.1 Specification Probelm Areas

It is presumed that most military electro-optical systems are

233

procured with some intended end purpose in mind. Ordinarily, the end purpose is to enable an observer to detect, recognize or identify a class of targets at a useful range and, for the purposes of specification, a few targets can be readily singled out as being representative. However, the main specification problem area comes in defining the target and scene parameters. Too often, the target is specified to be of low contrast, of low reflectivity, in near total darkness and at long range through an atmosphere of poor visibility. These parameters, taken in combination become impossible to meet with a system of reasonable size and complexity. Faced with unreasonable requirements, the designer can, however, exercise some options which tend to offset the unduly strict requirements by selecting the most favorable contrast definition of the many available, neglecting such factors as sky-to-ground luminance ratio in the atmospheric model, neglect image motion effects, adopt the easiest detection criteria and neglect certain MTF's such as those associated with the display or the observer's eye. By these means, and others, a system design, on paper may approach the specified goal. This manner of cancelling the effects of an unrealistic requirement may nevertheless result in a realistic and useful system but the practice is to be deplored because it is first of all unethical, and secondly, because the comparing of various system proposals becomes all but impossible — particularly if the definitions used are not carefully documented.

In many other cases, the sensor parameters rather than the mission requirements are specified. Again, a variety of definition problems are encountered. One of the most usual is to confuse the contrast transfer function or CTF with the modulation transfer function or MTF. The former

234

is much more optimistic. Some sensors such as the image orthicon have MTF's which are light level dependent but no note is made of it. It is also not uncommon to see MTF quoted including electronic aperture correction.

While the picture painted above may be overly black, there are both intentional and unintentional abuses in the specification game. Many of these could be eliminated by creating specification standards and definitions. In the following, a number of scene and system parameters will be discussed with a view toward pointing out problem areas. In certain instances, definitions will be proposed. The need for standards in certain areas will be highlighted. However, the discussion below represents only beginning effort which needs considerable refinement.

6.2 Scene Parameters

As we discussed in Section 2, scenes and objects in them can assume infinite variety depending on the type of scene irradiance, its directivity, the atmospheric condition, the foreground, etc. For passive TV sensors, it is recommended that the scene irradiance be considered diffuse so that the general contrast models developed by Middleton [Eqs. (8-13)] can be used. Particular attention should be paid to the air-to-ground imaging case for which the curves of Fig. 6 are drawn. These curves are a function of the ratio of sky to ground radiance. Many designers use the curve for $S_K/G_D = 1$, which is usually quite optimistic. With sensors limited to the near infrared band, where reflectivity differences are generally higher, values for S_K/G_D of 2 to 4 might be more appropriate.

The reflectivity of the object and its background can be specular or diffuse or combinations thereof. In general, the diffuse case is more

235

commonly encountered. Scene reflectivities, particularly in the near infrared, tend to be quite high — nearer 50% than the 10% usually specified but again, considerable variation can be encountered. Reflectivity differences, leading to contrast differences are also usually higher than the 10% values often specified. This is particularly true of active systems where man-made objects tend to stand out in strong relief against their backgrounds. Ships, for example, appear nearly white against a black background. We note in this regard that we speak of an inherent object contrast as if the contrast were a fundamental property of the object. This is not the case. Object contrast will usually be a continuous function of the viewing angle, the directivity and direction of the scene irradiators, and the properties of the foreground and the background. For example, the contrast of a ship imaged against the horizon sky is much different than its contrast when viewed straight down. Image contrast is also not numerically equal to the differential reflectivity of the object and its background except in very special cases as is extensively discussed by Middleton[4]. For calculation purposes, it will probably be necessary to assume the object-to-background contrast has some near constant value but its continuously varying nature will lead to considerable apparent errors when efforts are made to correlate predicted and measured results.

It has been said that there are at least 14 different definitions of contrast. The isolated image contrast definition of Eq. (1) has, perhaps, been the most widely used but we are recommending the use of Eq. (2) since it leads to analytical simplicity because the use of Eq. (1) leads to the inclusion of contrast in the sensor noise expression. Note in Fig. 2, that at low contrasts, the isolated image contrast, C_I, is nearly twice as

236

large (in magnitude) as C_M, the modulation contrast.

The atmospheric extinction coefficients for the visible spectrum is tabulated in Fig. 3 and is in general use. As we noted in Section 2, the extinction coefficient is a function of wavelength. To show this dependence, we have elected to use the Steingold and Strauch expression of Eq. 20. Alternative curves are given in the RCA Electro-Optics Handbook, SCN 102-67. The RCA curves are somewhat more pessimistic. We have no strong feelings about either approach. The extinction coefficient is also a function of altitude as noted either by the slant range approach of Eq. (6) or by the correction factor approach of Fig. 4. Since the correction factor approach is easier to use, we tentatively recommend it for the near term at least.

Object radiation can also be modulated both temporarily and spatially by the atmosphere -- primarily due to thermal refraction effects. We have not studied these effects with sufficient detail to include them in our models. With the current increase in interest in high resolution systems, these effects become ever more important and more effort in this area is recommended.

Range-gated-active sensors are also becoming of increased importance because of their ability to increase scene lighting levels, reduce atmospheric contrast degradation and increase the contrast of man-made objects. The analysis of scene parameters should be much more straightforward for active sensors since the source location and the directivity are known. A start has been made in this area in Section 2 but much more can be done. In the passive system case, the scene can take on near infinite variety and defining a small group of typical imaging

237

situations becomes near impossible. For active sensor, we should be able to define a standard set of typical scenes.

The scene object is characterized by dimensions. However, the dimensions of interest are not necessarily the object's overall length and width but rather, some more elemental area such as is suggested by the "equivalent bar pattern" approach wherein the object is replaced by a bar pattern with bar widths equal to the vehicle's minimum dimension divided by k_d, the level of discrimination factor. The equivalent bar pattern approach is shown schematically in Figs. 20 and 44, and the level of discrimination factor may be inferred from Fig. 45.

The current range gated active systems employ a monochromatic source whose wavelength is precisely known. If the scene reflectivity and geometric factors are known, then the differential radiance can presumably be specified in radiometric form. For naturally lighted scenes, it has been customary to use luminous measures of the light level in spite of the fact that the visible is entirely filtered out. This practice can lead to substantial errors as will be discussed below.

6.3 Sensor Parameters

For the purpose of discussion, we will define the sensor to consist of the lens and photosurface only. The various first order lens parameters have been discussed at some length in Section 2.6. One of the most important lens parameters is its MTF, particularly for long focal length lenses. The MTF of any aperture whether it is a lens, a target or an electron beam is quite often confused with its contrast transfer function or CTF. The CTF is synonymous with the square wave amplitude response which can be substantially higher than the MTF as shown in Fig. 42.

238

The problem with CTF as a descriptor is that it cannot be multiplied by other system MTF's to obtain the overall system MTF. Neither can the CTF be used to obtain the square wave flux response, $R_{SF}(N)$.

The primary merit of the CTF is that it is easy to measure because bar test patterns are easier to construct than sine wave test patterns. The CTF is not a well behaved analytical function, however, and the MTF cannot be obtained from the CTF directly. When only CTF is provided, the only recourse to finding the MTF is to use the approximate technique developed by John Coltman and reported in JOSA in Vol. 44, No. 6, June 1954.

The lens MTF should be reported at the center of its field of view, half way between the center and edge and at the edges. It should be clearly stated that the MTF rather than the CTF is reported to avoid confusion. Also, the relative focal plane irradiance should be given as a function of the angle off-axis.

The photosurface sensitivity has been reported in many ways. The most desirable from a systems viewpoint is a spectral response vs wavelength curve such as is shown in Fig. 18. The curves of Fig. 18 are only appropriate for photosurfaces which have unity gamma. For surfaces such as the vidicon which have gammas which are approximately constant, the specific responsivity curves obtained as discussed in Ref. 2, Section XII.

In many cases, it is desired to characterize the sensitivity of photosurfaces by a single number. For photosurfaces which are sensitive in the visible and near infrared, it has been customary to use a quantity "microamperes per lumen" measured using a tungsten bulb operated at 2654° K. This is not an unreasonable quantity when the photosurface has a response

239

tailo. ed to match the spectral response of the eye and where the scene illuminance is mainly tungsten as is often the case in commercial television broadcast studios. It can be very misleading in military usage. For example, one tube could have a specific luminous response of 200 μa/lumen but have its response only in the near infrared, while another tube has the same luminous response but span both the visible and near infrared. For military reconnaissance, the former tube would be much more valuable most of the time.

One alternate solution proposed is to convert luminous response to radiant response by noting that a tungsten bulb generates 20 lumens/watt and that there is 10^{-3} mA/μa. Thus, 200 μa/lumen corresponds to 4 mW/W. But this is merely exchanging one number for another. A more appropriate method would be to give the average response over a given wavelength interval. The S-20VR of Fig. 18, has an average response of about 30-40 mA/W in the 0.7 to 0.9 micron spectral interval while its response to $\approx 2854^\circ$ K light is only 6-8 ma/W. As we indicated in Section 2.11, the radiometric sensitivity of the S-25 photosurface to a combination of moonlight and airglow is approximately 23.4 mA/Watt when the entire spectral bandwidth is used.

No single standard can be proposed because the desired standard will be a function of the application. For example, if the sensor is to be used only in conjunction with a 0.86 micron scene irradiator, only sensitivity at 0.86 micron is of interest. On the other hand, a number of spectral bands appropriate to various reconnaissance tasks can be defined and the manufacturer can be required to provide average sensitivities within these bands.

It should also be noted that the MTF of both the lens and the photosurface can be wavelength dependent. Thus, if the spectral bandpass of the system is to be restricted, the MTF should be specified and measured in the restricted wavelength band.

6.4 Signal Processor Parameters

Ordinarily, the signal processor represents all those elements within the sensory system following the input photocathode but preceding the display phosphor but in some either the photosurface or the display or both may be included when discussing certain signal processor parameters. The primary function of the signal processor is to transmit the image from the photosurface to the display and to amplify and magnify the image as necessary so that the output displayed images can be easily and comfortably viewed by an observer.

One function, which combines the parameters of the photosurface and a portion of the signal processor is the light transfer characteristic which is a plot of the signal output of a TV camera tube vs its photosurface irradiance or illuminance as shown in Fig. 53. Often, when the input photosurface is linear, a single point on the signal transfer curve is given. For example, with a 16 mm SEBIR, a number such as 1 mA/W/m^2 or 500 μa/ft-candle might be given. While this single number serves to define the light transfer characteristic, neither the curve nor any number on it can be used to specify the camera tube's sensitivity as is often done. This is improper because the camera tube's signal current is the product of the photosurface sensitivity, photosurface area, prestorage signal current gain, the gains of any internal electron multiplier and the inverse of the readout scan efficiency and these quantities are not interchangeable in the signal-to-

241

noise ratio expression.

For example, an image signal-to-noise ratio is established by the photosurface which inherently limits its detectability. The more sensitive the photosurface, the higher this signal-to-noise ratio will be. The prestorage signal current gain, usually associated with the camera tube's target, amplifies the image signals and noises alike. Thus, a high prestorage gain cannot compensate for a low photosurface conversion efficiency. A high prestorage gain is, however, desirable for two reasons. First, it is used to bring the signal and noise levels up to a point where the preamp noise added in the next step of signal processing becomes less of a factor. This preamp noise may be added either in the input of the first dynode of an internal preamp or in the input resistor of a preamp external to the camera tube. Secondly, a high prestorage signal gain is desired because it tends to reduce the sensor time constant. Again it should be clear that prestorage gain and internal preamp gain is not interchangeable nor is the internal preamp noise interchangeable with photoconversion efficiency. The scan efficiency is a form of prestorage signal current gain but not quite because a low scan efficiency (high gain) results in a need for an increased video bandwidth which can impact on preamp noise. The motivation for characterizing camera tube sensitivity by a single number on the light transfer curve is a simple one -- fewer reject tubes and simpler acceptance testing.

It is therefore recommended that any sensor specification call out the minimum photosurface sensitivity and internal sensor gains separately. It must, of course, be realized that acceptance on the basis of the individual photosurface and gain parameters may increase the rejection

242

rate and costs in turn unless reasonable minimums are set for these quantities. Since the light transfer characteristic has no fixed relationship to the sensor's sensitivity, it is a very poor way to compare tubes of different types. The signal transfer curves of tubes containing internal preamplifiers should never be plotted on the same curve as tubes which do not. Specifically, the light transfer curves of image orthicons or image isocons should not be plotted together with tubes such as the SEBIR or SEC camera tubes. It is, however, acceptable to plot comparative curves of video signal-to-noise ratios (properly compensated for equal video bandwidth) as a function of photosurface irradiance level.

We have observed that the photoconversion efficiency and the various internal sensor gains are not interchangeable quantities. There may be a number of MTF's in a sensory system and while the overall sensory system MTF is a product of the individual MTF's, the individual MTF's are not interchangeable with respect to their location.

To illustrate the effect of MTF location consider the case of a sensor with two principal MTF's and two principal noise sources. Let the two MTF's be that of the lens and the target as was the case in Section 2.9 and let the noises be the photoelectron noise and the preamp noise. Consider first, a periodic image input. In this case, the signal modulation is reduced by the combined effect of the lens and target MTF's. The photoelectron noise is generated after the lens but before the target. Thus, the photoelectron noise is unaltered by the lens but filtered by the target. The preamp noise which is inserted after the lens and target is unaffected by either MTF.

For isolated aperiodic images, the lens and target MTF's have
no effect on signal except to distort the image. The lens MTF increases
the observed photoelectron and preamp noise but filters neither. The target
MTF filters the photoelectron noise while increasing the observed preamp
noise. The point of the above discussion is that the location of the MTF's
relative to the points of noise insertion does matter. Sensor and sensory
system manufacturers should be required to detail the MTF locations, all
noise sources and their points of insertion.

Before continuing, we note that it is usual to assume that
apertures such as the lens are assumed to be linear components, i.e.,
that their response to several stimuli acting simultaneously is identical
to the sum of the responses that each of the component stimuli would
produce individually. In practice, imaging systems are seldom linear over
their entire object field but it is usually possible to divide the object
field into small regions called isoplanatic patches over which the system
is approximately linear. If a system aperture is linear, or nearly so,
then an MTF can be defined and the MTF will have three properties. First,
it will have a value of unity at zero spatial frequency. Secondly, its
value at any other spatial frequency will be less than its value at zero
frequency, i.e., smaller than 1. Thirdly, the MTF will be symmetrical
about zero frequency although it is customary to plot only the positive
frequency position. Sometimes, functions are plotted which have values
greater than unity but are called MTF's. While the definition of MTF might
be extended to include these functions, the apertures that they represent
are not linear and this fact should be noted. The super response of the
image orthicon noted when the tube is operated above the "knee" of its

244

light transfer characteristic is an example of a non-linear response. The "MTF" of a non-linear aperture cannot be multiplied by the MTF of some other aperture to obtain the overall MTF.

We have noted that the positions of the internal sensor gain elements are important. In particular, we noted a desire for high gain before readout by the electron beam and prior to the insertion of preamp noise. This is the case when imaging at very low light levels, but as scene light level is increased, the reverse may be true, i. e., gain before readout should be reduced to a minimum. This apparent anomalty results from the following reasoning. Under very low light levels, maximum gain is desired to achieve the photoelectron-noise-limited condition. As the light level increases, a point will be reached where the scene high-lights saturate the camera tube. At this point, it will be found that the maximum video signal-to-noise ratio obtained at low spatial frequencies is about 10 or 20:1. With further increase in light level, the system operator has three options. He can reduce the lens iris opening, decrease sensor exposure time, or he can reduce sensor gain. With a poor lens, he may elect to reduce the iris opening somewhat in order to improve the lens' MTF. The low frequency video SNR remains limited to 10 or 20:1 as before but high frequency SNR may be improved somewhat due to the MTF improvement.

With a good lens, or after the lens opening has been reduced enough to gain an MTF improvement, the proper procedure with further light level increase is to reduce sensor gain by an amount sufficient to keep the scene highlights just below the camera tube saturation level. When this is done, the signal-to-photoelectron noise ratio keeps increasing but eventually as gain is sufficiently reduced, the preamp noise becomes a factor.

Nevertheless, the low spatial frequency video SNR improves and may become as high as 100 to 300:1. The high spatial frequency video SNR also improves proportionately. In no case should the exposure gating be used until the sensor gain has been reduced to its minimum. The gain reduction is usually obtained by reducing the voltage across the intensifier, if used, and the voltage across the image section. There is a limit to the gain reduction which may be obtained because the electron image may tend to rotate or lose focus. In certain cameras, such as those employing vidicons, no gain reduction options are available.*

When a gain control option is available within a sensor, the system's designer should specify the sequence he will employ in controlling the overall light level and to show that the control sequence is such as to optimize picture quality.

It is quite common to provide aperture correcting networks within a camera tube. At very high light levels, such aperture correction networks have been shown to be effective in sharpening image detail and may enhance object recognizability or identifiability; at low light levels, the reverse has been true in the past although some of the newer high gain sensors such as the SEBIR camera tube should, and do, benefit somewhat from corrective networks.

The effect of most finite sensor apertures is to reduce the amplitude of high spatial frequency signals. The purpose of an aperture

---

* Although it may be desirable to decrease target voltage in order to reduce dark current.

246

correction circuit is to restore these signal amplitude losses by means of
an amplifier whose gain increases with increase in spatial frequency. While
such correcting circuits can be readily constructed, they may or may not be
effective in increasing SNR. When an aperture, or OTF, precedes a point of
noise insertion, a corrective network following the point of noise insertion
will increase both signal and noise alike. For sensors in which the pre-
amp noise is a substantial factor, the effect of the correcting network
is usually deleterious because the preamp noise itself is an increasing
function of frequency. In the case of an intensifier-SEBIR camera, the
gain is so high prior to the insertion of preamp noise that the preamp
noise can be neglected. The photoelectron noise is inserted prior to the
MTF of the phosphor of the intensifier or the MTF of the SEBIR target.
Aperture correction of these MTF's should be effective since signal is
increased at a faster rate than the noise. The most effective aperture
correction can be obtained when the correcting network precedes the MTF.
For example, a display MTF can be corrected in the video amplifier without
addition of noise unless the noise of sources prior to the aperture corrector
become adversely affected.

The main point is that aperture correction may or may not be of
bene.it depending on the location of the corrector relative to noise
sources and the nature of the noise. When an aperture corrector is included
in a system design, the proposer should be prepared to show its probable
effectiveness.

Sensor time constants are very important system parameters but
are ignored in most system analyses including the work discussed herein.
The reason for this neglect is the poor understanding of the processes

247

involved and the lack of a good analytical model. Several measures of sensor time constant are in current vogue. One is the discharge time constant which is measured by illuminating an area on the photosurface until steady state is achieved. Then, the illumination is suddenly cut off and the current in the previously illuminated area is monitored on successive readouts. The reported measure is the percentage of current remaining in the third field. While discharge time constant is important, the signal buildup time must be given equal weight. Unfortunately signal buildup times are seldom reported. The main problem with either signal buildup or discharge measures is that methods of using them in system range prediction have not been developed. Only qualitative statements have been made such as the lag on 3 field should be less than 5% or 10% at the average photosurface light level of interest.

A third measure is the dynamic resolution vs photosurface irradiance characteristic. This measure is considered the best of the lot at the moment although the methods of using this characteristic have not been developed either. Typical dynamic resolution vs photosurface illuminance curves are shown in Figs. 150 and 151. It is seen that a factor of 4 to about 80 in apparent sensitivity can be lost due to even very slow image motions. It was also shown in Section 5 that motions of the order to be troublesome are the rule rather than the exception in airborne imaging environments.

The surprising feature of the results shown in Figs. 150 and 151 is that so much sensitivity is lost at low line numbers. With a bar pattern of 100 lines per picture width, a pattern velocity rate of only 20 sec per picture width results in a large sensitivity loss, yet, each bar in the

pattern moves only a small fraction of a line width between successive readouts. It was also noted that the signal amplitudes did not seem to decrease enough to account for the very significant apparent sensitivity loss. The motion aspects of sensitivity loss obviously require more study and it is planned to emphasize the study of motion in the follow-on effort. In the interim, it is recommended that manufacturers depreciate the sensitivity of their cameras by an amount equal to the shift of the limiting resolution vs light level curve at some line number, say 200 lines/ picture height when the pattern speed is 20 sec/picture width and when the input image contrast is 100%.

The intrascene dynamic range which can be tolerated within any given scene is an often discussed but undefined quantity. It may also be a variable quantity depending on the camera tube's operating point. For example, the intrascene dynamic range should be higher for a SEBIR camera when it is operated at low gain than when it is operated at high gain. Most camera tubes have some limitation to the maximum signal current it can store or readout either because of limited signal storage capability or because of a limited beam current. Sometimes the maximum is well defined due to a reasonably hard knee in the signal transfer characteristic while at other times, the knee is quite rounded. However, the maximum signal current, which can be translated to light level, is easier to define than the minimum light level which is mainly dependent upon the noise level in some functional way. It is a temptation to use some measure such as a video signal-to-noise ratio of unity in defining the lower light level limit but video signal-to-noise ratio is not a fundamental quantity for systems whose displays are viewed by humans.

In the past, shades of grey have been used as a measure of dynamic range although it is not a good one as currently used because it lacks analytical and quantitative precision. However, shades of grey represent a viable concept and is considered a worthy contender. In some future effort, it is proposed to develop a grey shade pattern which might take the form of a number of isolated square images in vertical, but not contiguous array. A number of vertical arrays would be provided, each with squares of different sizes, e. g., 8 x 8, 4 x 4, 2 x 2 scan lines, etc. Then psychophysical experiments would be performed to quantitatively associate the various patterns with display signal-to-noise ratio. The suitability of other patterns such as Air Force "three bar" patterns should also be investigated. The use of different square sizes or bar patterns of varying spatial frequency overcomes one of the current objections to the grey shade measure, i. e., that the dynamic range is also a function of spatial frequency. In the interim, it is recommended that as a minimum, the grey shade scales dimensions should be standardized.

Along the same lines, we note that various camera types differ substantially with respect to their ability to withstand bright light overloads. Some quantitative measures are now being developed and some results reported are that they are isolated from the camera tube's sensitivity. A camera with low sensitivity should in general be capable of withstanding larger overloads then one which is photoelectron limited. Similarly tubes with large signal storage capacity are more effective in handling overloads but the large storage capacity can result in a long sensor time constant. Since trade-offs exist between signal storage capacity, sensitivity and time constant, or means of showing these

characteristics in some composite way. In no event should the overload

capacities of different tube types be plotted on the same coordinates

without some indication of the other significant tube properties.

6.5 Observer Parameters

The primary objective of the psychophysical experimentation

is to obtain the necessary "constants" for use in the analytical models.

These constants take the form of SNR thresholds for a given level of

probability of success in performing a desired level of object discrimina-

tion. A large number of these constants are reported in Section IV. We

note that these constants hold only when the calculations are made using

the methods used in obtaining the constants in the first place. For

example, if a different integration time is used for the eye, a

different constant would result.

With regard to detection, we have established two tentative

criteria; one for cluttered and the other for uncluttered environments.

As we saw in Fig. 33, the threshold range differs markedly for the two

cases. In general, the uncluttered object case is seldom encountered.

On the other hand, the cluttered object case probably leads to somewhat

pessimistic predictions. As an interim recommendation, we have been leaning

toward analyzing the detectability of objects in moderate clutter (vehicles

on roads) by using a one line per minimum object width criteria but using

the analytical treatment as for the cluttered case as is exemplified by

Eq. 67.

For recognition and identification of objects, the equivalent

bar pattern approach is felt to have some merit. Here, we substitute a

bar pattern for the "real world" object with bars equal in length to the

251

length of the object and of spacing 1/8 or 1/13 the minimum object dimension for recognition and identification respectively. The notion of replacing the "real world" object with a bar pattern has appeal because we know a great deal about the discernability of bar patterns. In the Section 4, it was seen that the discernability equivalent bar patterns as measured by a threshold SNR was similar to the SNR's required to recognize or identify the objects. On the other hand, the SNR for the object was calculated on the basis of the peak signal excursion relative to background while for discerning bar patterns, the observer must be able to see modulation within the pattern. We observe that real objects are not usually periodic but rather, are assemblages of aperiodic objects. Generally speaking, we would expect the effect of MTF's to be less severe on aperiodic objects than on periodic objects and thus, the equivalent bar pattern approach may lead to pessimistic range predictions. While we recognize and even emphasize these differences, we do not now have better criteria to suggest. For the moment, we suggest that the equivalent bar pattern approach be adopted, using thresholds such as those tabulated in Fig. 46 with the understanding that the results predicted are probably pessimistic.

6.6 Range Prediction

We mentioned that the objective of an overall system specification is to provide the procuring agency with some assurance that the equipment being proposed for a given mission will have some reasonable expectation of actually meeting the mission requirement. While range prediction for electro-optical sensors must still be considered an art, needing considerable refinement; nevertheless, the first order effects have been investigated and accounted for. Methods of predicting range were developed and presented in

252

the previous report (REF 2) and again in Section 2 of this report. We have used these techniques to predict system range performance and we find that the predictions are generally consistent with those measured in field and tower tests when due account is taken of unknowns such as meteorological visibility. These predictions were particularly good for field test targets which are similar to those used in the laboratory such as bar patterns and for the active system where the scene irradiance could be measured.

It is felt that any reasonably competent system manufacturer can perform a range prediction and that range predictions should be a require- ment in any proposed effort. It is not necessary that the procedures proposed in this document be followed precisely but in view of the rather considerable general acceptance of the methods used herein, any large deviations in method should be explained.

6.7 Formation of a Specifications Committee

In the past, committees such as those formed by the IEEE have generated standards, specifications and guides for television sensors. How- ever, these committees have dwelled upon the measurement of specific sensor parameters such as photosurface spectral sensitivity, target gain, synchronization standards and the like. Little thought has been given to the overall sensory system performance including the observer as an integral part of the sensory system. The authors of this report are active in and are contributing to the work of the current IEEE committee on imaging tube specifications. While some image quality guides, based on image signal-to- noise ratio concepts may be incorporated, the major emphasis is on specific sensors parameters as in the past. This is partially due to the comparative newness of the electro-optical image quality analysis and partially due to

253

the greater commercial orientation of the IEEE standards group.

Thus, it seems quite clear that if standards are desired for military purposes in the new terms, it will be necessary to form a joint committee composed of industrial and military organizations. The committee approach is necessary to obtain general standards acceptability. The advantage of a committee with military orientation is that it can focus on the long range detection of objects under marginal viewing conditions as opposed to the meeting of commercial broadcast standards.

Appendix 1 – Characterization of the Signal Readout Process from a Resistive Sea Type Silicon Diode Array Target Tube

In the following, the resistive sea type EBS target will be discussed. A simplified equivalent charging and discharging circuit for the resistive sea EBS target is shown in Fig. 154 A. The circuit elements have the following meaning:

C_R = capacitance/area of resistive sea

R_R = resistance through unit area of resistive sea

C_d = capacitance/area of diode depletion region (i.e., storage capacitance)

R_d = diode leakage resistance

I = target charging source

T = frame time

T' = beam dwell time

To further simplify the circuit, we will assume that

$$T' \ll C_R R_R \ll T \tag{174}$$

and the equivalent circuit is shown in Fig. 154 B.
Now let

$$\frac{C_R + C_d}{C_d} = r \tag{175}$$

The general solution for buildup of odd fields proceeds as follows and is depicted in Fig. 155.

Field No.	Peak	Base	Readout
1	$\frac{1}{4}$	$\frac{1}{4r}$	$\frac{1}{4}\left(1 - \frac{1}{r}\right)$
3	$1 + \frac{1}{4r}$	$\frac{1}{r} + \frac{1}{4r^2}$	$\left(1 + \frac{1}{4r}\right)\left(1 - \frac{1}{r}\right)$
5	$1 + \frac{1}{r} + \frac{1}{4r^2}$	$\frac{1}{r} + \frac{1}{r^2} + \frac{1}{4r^3}$	$\left(1 + \frac{1}{r} + \frac{1}{4r^2}\right)\left(1 - \frac{1}{r}\right)$
7	$1 + \frac{1}{r} + \frac{1}{r^2} + \frac{1}{4r^3}$	$\frac{1}{r} + \frac{1}{r^2} + \frac{1}{r^3} + \frac{1}{4r^4}$	$\left(1 + \frac{1}{r} + \frac{1}{r^2} + \frac{1}{4r^3}\right) \cdot$ $\cdot \left(1 - \frac{1}{r}\right)$
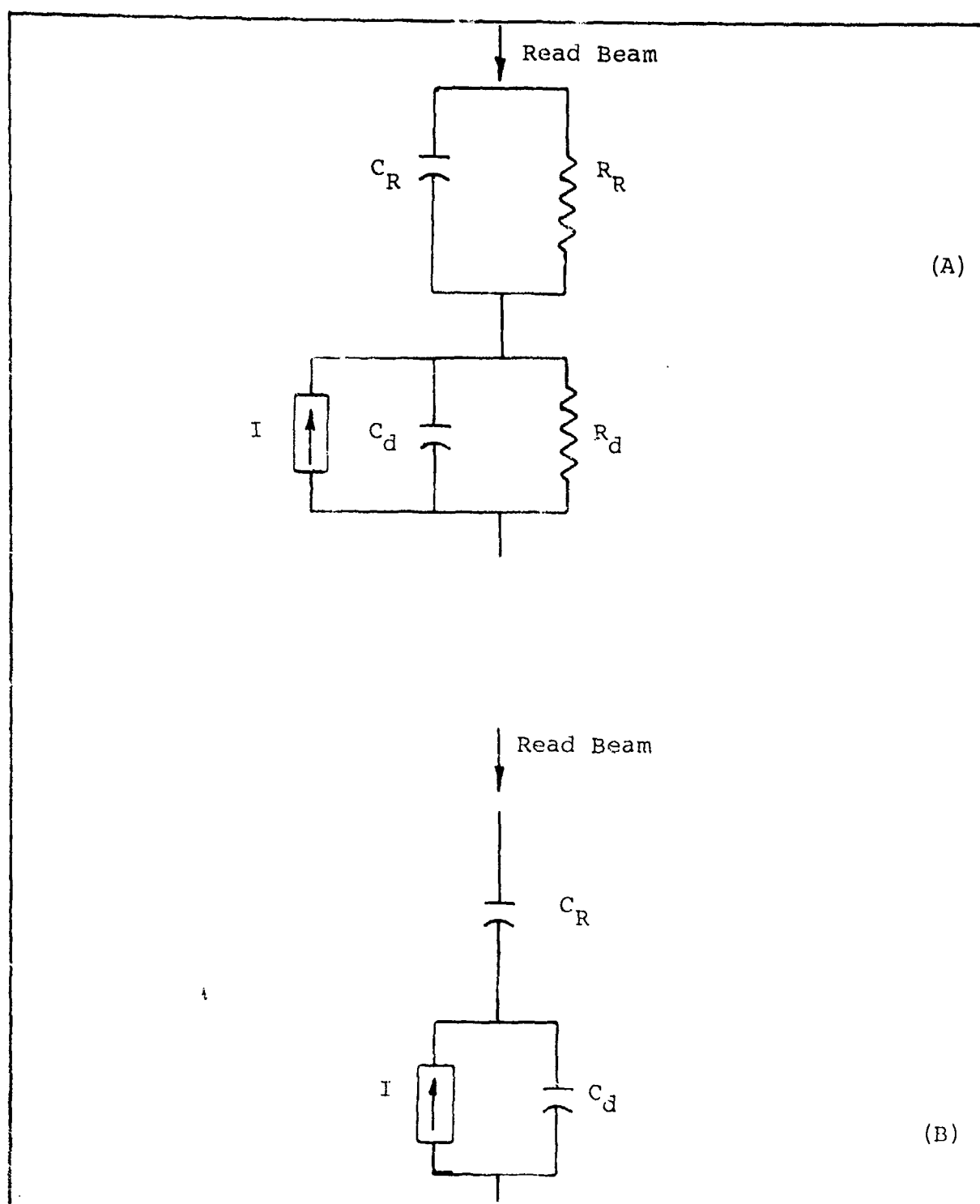
Fig. 154   Equivalent Circuits for Resistive Sea EBS Target
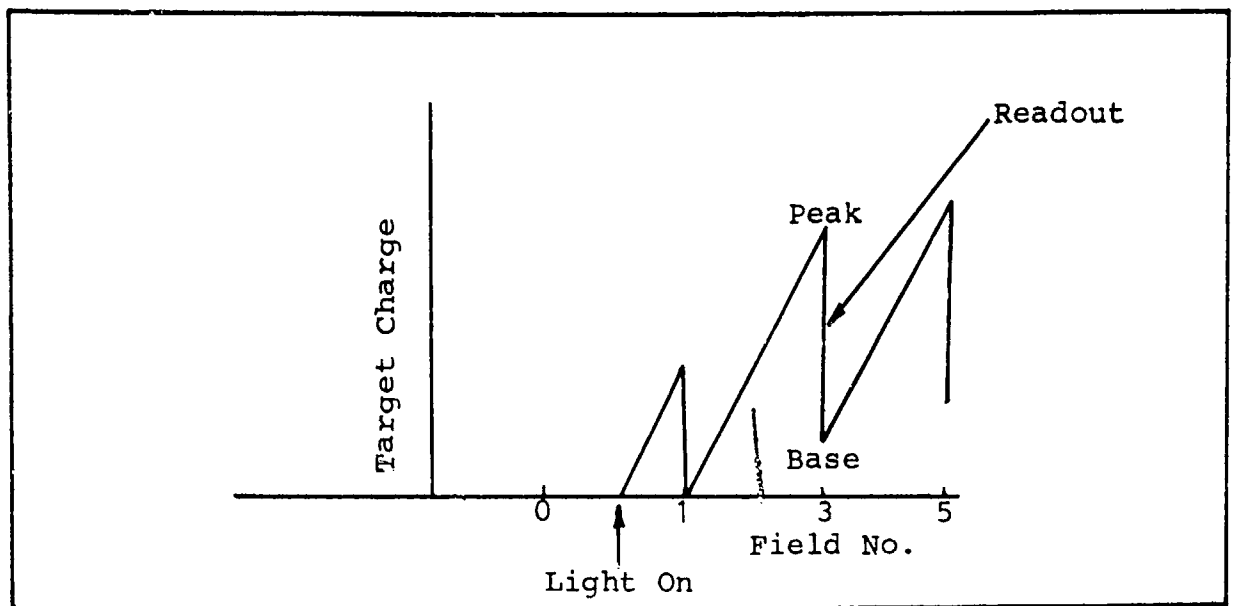
Fig. 155   Charge Buildup - Odd Fields
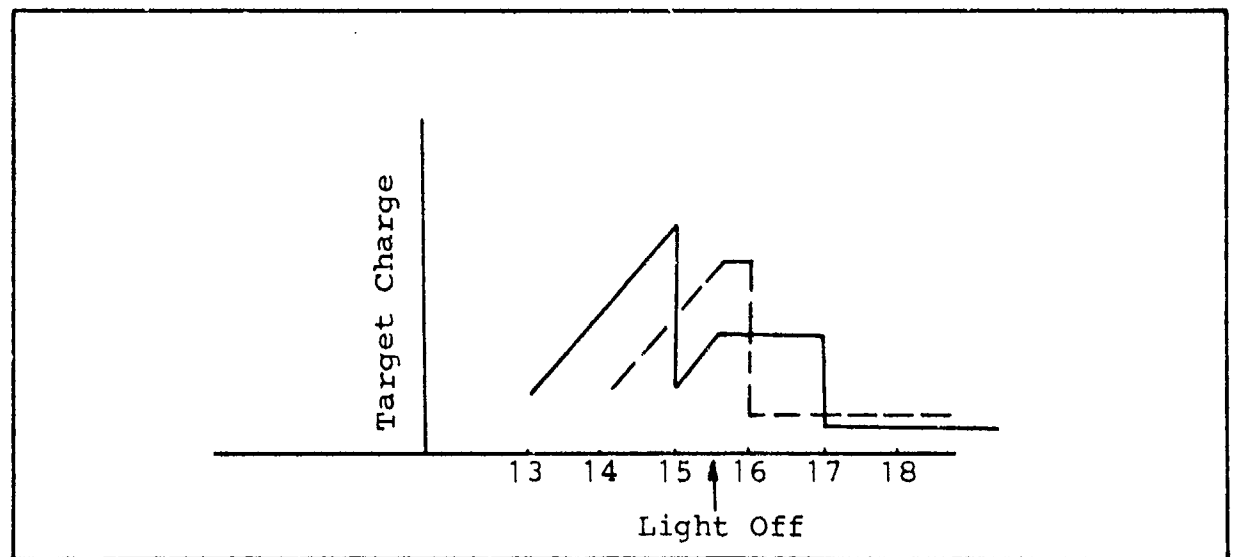
Fig. 156   Decay

So we see that the base tends to $\frac{1}{r-1} = \frac{C_d}{C_r}$ and the readout tends to 1.

For ideal target $r \longrightarrow \infty$

The general solution for buildup of even field is developed similarly below.

Field No.	Peak	Base	Readout
2	$\frac{3}{4}$	$\frac{3}{4r}$	$\frac{3}{4}(1 - \frac{1}{r})$
4	$1 + \frac{3}{4r}$	$\frac{1}{r} + \frac{3}{4r^2}$	$(1 + \frac{3}{4r})(1 - \frac{1}{r})$
6	$1 + \frac{1}{r} + \frac{3}{4r^2}$	$\frac{1}{r} + \frac{1}{r^2} + \frac{3}{4r^3}$	$(1 + \frac{1}{r} + \frac{3}{4r^2})(1 - \frac{1}{r})$
8	$1 + \frac{1}{r} + \frac{1}{r^2} + \frac{3}{4r^2}$	$\frac{1}{r} + \frac{1}{r^2} + \frac{1}{r^3} + \frac{3}{4r^4}$	$(1 + \frac{1}{r} + \frac{1}{r^2} + \frac{3}{4r^3}) \cdot (1 - \frac{1}{r})$

and we see that the base tends to $\frac{1}{r-1} = \frac{C_d}{C^r}$ as was the case for odd fields.

The readout tends to 1.

Now, let $\gamma = (\frac{r-1}{r})$ where γ is the parameter defined in Section as the fraction of the total charge readout in a single scan. The solution for decay is depicted in Fig. 156 and is developed below.

During Steady State

Readout $= 1$

Base $= (\frac{1}{r-1})$

Peak $= (\frac{r}{r-1})$ $\gamma = (\frac{r-1}{r})$

For odd fields, we have the following,

Odd Fields	Readout
15	1
17	$\frac{1}{4} \left(\frac{1}{r}\right) (r + 3)$
19	$\frac{1}{r^2} \left(\frac{1}{4}\right) (r + 3)$
21	$\frac{1}{r^3} \left(\frac{1}{4}\right) (r + 3)$
23	$\frac{1}{r^4} \left(\frac{1}{4}\right) (r + 3)$
25	$\frac{1}{r^5} \left(\frac{1}{4}\right) (r + 3)$

whereas, for even fields, we have

Even Fields	Readout
14	1
16	$\frac{1}{r} \left(\frac{1}{4}\right) (3r + 1)$
18	$\frac{1}{r^2} \left(\frac{1}{4}\right) (3r + 1)$
20	$\frac{1}{r^3} \left(\frac{1}{4}\right) (3r + 1)$
22	$\frac{1}{r^4} \left(\frac{1}{4}\right) (3r + 1)$
24	$\frac{1}{r^5} \left(\frac{1}{4}\right) (3r + 1)$

For the ideal tube $r \longrightarrow \infty$.

For WX-31841 tested, R = 4 gives excellent agreement with measurements at $V_T = 15V$, $I_s = 400$ nA. This implies $C_R = 3C_d$. With decreasing V_T, C_d increases although C_R remains fixed. Thus r decreases with increasing V_T.

Nominal buildup lag on basis of the series capacitance model is $\approx$ 80%.

Nominal decay lag is $\approx$ 20%.

Appendix 2 – Measured Signal Buildup and Decay Data

RELATIVE SIGNAL AMPLITUDE

Field No.	3	6	9	12	15	18	21	24	27	30
I_S = 100 nA, V_T = 7.5 V	1.9	2.8	3.2	3.4	3.5	1.7	.8	.4	.3	.2
I_S = 100 nA, V_T = 10 V	2.3	3.0	3.5	3.5	3.5	1.3	.6	.4	.2	.1
I_S = 100 nA, V_T = 12.5 V	2.6	3.2	3.4	3.5	3.5	1.0	.45	.3	.2	.2
I_S = 100 nA, V_T = 15 V	2.7	3.3	3.4	3.4	3.4	.9	.4	.3	.2	.2
I_S = 100 nA, V_T = 20 V	3.0	3.3	3.4	3.5	3.5	.7	.3	.2	.2	.2

RELATIVE SIGNAL AMPLITUDE

Field No.	3	6	9	12	15	18	21	24	27	30
I_S = 200 nA V_T = 7.5 V	1.5	2.6	3.1	3.4	3.5	1.7	1.0	.6	.4	.3
I_S = 200 nA V_T = 10 V	1.9	2.8	3.4	3.4	3.5	1.3	.7	.4	.3	.2
I_S = 200 nA V_T = 12.5 V	2.3	3.0	3.4	3.5	3.5	1.0	.5	.3	.3	.3
I_S = 200 nA V_T = 15 V	2.5	3.1	3.4	3.5	3.5	.9	.4	.3	.3	.3
I_S = 200 nA V_T = 20 V	2.7	3.2	3.4	3.4	3.5	.7	.3	.3	.3	.3

RELATIVE SIGNAL AMPLITUDE

Field No.	1	2	3	6	9	12	15	16	17	18	21	24	27	30
$I_S = 400$ nA, $V_T = 7.5$ V			1.8	2.8	3.3	3.5	3.5			1.5	.8	.5	.3	.2
$I_S = 400$ nA, $V_T = 10$ V	.6	1.5	2.2	2.9	3.3	3.4	3.5	2.8	1.8	1.2	.6	.3	.2	.1
$I_S = 400$ nA, $V_T = 12.5$ V			2.6	3.1	3.4	3.5	3.5			.9	.4	.2	.1	.1
$I_S = 400$ nA, $V_T = 15$ V	.8	2.0	2.7	3.3	3.5	3.5	3.5	2.6	1.3	.8	.3	.2	.1	.1
$I_S = 400$ nA, $V_T = 20$ V			2.9	3.3	3.4	3.5	3.5			.6	.3	.1	.1	.1

RELATIVE SIGNAL AMPLITUDE

Field No.	3	6	9	12	15	18	21	24	27	30
$I_S = 600$ nA, $V_T = 7.5$ V	2.0	2.8	3.2	3.4	3.5	1.6	.7	.4	.2	.2
$I_S = 600$ nA, $V_T = 10$ V	2.3	3.1	3.4	3.5	3.5	1.3	.6	.3	.2	.1
$I_S = 600$ nA, $V_T = 12.5$ V	2.5	3.1	3.4	3.4	3.5	1.0	.4	.2	.1	.1
$I_S = 600$ nA, $V_T = 15$ V	2.6	3.1	3.4	3.5	3.5	.8	.3	.2	.1	.1
$I_S = 600$ nA, $V_T = 20$ V	2.8	3.2	3.4	3.5	3.5	.7	.3	.1	.1	.1

Appendix 3 - Charge Readout with Signal Mixing and Lag Effects Included

Consider a photoelectron flux density incident on the target. The flux density is independent of position normal to the x-axis. The number of photoelectrons per cm^2 per sec. falling on an elemental area of unit length and width Δx in the time interval dt at time, t, is proportional to

$$J \quad \propto \quad 1 + \sin \frac{2\pi}{\lambda} (x - vt) \tag{176}$$

where λ is the spatial wavelength of the periodic pattern and v is its velocity of motion parallel to the x axis.

Consider the pattern, initially, to be stationary and with a steady state condition achieved. Each readout by the read electron beam consists of neutralizing a fraction γ of the total accumulated charge. Steady state requires that

$$\gamma Q_T = Q_f \qquad Q_T = \text{total charge density} \tag{177}$$

where Q_f is the charge per unit area integrated onto the target during a single frame. After each readout a residue charge density $Q_R = (1 - \gamma) Q_T$ remains upon which Q_f is subsequently deposited. Thus $Q_T = Q_f + Q_R$. Assume now that the pattern is put in motion with velocity v. During one frame time T_1 the new charge per unit area integrated onto the target will be

$$Q_{f1} = \int_0^{T1} \left(1 + \sin \frac{2T}{\lambda} (x - vt) \right) dt. \tag{178}$$

The total charge density will be Q_{f1} plus the residual from the previous steady state readout, or

$$Q_{T1} = Q_{f1} + Q_{RO} \qquad \text{where} \tag{179}$$

$$Q_{RO} = (\frac{1-\gamma}{\gamma})\ Q_{fo} = \frac{1-\gamma}{\gamma} \int_{0}^{T_0} \left(1 + \frac{\sin 2\pi x}{\lambda} \right) dt \qquad (180)$$

$$Q_{RO} = (\frac{1-\gamma}{\gamma})\ (1 + \frac{\sin 2\pi x}{\lambda})\ T_0 \qquad (181)$$

and

$$Q_{f1} = T_1 + \frac{\lambda}{2\pi v} \left(\cos \frac{2\pi}{\lambda} (x - vT_1) - \cos \frac{2\pi x}{\lambda} \right) . \qquad (182)$$

$$Q_{T1} = K + T_1 + \frac{\lambda}{2\pi v} \left(\cos \frac{2\pi}{\lambda} (x - vT_1) - \cos \frac{2\pi x}{\lambda} \right) \qquad (183)$$

$$\text{where } K = Q_{RO} = (\frac{1-\gamma}{\gamma})\ (1 + \frac{\sin 2\pi x}{\lambda})\ T_0 \qquad (184)$$

At time $t = T_1$ the charge density γQ_{T1} is read out.

$$\gamma Q_{T1} = \gamma K + \gamma T_1 + \frac{\gamma \lambda}{2\pi v} \left(\cos \frac{2\pi}{\lambda} (x - vT_1) - \cos \frac{2\pi x}{\lambda} \right) . \qquad (185)$$

A residual $Q_{R1} = (1 - \gamma)\ Q_{T1}$ then exists.

$$Q_{R1} = (1 - \gamma)\ K + (1 - \gamma)T_1 + \frac{(1 - \gamma)\lambda}{2\pi v} \left(\cos \frac{2\pi}{\lambda} (x-vT_1) - \cos \frac{2\pi x}{\lambda} \right) \qquad (186)$$

During interval $T_2 = (T_1 + T_2) - (T_1)$ a charge per unit area Q_{f2}
will be integrated onto the target giving a total accumulated
charge per unit area of

$$Q_{T2} = (1 - \gamma)\ K + (1 - \gamma)T_1 + (1 - \gamma)\ \frac{\lambda}{2\pi v} \left(\cos \frac{2\pi}{\lambda} (x-vT_1) - \cos \frac{2\pi x}{\lambda} \right)$$

$$+ (T_2) + \frac{\lambda}{2\pi v} \left(\cos \frac{2\pi}{\lambda} (x - v (T_1 + T_2) - \cos \frac{2\pi}{\lambda} (x - vT_1) \right) \qquad (187)$$

The readout will be γQ_{T2}.

266

$$\gamma\, Q_{T2} = \gamma(1-\gamma)\ K + \ (1-\gamma)\ T_1 + \gamma T_2 + \gamma(1-\gamma)\ \frac{\lambda}{2\pi v}. \quad (188)$$

$$\left(\cos\frac{2\pi}{\lambda}\ (x - vT_1) - \cos\frac{2\pi x}{\lambda} \right)$$

$$+ \frac{\gamma\lambda}{2\pi v}\left(\cos\frac{2\pi}{\lambda}\ (x - v\ (T_1 + T_2)) - \cos\frac{2\pi x}{\lambda}(x - vT_1) \right)$$

The residual $Q_{R2} = (1-\gamma)\ Q_{T2}$.

In general a residual charge density will be

$$Q_{RN} = (1-\gamma)^N\ K + \sum_{n=1}^{N}\ (1-\gamma)^n T^n \qquad (189)$$

$$+ \sum_{n=1}^{N}\ (1-\gamma)^{N-(n-1)}\ \frac{\lambda}{2\pi v}\left(\cos\frac{2\pi}{\lambda}(x - vnT) - \cos\frac{2\pi}{\lambda}(x - v(n-1)T) \right)$$

where N is the last frame number and n has values 1, 2, 3,
The readout at the end of frame period T_n is given by

$$(\frac{\gamma}{1-\gamma})\ Q_{RN} \qquad (190)$$

or

$$\gamma\, Q_{TN} = \gamma(1-\gamma)^{N-1} K + \sum_{n=1}^{N}\ \gamma(1-\gamma)^{n-1}\ T^{n-1} \qquad (191)$$

$$+ \sum_{n=1}^{N}\ \gamma(1-\gamma)^{N-n}\ \frac{\lambda}{2\pi v}\left(\cos\frac{2\pi}{\lambda}\ (x - vnT) - \cos\frac{2\pi}{\lambda}(x - v(n-1)T) \right).$$

If $N = 1$ integration of charge occurs over only one frame, and if
$\gamma = 1$, the charge readout reflects the effect of signal mixing
alone. The relative modulation in this case is given by

$$\frac{Q_{T1}\ (max)}{Q_{To}\ (max} = \frac{Q_{T1}\ (max)}{T} \qquad (192)$$

$$\frac{Q_T}{Q_{To}} = \frac{\lambda}{2\pi vT}\left(\cos 2\pi\ (\frac{x}{\lambda} - \frac{vT}{\pi}) - \cos 2\pi\ (\frac{x}{\lambda}) \right). \qquad (193)$$

267

To determine the value of x/λ which maximizes this expression
the quantity in the brackets is differentiated with respect to
x and set equal to zero. Doing this, we find,

$$\frac{x}{\lambda} = \frac{vT}{2\lambda} + \frac{1}{4} \quad \text{satisfies this condition.} \tag{194}$$

For signal mixing along the relative modulation or contrast
becomes, for a sinusoidal input

$$M = \frac{\lambda}{2\pi vT} \quad \cos 2\pi \left(\frac{-vT}{2\lambda} + \frac{1}{4}\right) - \cos 2\pi \left(\frac{vT}{2\lambda} + \frac{1}{4}\right) \quad . \tag{195}$$

The relative signal mixing contrast for the sine wave is shown
in Fig. 157 where it may be compared with the corresponding
quantity for square wave input taken from Fig. 128. The
frame time T was taken as 1/30 sec.
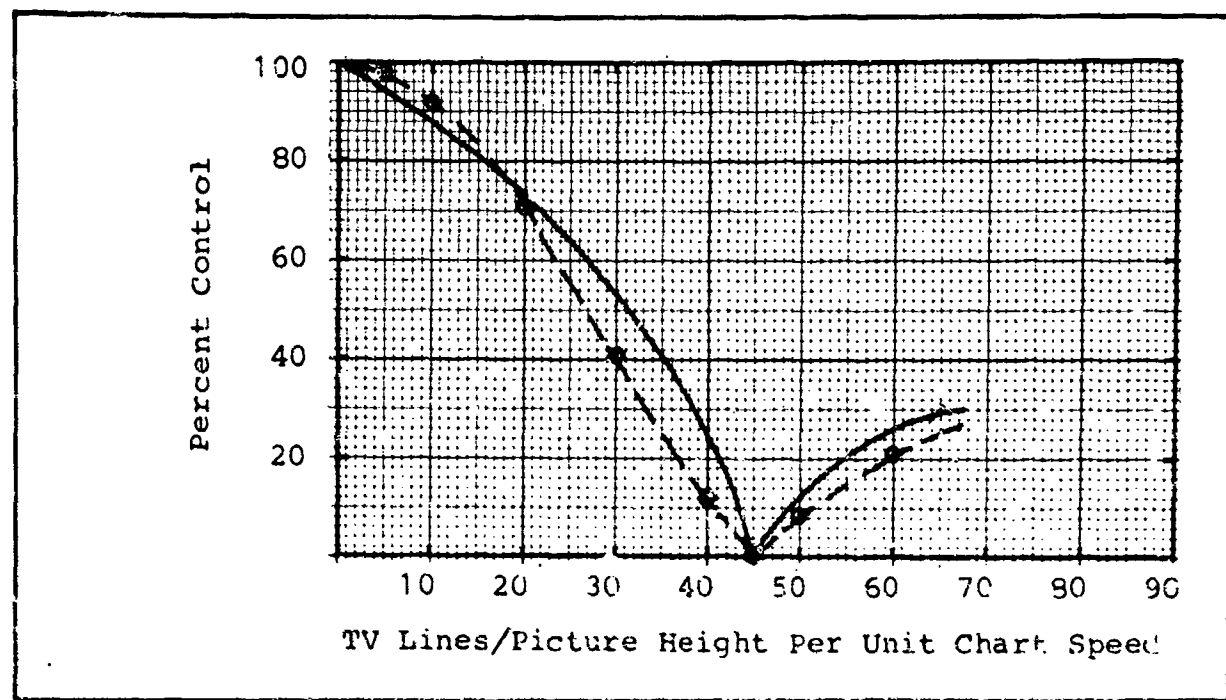
Fig. 157   Signal Mixing for Different Inputs

O   Sinusoidal Input   T = 1/30 Sec.

—— Square Wave Input T = 1/30 Sec.

REFERENCES

1. Bond, D. S., and Henderson, F. P., "The Conquest of Darkness", AD 346297, DDC, July 1963.

2. Rosell, F. A., and Willson, R. H., "Performance Synthesis – Electro-Optical Sensors", Tech. Rpt. No. AFAL-TR-71-137, Air Force Avionics Laboratory, WPAFB, Ohio, May 1971.

3. Biberman, L. M., and Nudelman, S., "Photoelectronic Imaging Devices", Vol. 1, Plenum Press, New York, 1971.

4. Middleton, W. E. K., "Vision Through the Atmosphere", University of Toronto Press, Canada, 1952.

5. "Electro-Optics Handbook", RCA Defense Electronics Products, Burlington, Mass., 1968.

6. Steingold, H., and Strauch, R., Applied Optics, Jan. 1969.

7. Johnson, J., "Analysis of Image Forming Systems", Image Intensifier Symposium, Ft. Belvoir, Va., AD220 160, Oct. 1958.

8. Schade, O. H., Sr., RCA Review, Sept. 1967.

9. Barnes, R., and Czerny, M., Z. Physik, 79, 1932.

10. de Vries, H. L., Physica X, No. 7, July 1943.

11. Rose, A., J. Opt. Soc. Am., 38, 196, 1943.

12. Blackwell, H. R., J. Opt. Soc. Am., 59, 539, 1941.

13. Coltman, J. W., and Anderson, A. E., Proc. IRE, 48, 858, 1960.

14. Rosell, F. A., J. Opt. Soc. Am., 59, 539, 1969.

15. Coltman, J. W., J. Opt. Soc. Am., 44, 6, 1954.

16. "NASA Biostronautics Data Book", NASA SP-3006, U. S. Government Printing Office, 1964.

17. Krittmann, I. M., IEE Transactions on Electron Devices, Vol. 10, Nov. 1963.

18. Cope, A. D., atal., "Photoelectronic Imaging Devices", (L. M. Biberman and S. Nudelman, editors), Plenum Press, Vol. 2, Chapter 2, New York 1971.

19. Schade, O. H., Sr., "Photoelectronic Imaging Devices", (L. M. Biberman and S. Nudelman, editors), Plenum Press, Vol. 2, Chapter 16, New York 1971.

20. Zucchino, P. M., and Lowrance, J. L., Progress Report on Development of the SEC Vidicon for Astronomy, Proceedings of a symposium on Astronomical Use of Television-Type Image Sensors held at Princeton University, NASA SP-256, May 20-21, 1970.

21. Anderton, H., and Beyer, R. R., "Advances in Electronics and Electron Physics", (Academic Press, L. Marton, editor), Vol. 28A, p. 229, 1969.

22. Coltman, J, JOSA, 44, 6, June 1954.

DOCUMENT CONTROL DATA · R&D

(Security classification of title, body of abstract and indexing annotation must be entered when the overall report is classified)

1 ORIGINATING ACTIVITY *(Corporate author)*	2a. REPORT SECURITY CLASSIFICATION
Westinghouse Defense and Space Center	Unclassified
Aerospace Division, Baltimore, Maryland	2b GROUP None

3 REPORT TITLE

Performance Synthesis
(Electro-Optical Sensors)

4 DESCRIPTIVE NOTES *(Type of report and inclusive dates)*

Final Report

5 AUTHOR(S) *(Last name, first name, initial)*

Rosell, Frederick A.
Willson, Robert H.

6 REPORT DATE	7a. TOTAL NO. OF PAGES	7b NO OF REFS
Aug. 1971	271	22

8a. CONTRACT OR GRANT NO. F33615-70C-1461	9a. ORIGINATOR'S REPORT NUMBER(S)
b. PROJECT NO	
c. 698DF	9b. OTHER REPORT NO(S) *(Any other numbers that may be assigned this report)*
d.	AFAL-TR-72- 279

10 AVAILABILITY/LIMITATION NOTICES

Distribution limited to United States government agencies only; test and evaluation; 11 August 1972. Other requests for this document must be referred to Air Force Avionics Laboratory (NVA-698DF), Wright-Patterson Air Force Base, Ohio 45433.

11 SUPPLEMENTARY NOTES	12 SPONSORING MILITARY ACTIVITY
	Air Force Avionics Laboratories Wright Patterson AFB, Ohio 45433

13 ABSTRACT

This effort is a continuation of the Performance Synthesis Study (Electro-Optical Sensors) reported in Technical Report AFAL-TR-71-137, dated May 1971. Analytical models are developed for evaluating and predicting the performance of observers augmented by electro-optical sensors for laboratory test images such as rectangles and periodic bar patterns and for a limited number of real world objects. The models developed are improved, and modified to bring them into closer agreement with those models proposed by other investigators for the purpose of obtaining greater acceptance and making available a wider body of technical literature. In the models developed, a signal-to-noise ratio is associated with an image based on the image's irradiance and spatial dimensions. Through psychophysical experimentation, the observer's thresholds for discrimination of these images are determined.

Methods of predicting the range capability of sensor-augmented observers are developed and applied to both range-gated active and passive low-light-level television systems. These models take into account properties of the scene, atmosphere and level of target discrimination. Also, pure image motion effects, observer effects due to motion, and sensor effects due to motion are analyzed. The general area of system specification is discussed.

DD FORM 1473

14 KEY WORDS	LINK A		LINK B		LINK C	
	ROLE	WT	ROLE	WT	ROLE	WT
Synthesis						
698DF						
Low-Light-Level Television						
Model						
Range						
Electro-Optics						
Sensors						
Video						
Perception						
Vision						
Signal-to-Noise Ratio Display						